Doctoral Dissertation
Doctoral Program in Civil and Environmental Engineering (32.nd cycle)

Static, Dynamic, and Stability Analysis of High-rise Buildings

Giuseppe Nitti
* * * * * *

Supervisors
Prof. Alberto Carpinteri, Supervisor
Prof. Giuseppe Lacidogna, Co-supervisor

Doctoral Examination Committee:
Prof. A.M. Tarantino, Referee, Università di Modena e Reggio Emilia
Prof. F. Tubino, Referee, Università di Genova
Prof. G.C. Marano, Politecnico di Torino
Prof. F. Mollaioli, Università di Roma "La Sapienza"
Prof. F. Tornabene, Università del Salento

Politecnico di Torino
September, 2020

. . . . . .

Giuseppe Nitti

Turin, September, 2020

Summary

The analytical formulation of a simplified method that allows the static, dynamic, and stability analysis of a high-rise building is proposed in the present work.

This thesis is the natural extension, development and improvement of a project started a few years ago by Prof. Alberto Carpinteri, author of a formulation that allows the preliminary analysis of a tall building. Originally this formulation was rather limited and only allowed the analysis of a few types of structures. Over the years, also thanks to the contribution of Prof. Giuseppe Lacidogna and Dr. Sandro Cammarano, new models have been introduced and a more advanced calculation code has been created.

In 2016, after completing a Master Thesis and joining the Doctoral Program in Civil and Environmental Engineering (32nd cycle) at the Politecnico di Torino, I became involved in this project.

As a matter of fact, I created the graphical interface of the calculation code, greatly simplifying its use and improving the interpretation of the results. Subsequently, to make a further improvement to the formulations relating to static and dynamic analysis, with a focus on structures that present irregularities in plan and height, I implemented the analysis of framed tube structures, and diagrid (in collaboration with Eng. Domenico Scaramozzino). Eventually, I dealt with the stability analysis, a topic which is important but virtually absent in the literature.

The objectives of this thesis are to illustrate the analytical formulations and the operational methodology underlying the calculation code developed. In this context, simplified analytical formulations have been developed which describe the behavior of tall buildings in a simple, intuitive way and with the use of simple resources and techniques. This computer tool combines the advantages of analytical formulations, including simple and intuitive input, absence of mesh and few unknowns, with the advantages of computer software, such as its great potential for calculation and the ability to view the results on screen with graphs and three-dimensional models.

However, the greatest strength of this analytical code is the reduced processing time, which makes it suitable for use in preliminary analysis and structural optimization. In these phases, in order to find the best compromise between material

strength, deformation and construction cost, it is necessary to vary one parameter at a time (thickness of each shear wall, size of cross sections of beams and columns, etc.) making it necessary to create thousands of different models. In this context, as can be easily understood, the speed of calculation is a determining factor that has a significant impact on the cost and on the planning times.

The thesis is divided into six chapters, each of which is dedicated to a particular aspect of the study of high-rise buildings. It was important to give ample space to bibliographical references, as, in addition to providing a description of the problem from multiple points of view, it can be an important starting point if the reader wants to delve deeper into the topics covered.

Chapter 1 provides an overview of the evolution of tall buildings. It also reviews the main construction typologies, as well as providing a basic description of structural behavior.

Chapter 2 illustrates the simplified analytical formulations that lead to the determination of the stiffness matrices of the vertical bracings that are mainly used to contrast the transversal displacements caused by the horizontal loads acting on a building.

Chapter 3 describes the analytical procedure that allows the static analysis of a tall building, by means of which it is possible to determine the floor displacements and the stresses in each structural element.

Chapter 4 shows a simplified procedure that permits the mode shapes, natural frequencies, and periods of vibration of a high-rise building to be determined. To demonstrate the effectiveness of the algorithm, the results of the analysis of a tall building recently built in Turin are presented: the Piedmont Region Headquarters Tower. The comparison between the results obtained using the analytical algorithm and those obtained using a commercial Finite Element software allows the accuracy of the proposed formulation to be verified.

In Chapter 5, an analytical formulation is presented which allows the stability analysis of a thin-walled open-section beam and, by extension of the method, of a high-rise building. With this method, a generalization of Euler's Theory (axial buckling) and of Prandtl's Theory (lateral-torsional buckling) is introduced. Furthermore, an energy-based method is defined that allows the non-uniform torsion equation obtained by Vlasov to be determined through a procedure described in Chapter 2.

Finally, Chapter 6 is dedicated to the conclusions drawn and to a concise description of the results achieved, also making reference to future possible developments.

Acknowledgements

I would like to express my gratitude and appreciation for Professor Alberto Carpinteri and Professor Giuseppe Lacidogna for their consistent support and guidance during the running of this project. They have made this experience inspiring for me.

I would like also to thank Professor Giulio Ventura, for his conscientious coordination activities of the Doctoral Program in Civil and Environmental Engineering.

Finally, I would like to thank my family, colleagues and friends who have supported me over these challenging years.

One repays a teacher badly if one always remains nothing but a pupil

Friedrich Nietzsche

Contents

List of Tables

List of Figures

Chapter 1

Historical notes and structural models of tall buildings

1.1 Short historical review

Since ancient times, Man has shown interest in the construction of high structures, and those who lived there were seen as privileged because they could defend themselves from attacks by predatory animals and from frequent flooding of rivers.

Throughout history, elevated structures have also assumed a religious significance, as they were a way for man to approach the sky where the *Divine Power* was thought to live. In this regard, many examples come to mind, such as ancient Mesopotamia, or the pyramids built by the Egyptians and the peoples of pre-Columbian America, up to Gothic cathedrals or the minarets erected by Muslim peoples. The tower also assumes a symbolic role in some religious texts, as in the case of the Tower of Babel mentioned in the Bible. Over the centuries, the tower also assumed other roles, mainly related to height.

Around 280 BCE the Faro (Lighthouse) of Alexandria was erected, a particular construction which, reaching a notable height of around 130 meters for the time, was classified among the Seven Wonders of the Ancient World. Due to a violent earthquake, the building was destroyed in the 14^{th} Century.

In Roman times, the tower took on the role of defense, control and surveillance of the city perimeter. For this reason it was often located near the city walls or at the access gates to the city.

In Medieval times, the tower was incorporated into the castles, again with the function of defense. However, in this historical period the tower also began to assume a prestigious role, as the height and size of the castle tower indicated the power and wealth of the noble family who lived there, and consequently the importance and the size of the fiefdom.

In the Renaissance, the tower began to lose the military function that had characterized it for centuries, and increasingly assumed a symbolic role of power

and prestige. In fact, it was incorporated into the palaces of aristocratic families.

Often it did not even have a residential function, but was adorned with the family crests and its height was proportional to the importance of the family in society. In this regard, it is curious to remember that in the event that two rival families faced each other in battle, the family that was defeated was forced to knock down the top of its tower as a sign of scarring and shame. The towers were historically made of masonry, with a circular or square floor plan. The thickness of the walls was proportional to the height; consequently, at the base it could even reach a few meters. The openings were reduced to the essentials; often only small slits were present as these structures were not intended for residential use.

1.1.1 The Chicago School

The Chicago School [43], [181] is an architectural movement that developed in Chicago in the late 19^{th} Century. A dramatic episode that gave birth to this movement was the disastrous fire which in 1871 destroyed much of the city [73].

Following this event, it was necessary to quickly rebuild the buildings with materials that made them safer, such as steel, to replace wood and masonry. The rising prices of building areas led designers to build large buildings, mainly intended for commercial activities and offices, on sites of limited surface area. This need led to the conception of a new building typology: the skyscraper. The solution of increasing the number of building floors was made possible by recent technological inventions. In 1870 Cyrus W. Baldwin invented and built the first hydraulic lift in Chicago, while in 1887 the electric lift began to become widely used. Lifts, water pumps, telephones, and pneumatic mail allowed the easy use of homes, offices and warehouses at any height. Among the first architects that had the role to build new high-rise buildings are prestigious names [91], including William Le Baron Jenney (1832-1907), an engineer who graduated from the École Polytechnique in Paris, active in the military engineer corps during the War of Secession and operating in Chicago since 1867. The steel skeleton structure consisting of beams and columns bolted together, designed by Le Baron Jenney as an alternative to a massive masonry structure, allowed the height of the building to be increased without having to worry about encumbrance on the lower floors.

Furthermore, with this construction method, it is possible to create large glazed openings in the facades that allow well-lit indoor environments to be created. Finally, to support the concentrated loads of the columns, new stone foundation systems were proposed in 1873 by Frederick Baumann, which would lead to the use of caisson substructures, adopted for the first time in 1894. William Le Baron Jenney can be considered the founder of the First Chicago School, which combined purely structural needs with aesthetic standards, found above all in the recurring design of the motifs of the facades, influenced by the corresponding development of the architectural avant-garde in Europe. The first and most important architects who

shared the ideas of the School we can remember Daniel Burnham (1846-1912) who works with John Root (1850-1891), Martin Roche (1853-1927), and Louis Sullivan (1856-1924), who associates with Dankmar Adler (1844-1900) [105].

The most notable buildings designed by these architects are: Wainwright Building (St. Louis, 1891, Adler and Sullivan), Guaranty Building (Buffalo, 1896, Adler and Sullivan), Monadnock Building (Chicago, 1891, Root and Burnham), Reliance Building (Chicago, 1895, Root and Burnham), and Marquette Building (Chicago, 1895, Roche).

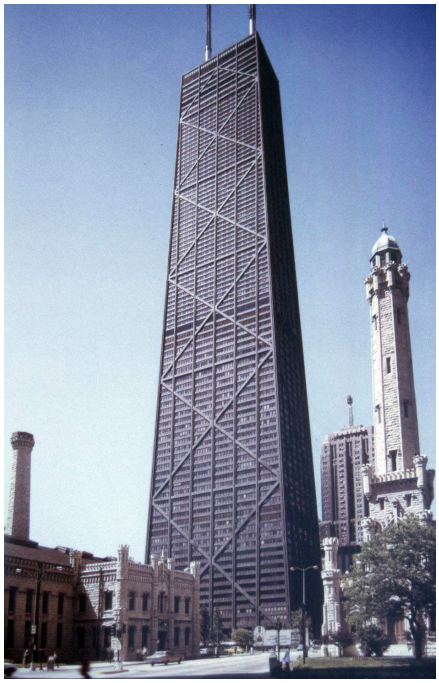

Figure 1.1: John Hancock Center (web source)

Even a very young Frank Lloyd Wright (1867-1959) started his working experience in the studio of Adler and Sullivan but soon distanced himself from the stylistic canons of the School. Brilliant architect, but with ideas that were too daring for the time, in 1956, Frank Lloyd Wright, then nearly 90 years old, presented the project for a 528-storey skyscraper that would have to soar an entire mile (1609 meters) above Chicago. Similar in shape to a gigantic dagger, the steel and aluminum building would have contained offices for 100,000 employees, a parking lot for 15,000 cars and landing areas for helicopters.

Many years later, another great name of modern architecture, Ludwig Mies van der Rohe (1886-1969), after the fundamental German experience of the Bauhaus, arrived in Chicago in 1938 and took over the direction of the prestigious Illinois Institute of Technology [33]. Defined by some architectural critics as the legitimate

inheritor of the great tradition of skyscraper architects, his most important works include the Lake Shore Drive Buildings in Chicago and the Seagram Building in New York.

Another great design studio that shared the stylistic canons of the Second Chicago School was the office founded by Skidmore, Owings & Merrill (SOM).

Many famous engineers and architects linked their name to the SOM studio, such as Myron Goldsmith, Walter Netsch, Bruce Graham, and Fazlur Khan [25].

The latter is considered the father of the framed tube, an innovative structural system that has allowed skyscrapers to reach remarkable heights, and one of the pioneers of Computer Aided Design (CAD). Among the major works by Khan made in Chicago, we can mention the John Hancock Center (Figure 1.1), a tapered building of 100 floors and 344 meters high, characterized by the presence on the façade of long diagonal braces about ten floors high, and the Sears Tower (now Willis Tower), which with its 443 meters held the record of height from 1973 to 1998.

1.1.2 The long race to the record

Conventionally, the birth of the skyscraper coincides with the construction in Chicago of the Home Insurance Building (Figure 1.2), inaugurated in 1885 and demolished in 1931.

Figure 1.2: Home Insurance Building (web source)

This building, designed by William Le Baron Jenney, had only twelve floors for 42 meters height.

This was only the first of long series, higher and more innovative buildings were designed and built, which allow both the decrease in the incidence of land prices and the possibility of housing a multitude of people, who at that time began to flow into the big cities. In 1890 the construction of a twenty-story building, the New York World Building (Figure 1.3a), was completed in New York. Since then, and for many years to follow, financial groups and banking companies in New York challenge each other in the construction of towers of glass, concrete and steel always of greater heights, such as the Manhattan Life Insurance Building completed in 1894 and which reaches the height of 106 meters.

(a) (b) (c)

Figure 1.3: (a) New York World Building; (b) Metropolitan Life Tower; (c) Woolworth Building (web source)

The 20$^{\text{th}}$ Century sees the beginning of a real competition that sees on the one hand the investors, who want to own the tallest skyscraper in the world to declare the economic prestige of their companies, on the other the architects who with their daring and futuristic projects want to demonstrate their skills. The race for the world's tallest building record had begun. The cities where tall buildings were mostly built are Chicago and New York, where the Singer Building, the Metropolitan Life Tower (Figure 1.3b), and the Woolworth Building (Figure 1.3c) are built in a few years, reaching a height of over 241 meters.

(a) (b) (c)

Figure 1.4: (a) Chrysler Building; (b) Empire State Building; (c) World Trade Center (web source)

(a) (b) (c)

Figure 1.5: (a) Sears Tower; (b) Petronas Towers; (c) Taipei 101 (web source)

Figure 1.6: Burj Khalifa (web source)

With the outbreak of the First World War and with the following American crisis, there is a setback. But as early as 1930 the Chrysler Building (Figure 1.4a) was inaugurated with its 319 meters dominating the panorama of New York. But only a year later, the world's tallest building record passes to the Empire State Building (Figure 1.4b) which, with a height of 381 meters, is perhaps the most famous and iconic skyscraper in the world. This building held the height record until the inauguration in 1971 of the sadly famous World Trade Center in New York (Figure 1.4c), which reached a height of 417 meters. But this record lasted only two years because it had to give up the scepter in Chicago where the Sears Tower was built (Figure 1.5a), which with the height of 443 meters held the highest building record in the world from 1973 to 1998.

1998 is a crossroads year in the history of tall buildings because the height record leaves the United States and moves to Asia where just that year were inaugurated in Kuala Lumpur, Malaysia, the Petronas Towers (Figure 1.5b). There was much controversy about this record as these towers are surmounted by a very high not habitable cusp, whose function was purely aesthetic. The Council on Tall Buildings and Urban Habitat (CTBUH), the international committee that is responsible for

(a) (b)

Figure 1.7: Kingdom Tower. (a) Picture taken on August 2019; (b) Artist conception (web source)

high-rise building statistics, awarded the record for the world's tallest building to the Petronas Tower (452 meters) establishing that their cusps, even if they had a purely aesthetic function, were an integral and non-removable part of the building, as opposed to telecommunications antennas that are not taken into account. The Sears Tower was instead given the recognition of building with the highest habitable room in the world.

However, all controversies were quelled in 2004 when the record passed to Taipei 101 (Figure 1.5c), 509 meters high, built in Taipei, Republic of China (Taiwan).

In 2010 the construction of a real giant was completed, the Burj Khalifa (Figure 1.6) built in Dubai, United Arab Emirates. With its 163 floors and 828 meters high, it is today (2020) the tallest building in the world, although perhaps its record will soon be broken. In fact, the Kingdom Tower (Figure 1.7), also known as Jeddah Tower, a skyscraper that will be 1008 meters high, is under construction in Jeddah, Saudi Arabia. When its construction will be completed (expected in 2024) it will become the tallest building in the world.

1.1.3 Statistics

This section shows the data and the geographical distribution of the major tall buildings built in the world. All data are updated to September 2020 and refer to studies published by the Council on Tall Buildings and Urban Habitat (CTBUH).

Table 1.1 and Figure (1.8) show the timeline of the skyscraper height record.

Table 1.1: Timeline of record tallest buildings

Name	Height	City	Years of record
Home Insurance Building	42 m	Chicago	1885 - 1889
Auditorium Building	73 m	Chicago	1889 - 1890
New York World Building	94 m	New York City	1890 - 1894
Manhattan Life Insurance Build.	106 m	New York City	1894 - 1895
Milwaukee City Hall	108 m	Milwaukee	1895 - 1899
Park Row Building	119 m	New York City	1899 - 1901
Philadelphia City Hall	167 m	Philadelphia	1901 - 1908
Singer Building	187 m	New York City	1908 - 1909
Metropolitan Life Tower	213 m	New York City	1909 - 1913
Woolworth Building	241 m	New York City	1913 - 1929
40 Wall Street	283 m	New York City	1929 - 1930
Chrysler Building	319 m	New York City	1930 - 1931
Empire State Building	381 m	New York City	1931 - 1971
World Trade Center	417 m	New York City	1971 - 1973
Sears Tower	443 m	Chicago	1973 - 1998
Petronas Towers	452 m	Kuala Lumpur	1998 - 2004
Taipei 101	509 m	Taipei	2004 - 2010
Burj Khalifa	828 m	Dubai	2010 - present

Table 1.2 shows the 35 tallest buildings in the world. As can be seen, 23 of them are in the Eastern Asia (China, Taiwan, Malaysia, South Korea, and Vietnam); 6 are in the Middle East (United Arab Emirates, Saudi Arabia, and Kuwait); 5 in the United States of America (historically considered the home of the skyscraper) and only one in Europe, in Saint Petersburg. Noteworthy buildings are the Shanghai Tower (the tallest twisted building and the highest observation deck at 562 m), the Royal Clock Tower in Mecca (also known as Abraj Al-Bait Clock Tower), the tallest building with a clock face, and the Central Park Tower, currently under construction, once completed (estimated 2021), will become the tallest residential building in the world.

In Table 1.3, the 35 tallest buildings in Central and North America are shown. The first 9 places in the ranking are occupied by skyscrapers built in Chicago

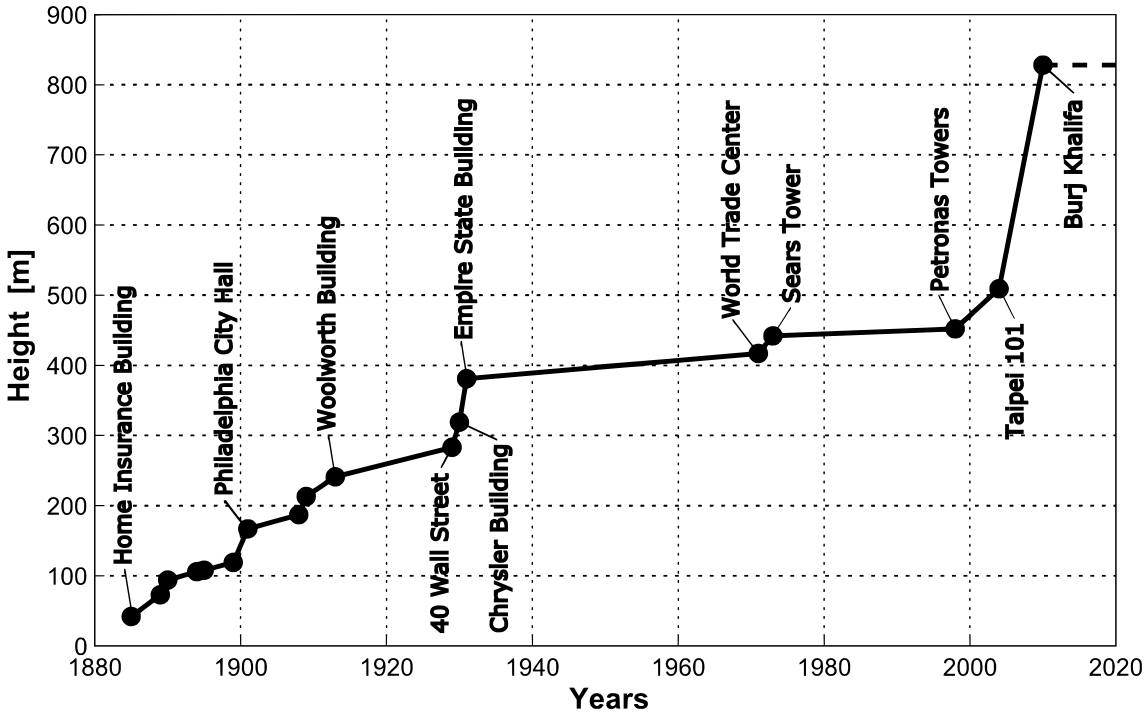

Figure 1.8: Timeline of record tallest buildings

and New York, while the tallest building outside the USA rises in Canada and is in the 26th place.

In Table 1.4, the 35 tallest buildings in South America are shown. The tallest building is the Gran Torre Santiago, 300 meters high, built in 2014 in Chile, while the oldest among these is the Altino Arantes Building, built in 1947 in São Paulo, Brazil.

In Table 1.5, the 35 tallest buildings in Asia are shown. Most of these buildings are located in China, and are of a very low age as the oldest building is Shun Hing Square, built in 1996 in Shenzhen, China.

In Table 1.6 the 35 tallest buildings in Africa are shown. The heights are modest in this continent, the record for height belongs to The Leonardo, 234 meters high, built in 2019 in Johannesburg, South Africa. The major part of the skyscrapers rise in the rich States of the continent, as South Africa and Egypt.

In Table 1.7, the 35 tallest buildings in Europe are shown. To date, the State with the tallest buildings is Russia, where 16 of the first 35 tallest buildings in Europe are located. These buildings have a very low average age with the exception of the tower of the Moscow State University, built in 1959 and one of the symbols of Soviet Power. Italy ranks 33rd with the Unicredit Tower in Milan.

In Table 1.8, the 35 tallest buildings in Oceania are shown. As it was easy to

foresee, all these buildings rise in the major coastal cities of Australia.

Finally in Table 1.9, the 35 tallest buildings in Italy are shown. In the Italian historical context [188], worthy of note are the Piacentini Tower (1940 – 108 m) in Genoa, which was the highest Italian and European reinforced concrete construction until 1952, the Pirelli Tower (1960 – 127 m) designed by Giò Ponti and Pier Luigi Nervi in Milan, which was the tallest tower in Italy until 1995, and the Telecom Tower in Naples (1995 – 129 m).

In recent years, only the cities of Milan and Turin have considered building skyscrapers in Italy (Figure 1.9). In particular, an urban plan involving the construction of skyscrapers in the City of Milan was prepared in order to redevelop and reuse the large building zones deriving from exhibition areas (CityLife Area) and brownfield sites (Portobello Area). As a result of this urban plan, the Unicredit Tower (231 m at its tip, and 218 m on the roof level) was completed in 2011. This tower is now the tallest building in Italy.

On the other hand, the City of Turin underwent rapid development due to urban restyling related to the XX Olympic Winter Games in 2006. In this period, the Intesa-Sanpaolo Tower, 167 meters high, was designed and subsequently completed in 2012. It was the newest tall building built in Turin since 1934 (Reale Mutua Tower, 109 m). Moreover, on November 30, 2011, the construction of the Piedmont Region Headquarters Tower, 209 meters high, began. It is now the tallest building in Turin and the third tallest building in Italy.

(a) (b) (c)

Figure 1.9: (a) Unicredit Tower; (b) CityLife Area (PWC Tower, Generali Tower, Allianz Tower); (c) Intesa-Sanpaolo Tower

Table 1.2: The 35 tallest buildings in the World

Name	**City**	**Country**	**Height**	**Year**
Burj Khalifa	Dubai	UAE	828 m	2010
Shanghai Tower	Shanghai	China	632 m	2016
Royal Clock Tower	Mecca	SA	601 m	2012
Goldin Finance 117	Tianjin	China	597 m	2018
Ping An Finance Center	Shenzhen	China	592 m	2017
Lotte World Tower	Seoul	S. Korea	555 m	2016
One World Trade Center	New York City	USA	541 m	2014
Guangzhou Finance Centre	Guangzhou	China	530 m	2016
Tianjin Finance Centre	Tianjin	China	530 m	2019
China Zun	Beijing	China	528 m	2018
Taipei 101	Taipei	Taiwan	509 m	2004
World Financial Center	Shanghai	China	492 m	2008
Int. Commerce Centre	Hong Kong	China	484 m	2010
Lakhta Center	S. Petersburg	Russia	462 m	2019
Landmark 81	Ho Chi Minh	Vietnam	461 m	2018
Petronas Tower 1	Kuala Lumpur	Malaysia	452 m	1998
Petronas Tower 2	Kuala Lumpur	Malaysia	452 m	1998
Changsha IFS Tower	Changsha	China	452 m	2017
Zifeng Tower	Nanjing	China	450 m	2010
The Exchange 106	Kuala Lumpur	Malaysia	445 m	2019
Sears Tower	Chicago	USA	443 m	1973
Kingkey 100	Shenzhen	China	442 m	2011
Int. Finance Center	Guangzhou	China	440 m	2010
Wuhan Center	Wuhan	China	438 m	2017
432 Park Avenue	New York City	USA	426 m	2015
Marina 101	Dubai	UAE	425 m	2017
Trump International Hotel	Chicago	USA	423 m	2009
Jin Mao Tower	Shanghai	China	421 m	1999
Int. Finance Center	Hong Kong	China	415 m	2003
Princess Tower	Dubai	UAE	414 m	2012
Al Hamra Firdous Tower	Kuwait City	Kuwait	413 m	2011
23 Marina	Dubai	UAE	395 m	2012
China Resources Head.	Shenzhen	China	392 m	2018
CITIC Plaza	Guangzhou	China	391 m	1997
30 Hudson Yards	New York City	USA	387 m	2019

Table 1.3: The 35 tallest buildings in Central and North America

Name	**City**	**Country**	**Height**	**Year**
One World Trade Center	New York City	USA	541 m	2014
Sears Tower	Chicago	USA	443 m	1973
432 Park Avenue	New York City	USA	426 m	2015
Trump International Hotel	Chicago	USA	423 m	2009
30 Hudson Yards	New York City	USA	387 m	2019
Empire State Building	New York City	USA	381 m	1931
Bank of America Tower	New York City	USA	366 m	2009
Aon Center	Chicago	USA	346 m	1973
John Hancock Center	Chicago	USA	344 m	1969
Comcast Technology Center	Philadelphia	USA	342 m	2018
Wilshire Grand Center	Los Angeles	USA	335 m	2017
3 World Trade Center	New York City	USA	329 m	2018
Salesforce Tower	San Francisco	USA	326 m	2018
53W53	New York City	USA	320 m	2018
Chrysler Building	New York City	USA	319 m	1930
The New York Times Building	New York City	USA	319 m	2007
Bank of America Plaza	Atlanta	USA	311 m	1992
U.S. Bank Tower	Los Angeles	USA	310 m	1989
35 Hudson Yards	New York City	USA	308 m	2019
Franklin Center	Chicago	USA	307 m	1989
One57	New York City	USA	306 m	2014
JPMorgan Chase Tower	Houston	USA	305 m	1982
Two Prudential Plaza	Chicago	USA	303 m	1990
One Manhattan West	New York City	USA	303 m	2019
Wells Fargo Plaza	Houston	USA	302 m	1983
First Canadian Place	Toronto	Canada	298 m	1975
4 World Trade Center	New York City	USA	298 m	2013
Comcast Center	Philadelphia	USA	297 m	2007
JW Marriott Panama	Panama City	Panama	293 m	2011
311 South Wacker Drive	Chicago	USA	293 m	1990
70 Pine Street	New York City	USA	290 m	1932
220 Central Park South	New York City	USA	290 m	2017
Key Tower	Cleveland	USA	289 m	1991
One Liberty Place	Philadelphia	USA	288 m	1987
Columbia Center	Seattle	USA	284 m	1985

Table 1.4: The 35 tallest buildings in South America

Name	**City**	**Country**	**Height**	**Year**
Gran Torre Santiago	Santiago	Chile	300 m	2014
Yachthouse Residence	Balneário Camboriú	Brazil	281 m	2020
Alvear Tower	Buenos Aires	Argentina	241 m	2018
Infinity Coast	Balneário Camboriú	Brazil	235 m	2019
Parque Central Complex	Caracas	Venezuela	225 m	1983
BD Bacatá	Bogotá	Colombia	216 m	2015
Epic Tower	Balneário Camboriú	Brazil	209 m	2020
Estelar Hotel	Cartagena de Indias	Colombia	202 m	2017
Torre Colpatria	Bogotá	Colombia	196 m	1978
Titanium La Portada	Santiago	Chile	194 m	2010
Centro de Comercio Int.	Bogotá	Colombia	192 m	1977
Orion Complex	Goiânia	Brazil	191 m	2018
Centro Financiero Conf.	Caracas	Venezuela	190 m	1994
Museo Parque Central	Bogotá	Colombia	185 m	2017
Krystal Tower	Bogotá	Colombia	184 m	2017
Cali Tower	Cali	Colombia	183 m	1984
Tour Geneve	João Pessoa	Brasil	183 m	2018
Mercantil Tower	Caracas	Venezuela	179 m	1984
Millennium Palace	Balneário Camboriú	Brazil	177 m	2014
Coltejer Building	Medellín	Colombia	175 m	1972
Torre Cavia	Buenos Aires	Argentina	172 m	2009
E Tower North Point	Bogotá	Colombia	172 m	2018
Ciudadela San Martín	Bogotá	Colombia	171 m	1983
Mirante do Vale	São Paulo	Brazil	170 m	1960
Grand Bay Club	Cartagena de Indias	Colombia	170 m	2009
Mirage 57	Barranquilla	Colombia	162 m	2016
Edifício Itália	São Paulo	Brazil	165 m	1965
Rio Sul Center	Rio de Janeiro	Brazil	164 m	1982
Majestic Building	Bucaramanga	Colombia	163 m	2015
Altino Arantes Building	São Paulo	Brazil	161 m	1947
Avianca Building	Bogotá	Colombia	161 m	1969
Mulieris towers	Buenos Aires	Argentina	161 m	2008
Torre del Café	Medellín	Colombia	160 m	1975
El Faro Towers	Buenos Aires	Argentina	160 m	2005
Palmetto	Cartagena de Indias	Colombia	160 m	2009

Table 1.5: The 35 tallest buildings in Asia

Name	**City**	**Country**	**Height**	**Year**
Burj Khalifa	Dubai	UAE	828 m	2010
Shanghai Tower	Shanghai	China	632 m	2016
Royal Clock Tower	Mecca	SA	601 m	2012
Goldin Finance 117	Tianjin	China	597 m	2018
Ping An Finance Center	Shenzhen	China	592 m	2017
Lotte World Tower	Seoul	S. Korea	555 m	2016
Guangzhou Finance Centre	Guangzhou	China	530 m	2016
Tianjin Finance Centre	Tianjin	China	530 m	2019
China Zun	Beijing	China	528 m	2018
Taipei 101	Taipei	Taiwan	509 m	2004
World Financial Center	Shanghai	China	492 m	2008
Int. Commerce Centre	Hong Kong	China	484 m	2010
Landmark 81	Ho Chi Minh	Vietnam	461 m	2018
Petronas Tower 1	Kuala Lumpur	Malaysia	452 m	1998
Petronas Tower 2	Kuala Lumpur	Malaysia	452 m	1998
Changsha IFS Tower	Changsha	China	452 m	2017
Zifeng Tower	Nanjing	China	450 m	2010
The Exchange 106	Kuala Lumpur	Malaysia	445 m	2019
Kingkey 100	Shenzhen	China	442 m	2011
Int. Finance Center	Guangzhou	China	440 m	2010
Wuhan Center	Wuhan	China	438 m	2017
Marina 101	Dubai	UAE	425 m	2017
Jin Mao Tower	Shanghai	China	421 m	1999
Int. Finance Center	Hong Kong	China	415 m	2003
Princess Tower	Dubai	UAE	414 m	2012
Al Hamra Firdous Tower	Kuwait City	Kuwait	413 m	2011
23 Marina	Dubai	UAE	395 m	2012
China Resources Head.	Shenzhen	China	392 m	2018
CITIC Plaza	Guangzhou	China	391 m	1997
Capital Market Auth.	Riyadh	SA	385 m	2014
Shun Hing Square	Shenzhen	China	384 m	1996
Dalian Eton Center	Dalian	China	384 m	2015
Forum 66 Tower 1	Shenyang	China	384 m	2015
Elite Residence	Dubai	UAE	381 m	2012
Burj Bin Rashid	Abu Dhabi	UAE	381 m	2014

Table 1.6: The 35 tallest buildings in Africa

Name	**City**	**Country**	**Height**	**Year**
The Leonardo	Johannesburg	South Africa	234 m	2019
Carlton Centre	Johannesburg	South Africa	223 m	1973
Britam Tower	Nairobi	Kenya	200 m	2017
Cairo Tower	Cairo	Egypt	187 m	1961
Ponte City Apart.	Johannesburg	South Africa	173 m	1975
UAP Tower	Nairobi	Kenya	163 m	2016
NECOM House	Lagos	Nigeria	160 m	1979
Tanzania Ports Auth.	Dar Es Salaam	Tanzania	157 m	2016
PSPF Towers	Dar Es Salaam	Tanzania	153 m	2014
Marble Towers	Johannesburg	South Africa	152 m	1973
Pearl Dawn	Durban	South Africa	152 m	2010
South African Bank	Pretoria	South Africa	150 m	1988
88 on Field	Durban	South Africa	147 m	1985
IMOB Tower	Luanda	Angola	145 m	2018
MNF Square I	Dar Es Salaam	Tanzania	145 m	2019
Burj Bulaya Office	Tripoli	Libya	144 m	2007
Min. of Foreign Aff.	Cairo	Egypt	143 m	1994
El Gezira Tower	Cairo	Egypt	142 m	1996
Grand Hyatt	Cairo	Egypt	142 m	2002
Nile City Tower	Cairo	Egypt	142 m	2003
KwaDukuza eGoli	Johannesburg	South Africa	140 m	1970
Trust Bank Build.	Johannesburg	South Africa	140 m	1970
ABSA Building	Johannesburg	South Africa	140 m	1970
El Maadi Tower	Cairo	Egypt	140 m	1987
Times Tower	Nairobi	Kenya	140 m	2000
Michelangelo Towers	Johannesburg	South Africa	140 m	2005
Standard Bank Build.	Johannesburg	South Africa	139 m	1968
Southern Life Centre	Johannesburg	South Africa	138 m	1973
Old Mutual Centre	Durban	South Africa	137 m	1995
Portside Tower	Cape Town	South Africa	136 m	2014
National Bank of Egypt	Cairo	Egypt	135 m	1986
Cairo Plaza Building	Cairo	Egypt	135 m	1986
S. Stefano Grand Plaza	Alexandria	Egypt	135 m	2006
Tour Mpila 1	Brazzaville	Rep. Congo	135 m	2019
Mzizima Tower	Dar Es Salaam	Tanzania	134 m	2018

Table 1.7: The 35 tallest buildings in Europe

Name	**City**	**Country**	**Height**	**Year**
Lakhta Center	S. Petersburg	Russia	462 m	2019
Feder. East Tower	Moscow	Russia	374 m	2016
OKO: South Tower	Moscow	Russia	354 m	2015
Neva Tower 2	Moscow	Russia	345 m	2019
Mercury Tower	Moscow	Russia	339 m	2013
The Shard	London	UK	310 m	2012
Eurasia	Moscow	Russia	309 m	2014
CoC: Moscow	Moscow	Russia	302 m	2010
Neva Tower 1	Moscow	Russia	302 m	2019
Skyland	Istanbul	Turkey	293 m	2017
Metropol	Istanbul	Turkey	280 m	2017
22 Bishopsgate	London	UK	278 m	2019
Baku Tower	Baku	Azerbaijan	276 m	2020
Naberezhnaya Tower C	Moscow	Russia	268 m	2007
Triumph Palace	Moscow	Russia	264 m	2005
Commerzbank Tower	Frankfurt	Germany	259 m	1997
CoC: S. Petersburg Tower	Moscow	Russia	257 m	2010
Messeturm	Frankfurt	Germany	256 m	1990
Nurol Life	Istanbul	Turkey	252 m	2017
Torre de Cristal	Madrid	Spain	249 m	2008
Torre Cepsa	Madrid	Spain	248 m	2008
Evolution Tower	Moscow	Russia	246 m	2014
OKO: North Tower	Moscow	Russia	245 m	2014
Federation: West Tower	Moscow	Russia	243 m	2007
Moscow State Univ.	Moscow	Russia	240 m	1953
Imperia Tower	Moscow	Russia	239 m	2011
Palace of Science	Warsaw	Poland	237 m	1955
Torre PwC	Madrid	Spain	236 m	2008
1 Canada Square	London	UK	235 m	1991
Istanbul Sapphire	Istanbul	Turkey	235 m	2010
Landmark Pinnacle	London	UK	233 m	2019
Tour First	Paris	France	231 m	2011
Unicredit Tower	Milan	Italy	231 m	2011
Heron Tower	London	UK	230 m	2011
Torre Espacio	Madrid	Spain	228 m	2008

Table 1.8: The 35 tallest buildings in Oceania

Name	**City**	**Country**	**Height**	**Year**
Q1 Tower	Surfers Paradise	Australia	323 m	2005
Australia 108	Melbourne	Australia	316 m	2020
Eureka Tower	Melbourne	Australia	297 m	2006
Aurora Central	Melbourne	Australia	271 m	2019
Brisbane Skytower	Brisbane	Australia	270 m	2019
120 Collins Street	Melbourne	Australia	265 m	1991
101 Collins Street	Melbourne	Australia	260 m	1991
1 William Street	Brisbane	Australia	260 m	2016
Prima Pearl	Melbourne	Australia	254 m	2014
Rialto Towers	Melbourne	Australia	251 m	1986
Central Park	Perth	Australia	249 m	1992
Infinity Tower	Brisbane	Australia	249 m	2013
Chifley Tower	Sydney	Australia	244 m	1992
City Square	Perth	Australia	244 m	2011
Citigroup Centre	Sydney	Australia	243 m	2000
Soleil	Brisbane	Australia	243 m	2011
Soul	Gold Coast	Australia	243 m	2012
Victoria One	Melbourne	Australia	241 m	2018
Deutsche Bank	Sydney	Australia	239 m	2005
Swanston Central	Melbourne	Australia	236 m	2019
World Tower	Sydney	Australia	230 m	2004
Vision Apartments	Melbourne	Australia	229 m	2016
MLC Centre	Sydney	Australia	228 m	1977
Governor Phillip	Sydney	Australia	227 m	1993
Bourke Place	Melbourne	Australia	224 m	1991
Ernst & Young Tower	Sydney	Australia	222 m	2004
Circle on Cavill	Gold Coast	Australia	220 m	2007
Aurora Place	Sydney	Australia	219 m	2001
Telstra Corporate	Melbourne	Australia	218 m	1992
International Tower	Sydney	Australia	217 m	2016
108 St Georges Terrace	Perth	Australia	214 m	1988
Melbourne Central	Melbourne	Australia	211 m	1991
Aurora Tower	Brisbane	Australia	207 m	2006
Freshwater Place	Melbourne	Australia	205 m	2005
Riparian Plaza	Brisbane	Australia	200 m	2005

Table 1.9: The 35 tallest buildings in Italy

Name	**City**	**Region**	**Height**	**Year**
Unicredit Tower	Milan	Lombardia	231 m	2011
Allianz Tower	Milan	Lombardia	209 m	2015
Piedmont Region Head.	Turin	Piemonte	209 m	2015
Generali Tower	Milan	Lombardia	191 m	2016
Intesa Sanpaolo Tower	Turin	Piemonte	167 m	2012
Lombardia Building	Milan	Lombardia	161 m	2010
Solaria Tower	Milan	Lombardia	143 m	2013
Diamante Tower	Milan	Lombardia	140 m	2012
Telecom Italia Tower	Naples	Campania	129 m	1995
Pontina Tower	Latina	Lazio	128 m	2010
Pirelli Tower	Milan	Lombardia	127 m	1960
Unipol Tower	Bologna	Emilia Romagna	127 m	2012
Enel Tower	Naples	Campania	122 m	1990
Eurosky Tower	Rome	Lazio	120 m	2012
Europarco Tower	Rome	Lazio	120 m	2012
Marinella Tower	Cesenatico	Emilia Romagna	118 m	1958
Saverio Tower	Naples	Campania	118 m	1990
Francesco Tower	Naples	Campania	118 m	1990
Breda Tower	Milan	Lombardia	116 m	1954
Regional Council Tower	Naples	Campania	115 m	1992
Bosco Verticale	Milan	Lombardia	111 m	2014
Crystal Palace	Brescia	Lombardia	110 m	1990
Court of Justice	Naples	Campania	110 m	1991
Reale Mutua Tower	Turin	Piemonte	109 m	1934
Il Matitone	Genoa	Liguria	109 m	1992
Piacentini Tower	Genoa	Liguria	108 m	1940
Velasca Tower	Milan	Lombardia	106 m	1958
San Vincenzo Tower	Genoa	Liguria	105 m	1968
Galfa Tower	Milan	Lombardia	103 m	1959
World Trade Center	Genoa	Liguria	102 m	1992
Ambassador's Hotel	Naples	Campania	100 m	1957
Rimini Skyscraper	Rimini	Emilia Romagna	100 m	1960
Garibaldi Tower A	Milan	Lombardia	100 m	1994
Unicredit Tower B	Milan	Lombardia	100 m	2011
Compartimento 2 Tower	Genoa	Liguria	100 m	2014
Aria Tower	Milan	Lombardia	100 m	2014

1.2 Lateral load resisting systems for high-rise buildings

The design of tall buildings represents a challenging problem from an architectural point of view, especially considering structural analysis. The main difficulties are represented by the limitation of transversal displacements due to wind or seismic lateral load [17], [44], [119], [134]. The demanding design formulation is due to the choice of a static scheme because of the great height. In response to this problem, some authors [228], [242], and [243], suggested identifying the appropriate structural system according to the number of storeys.

1.2.1 Rigid nodes frame buildings

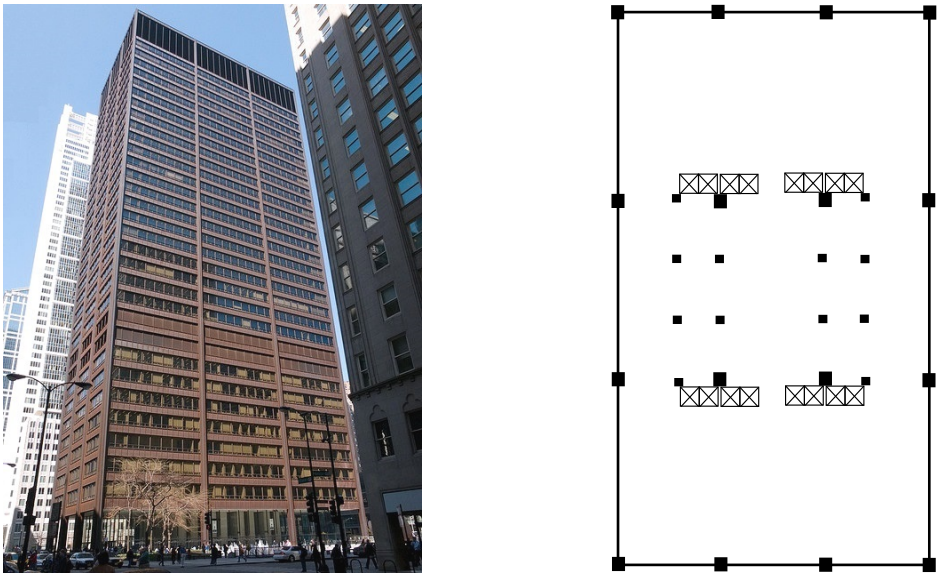

(a) (b)

Figure 1.10: Daley Center. (a) Exterior view; (b) Typical floor plan (web source)

The structures of this type are built from beams and columns connected by rigid nodes, following the deformation induced by external forces, they keep the angles between the elements they connect unchanged. The dimensions of the columns are mainly determined according to the vertical forces while the dimensions of the beams are fixed so that the frame has a limited deformability with respect to the horizontal displacements. In particular, the horizontal stiffness is proportional to the dimensions of the cross sections of the columns and beams, and is inversely proportional to the distance between the columns. To obtain a rigid frame, therefore, low distance between columns and high beams are used. An example of a rigid

frame structure is the Daley Center in Chicago (Figure 1.10). The main advantage of this structural scheme lies in the fact that the structure leaves large rectangular meshes free in the façade (Figure 1.10a) within which the necessary openings (doors and windows) can be placed, also allowing great flexibility in floor plan (Figure 1.10b). If the rigid frame is the only structural element to which the absorption of horizontal forces is given, its use is efficient for buildings up to 25-30 floors. For a greater number of storeys, the height of the beams necessary to ensure sufficient rigidity becomes uneconomical. In general, this structural scheme is suitable for reinforced concrete structures due to the intrinsic stiffness of the nodes.

The disadvantages are due to the size of the beams and columns, especially in the lower floors of the construction.

1.2.2 Braced frame buildings

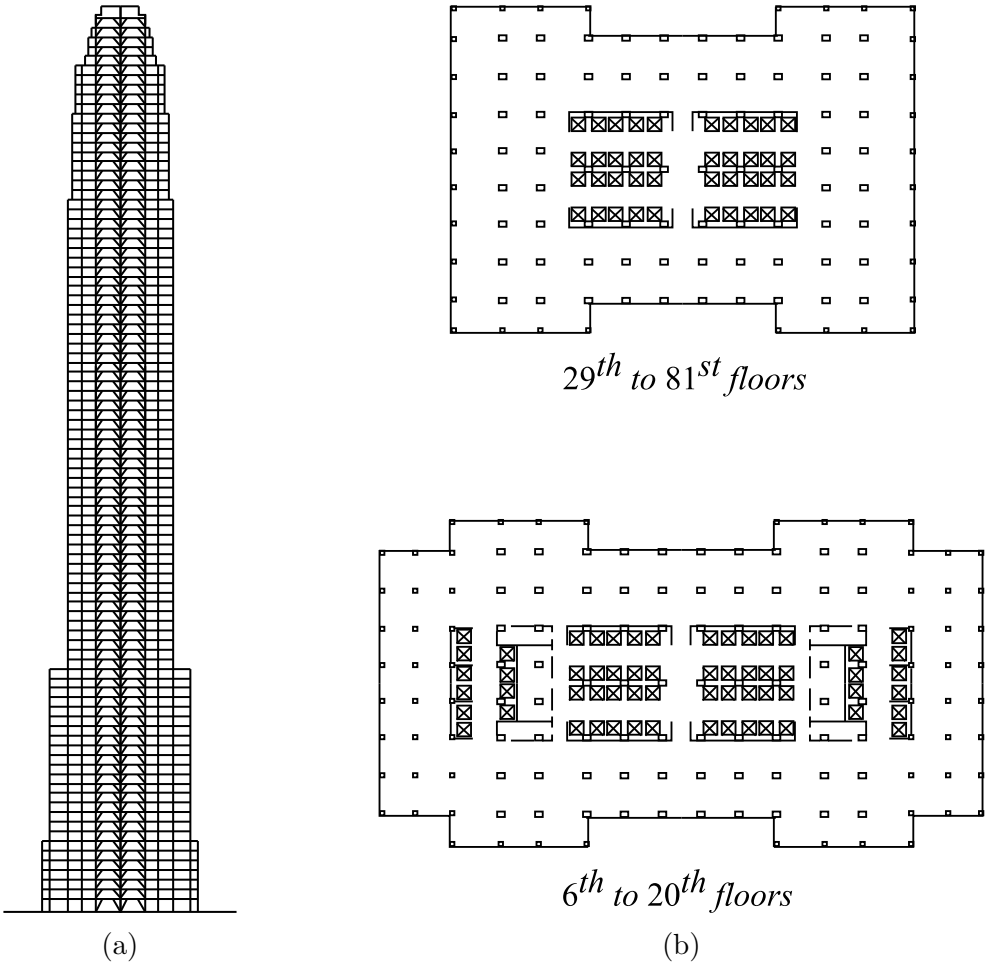

Figure 1.11: Empire State Building. (a) Vertical section; (b) Floor plans

The structural scheme of braced frame is mainly used in steel structures as the goal is to improve the efficiency of rigid node frames. In general, the buildings designed following this model are made of steel. The main advantage of this structural solution lies in the truss scheme which makes the structure very efficient.

Another advantage consists in the fact that the horizontal beams participate to a minimal extent in the absorption of the horizontal forces and are therefore dimensioned on the basis of the vertical forces transmitted by the floors only, and consequently they will have the same dimensions for all floors of the building, which results into a reduction in construction costs. A disadvantage of this type of structures consists in the fact that the presence of diagonal currents constitutes a strong constraint for the location of the openings. For this reason, the braces are often placed inside the building in correspondence with the stairwells and the lift. An example of tall buildings built with this technique is the Empire State Building (Figure 1.11), where the construction scheme adopted was not particularly innovative, but proved extremely functional: the construction times were so short as to become one of the most difficult records to pass [270].

1.2.3 Shear walls buildings

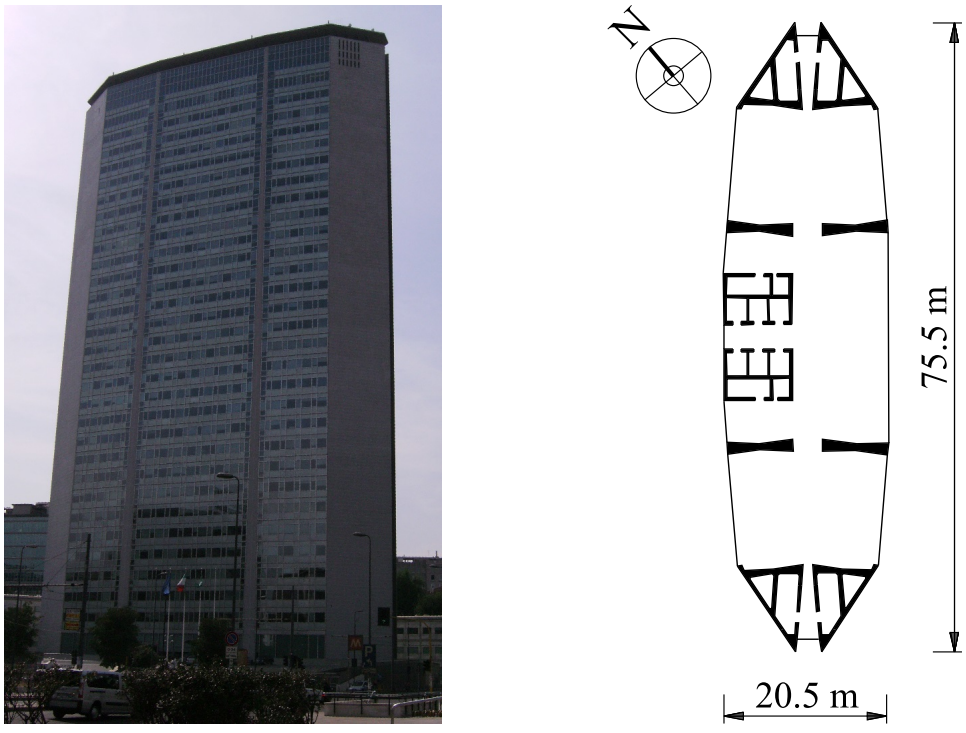

(a) (b)

Figure 1.12: Pirelli Tower. (a) South-east view; (b) Typical floor plan

In these structures, resistance to horizontal actions is entirely given to shear walls in concrete, which work mainly as cantilever beams. For buildings with up to 35 floors they are efficient both in terms of resistance to horizontal and vertical actions and in general their placement in the plant is carried out in such a way that they can carry a proportion of the vertical loads such as to cancel the traction stresses induced on them from the bending moment. This reduces the amount of steel rebars. An example of a structure with shear walls is the Pirelli Tower in Milan (Figure 1.12).

1.2.4 Shear wall-frame interacting systems

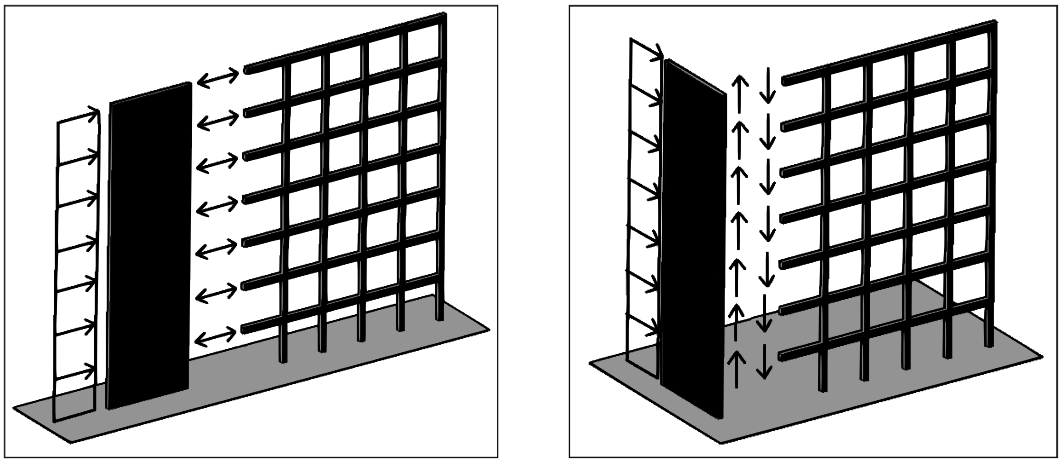

(a) (b)

Figure 1.13: Relative position between the shear walls and the frames. (a) Placed in series; (b) Orthogonal to each other

Rigid frames become inefficient above 30 floors as they require excessive dimensions of the structural elements. Buildings with only shear walls made of reinforced concrete or by means of truss elements, are efficient for buildings between 10 and 35 floors high. However, by combining and connecting the shear walls with the rigid frames with each other, a resistant mechanism is developed that allows reaching heights between 40 and 70 floors in an efficient way. In fact, the two types of structural elements have a different behavior towards horizontal actions and in particular, while the shear walls behave like cantilevers, that is, with minimal displacements in the lower floors and elevated at the top, the frames are deformed presenting high displacements at the base and modest at the top. If the two types of structure are rigidly connected, and therefore constrained to undergo the same displacements, the result is a less deformable structure along the entire height of the building.

Depending on the relative position between the shear walls and the frames, two limit cases can be distinguished whose structural behavior is clearly different that is:

- frames and shear walls placed in series (Figure 1.13a): in this case the exchanged actions are axial forces which have repercussions in the non-linearity of the shear forces;
- frames and shear walls orthogonal to each other (Figure 1.13b): in this case the exchanged actions are shear forces that affect the non-linearity of the axial forces in the columns of the frame.

1.2.5 Framed tube buildings

The philosophy behind this type of building is to bring most of the structural elements to which the resistance to horizontal actions is given towards the perimeter of the structure. This solution increases the inertia of the building's cross section and therefore its stiffness. In these buildings the structure is built from rigid frames that in the plant form a closed polygonal. In this way, the cross section of the building functions as a hollow profile to which resistance to horizontal actions is given. To ensure that each frame in its plane can be assimilated to a rigid panel, beams are made with high rigidity obtained by placing the columns at close range.

Figure 1.14: New York World Trade Center in 1965 (web source)

Furthermore, the uniformity of this system allows the use of prefabrication techniques which considerably reduce construction times and costs. An increase in stiffness in the buildings with a tubular casing can be obtained by coupling an internal core to the external tube, generally used to accommodate the lifts and systems, which collaborates in absorbing horizontal actions. This type of structure is called *tube-in-tube building*. This technique was adopted in the design of the two main towers of the World Trade Center (Figure 1.14) in which along the perimeter, it was composed of rigid frames formed by 59 steel columns with a square section of about 0.36 meters on each side placed at a center distance of about 1 meter. To obtain frames of high stiffness, the connection beams between the columns had a height of about 1.3 meters.

For very tall buildings the single-tube structure becomes inefficient due to excessive normal stress on the columns. These stresses can be significantly reduced by using internal frames which constitute additional cores which stiffen the tubular casing. This technique allows the building to be tapered in height by imposing different heights for the individual pipes that make it up. The torsion resulting from the consequent section asymmetry is easily absorbed thanks to the tubular shape of the section. A significant example of this structural scheme is the Sears Tower (Figure 1.15) designed by Khan.

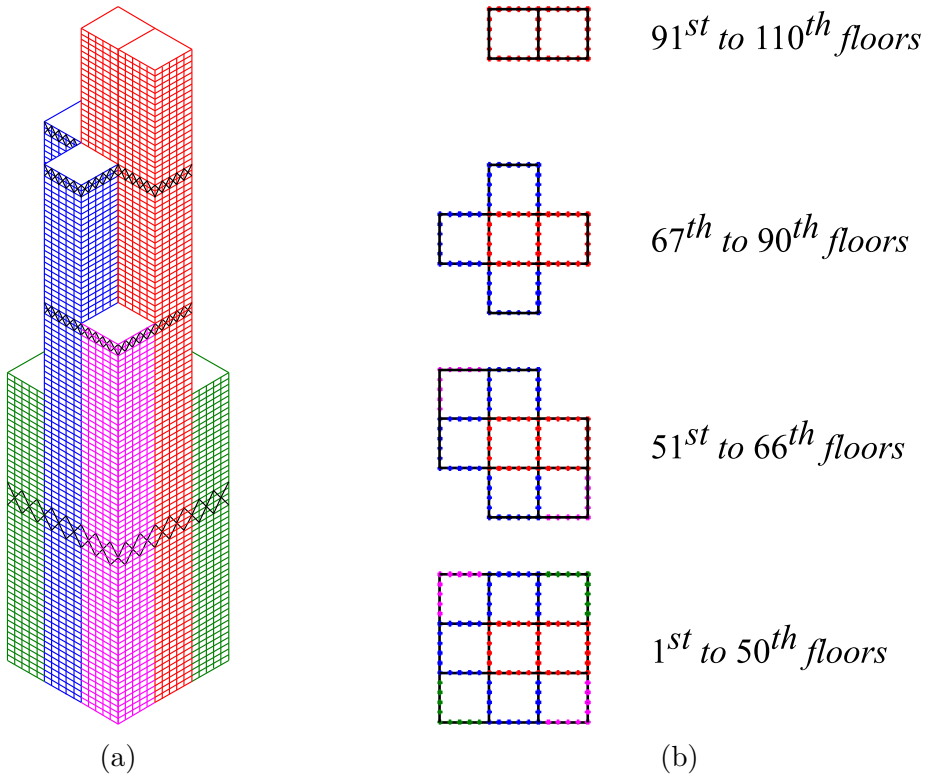

Figure 1.15: Sears Tower. (a) 3D-model; (b) Floor plans

1.2.6 Diagrid buildings

The structural conception of these structures derives from the framed tube systems but, differently from these, do not have the presence of orthogonal elements.

The vertical actions, as well as the horizontal ones, are absorbed by a grid of diagonal elements (diagonal grid, hence the name) placed along the perimeter of the building. Compared to tubular systems, the advantage of diagrid structures consists in the fact that the presence of the diagonal elements also increases the shear stiffness in addition to the purely flexural one. One of the first examples of this type of structure is the United Steelworkers Building built in Pittsburgh in 1963 with a height of only 13 floors. Only recently has the diagrid structure been used for tall buildings such as in the 30 St. Mary Axe Building (Figure 1.16a) in London, also know as Swiss Re Building, in the Hearst Headquarters designed in New York by Norman Foster or in the Capital Gate (Figure 1.16b) in Abu Dhabi.

In most of these structures the diagrid scheme was made using steel structural elements, but it is also possible to use reinforced concrete as was done in the COR building in Miami designed by Oppenheim Architecture or in the O-14 Building (Figure 1.16c) in Dubai, designed by RUR Architecture. The openings, apparently placed randomly, actually follow a precise pattern that traces the diagonal trend of the reinforced concrete elements to which the absorption of both horizontal and vertical forces is given.

(a) (b) (c)

Figure 1.16: (a) 30 St. Mary Axe Building; (b) Capital Gate; (c) O-14 Building (web source)

Chapter 2

Stiffness matrix for the most common types of vertical bracings

In this chapter the calculation methodology will be shown to roughly determine the stiffness matrix of the types of vertical resistant elements that are commonly used in tall buildings. The importance of defining the stiffness matrix consists in the possibility of releasing the calculation from the type of load acting on the structure, or rather, it is possible to solve the problem also with distributed forces that vary linearly, or that contain exponential or logarithmic functions within them (as in the case of actions due to wind or earthquake).

Furthermore, it is possible to evaluate the effects deriving from the simultaneous presence of several types of load such as, for example, the concomitant presence of distributed and concentrated actions or of the same entity but applied at different points of the building. Another great advantage of having defined the stiffness matrix of the structure consists in the possibility of coupling several resistant systems, such as, for example, the insertion of closed- or open-section shear walls, all simply by manipulating and condensing the stiffness matrices of the individual elements as will be shown in Chapter 3.

2.1 Shear walls

In the scientific literature there are many calculation procedures developed to analyze the shear walls with the help of stiffness matrices, some of these introduced mainly for the study of aeronautical constructions [154]. These methods are described in numerous scientific texts, among the works written in Italian we can mention, among others, the works of Belluzzi [23], Giangreco [112], Franciosi [103], Baldacci [19], and Pozzati [204], while in the international context this topic has been widely studied by Timoshenko [251], Gallangher [106], and Stafford Smith [228]. In this section, a simple analytical procedure [204] is briefly recalled, which

has been extended in order to be able to determine the three-dimensional stiffness matrix of a shear wall.

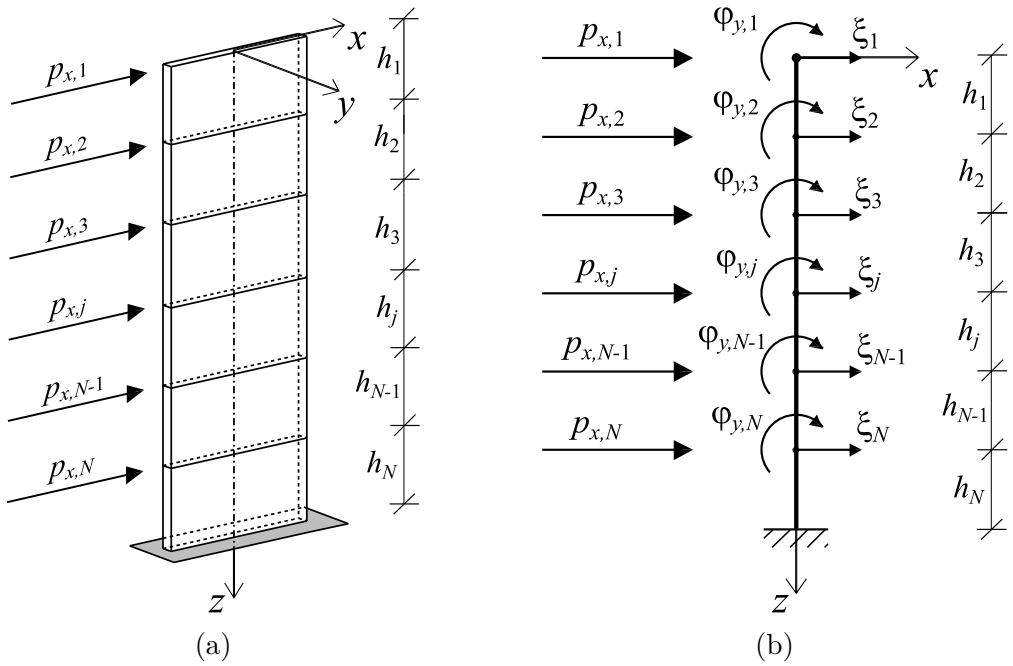

Figure 2.1: (a) 3D-model of a plane shear wall; (b) Projection of the shear wall on the plane xz

Consider the shear wall composed by N floors, each of h_j height, consisting of a continuous, isotropic, linear, and elastic material, characterized by Young's modulus E and shear elastic modulus G (Figure 2.1a). The section, which is maintained unchanged for the entire height of the bracing, is defined through the moments of inertia J_x and J_y referred to the axes of the right-handed local coordinate system with origin in the shear center of the element.

In the local reference coordinate system, the $3N$-vector $\{F^*\}$

$$\{F^*\} = \left\{ \begin{array}{c} \{p_x\} \\ \{p_y\} \\ \{m_z\} \end{array} \right\} \tag{2.1}$$

in which $2N$ shearing forces $\{p_x\}$, $\{p_y\}$, and N torsional moments $\{m_z\}$ are included, is connected to the $3N$ displacement vector $\{\delta^*\}$

$$\{\delta^*\} = \left\{ \begin{array}{c} \{\xi\} \\ \{\eta\} \\ \{\vartheta\} \end{array} \right\} \tag{2.2}$$

constituted by $2N$ translations $\{\xi\}$, $\{\eta\}$, and N rigid rotations about the z axis $\{\vartheta\}$, by the $3N \times 3N$ stiffness matrix of the entire shear wall $[K^*]$

$$[K^*] = \begin{bmatrix} [K_x] & 0 & 0 \\ 0 & [K_y] & 0 \\ 0 & 0 & [K_\vartheta] \end{bmatrix} \tag{2.3}$$

where each term is a $N \times N$ sub-matrix.

Under these hypotheses, the three-dimensional problem

$$\begin{Bmatrix} \{p_x\} \\ \{p_y\} \\ \{m_z\} \end{Bmatrix} = \begin{bmatrix} [K_x] & 0 & 0 \\ 0 & [K_y] & 0 \\ 0 & 0 & [K_\vartheta] \end{bmatrix} \begin{Bmatrix} \{\xi\} \\ \{\eta\} \\ \{\vartheta\} \end{Bmatrix} \tag{2.4}$$

or in compact form,

$$\{F^*\} = [K^*]\,\{\delta^*\} \tag{2.5}$$

can be analyzed considering independent stiffness terms $[K_x]$ and $[K_y]$, for x and y axes, respectively, and the torsional term $[K_\vartheta]$.

Numbering the floors from 1 to N, as shown in Figure (2.1b), the term $[K_x]$ can be determined by considering the projection of the shear wall on the xz plane.

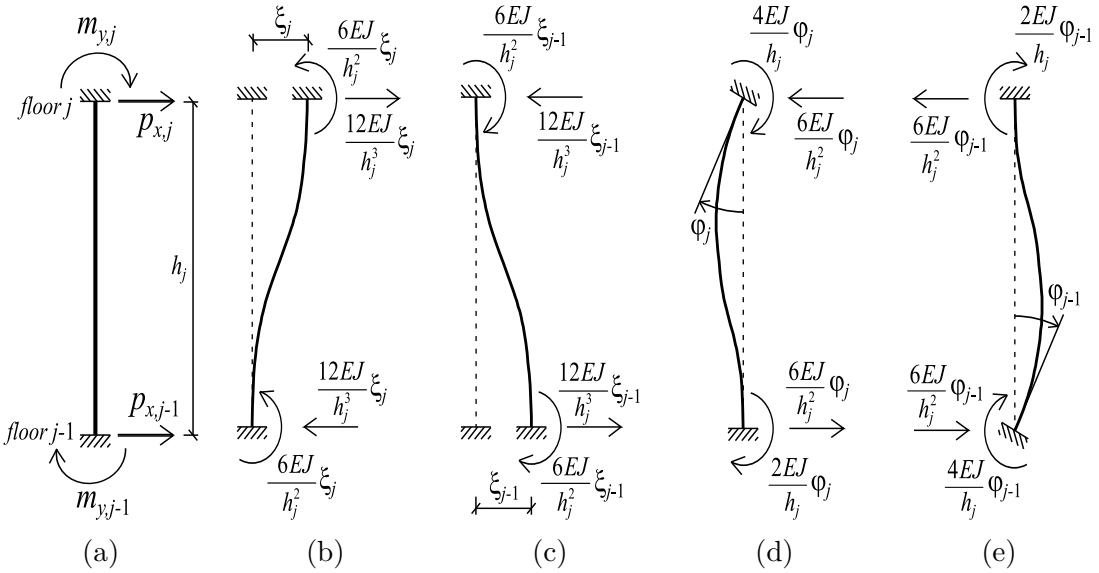

Figure 2.2: Static beam diagrams. (a) Nodal forces; (b) Imposed deformation ξ_j; (c) Imposed deformation ξ_{j-1}; (d) Imposed rotation φ_j; (e) Imposed rotation φ_{j-1}

In this model, extrapolates the generic portion of the shear wall between floors j and $j-1$ (length h_j), imposing the nodal displacements ξ and bending rotations φ_y with respect to y axis, referring to the static beam diagrams in Figure (2.2), for each floor it is possible to write the following relationship:

$$\begin{Bmatrix} p_{x,j} \\ p_{x,j-1} \\ m_{y,j} \\ m_{y,j-1} \end{Bmatrix} = EJ_y \begin{bmatrix} 12/h_j^3 & -12/h_j^3 & -6/h_j^2 & -6/h_j^2 \\ -12/h_j^3 & 12/h_j^3 & 6/h_j^2 & 6/h_j^2 \\ -6/h_j^2 & 6/h_j^2 & 4/h_j & 2/h_j \\ -6/h_j^2 & 6/h_j^2 & 2/h_j & 4/h_j \end{bmatrix} \begin{Bmatrix} \xi_j \\ \xi_{j-1} \\ \varphi_j \\ \varphi_{j-1} \end{Bmatrix} \tag{2.6}$$

where its 4×4 stiffness matrix $[k_{xx,j}]$ can be written as:

$$[k_{xx,j}] = EJ_y \begin{bmatrix} 12/h_j^3 & -12/h_j^3 & -6/h_j^2 & -6/h_j^2 \\ -12/h_j^3 & 12/h_j^3 & 6/h_j^2 & 6/h_j^2 \\ -6/h_j^2 & 6/h_j^2 & 4/h_j & 2/h_j \\ -6/h_j^2 & 6/h_j^2 & 2/h_j & 4/h_j \end{bmatrix} \tag{2.7}$$

Considering all floors, the stiffness matrix of the entire shearwall can be obtained by assembling the stiffness matrices related to j-th floors (Equation 2.7) to obtain a $2N \times 2N$ stiffness matrix:

$$\begin{Bmatrix} p_x,1 \\ p_x,2 \\ \vdots \\ p_x,N \\ m_y,1 \\ m_y,2 \\ \vdots \\ m_y,N \end{Bmatrix} = \begin{bmatrix} [k_{xx}] & \left[k_{x\varphi_y}\right] \\ \left[k_{\varphi_y x}\right] & \left[k_{\varphi_y \varphi_y}\right] \end{bmatrix} \begin{Bmatrix} \xi_1 \\ \xi_2 \\ \vdots \\ \xi_N \\ \varphi_{y,1} \\ \varphi_{y,2} \\ \vdots \\ \varphi_{y,N} \end{Bmatrix} \tag{2.8}$$

As shown in Figure (2.1b), by considering the projection of the shear wall on the xz plane, the degrees of freedom are two for each floor, that is the translation in x-direction (ξ) and rotation around y axis (φ_y), while the forces acting on the system are only the horizontal ones $\{p_x\}$, whereas the bending moment $\{m_y\}$ are null. Therefore, the force-displacement relationship can be written as:

$$\begin{Bmatrix} \{p_x\} \\ \{0\} \end{Bmatrix} = \begin{bmatrix} [k_{xx}] & \left[k_{x\varphi_y}\right] \\ \left[k_{\varphi_y x}\right] & \left[k_{\varphi_y \varphi_y}\right] \end{bmatrix} \begin{Bmatrix} \{\xi\} \\ \{\varphi_y\} \end{Bmatrix} \tag{2.9}$$

where, considering that the j-th portions of bracing between two consecutive floors are connected in series, each sub-matrices of size $N \times N$ take a recursive form and can generally be written as:

$$[k_{xx}] = 12EJ_y \begin{bmatrix} 1/h_1^3 & -1/h_1^3 & 0 & \cdots & 0 \\ -1/h_1^3 & 1/h_1^3 + 1/h_j^3 & -1/h_j^3 & \cdots & 0 \\ 0 & -1/h_j^3 & 1/h_j^3 + 1/h_{j+1}^3 & \cdots & 0 \\ \vdots & \vdots & \vdots & \ddots & \vdots \\ 0 & 0 & 0 & \cdots & 1/h_N^3 \end{bmatrix} \tag{2.10a}$$

$$\left[k_{x\varphi_y}\right] = 6EJ_y \begin{bmatrix} -1/h_1^2 & -1/h_1^2 & 0 & \cdots & 0 \\ 1/h_1^2 & 1/h_1^2 - 1/h_j^2 & -1/h_j^2 & \cdots & 0 \\ 0 & 1/h_j^2 & 1/h_j^2 - 1/h_{j+1}^2 & \cdots & 0 \\ \vdots & \vdots & \vdots & \ddots & \vdots \\ 0 & 0 & 0 & \cdots & 1/h_N^2 \end{bmatrix} \tag{2.10b}$$

$$\left[k_{\varphi_y x}\right] = 6EJ_y \begin{bmatrix} -1/h_1^2 & 1/h_1^2 & 0 & \cdots & 0 \\ -1/h_1^2 & 1/h_1^2 - 1/h_j^2 & 1/h_j^2 & \cdots & 0 \\ 0 & -1/h_j^2 & 1/h_j^2 - 1/h_{j+1}^2 & \cdots & 0 \\ \vdots & \vdots & \vdots & \ddots & \vdots \\ 0 & 0 & 0 & \cdots & 1/h_N^2 \end{bmatrix} \tag{2.10c}$$

$$\left[k_{\varphi_y \varphi_y}\right] = EJ_y \begin{bmatrix} 4/h_1 & 2/h_1 & 0 & \cdots & 0 \\ 2/h_1 & 4/h_1 + 4/h_j & 2/h_j & \cdots & 0 \\ 0 & 2/h_j & 4/h_j + 4/h_{j+1} & \cdots & 0 \\ \vdots & \vdots & \vdots & \ddots & \vdots \\ 0 & 0 & 0 & \cdots & 4/h_N \end{bmatrix} \tag{2.10d}$$

Equation (2.9) can be rewritten as follows:

$$[k_{xx}]\{\xi\} + \left[k_{x\varphi_y}\right]\{\varphi_y\} = \{p_x\} \tag{2.11a}$$

$$\left[k_{\varphi_y x}\right]\{\xi\} + \left[k_{\varphi_y \varphi_y}\right]\{\varphi_y\} = \{0\} \tag{2.11b}$$

From Equation (2.11b) it is easy to determine the displacements $\{\varphi_y\}$, so Equation (2.11a) can be written as follows:

$$\left[[k_{xx}] - \left[k_{x\varphi_y}\right]\left(\left[k_{\varphi_y\varphi_y}\right]^{-1}\left[k_{\varphi_y x}\right]\right)\right]\{\xi\} = \{p_x\} \tag{2.12}$$

The $N \times N$ condensed stiffness matrix in the x-direction was determined:

$$[K_x] = \left[[k_{xx}] - \left[k_{x\varphi_y}\right]\left(\left[k_{\varphi_y\varphi_y}\right]^{-1}\left[k_{\varphi_y x}\right]\right)\right] \tag{2.13}$$

Similar considerations can be made making an allowance for the projection of the wind on the yz plane obtaining the following local stiffness matrix:

$$[K_y] = \left[[k_{yy}] - [k_{y\varphi_x}]\left([k_{\varphi_x\varphi_x}]^{-1}[k_{\varphi_x y}]\right)\right] \tag{2.14}$$

where the sub-matrices are defined as follows:

$$[k_{yy}] = 12EJ_x \begin{bmatrix} 1/h_1^3 & -1/h_1^3 & 0 & \cdots & 0 \\ -1/h_1^3 & 1/h_1^3 + 1/h_j^3 & -1/h_j^3 & \cdots & 0 \\ 0 & -1/h_j^3 & 1/h_j^3 + 1/h_{j+1}^3 & \cdots & 0 \\ \vdots & \vdots & \vdots & \ddots & \vdots \\ 0 & 0 & 0 & \cdots & 1/h_N^3 \end{bmatrix} \tag{2.15a}$$

$$[k_{y\varphi_x}] = 6EJ_x \begin{bmatrix} -1/h_1^2 & -1/h_1^2 & 0 & \cdots & 0 \\ 1/h_1^2 & 1/h_1^2 - 1/h_j^2 & -1/h_j^2 & \cdots & 0 \\ 0 & 1/h_j^2 & 1/h_j^2 - 1/h_{j+1}^2 & \cdots & 0 \\ \vdots & \vdots & \vdots & \ddots & \vdots \\ 0 & 0 & 0 & \cdots & 1/h_N^2 \end{bmatrix} \tag{2.15b}$$

$$[k_{\varphi_x y}] = 6EJ_x \begin{bmatrix} -1/h_1^2 & 1/h_1^2 & 0 & \cdots & 0 \\ -1/h_1^2 & 1/h_1^2 - 1/h_j^2 & 1/h_j^2 & \cdots & 0 \\ 0 & -1/h_j^2 & 1/h_j^2 - 1/h_{j+1}^2 & \cdots & 0 \\ \vdots & \vdots & \vdots & \ddots & \vdots \\ 0 & 0 & 0 & \cdots & 1/h_N^2 \end{bmatrix} \tag{2.15c}$$

$$[k_{\varphi_x \varphi_x}] = EJ_x \begin{bmatrix} 4/h_1 & 2/h_1 & 0 & \cdots & 0 \\ 2/h_1 & 4/h_1 + 4/h_j & 2/h_j & \cdots & 0 \\ 0 & 2/h_j & 4/h_j + 4/h_{j+1} & \cdots & 0 \\ \vdots & \vdots & \vdots & \ddots & \vdots \\ 0 & 0 & 0 & \cdots & 4/h_N \end{bmatrix} \tag{2.15d}$$

As regards to the torsional stiffness matrix $[K_\vartheta]$, which connects the torque moments to the floor rotations, it can be easily obtained by assembling the terms related to the j-th portions of shear wall:

$$[K_\vartheta] = GJ_t \begin{bmatrix} 1/h_1 & -1/h_1 & 0 & \cdots & 0 \\ -1/h_1 & 1/h_1 + 1/h_j & -1/h_j & \cdots & 0 \\ 0 & -1/h_j & 1/h_j + 1/h_{j+1} & \cdots & 0 \\ \vdots & \vdots & \vdots & \ddots & \vdots \\ 0 & 0 & 0 & \cdots & 1/h_N \end{bmatrix} \tag{2.16}$$

where the term J_t indicates the torsional shear factor of the shear wall cross section.

2.1.1 Pierced shear walls

In the constructive planning, many times it is necessary to create small openings inside the shear walls, for example to allow access to stairs or elevator doors, as shown in Figure (2.3).

The presence of these openings obviously causes a stiffness reduction, and consequently, an increase of the displacements. The first analytical studies of this type of structure were made by Rosman [221], [222] in the 1960s which proposed a procedure, called *Continuum Medium Technique*. This procedure consists in modeling the portion of structure affected by the openings as a distribution of shearing forces applied to the remaining parts of the shear wall. This technique, relatively simple, was later deepened and improved by other authors, among whom we remember Schwaighofer [225], [226], Coull et al. [78], [80], [82], [85], [86], and Capuani et al. who addressed the problem both statically [49], [51], and dynamically [50].

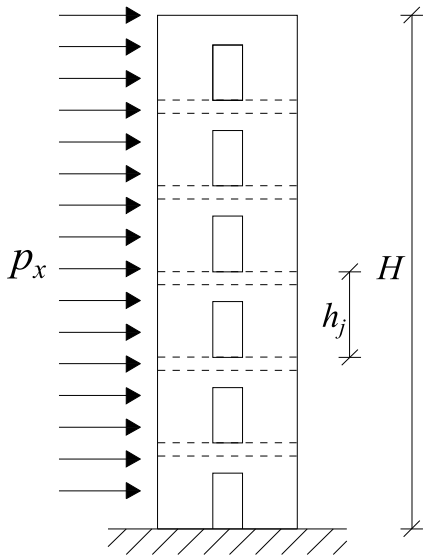

Figure 2.3: Pierced shear walls

A three-dimensional analytical approach described by simple differential equations which also define the torsional effects, was obtained in 1969 by Michael [179].

Extensions of this method, able to analyze also asymmetric structures, were presented by Glück [113] and Heidebrecht [124]. The latter fomulation is based on the stiffness matrix approach. In the procedures mentioned above there are no possibility of considering axial deformations, which is instead done by Tso [256], [257].

In 1975, Liauw and Leung [163] propose the transfer matrix method that allows analyzing structures that have different heights and non-constant shear walls

thicknesses, while Rutenberg and Heidebrecht [223] proposed a procedure for approximate analysis of asymmetric wall-frame structures.

Only many years later Wdowicki and Wdowicka [267], [268] proposed a further refinement of this formulation for evaluation of the stress state in non-planar asymmetric shear wall structures having stepwise changes in cross section.

For an analytical description of the main calculation methods, reference can be made to Stafford Smith's [228] and Taranath's [242], [243] books, in addition to Dr. Cammarano's Ph.D Thesis [47].

2.1.2 Twisted and tapered shear walls

Figure 2.4: HSB Turning Torso (web source)

Since the beginning, the design of high-rise buildings has been guided by the engineering issues [230] and the minimum performance requirements necessary by technical regulations [132], [232], [233] For this reason, tall buildings often have the shape of huge parallelepipeds embedded in the ground, however, most show graded tapering as in the case of the Empire State Building in New York or the Sears Tower in Chicago. In recent decades, this trend has been questioned in how much buildings have been designed by unusual architectural forms. Many times the tapered shape is

due only to the external covering while the core is of traditional type, as in the case of Shanghai Tower; in other cases it is a consequence of structural optimisation [274], while in other cases it is the supporting structure itself to be part of the architectural form, as illustrated by Sarkisian in his book [224]. They are part of this last category the diagrid structures that have represented the turning point regarding the architectural design of the high buildings, such as the Capital Gate in Abu Dhabi or the Tornado Tower in Doha. Another interesting typology are twisted, tapered, and tilted high-rise buildings. In many of these buildings, the core changes its plant continuously starting from the base to the top, as in the case of HSB Turning Torso of Malmo in Sweden (Figure 2.4), a twisted high-rise building of 54 floors and 190 meters high. In many cases, the particular architectural form of this type of building involves the creation of specific mathematical models to correctly describe the action of wind [142], [240], while in other cases, to estimate the pressure coefficients shall be carried out experimentally [143], [175].

The analytical method presented in the previous section can also be applied to the case of tapered and twisted shear walls. In these cases the geometric characteristics of the shear wall are discredited considering them constant between one floor and the other. For details of this analytical procedure, you can see the works of Carpinteri [60], Lacidogna [151], and Cammarano [47], while other formulations to analyze the same problem were proposed, among others, by Rajasekaran [211], Eisenberger [98], and Zupan [286].

2.2 Thin-walled open-section shear walls

Most of the resistant solutions employed in tall buildings are represented by vertical elements arranged as parallel cantilevers clamped at the base and designed to absorb the total horizontal force coming from earthquakes and winds. These members, commonly known as shear walls, can be freely located in the floor plan of the building and used with or without other vertical bracings to obtain an adequate stability. In the case of not excessive heights, they can be constituted by a simple plane element whose resistance is proportional to the maximum size of the section.

For greater heights, they are designed to behave as three-dimensional elements, having an appropriate bending resistance in the two principal directions, as well as a good torsional stiffness, giving rise to thin-walled hollow or open-section walls.

Beyond the mechanical function, these members allow to house stairwells and/or lift shafts, which are indispensable in a tall building.

Unlike hollow sections, in presence of torsional actions, thin-walled open-section elements reveal a particular behaviour, which is far from Saint Venant's results.

Once the torsional deformation takes place, the section twists around its shear centre but, at the same time, does not remain plane, since it undergoes different longitudinal extensions causing an out-of-plane distortion, the so-called *warping of*

the section [48], [59], [93], [178], [215]. As a consequence, a further longitudinal stress, absent in the theory of primary torsion, develops in the thickness of the section.

The analytic study of the behavior of this type of sections began more than a century ago, when in 1909 Bach [18] conducting experiments on metal channel section beams, observed that a transversal load applied in its center of gravity causes, besides bending, also torsional deformations. Moreover, Bach observes that the four fibers placed in correspondence of the edges of the beam do not show dilations compatible with the hypothesis of the plane sections introduced by Navier. In his work, Bach attributed this anomaly to the asymmetry of the section. In the same years S.P. Timoshenko, studying the stability of thin-walled section beams [247], determined experimentally the torsional stiffness value of I-section beams subject to torsional moment. In this work, it is defined that the torque, in addition to shearing stresses, also generates axial stresses, which are not determined analytically.

In 1921, Maillart published a work dedicated to the problem of torsion in thin-section metal beams [169], in which he analyzed Bach's experiments, commenting that the sections do not keep flat even in the beams having symmetrical cross section. In 1926 Weber [269] presents a generalization of the results obtained by Timoshenko, which allows correlating the shear center and the torsion center that is the point of the cross section that remains fixed in following a torsional stress, and he demonstrated that, in case of torsional stress, these two points coincide.

In the second half of the 1930s, Vlasov published some works [258], [259], [260], in which highlights a new method for determining strains and stresses in thin-walled open-section beams. This procedure, which takes the name of *Sectorial Area Theory*, is an extension of the Navier's Theory. A few years later, the same author formalizes further this theory [262] introducing a new flexo-torsional stress: the *bimoment*. The scientific and methodological meaning theory of the thin-walled beams also resides in the fact that, basing itself on hypotheses more general than those of Saint Venant's classical Theory (which essentially reaffirms it in terms of shear forces and bending moments), this theory allows you to create a mathematical model of the beam that better describes the real behavior of the beam and thus allows better use of the materials.

In 1945 Timoshenko publishes an extensive paper on the thin-walled open-section beam theory [249] in which he analyses the open-section thin beam subject to torsional moment. The analytical formulation, although having a different notation, has extensive references to the work of Vlasov [262]. This work has a remarkable international success, probably because it was published in English (unlike the works by Vlasov, which were published in Russian) and thus accessible to more researchers. From this moment on, interest in the study of open thin sections increased significantly to such an extent that The Israel Program for Scientific Translations, a government company focused on translation and publication

of scientific and technical manuscripts from Russian to English, recognized the importance of the work of Vlasov (who died on August 7, 1958), publishing in 1961 the English translation [261] of his 1940 volume. This book, Thin-walled Elastic Beams, remains a milestone in the scientific literature.

In 1964 Capurso [53], [54] further extended Vlasov's Theory removing the hypothesis of the indeformability of section, going in this way to further generalize the problem of Saint Venant for thin-walled open-section beams. This theme was also taken up by other authors, including Aggarwal [2], Taranath [245], Takabatake [238], [239], Prokic [206], and Boswell [36].

In the 1980s, Capurso introduced a method [52] to analyze an n thin-walled open-section beam system connected in series by elements infinitely rigid in its own plane and infinitely deformable out of the plane. The originality of this work consists in having introduced a formulation like the well-known equations of Huygens, by which it is possible to transpose the moment of sectorial inertia from one reference system to another. This formulation has allowed defining a matrix containing all the geometric and sectorial stiffness terms useful for defining the global stiffness matrix of the entire n thin-walled open sections connected in series.

2.2.1 Vlasov's Theory

Let us consider the case of a cantilever channel-beam subjected to a flexural, axial, and torsional actions.

Based on the Superposition Principle, this load can be reduced to the sum of four different loading cases: one is purely axial (Figure 2.5a), two are purely flexural (Figures 2.5b and 2.5c); whilst the other is defined as flexural torsion (Figure 2.5d). In the latter case, the section does not remain plane (warping effect) and additional normal stresses appear. These additional normal stresses give rise to a generalised action, called *bimoment*, which is directly connected to the warping of the section. The intensity of this stress state cannot be neglected for these profiles and the application of Saint Venant's Theory could lead to gross errors. Two main geometrical hypotheses are at the basis of Vlasov's Theory:

- the section is considered rigid and, therefore, its shape is undeformable;
- the shearing strains on the midline of the section are assumed to vanish.

The formulation of Vlasov's Theory, has already been widely published in various works [55], [63], [189], and it is summarized in the following.

Let us consider a free shaped thin-walled open-section beam, located in a generic coordinate system, in which the Z axis is parallel to the longitudinal axis of the beam. Defined a specific cross section at $z = constant$, X and Y axes complete the right-handed coordinate system XYZ. Each point of the midline can be identified

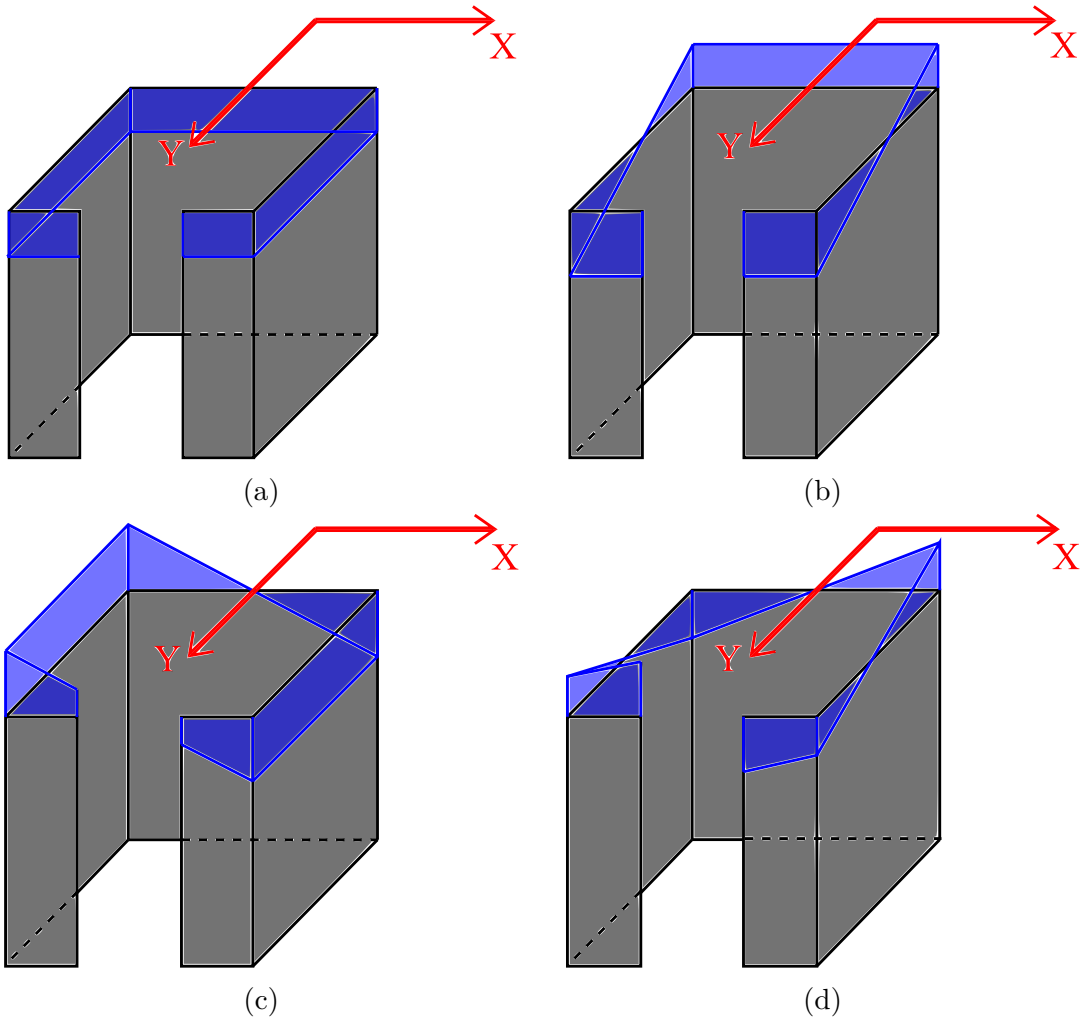

Figure 2.5: Cantilever channel-beam with four different loading cases. (a) Axial deformation; (b) Bending with respect to x axis; (c) Bending with respect to y axis; (d) Warping

by using the coordinates (x, y) or, along the midline, the curvilinear coordinate s (Figure 2.6).

With the aim of defining the equations which govern the structural behaviour of thin-walled open profiles, it is assumed that the beam is subjected to some torsional deformations. As a result of these, each point of the section is characterised by a new position in the general coordinate system XYZ. Therefore, it behaves as a perfectly rigid body, whose position can be evaluated by means of three independent variables corresponding to the three generalized displacements of an arbitrarily chosen point: two translations ξ and η in the X and Y directions, respectively, and the rotation ϑ.

Introducing the unit vector $\{u_t\}$ tangent to the midline of the section

$$\{u_t\} = \left\{ \frac{\mathrm{d}x}{\mathrm{d}s} \quad \frac{\mathrm{d}y}{\mathrm{d}s} \right\} \tag{2.17}$$

and the displacements vector $\{\delta\}$ of any point belonging to the cross section,

$$\{\delta\} = \left\{ \begin{array}{cc} u & v \end{array} \right\} \tag{2.18}$$

identified by the translations u and v in the X and Y directions, respectively, which can be determined through the well-known expressions:

$$u = \xi(z) - \vartheta(z)y \tag{2.19a}$$

$$v = \eta(z) + \vartheta(z)x \tag{2.19b}$$

the tangential displacement δ_t, related to the generic point of the section, can be computed by

$$\delta_t = \{\delta\}\{u_t\}^{\mathrm{T}} = u\frac{\mathrm{d}x}{\mathrm{d}s} + v\frac{\mathrm{d}y}{\mathrm{d}s} \tag{2.20}$$

and then:

$$\delta_t = \xi\frac{\mathrm{d}x}{\mathrm{d}s} + \eta\frac{\mathrm{d}y}{\mathrm{d}s} + \vartheta h(s) \tag{2.21}$$

in which the term $h(s)$ represents the distance between origin of the reference system and tangent line to the section midline (Figure 2.6)

$$h(s) = \{r\}^{\mathrm{T}}\{u_n\} = x\frac{\mathrm{d}y}{\mathrm{d}s} - y\frac{\mathrm{d}x}{\mathrm{d}s} \tag{2.22}$$

where r indicates the position vector $\{x \; y\}$ of the generic midline section point in the reference system, while $\{u_n\}$ is the unit vector normal to the section midline.

The longitudinal displacement component w can be obtained by the second Vlasov's hypothesis, according to which the shearing strains on the midline are considered negligible:

$$\gamma_{zs} = \frac{\partial w}{\partial s} + \frac{\partial \delta_t}{\partial z} = 0 \tag{2.23}$$

Taking into account the following relationship:

$$\omega(s) = \int_0^s h(s)\mathrm{d}s \tag{2.24}$$

the analytical expression of w is derived by integration,

$$w = \zeta(z) - \int_0^s \frac{\partial \delta_t}{\partial z}\mathrm{d}s = \zeta(z) - \xi' x - \eta' y - \vartheta'\omega \tag{2.25}$$

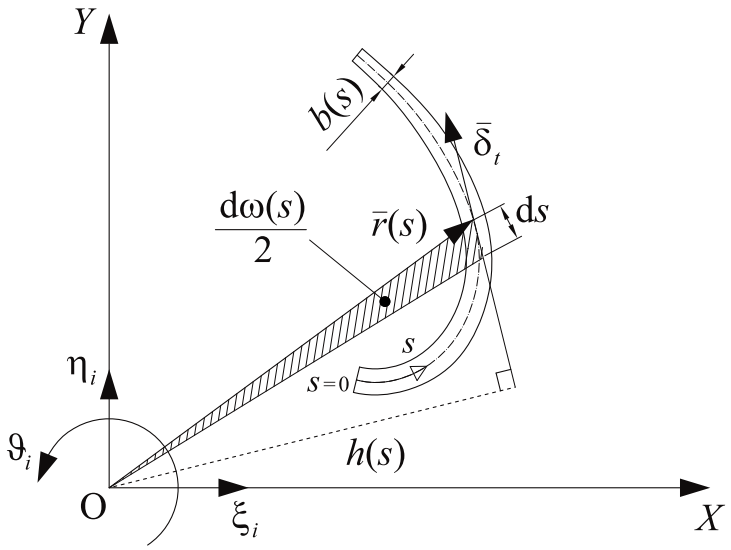

Figure 2.6: Computation of the sectorial coordinate ω [63]

The term $\zeta(z)$ is an arbitrary function, depending only on z, which describes a longitudinal translation of the entire section (Figure 2.5a); $\omega(s)$ is the *sectorial area*, *i.e.* the double of the area swept by the radius vector $\{r\}$ from $s = 0$ to the current point s of the section's midline. The points O and $s = 0$ are the *sectorial pole* and the *sectorial origin*, respectively (Figure 2.6). The longitudinal component w is composed by four terms: the first three are well-known and arise from extension and bending in the XZ and YZ planes (Figures 2.5b and 2.5c). The component which describes the warping of the section (Figure 2.5d) is expressed by the fourth term and, in particular, ϑ' can be considered as an amplification factor, whereas ω as the shape of the warped section. By differentiating w with respect to z, it is possible to obtain the expression of the longitudinal deformation ε_z:

$$\varepsilon_z = \frac{\partial w}{\partial z} = \zeta' - \xi'' x - \eta'' y - \vartheta'' \omega \tag{2.26}$$

The fourth term of Equation (2.26) demonstrates that the hypothesis of primary torsion, according to which the unit angle of torsion should be constant, in general can be removed. The general expression of the normal stress σ_z is obtained multiplying Equation (2.26) by the elastic modulus E:

$$\sigma_z = E\left(\zeta' - \xi'' x - \eta'' y - \vartheta'' \omega\right) \tag{2.27}$$

In each section of the beam, the normal stress σ_z is the sum of two contributions:

$$\sigma_z = \sigma_z^{SV} + \sigma_z^{VL} \tag{2.28}$$

where:

$$\sigma_z^{VL} = -E\vartheta''\omega \tag{2.29}$$

This expressions demonstrate that normal stresses can appear not only in presence of uniform extension and bending of the beam, but also as a result of the non-uniform torsion of the cross section. On the other hand, this specific contribution is usually assumed to vanish in the theory of primary torsion.

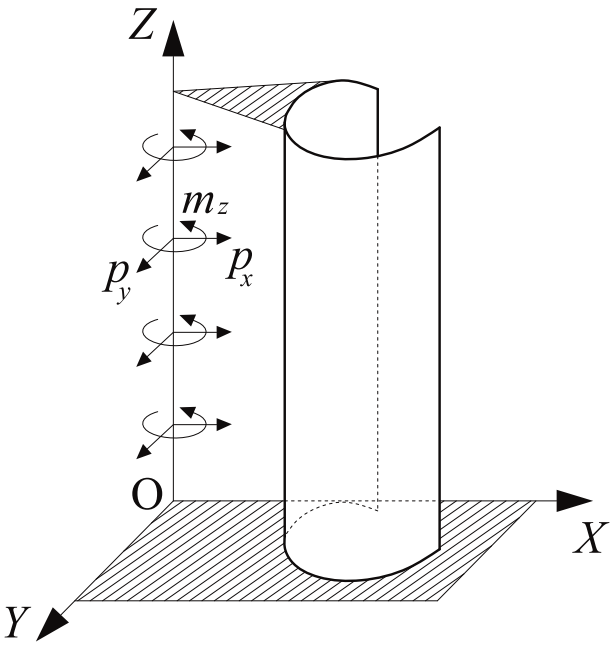

Figure 2.7: Thin-walled open-section beam subjected to transversal actions [63]

The computation of the sectorial terms is carried out considering the origin of the generic right-handed system XYZ as sectorial pole and a generic sectorial origin on the midline (Figure 2.7), the expression (2.27) allows to define, by integration, the normal stress acting along cantilever beam:

$$N = \int_A \sigma_z \mathrm{d}A = E \int_A \Big[(\zeta' - \xi'' x - \eta'' y - \vartheta''\omega) \Big] \mathrm{d}A \tag{2.30}$$

Noting that:

$$\int_A \zeta' \mathrm{d}A = \zeta' \int_A \mathrm{d}A = \zeta' A \tag{2.31a}$$

$$\int_A \xi'' x \mathrm{d}A = \xi'' \int_A x \mathrm{d}A = \xi'' S_y \tag{2.31b}$$

$$\int_A \eta'' y \mathrm{d}A = \eta'' \int_A y \mathrm{d}A = \eta'' S_x \tag{2.31c}$$

$$\int_A \vartheta'' \omega \mathrm{d}A = \vartheta'' \int_A \omega \mathrm{d}A = \vartheta'' S_\omega \tag{2.31d}$$

where the terms S_x and S_y are the static moments of the section with respect to the y and x axis, while S_ω is the sectorial static moment of the section, Equation (2.30) can be rewritted as:

$$N = \int_A \sigma_z \mathrm{d}A = E\left(A\zeta' - S_y\xi'' - S_x\eta'' - S_\omega\vartheta''\right) \tag{2.32}$$

Supposing null the axial force in the vertical bracing, the term ζ' can be eliminated in Equation (2.32):

$$\zeta' = \frac{S_y}{A}\xi'' + \frac{S_x}{A}\eta'' + \frac{S_\omega}{A}\vartheta'' = x_G\xi'' + y_G\eta'' + \omega_0\vartheta'' \tag{2.33}$$

The substitution of Equation (2.33) into Equation (2.27) permits to define the internal actions related to the flexural behaviour of the beam:

$$M_y = \int_A \sigma_z x \mathrm{d}A = -E\left(J_{yy}\xi'' + J_{yx}\eta'' + J_{y\omega}\vartheta''\right) \tag{2.34a}$$

$$M_x = \int_A \sigma_z y \mathrm{d}A = -E\left(J_{xy}\xi'' + J_{xx}\eta'' + J_{x\omega}\vartheta''\right) \tag{2.34b}$$

$$B = \int_A \sigma_z \omega \mathrm{d}A = -E\left(J_{\omega y}\xi'' + J_{\omega x}\eta'' + J_{\omega\omega}\vartheta''\right) \tag{2.34c}$$

Equation (2.34c) defines the bimoment action, which represents a generalized self-balanced force system equivalent to two bending moments, having the same magnitude but opposite signs.

The moments and product of inertia, with respect to the centroid of the section, can be obtained *via* the inverse application of Huygens-Steiner theorem:

$$J_{yy} = I_{yy} - Ax_G^2 \tag{2.35a}$$

$$J_{xx} = I_{xx} - Ay_G^2 \tag{2.35b}$$

$$J_{xy} = I_{xy} - Ay_G x_G \tag{2.35c}$$

By using the similar formulations proposed by Capurso [52], which transfers the sectorial moments of inertia from the generic origin to the sectorial centroid of the section ω_0, can be obtained:

$$J_{\omega\omega} = I_{\omega\omega} - A\omega_0^2 \tag{2.36a}$$

$$J_{\omega y} = I_{\omega y} - Ax_G\omega_0 \tag{2.36b}$$

$$J_{\omega x} = I_{\omega x} - A y_G \omega_0 \tag{2.36c}$$

Introducing the matrix of inertia $[J]$, it is possible to write these terms in a compact form:

$$[J] = \begin{bmatrix} J_{yy} & J_{yx} & J_{y\omega} \\ J_{xy} & J_{xx} & J_{x\omega} \\ J_{\omega y} & J_{\omega x} & J_{\omega\omega} \end{bmatrix} \tag{2.37}$$

The shearing stresses τ_{zs}, supposed to be defined by a constant distribution on the thickness of the section, can be obtained considering the longitudinal equilibrium of an elementary portion of beam, whose dimensions are the length $\mathrm{d}z$, the width $\mathrm{d}s$, and the thickness b (Figure 2.8):

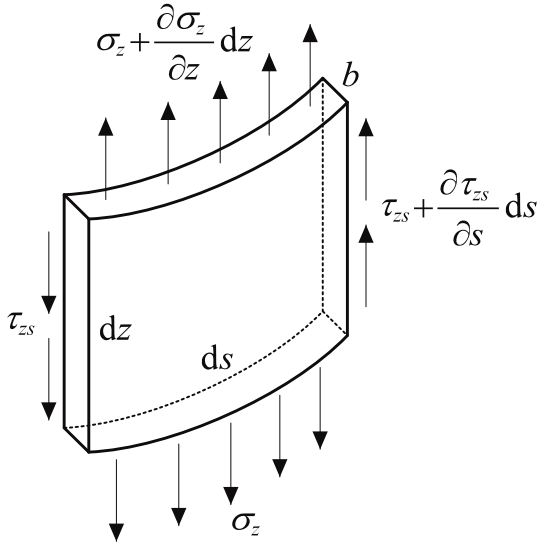

Figure 2.8: Longitudinal equilibrium of an infinitesimal strip of beam [63]

$$\frac{\partial (\tau_{zs} b)}{\partial s} + \frac{\partial (\sigma_z b)}{\partial z} = 0 \tag{2.38}$$

On the basis of Equation (2.38), three additional transverse internal actions, the shearing forces and the secondary torsional moment, can be defined:

$$T_x = \int_A \tau_{zs} \frac{\mathrm{d}x}{\mathrm{d}s} \mathrm{d}A \tag{2.39a}$$

$$T_y = \int_A \tau_{zs} \frac{\mathrm{d}y}{\mathrm{d}s} \mathrm{d}A \tag{2.39b}$$

$$M_z^{VL} = \int_A \tau_{zs} h \mathrm{d}A \tag{2.39c}$$

Integrating by parts and applying Equation (2.38), the following relations are obtained:

$$T_x = -\int_C \frac{\partial(\tau_{zs} b)}{\partial s} x \mathrm{d}s = \int_C \frac{\partial(\sigma_z b)}{\partial z} x \mathrm{d}s = \frac{\mathrm{d}}{\mathrm{d}z}\int_A \sigma_z x \mathrm{d}A \tag{2.40a}$$

$$T_y = -\int_C \frac{\partial(\tau_{zs} b)}{\partial s} y \mathrm{d}s = \int_C \frac{\partial(\sigma_z b)}{\partial z} y \mathrm{d}s = \frac{\mathrm{d}}{\mathrm{d}z}\int_A \sigma_z y \mathrm{d}A \tag{2.40b}$$

$$M_z^{VL} = -\int_C \frac{\partial(\tau_{zs} b)}{\partial s} \omega \mathrm{d}s = \int_C \frac{\partial(\sigma_z b)}{\partial z} \omega \mathrm{d}s = \frac{\mathrm{d}}{\mathrm{d}z}\int_A \sigma_z \omega \mathrm{d}A \tag{2.40c}$$

Equations (2.35 and 2.36) also affect the system (2.40), which becomes:

$$T_x = \frac{\mathrm{d}M_y}{\mathrm{d}z} = -E\left(J_{yy}\xi''' + J_{yx}\eta''' + J_{y\omega}\vartheta'''\right) \tag{2.41a}$$

$$T_y = \frac{\mathrm{d}M_x}{\mathrm{d}z} = -E\left(J_{xy}\xi''' + J_{xx}\eta''' + J_{x\omega}\vartheta'''\right) \tag{2.41b}$$

$$M_z^{VL} = \frac{\mathrm{d}B}{\mathrm{d}z} = -E\left(J_{\omega y}\xi''' + J_{\omega x}\eta''' + J_{\omega\omega}\vartheta'''\right) \tag{2.41c}$$

The last equation highlights that, due to the warping of the section, an unexpected torsional moment M_z^{VL} is generated, being it the first derivative of the bimoment action. The secondary torsional moment M_z^{VL} is generated by the τ_{zs} stresses due to the shearing actions T_x and T_y. A further step of differentiation leads to the equilibrium equations which take into account the distributed external loads p_x, p_y, and m_z (known terms):

$$p_x = -\frac{\mathrm{d}T_x}{\mathrm{d}z} = E\left(J_{yy}\xi^{IV} + J_{yx}\eta^{IV} + J_{y\omega}\vartheta^{IV}\right) \tag{2.42a}$$

$$p_y = -\frac{\mathrm{d}T_y}{\mathrm{d}z} = E\left(J_{xy}\xi^{IV} + J_{xx}\eta^{IV} + J_{x\omega}\vartheta^{IV}\right) \tag{2.42b}$$

$$m_z^{VL} = -\frac{\mathrm{d}M_z^{VL}}{\mathrm{d}z} = E\left(J_{\omega y}\xi^{IV} + J_{\omega x}\eta^{IV} + J_{\omega\omega}\vartheta^{IV}\right) \tag{2.42c}$$

Actually, the thin-walled open section is subjected to two different torsional moments: the first, due to a constant distribution of shearing stresses through the thickness, is related to the equilibrium with the normal stresses coming from the warping of the section; the second, according to Saint Venant's Theory, is due to a linear variation of shearing stresses through the thickness and is equal to zero on the midline. In each section of the beam, the torsional moment M_z is the sum of the two contributions:

$$M_z = M_z^{SV} + M_z^{VL} = GI_t\vartheta' - E\left(J_{\omega y}\xi''' + J_{\omega x}\eta''' + J_{\omega\omega}\vartheta'''\right) \tag{2.43}$$

where G is the shear elastic modulus, and I_t is the torsional stiffness factor of the section. Therefore, the global equilibrium Equation (2.42c) becomes:

$$m_z = -\frac{\mathrm{d}M_z}{\mathrm{d}z} = -GI_t\vartheta'' + E\left(J_{\omega y}\xi^{IV} + J_{\omega x}\eta^{IV} + J_{\omega\omega}\vartheta^{IV}\right) \tag{2.44}$$

If the vectors $\{\delta\}$, $\{M\}$, $\{T\}$, and $\{F\}$ are introduced,

$$\{\delta\} = \begin{Bmatrix} \xi \\ \eta \\ \vartheta \end{Bmatrix} \tag{2.45a}$$

$$\{M\} = \begin{Bmatrix} M_y \\ M_x \\ B \end{Bmatrix} \tag{2.45b}$$

$$\{T\} = \begin{Bmatrix} T_x \\ T_y \\ M_z^{VL} \end{Bmatrix} \tag{2.45c}$$

$$\{F\} = \begin{Bmatrix} p_x \\ p_y \\ m_z^{VL} \end{Bmatrix} \tag{2.45d}$$

it is possible to write systems (2.34), (2.41), and (2.42) in a compact form:

$$\{M\} = -E\,[J]\,\{\delta''\} \tag{2.46a}$$

$$\{T\} = -E\,[J]\,\{\delta'''\} \tag{2.46b}$$

$$\{F\} = E\,[J]\left\{\delta^{IV}\right\} \tag{2.46c}$$

The system of Equations (2.46) can be strongly simplified operating some choices. In fact, if a centroidal coordinate system is considered, the following conditions are all immediately satisfied:

$$S_y = \int_A x\mathrm{d}A = 0 \tag{2.47a}$$

$$S_x = \int_A y\mathrm{d}A = 0 \tag{2.47b}$$

Since the reference system is also principal, the product of inertia are null

$$J_{xy} = J_{yx} = \int_A xy\mathrm{d}A = 0 \tag{2.48}$$

On the other hand, if the sectorial pole coincides with the shear centre of the section, it can be shown that:

$$J_{\omega y} = J_{y\omega} = \int_A \omega y \mathrm{d}A = 0 \tag{2.49a}$$

$$J_{\omega x} = J_{x\omega} = \int_A \omega x \mathrm{d}A = 0 \tag{2.49b}$$

In addition, if the sectorial origin is in the sectorial centroid, by definition it follows that also the sectorial static moment is null

$$S_\omega = \int_A \omega \mathrm{d}A = 0 \tag{2.50}$$

When centroid and shear centre do not coincide, the diagonalization of Vlasov's Equations, namely, of the relationship between the diagonal terms of matrix $[J]$ and the second derivatives of the generalized displacements, is possible only in the case $N = 0$. If each of this hypothesis is satisfied, it is possible diagonalized the matrix $[J]$:

$$[J] = \begin{bmatrix} J_{yy} & 0 & 0 \\ 0 & J_{xx} & 0 \\ 0 & 0 & J_{\omega\omega} \end{bmatrix} \tag{2.51}$$

Taking into account this diagonal matrix, Equations (2.46) can be written in simplified form and the internal actions can be defined as:

$$M_y = -EJ_{yy}\xi'' \tag{2.52a}$$

$$M_x = -EJ_{xx}\eta'' \tag{2.52b}$$

$$B = -EJ_{\omega\omega}\vartheta'' \tag{2.52c}$$

The internal actions producing the shearing stresses are also diagonalized:

$$T_x = -EJ_{yy}\xi''' \tag{2.53a}$$

$$T_y = -EJ_{xx}\eta''' \tag{2.53b}$$

$$M_z^{VL} = -EJ_{\omega\omega}\vartheta''' \tag{2.53c}$$

This means that the system of Equations (2.42) is reduced to the following decoupled equilibrium equations:

$$p_x = EJ_{yy}\xi^{IV} \tag{2.54a}$$

$$p_y = EJ_{xx}\eta^{IV} \tag{2.54b}$$

$$m_z^{VL} = EJ_{\omega\omega}\vartheta^{IV} \tag{2.54c}$$

Therefore, the global equilibrium Equation (2.44) becomes:

$$m_z = -GI_t\vartheta'' + EJ_{\omega\omega}\vartheta^{IV} \tag{2.55}$$

Imposing the boundary conditions, the system can be solved and functions ξ, η, and, ϑ can be determined together with the normal and shearing stresses.

It is interesting to observe that Equation (2.55) is formally the same as the equation of the elastic line with effects of the second order due to a tensile axial load N and distributed load $q(z)$:

$$q(z) = EJ_{xx}v^{IV} - Nv'' \tag{2.56}$$

It is worthwhile to emphasize the formal analogy between the well-known equations of the elastic line describing the flexural behaviour of a beam and the diagonalized differential equations describing the torsional behaviour of thin-walled open-section beams. As in the case of flexural curvature, in the torsional behaviour the term ϑ'' vanishes where the bimoment is null, or, in other words, the bimoment is zero where the line describing the rotations of the beam shows an inflection point.

If the contribution related to the primary torsion $GI_t\vartheta''$ is negligible, Equation can be more easily integrated. Since the matrix of inertia is symmetrical and positive definite until the geometry of the section is such that the determinant of $[J]$ is different from zero, it can be inverted in order to obtain a relationship between the fourth derivatives of the displacements and the external distributed actions:

$$\{\delta^{IV}\} = \frac{1}{E}[J]^{-1}\{F\} \tag{2.57}$$

The transverse displacements of the section are obtained integrating Equation (2.57) and applying the boundary conditions at the base and at the top of the cantilever. At the constrained end:

$$\{\delta\} = \{0\} \tag{2.58a}$$

$$\{\delta'\} = \{0\} \tag{2.58b}$$

whereas, at the top:

$$\{\delta''\} = \{0\} \tag{2.59a}$$

$$\{\delta'''\} = \{0\} \tag{2.59b}$$

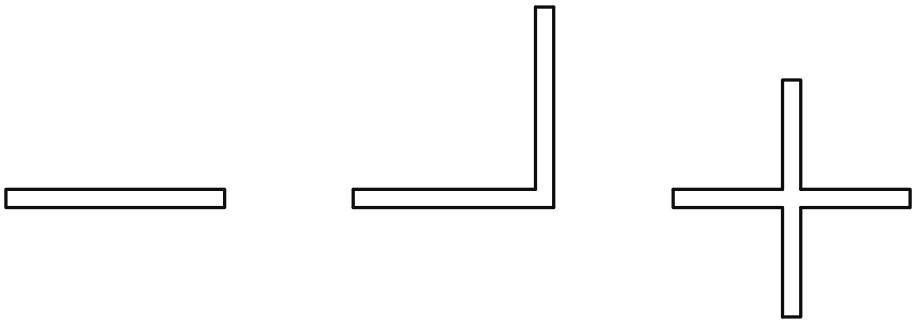

Figure 2.9: Shear walls constituted by thin plates converging in a single point [63]

Once ξ, η, and, ϑ are known, the application of Equation (2.33) yields the uniform axial displacement ζ with the corresponding boundary condition:

$$\zeta(z = 0) = 0 \tag{2.60}$$

Eventually, the displacement components δ_t and w can be easily derived from Equations (2.21) and (2.25). This analytical formulation cannot be applied in presence of specific sections for which the matrix $[J]$ is singular. These are the cases of shear walls constituted by a single thin rectangular plate or different thin plates converging into a single point, as shown in Figure (2.9). In these cases the warping function vanishes.

2.2.2 Stiffness matrix evaluation

Considering an N floors thin-walled open-section shear wall, in the local reference system with origin in the shear center of the section, the force-displacement relation can be defined as follows:

$$\begin{Bmatrix} \{p_x\} \\ \{p_y\} \\ \{m_z\} \end{Bmatrix} = \begin{bmatrix} [K_x] & 0 & 0 \\ 0 & [K_y] & 0 \\ 0 & 0 & [K_\vartheta] \end{bmatrix} \begin{Bmatrix} \{\xi\} \\ \{\eta\} \\ \{\vartheta\} \end{Bmatrix} \tag{2.61}$$

or in compact form:

$$\{F^*\} = [K^*]\,\{\delta^*\} \tag{2.62}$$

where the terms $\{p_x\}$, $\{p_y\}$, and $\{m_z\}$ represent the $N \times 1$ vectors containing the generalized floor forces; $[K_x]$, $[K_y]$, and $[K_\vartheta]$ represent the $N \times N$ stiffness matrices in the direction of referred to; while $\{\xi\}$, $\{\eta\}$, and $\{\vartheta\}$ represent the $N \times 1$ vectors containing the generalized floor displacements.

Numbering the N floors from top to bottom, assuming that the normal elastic modulus E is the same for the entire height of the shear wall, and considering valid Equation (2.57) for each floor, it is possible to write the following relation:

$$\begin{Bmatrix} \{\delta_1^{IV}\} \\ \{\delta_2^{IV}\} \\ \{\delta_j^{IV}\} \\ \vdots \\ \{\delta_N^{IV}\} \end{Bmatrix} = \frac{1}{E} \begin{bmatrix} [J_1]^{-1} & [0] & [0] & \cdots & [0] \\ [0] & [J_2]^{-1} & [0] & \cdots & [0] \\ [0] & [0] & [J_j]^{-1} & \cdots & [0] \\ \vdots & \vdots & \vdots & \ddots & \vdots \\ [0] & [0] & [0] & \cdots & [J_N]^{-1} \end{bmatrix} \begin{Bmatrix} \{F_1\} \\ \{F_2\} \\ \{F_j\} \\ \vdots \\ \{F_N\} \end{Bmatrix} \tag{2.63}$$

or in compact form:

$$\left\{\widehat{\delta^*}^{IV}\right\} = \frac{1}{E}\left[\widehat{J^*}\right]^{-1}\left\{\widehat{F^*}\right\} \tag{2.64}$$

where the 3×1 vectors $\{\delta_j\}$ and $\{F_j\}$, refferred to j-th floor, are:

$$\{\delta_j\} = \begin{Bmatrix} \xi_j \\ \eta_j \\ \vartheta_j \end{Bmatrix} \tag{2.65a}$$

$$\{F_j\} = \begin{Bmatrix} p_{x,j} \\ p_{y,j} \\ m_{z,j} \end{Bmatrix} \tag{2.65b}$$

$[0]$ is the 3×3 null matrix, while the 3×3 matrix $[J_j]$ is given by Equation (2.51) evaluated for the j-th floor.

As you can see, the vectors $\{\widehat{\delta^*}\}$ and $\{\delta^*\}$ differ only in the order of the their components, but it is possibile to write the following relationship:

$$\begin{Bmatrix} \xi_1 \\ \xi_2 \\ \vdots \\ \xi_N \\ \eta_1 \\ \eta_2 \\ \vdots \\ \eta_N \\ \vartheta_1 \\ \vartheta_2 \\ \vdots \\ \vartheta_N \end{Bmatrix} = \begin{bmatrix} 1 & 0 & 0 & 0 & 0 & 0 & \cdots & 0 & 0 & 0 \\ 0 & 0 & 0 & 1 & 0 & 0 & \cdots & 0 & 0 & 0 \\ \vdots & \vdots & \vdots & \vdots & \vdots & \vdots & \vdots & \vdots & \vdots & \vdots \\ 0 & 0 & 0 & 0 & 0 & 0 & \cdots & 1 & 0 & 0 \\ 0 & 1 & 0 & 0 & 0 & 0 & \cdots & 0 & 0 & 0 \\ 0 & 0 & 0 & 0 & 1 & 0 & \cdots & 0 & 0 & 0 \\ \vdots & \vdots & \vdots & \vdots & \vdots & \vdots & \vdots & \vdots & \vdots & \vdots \\ 0 & 0 & 0 & 0 & 0 & 0 & \cdots & 0 & 1 & 0 \\ 0 & 0 & 1 & 0 & 0 & 0 & \cdots & 0 & 0 & 0 \\ 0 & 0 & 0 & 0 & 0 & 1 & \cdots & 0 & 0 & 0 \\ \vdots & \vdots & \vdots & \vdots & \vdots & \vdots & \vdots & \vdots & \vdots & \vdots \\ 0 & 0 & 0 & 0 & 0 & 0 & \cdots & 0 & 0 & 1 \end{bmatrix} \begin{Bmatrix} \xi_1 \\ \eta_1 \\ \vartheta_1 \\ \xi_2 \\ \eta_2 \\ \vartheta_2 \\ \vdots \\ \eta_{N-1} \\ \vartheta_{N-1} \\ \xi_N \\ \eta_N \\ \vartheta_N \end{Bmatrix} \tag{2.66}$$

or in compact form:

$$\{\delta^*\} = [\Upsilon]\left\{\widehat{\delta^*}\right\} \tag{2.67}$$

An analogous relation can be written for the vector of static actions:

$$\{F^*\} = [\Upsilon] \left\{\widehat{F^*}\right\} \tag{2.68}$$

Substituting Equations (2.67 and 2.68) into Equation (2.64), and pre-multiplying the preceding expression by the transformation matrix $[\Upsilon]$ we get:

$$\left\{\delta^{*IV}\right\} = \frac{1}{E}\left([\Upsilon]\left[\widehat{J^*}\right]^{-1}[\Upsilon]^{-1}\right)\{F^*\} = \frac{1}{E}[J^*]^{-1}\{F^*\} \tag{2.69}$$

Integrating Equation (2.69) with the boundary conditions already detailed in Equations (2.58 and 2.59), we obtain the loads-displacements relation, that is the compliance matrix $[C^*]$ of the shear wall:

$$\{\delta^*\} = \left(\frac{L^3}{E}[J^*]^{-1}[Q^*]\right)\{F^*\} = [C^*]\{F^*\} \tag{2.70}$$

where L is the storey height, while the $3N \times 3N$ matrix $[Q^*]$ contains the non-dimensional influence coefficients determined through the integration. Its structure is block-diagonal, with three equal $N \times N$ submatrices $[Q]$ and six null $N \times N$ submatrices $[0]$:

$$[Q^*] = \begin{bmatrix} [Q] & [0] & [0] \\ [0] & [Q] & [0] \\ [0] & [0] & [Q] \end{bmatrix} \tag{2.71}$$

The computation of the terms of the submatrix $[Q]$ provides the generic recursive form [64]:

$$q_{a,b} = \frac{1}{6}(N - b + 1)^2(2N + b - 3a + 2) \tag{2.72}$$

where N is the number of the floors, while a and b are the position index of the term $q_{a,b}$.

By inverting the compliance matrix $[C^*]$ we finally get the expression of the stiffness matrix $[K^*]$ of the thin-walled open-section shear walls:

$$[K^*] = \frac{E}{L^3}[Q^*]^{-1}[J^*] \tag{2.73}$$

2.2.3 Capurso's Method

The previous formulation was extended by Capurso [52] to consider the case of M vertical cantilevers which represent the resistant skeleton of a tall building loaded by transverse actions applied to the floors with reference to the global coordinate system XYZ. The vertical bracings are connected to each other by means of in-plane rigid slabs, whose out-of-plane rigidity can be considered negligible. The unknown variables of the problem are the floor displacements, identified by the translations ξ and η in the X and Y directions, respectively, and the torsional rotation ϑ. Since $\{F_i\}$ indicates the vector of the transverse actions transmitted to the i-th cantilever, by virtue of Equation (2.46c) we have:

$$\{F_i\} = E\,[J_i]\left\{\delta^{IV}\right\} \tag{2.74}$$

where matrix $[J_i]$ contains the moments of inertia referred to the centroid of the section and to the sectorial centroid, whereas the vector $\left\{\delta^{IV}\right\}$ gathers the derivatives of the fourth order of the floor displacements ξ, η, and ϑ. If $\{F\}$ is the vector of the external loads, the equilibrium condition imposes:

$$\{F\} = \sum_{i=1}^{M}\{F_i\} = E\left(\sum_{i=1}^{M}[J_i]\right)\left\{\delta^{IV}\right\} = E\,[J]\left\{\delta^{IV}\right\} \tag{2.75}$$

Therefore, the combination of M cantilevers behaves as a single cantilever whose matrix of inertia is given by the sum of the M matrices related to the single cantilevers:

$$[J] = \sum_{i=1}^{M}[J_i] \tag{2.76}$$

Equation (2.75) can be solved following the procedure previously described in the case of a single vertical bracing. Once the floor displacements are known, the displacements of each cantilever can be deduced and information regarding the stress state can also be obtained. Finally, it is interesting to observe, from the relation between the vector $\{F_i\}$ of the i-th cantilever and the global vector $\{F\}$, that each bracing is subjected to an external load vector provided by the product of its own inertia matrix by the inverse of the global one, analogously to what emerges in the *General Algorithm* described in Chapter 3:

$$\{F_i\} = [J_i]\,[J]^{-1}\,\{F\} \tag{2.77}$$

In the case of a discrete distribution of transverse forces corresponding to the different floors, the 3×3 matrix $[J]$, which is a function of the longitudinal coordinate z, can be expanded to a $3N \times 3N$ stiffness matrix to be inserted in the General Algorithm.

Finally it is possible know the normal stress based on the corresponding internal actions substituting Equations (2.52) into Equation (2.27):

$$\sigma_z = \frac{M_x}{J_{xx}} y - \frac{M_y}{J_{yy}} x + \frac{B}{J_{\omega\omega}} \omega \tag{2.78}$$

The first two contributions derive from the well-known Saint Venant's Theory and are based on the hypothesis of plane sections; the third describes the normal stresses due to the out-of-plane warping of the profile. An expression of the shearing stresses τ_{zs} can be obtained substituting Equation (2.27) into Equation (2.38)

$$\frac{\partial(\tau_{zs} b)}{\partial s} + Eb(\zeta'' - \xi''' x - \eta''' y - \vartheta''' \omega) = 0 \tag{2.79}$$

and integrating with respect to s:

$$\tau_{zs} = -\frac{E}{b}\left[\zeta'' A(s) - \xi''' S_y(s) - \eta''' S_x(s) - \vartheta''' S_\omega(s)\right] \tag{2.80}$$

where the following geometrical expressions are used:

$$A(s) = b \int_0^s \mathrm{d}s \tag{2.81a}$$

$$S_y(s) = b \int_0^s x \mathrm{d}s \tag{2.81b}$$

$$S_x(s) = b \int_0^s y \mathrm{d}s \tag{2.81c}$$

$$S_\omega(s) = b \int_0^s \omega \mathrm{d}s \tag{2.81d}$$

The substitution of Equations (2.53) into Equation (2.80) gives an expression for the shearing stresses

$$\tau_{zs} = \frac{1}{b}\left[\frac{T_x}{J_{yy}} S_y(s) + \frac{T_y}{J_{xx}} S_x(s) + \frac{M_z^{VL}}{J_{\omega\omega}} S_\omega(s)\right] \tag{2.82}$$

The first two terms derive from Jourawski's Theory, whereas the last from Vlasov's Theory.

2.3 Plane frames

From a static point of view, a multi-storey plane frame is a many times hyperstatic structure, and as a result, using the traditional equilibrium techniques, its resolution can be laborious and very long computational time. Also, wanting to automate the calculation for implementation of the formulation in numerical codes, it becomes fundamental to define a matrix method, limiting the subjective intervention of the people. An iterative process was introduced by Cross in 1930 [88], [89] which can be used for resolution of frames in which the nodes rotate but do not translate. This procedure had an internationally noteworthy response, although Čališev [45], [46] announced that he had already proposed several years ago, a very similar procedure, but as this work was written in the Croatian language, it remained unknown to most of the international scientific community.

After the publication of the Cross Method, the focus was on the possibility of solving frames whose nodes, in addition to rotating, are also able to translate.

L.E. Grinter first indicated the iterative solution [115]. In the following years these procedures were further refined, including by introducing simplified assumptions [72], [104]. These calculation procedures, although providing accurate results, are iterative, laborious and difficult to implement in a automatic calculation code.

In addition, for the purposes of proper structural analysis, the correct estimation of the rigidity of the internal connections of the frame is of great importance [100], [128].

With a view to determining the approximate expression of the stiffness matrix of a plane frame, which will be implemented in an analytical calculation code that allows preliminary analysis of the static and dynamic behavior of a high building, it is necessary to consider a simplified model whose behavior provides comparable results with those obtained by using rigorous formulations. In order to do this, the following hypotheses are introduced:

- the frame has no flexural stiffness outside the plane containing it;
- the frame has no torsional stiffness;
- all nodes belonging to the j-th plane rotate of the same angle φ_j.

Consider the multi-storey plane frame, shown in Figure (2.10a), composed by n_c columns, of constant distance l clamped to the base, and N floors, each of h_j height, not necessarily constant for all storeys. A simplified literature method [204] is explained, by means of which the frame is assimilated to a continuous equivalent cantilever beam having flexural rigidity only in the plane that contains it, and torsional elastic constraints at each floor, as shown in Figure (2.10b).

Considering only horizontal forces p_x at the floor level, the frame of Figure (2.10a) assumes the deformed shape shown in Figure (2.11).

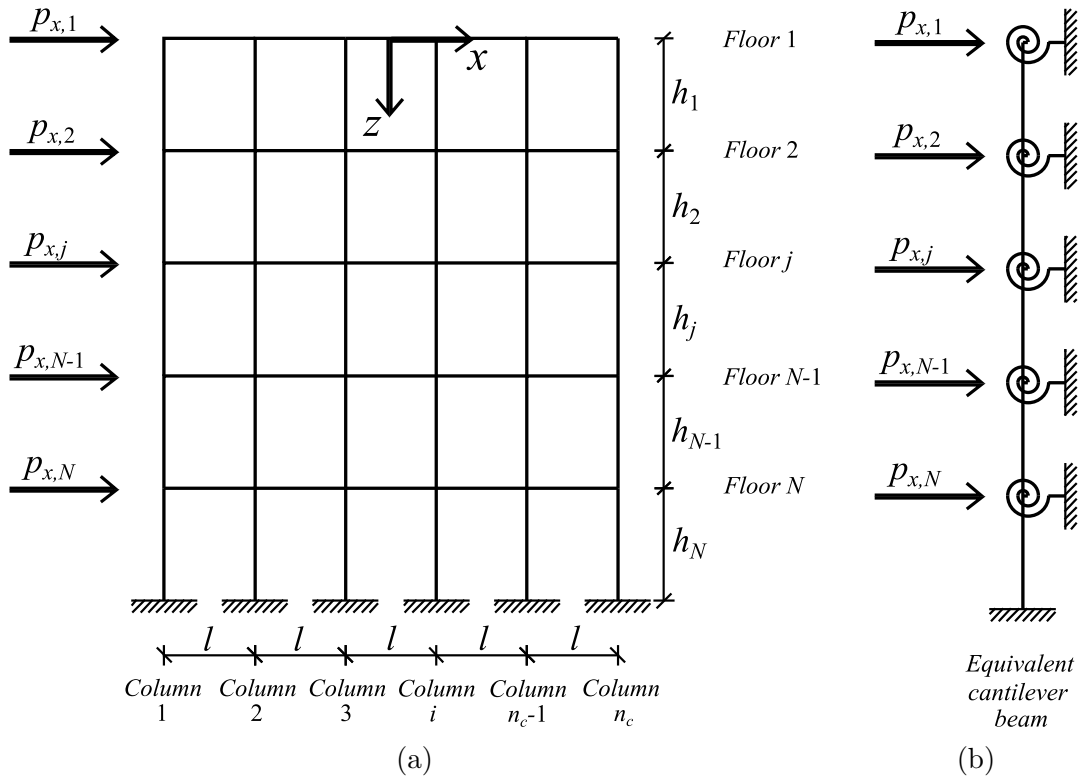

Figure 2.10: (a) Plane frame; (b) Continuous equivalent cantilever beam

Since each column of the frame has bending stiffness equal to:

$$k_c = \frac{12E_cJ_c}{h_j^3} \tag{2.83}$$

where E_c and J_c are the Young's modulus and second moment of inertia of the column, respectively, it is easy to determine that the stiffness of each portion of the continuous equivalent beam has flexural stiffness equal to the sum of the stiffness of the columns:

$$k_{c,eq} = \sum_{1}^{n_c} k_c = n_c k_c = n_c \frac{12E_cJ_c}{h_j^3} \tag{2.84}$$

Introducing the moment of inertia of the equivalent cantilever beam J_{eq} defined as:

$$J_{eq} = \sum_{1}^{n_c} J_c = n_c J_c \tag{2.85}$$

and neglecting the stiffening effect of the beams, the 4×4 stiffness matrix of the j-th portion between two consecutive floors of the equivalent cantilever can be written in the form:

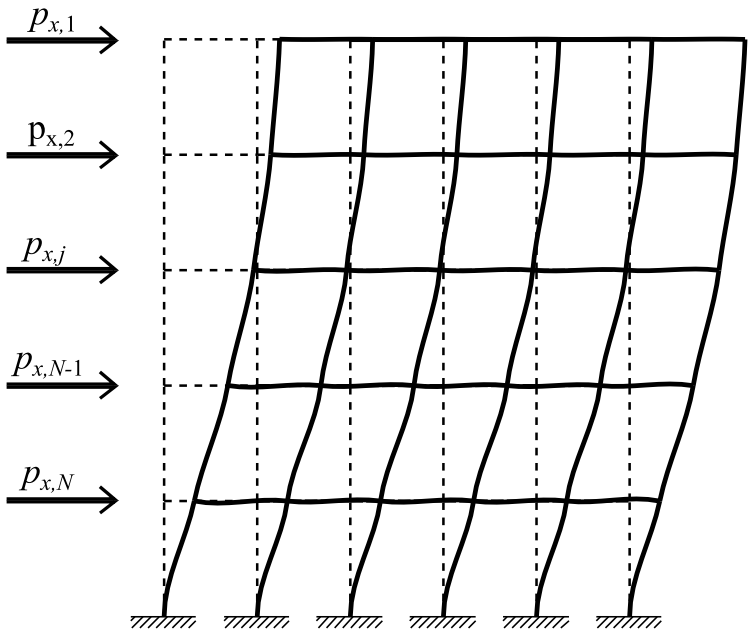

Figure 2.11: Deformed shape of the frame

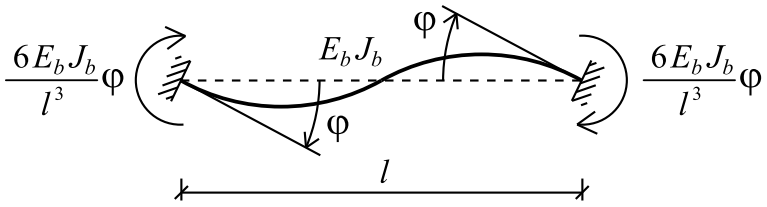

Figure 2.12: Beam static diagram with imposed rotations φ

$$[k_{x,j}] = EJ_{eq} \begin{bmatrix} 12/h_j^3 & -12/h_j^3 & -6/h_j^2 & -6/h_j^2 \\ -12/h_j^3 & 12/h_j^3 & 6/h_j^2 & 6/h_j^2 \\ -6/h_j^2 & 6/h_j^2 & 4/h_j & 2/h_j \\ -6/h_i j^2 & 6/h_j^2 & 2/h_j & 4/h_j \end{bmatrix} \tag{2.86}$$

This equation has a structure similar to Equation (2.7) obtained for shear walls.

Also in this case, considerations similar to the preceding ones apply, which make it possible to identify the stiffness matrix of the entire frame can be achieved by appropriately assembling the stiffness matrices relating to j-th floor, the following relationship is obtained:

$$\begin{Bmatrix} \{p_x\} \\ \{0\} \end{Bmatrix} = \begin{bmatrix} [k_{xx}] & [k_{x\varphi_y}] \\ [k_{\varphi_y x}] & [k_{\varphi_y \varphi_y}] \end{bmatrix} \begin{Bmatrix} \{\xi\} \\ \{\varphi_y\} \end{Bmatrix} \tag{2.87}$$

By analogy with the calculation procedure shown for shear walls (Equations 2.10), the $N \times N$ sub-matrices take a recursive form and can generally be written as:

$$[k_{xx}] = EJ_{eq} \begin{bmatrix} 1/h_1^3 & -1/h_1^3 & 0 & \cdots & 0 \\ -1/h_1^3 & 1/h_1^3 + 1/h_j^3 & -1/h_j^3 & \cdots & 0 \\ 0 & -1/h_j^3 & 1/h_j^3 + 1/h_{j+1}^3 & \cdots & 0 \\ \vdots & \vdots & \vdots & \ddots & \vdots \\ 0 & 0 & 0 & \cdots & 1/h_N^3 \end{bmatrix} \tag{2.88a}$$

$$\left[k_{x\varphi_y}\right] = EJ_{eq} \begin{bmatrix} -1/h_1^2 & -1/h_1^2 & 0 & \cdots & 0 \\ 1/h_1^2 & 1/h_1^2 - 1/h_j^2 & -1/h_j^2 & \cdots & 0 \\ 0 & 1/h_j^2 & 1/h_j^2 - 1/h_{j+1}^2 & \cdots & 0 \\ \vdots & \vdots & \vdots & \ddots & \vdots \\ 0 & 0 & 0 & \cdots & 1/h_N^2 \end{bmatrix} \tag{2.88b}$$

$$\left[k_{\varphi_y x}\right] = EJ_{eq} \begin{bmatrix} -1/h_1^2 & 1/h_1^2 & 0 & \cdots & 0 \\ -1/h_1^2 & 1/h_1^2 - 1/h_j^2 & 1/h_j^2 & \cdots & 0 \\ 0 & -1/h_j^2 & 1/h_j^2 - 1/h_{j+1}^2 & \cdots & 0 \\ \vdots & \vdots & \vdots & \ddots & \vdots \\ 0 & 0 & 0 & \cdots & 1/h_N^2 \end{bmatrix} \tag{2.88c}$$

Considering that each beam has a bending stiffness equal to (Figure 2.12):

$$k_b = \frac{6E_bJ_b}{l^3} \tag{2.89}$$

where E_b and J_b are the Young's modulus and second moment of inertia of the beam, and that on each floor there are $n_c - 1$ beams, and each beam has two ends connected to the columns, the stiffness of each torsional constraint applied at each floor is equal to:

$$k_{t,eq} = 2\sum_{1}^{n_c-1} k_b = 2(n_c - 1)\frac{6E_bJ_b}{l^3} = (n_c - 1)\frac{12E_bJ_b}{l^3} \tag{2.90}$$

This value shall be added to the terms present on the diagonal of the matrix $\left[k_{\varphi_y\varphi_y}\right]$ (Equation 2.10d) which takes the form:

$$\left[k_{\varphi_y\varphi_y}\right] = EJ_{eq} \begin{bmatrix} 4/h_1 + k_{t,eq} & 2/h_1 & \cdots & 0 \\ 2/h_1 & 4/h_1 + 4/h_j + k_{t,eq} & \cdots & 0 \\ \vdots & \vdots & \ddots & \vdots \\ 0 & 0 & \cdots & 4/h_N + k_{t,eq} \end{bmatrix} \tag{2.91}$$

Replacing Equations (2.88a, 2.88b, 2.88c, and 2.91) in Equation (2.87), by analogy to the procedure shown for the shear walls (Equations 2.11 and 2.12), the condensed shape of the $N \times N$ stiffness matrix in x-direction is obtained:

$$[K_x] = \left[[k_{xx}] - \left[k_{x\varphi_y}\right] \left(\left[k_{\varphi_y\varphi_y}\right]^{-1} \left[k_{\varphi_y x}\right] \right) \right] \tag{2.92}$$

Eventually, considering that the frame has no stiffness outside the plane that contains it and that it has no torsional stiffness, means the whole element stiffness matrix ($3N \times 3N$) expressed in the local reference system, shall take the following form:

$$[K^*] = \begin{bmatrix} [K_x] & 0 & 0 \\ 0 & 0 & 0 \\ 0 & 0 & 0 \end{bmatrix} \tag{2.93}$$

2.3.1 Braced frames

Since there are diagonal braces in the frame (Figure 2.13a), the method illustrated in the previous section can still be used with the foresight to add, at level of each floor, additional effective elastic constraints in the equivalent cantilever beam [47], as shown in Figure (2.13b).

By analyzing a single braced module of the frame in which the diagonal bar is present (Figure 2.14), neglecting the effect of the compressed rod, it is possible to determine the normal force N_d in it:

$$N_d = k_d\delta_d = \frac{E_d A_d}{\sqrt{l^2+h^2}}\delta_d = \left(\frac{E_d A_d}{\sqrt{l^2+h^2}}\right)\delta_x \cos\alpha \tag{2.94}$$

where k_d, E_d, and A_d are the axial stiffness, Young's modulus, and cross section area of the rod, respectively.

By projecting this force on the horizontal plane, we obtain:

$$p_{x,d} = N_d \cos\alpha = \left(\frac{E_d A_d}{\sqrt{l^2+h^2}}\right)\delta_x \cos^2\alpha = k_{x,d}\delta_x \tag{2.95}$$

where $k_{x,d}$ indicates a fictitious stiffness in x-direction due to the presence of the diagonal brace. This term, evaluated for each braced module of the frame in which the diagonal rod is present, shall be added to the terms present on the diagonal of the sub-matrix $[k_{xx}]$ described in Equation (2.88a):

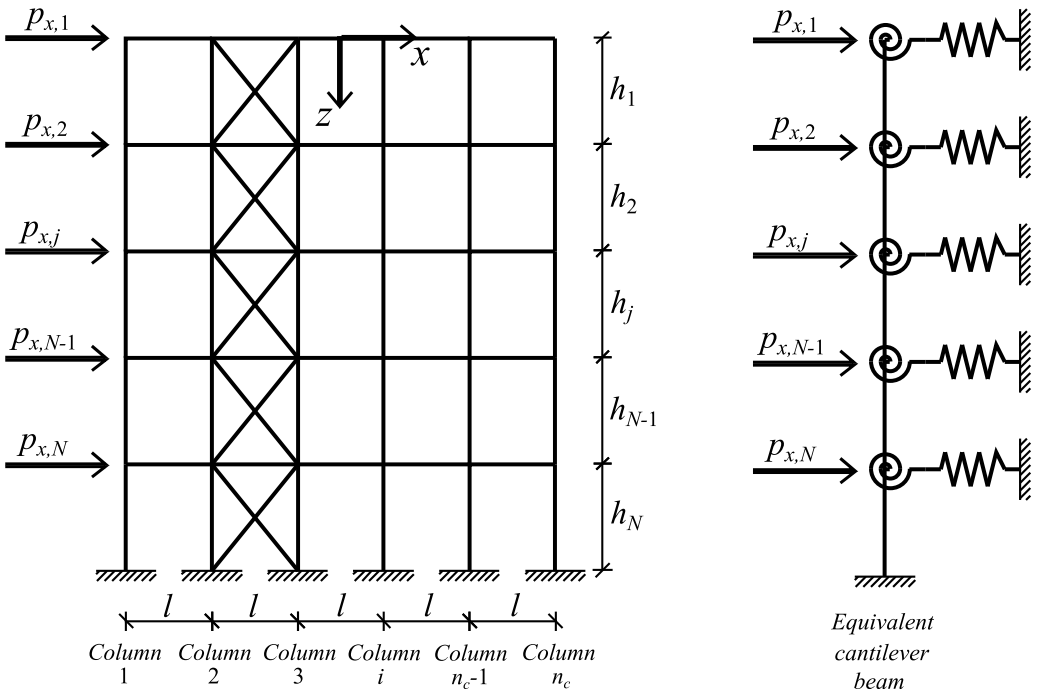

Figure 2.13: (a) Braced frame; (b) Continuous equivalent cantilever beam

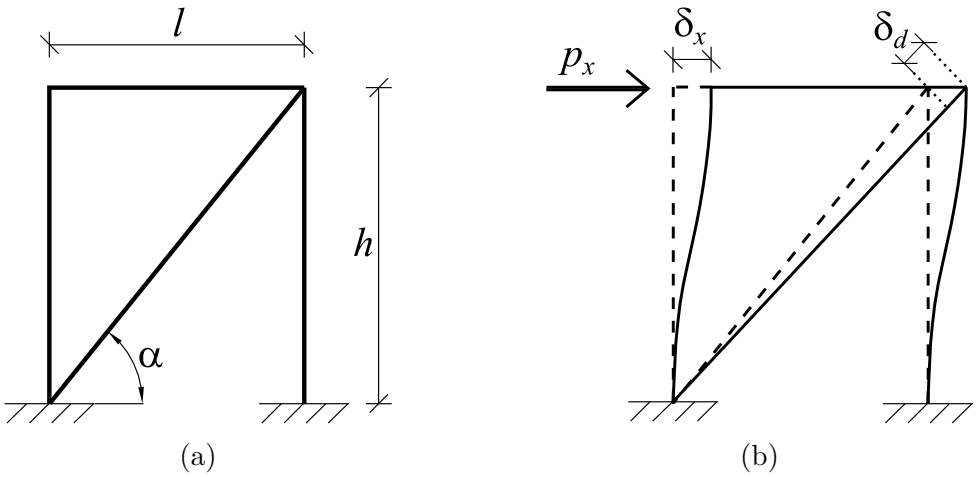

Figure 2.14: (a) Geometry of the single braced module of the frame; (b) Deformed shape

$$[k_{xx}] = EJ_{eq} \begin{bmatrix} 1/h_1^3 + n_b k_{x,d} & -1/h_1^3 & \cdots & 0 \\ -1/h_1^3 & 1/h_1^3 + 1/h_j^3 + n_b k_{x,d} & \cdots & 0 \\ \vdots & \vdots & \ddots & \vdots \\ 0 & 0 & \cdots & 1/h_N^3 + n_b k_{x,d} \end{bmatrix} \quad (2.96)$$

where n_b indicates the number of the braced module per each floor.

Then, by proceeding as described in the previous section, the condensed form of $N \times N$ stiffness matrix in x-direction is obtained.

$$[K_x] = \left[[k_{xx}] - \left[k_{x\varphi_y}\right] \left(\left[k_{\varphi_y\varphi_y}\right]^{-1} \left[k_{\varphi_y x}\right] \right) \right] \tag{2.97}$$

where the matrix $\left[k_{x\varphi_y}\right]$, $\left[k_{\varphi_y x}\right]$, and $\left[k_{\varphi_y\varphi_y}\right]$ can be evaluated with Equations (2.88b, 2.88c, and 2.91).

Eventually, considering that also in this case the frame has no stiffness outside the plane that contains it and that it has no torsional stiffness, means the whole element stiffness matrix ($3N \times 3N$) expressed in the local reference system, shall take the following form:

$$[K^*] = \begin{bmatrix} [K_x] & 0 & 0 \\ 0 & 0 & 0 \\ 0 & 0 & 0 \end{bmatrix} \tag{2.98}$$

2.4 Framed tube

The structural behavior of a high-rise building towards the horizontal actions in the first approximation is like that of a cantilever beam clamped at the base.

The bending moment induces tensile forces in the windward frames and compressive forces in the downwind frames with respect to the direction of the horizontal actions. Analyzing the theoretical distribution of axial stress in the columns of the frame, we observe a non-linear stress distribution with a significant increase in correspondence of the columns placed in the corners and a reduction in correspondence of the central zones of the respective sides, as shown in Figure (2.15). This singularity is called *shear lag effect*.

In the first half of the 1940s, the importance of this problem is understood, especially with regard to the components of airplane structures [148], [149], [213], [214], which were getting bigger and heavier in those years. The first applications in the field of civil engineering took place in the 1960s, for the design of box girder bridges [1], [246]. In particular, the work of Malcolm [170], convergent series expressions are used to represent the longitudinal and shear stresses in the flange. In the 1960s, the concept of an equivalent continuous elastic model was introduced by Rosman to study the shear walls provided with openings [219], [220], [222].

In 1973, Bažant and Christensen [21] modelled the rigid nodes frames of a high-rise building with an equivalent continuous system. This technique involved a series of different equations that were solved with the Finite Difference Method, obtaining with a good approximation.

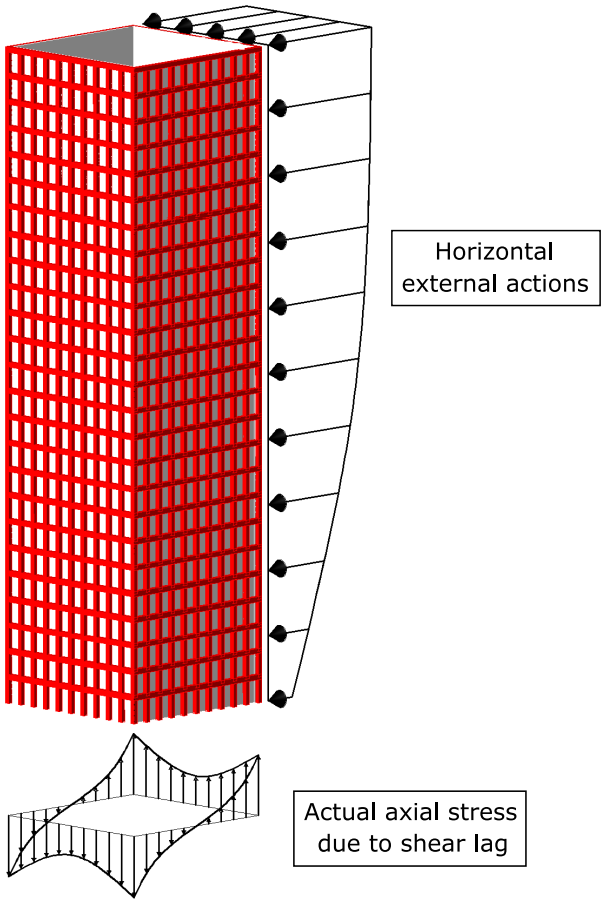

Figure 2.15: Distribution of axial stresses in the column of the framed tube building [187]

In 1974 Chan et al. [66] proposed a method to evaluate the stress intensification due to the shear lag effects in buildings composed of frames and shear walls rigidly connected to each other.

In those same years Coull et al. [75], [76], [77], [87], developed a formulation for analyzing framed tube that consists of modelling the frames using equivalent orthotropic membranes with equivalent mechanical characteristics. In this way they determined that the course of axial forces in the columns was approximate with cubic and parabolic functions. The concept of equivalent orthotropic membranes for modelling frames was also used by other authors, including which we cite the works of Khan [137], [138] and Ha [117]. The latter further developed this concept by introducing an orthotropic membrane having equivalent elastic properties by which it was possible to describe the deformations of the frame elements and the deformations of the beam-column joints. This approach is more refined than the

others, although the calculation burden becomes significant.

In the 1980s Foutch and Chang [102], and Chang and Zheng [67] observed that the distribution of normal forces on the upper floors of tubular structures shows an increase in the central pillars of the frames. They called this singularity *negative shear lag*.

In the following years many authors proposed more or less simple models to analyze the framed tubes, some based on the concept of equivalent membrane proposing different procedures to calculate the equivalent characteristics, such as the technique proposed by Kwan [150], which can be seen as the simplification of the method by Ha. Like these procedures is the formulation proposed by Connor and Poungare [74] in which the structure is modeled as a series of stringers and shear panels. Other authors proposed analytical methods based, for example, on Airy Stress Functions [118], or semi-analytically using shape functions to describe the shear lag [167].

Developments in these analytical models have been used to study framed tube structures and outrigger [158], [209], [210], or tube-in-tube structures [159].

The analytical formulation presented in this work was developed by Nitti [187] and is based on the Taylor series expansion method of shear stress [204]. The originality of the formulation is to model the frames as equivalent cantilever beams, whose geometrical and mechanical characteristics are obtained using appropriate simplified assumptions. By using this procedure it is possible to analyze buildings with frames orthogonal to each other or with a polygonal floor plan, thus making the spectrum of use of this analytical calculation methodology very broad.

2.4.1 Definition of the cantilever beam equivalent to the frame

A plane frame subject to a system of lateral forces contained in its own plane, in first approximation, is a *perforated wall*. Experimentally it can be noted that if distance between the columns of the frame is sufficiently small if compared to floor height, the deformation of the structure will tend to that of a cantilever beam. If we consider a frame having these characteristics, which is common in a high-rise framed tube buildings, we can isolate a *basic module* whose width is equal to the distance between the columns, while the height is equal to the interstorey, as shown in Figure (2.16).

Extrapolating the *basic module* from the frame, it is necessary to introduce appropriate constraints and, wishing to study relative displacements with respect to a local system; hinges are inserted at the ends because the presence of inflection points of the elastic line of the entire frame is assumed, as shown in Figure (2.17).

The concentrated load Q equivalent to the external distribuited load acting on the portion of the frame under examination, is applied to the system thus defined.

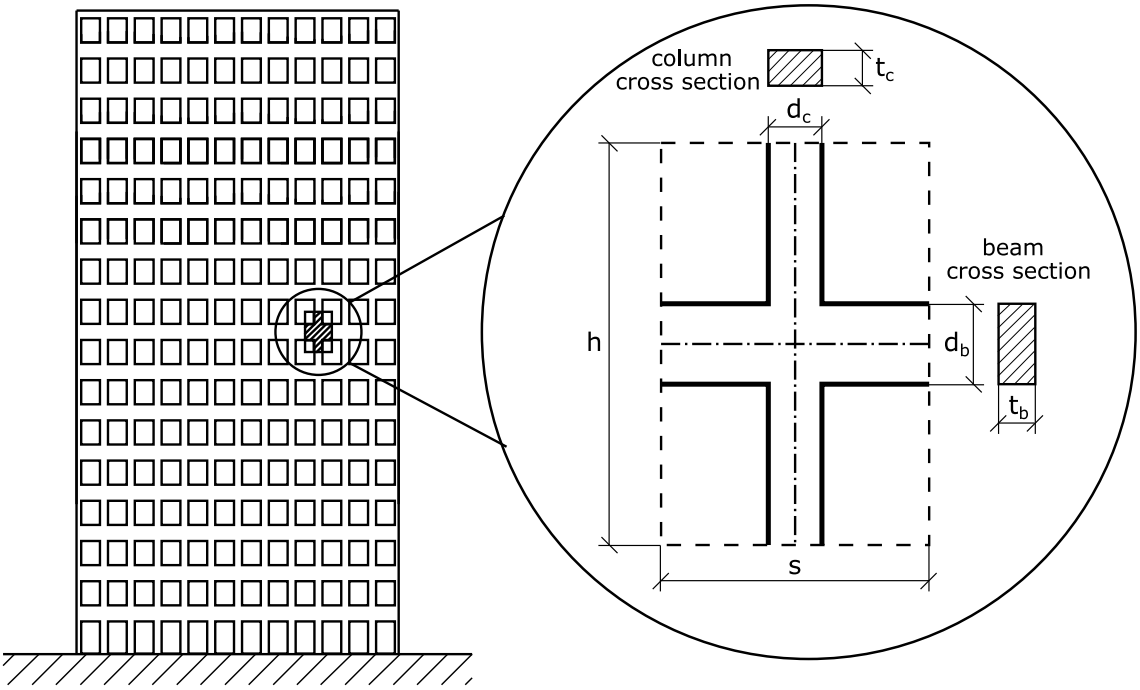

Figure 2.16: Geometry of the basic module [187]

Lateral displacement Δ is considered as the sum of the contribution due to the bending Δ_b, and shear forces Δ_v in the rods, respectively, and the contribution due to shear deformability of the beam-column joint, indicated by Δ_{vj}.

With reference to the static scheme shown in Figure (2.17), the displacements Δ_b, Δ_v, and Δ_{vj} can be evaluated by applying the Principle of Virtual Work, considering flexural and shearing deformability.

Applying the Superposition Principle,

$$\Delta = \Delta_b + \Delta_v + \Delta_{vj} \tag{2.99}$$

where the horizontal displacement due to the bending moment is equal to:

$$\Delta_b = Q\left[\frac{(h-d_b)^3}{12EI_c} + \frac{h^2}{s^2}\frac{(s-d_c)^3}{12EI_b}\right] \tag{2.100}$$

the frame displacement due to the shear force is equal to:

$$\Delta_v = Q\left[\frac{(h-d_b)}{GA_{sc}} + \frac{h^2}{s^2}\frac{(s-d_c)}{GA_{sb}}\right] \tag{2.101}$$

while the horizontal displacement contribution due to the deformability of the beam-column joint may be written as follows:

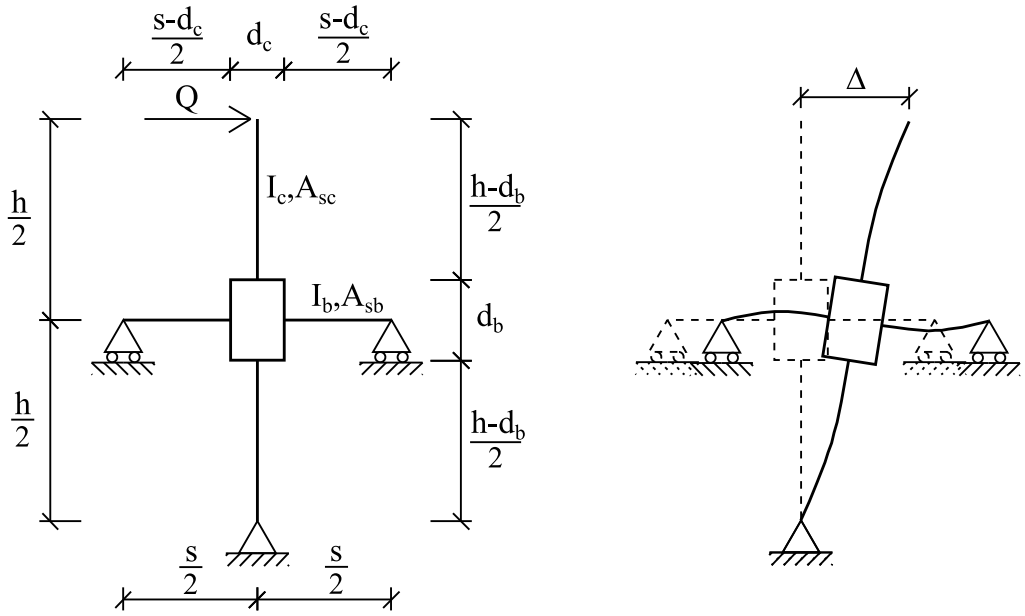

(a) (b)

Figure 2.17: (a) Geometry of basic module under lateral force Q; (b) Elastic line of the basic module [187]

$$\Delta_{vj} = \frac{Qh^2}{GA_{sj}d_b}\left(\frac{d_b}{h} + \frac{d_c}{s} - 1\right)^2 \tag{2.102}$$

where A_{sc} and A_{sb} are the shear area of beams and columns, respectively, while A_{sj} indicates the area of the joint defined as the product d_c by d_b. For the details, reference is made to [187].

Introducing an elastic membrane having dimensions equal to the height and width of the basic module, if subject to the same load, it is required to have the same Δ horizontal displacement (Figure 2.18).

Assuming, as permissible, that this membrane presents only shear deformability, it can be written that:

$$\Delta = \frac{Qh}{G_{xy}A_m} \tag{2.103}$$

where G_{xy} is the shear elastic modulus of the membrane and A_m is the area of its cross section defined as:

$$A_m = ts \tag{2.104}$$

Considering that the elastic modulus E of the membrane is the same as that of the frames, for congruence of deformations it must be imposed that the area of the

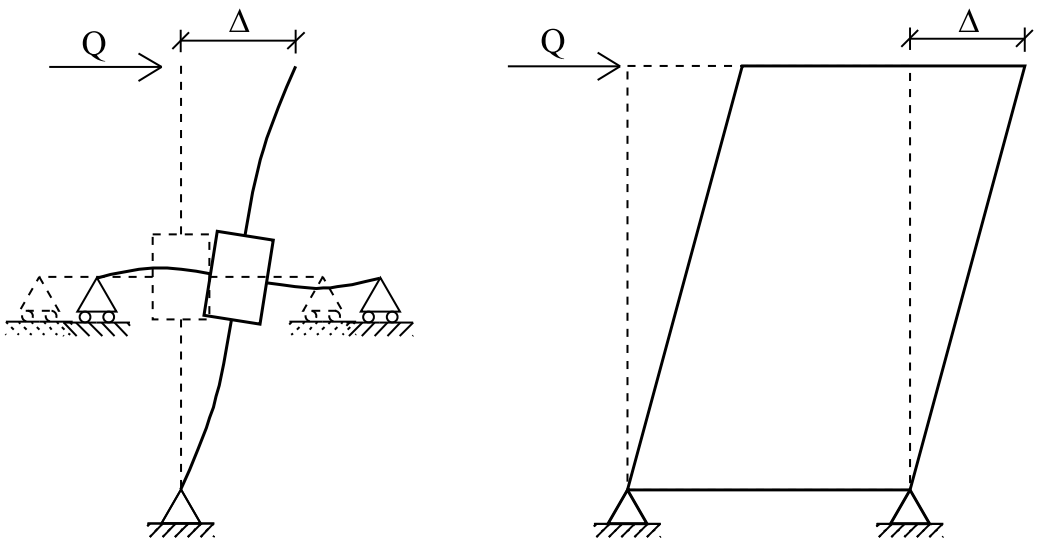

Figure 2.18: (a) Elastic line of the basic module Q; (b) Deformed shape of the equivalent membrane [187]

membrane is equal to the area of the column A_c, consequently it is determined the thickness of the membrane equivalent to the frame t_{eq}:

$$t_{eq} = \frac{A_c}{s} \tag{2.105}$$

By replacing the equations and performing some simple mathematical steps, it is possible to determine the coefficient C_G defined as:

$$\begin{aligned} C_G = & \frac{(h-d_b)^3}{12hI_c} + \frac{h}{s^2}\frac{(s-d_c)^3}{12I_b} + \\ & + \frac{E}{G}\left[\frac{h-d_b}{hA_{sc}} + \frac{h}{s^2}\frac{(s-d_c)}{A_{sb}} + \frac{h}{A_{sj}d_b}\left(\frac{d_b}{h} - 1 + \frac{d_c}{s}\right)^2\right] \end{aligned} \tag{2.106}$$

by means of which it is possible to calculate the shear elastic modulus of the membrane, formally expressed as:

$$G_{xy} = \frac{E}{C_G t_{eq} s} \tag{2.107}$$

Finally, considering that as whole tall buildings are being analyzed, it is intrinsic in the problem that the height of the frame prevails with respect to the width, consequently the two-dimensional effect of the membrane can be neglected by making it behave like a cantilever beam whose equivalent shear elastic modulus shall be equal to:

$$G_{eq} = G_{xy} = \frac{E}{C_G t_{eq} s} \tag{2.108}$$

It has thus been shown that this type of frame can be modelled like a equivalent cantilever beam having its same height and width, but with thickness as defined in Equation (2.105). However, regards the mechanical characteristics, the equivalent beam has the same Young's modulus as frame (assumed to be the same for beams and columns) while shear elastic modulus has been defined in Equation (2.108).

2.4.2 Analytical model of the framed tube

The analytical formulation is based on the fundamental hypotheses:

- the material of the beams and columns is isotropic, linear elastic and homogenous;
- the columns and beams are mutually constrained;
- the frames are externally constrained by fixed-joints;
- the frames are connected along the edges of the structures;
- the storeys have the same height throughout the entire structure;
- the frames have null stiffness outside own plane.

Consider a building of N rectangular floor plan, as shown in Figure (2.19), the force-displacement relationship can be defined as follows:

$$\begin{Bmatrix} \{F_x\} \\ \{F_y\} \\ \{m_z\} \end{Bmatrix} = \begin{bmatrix} [K_x] & 0 & 0 \\ 0 & [K_y] & 0 \\ 0 & 0 & [K_\vartheta] \end{bmatrix} \begin{Bmatrix} \{\xi\} \\ \{\eta\} \\ \{\vartheta\} \end{Bmatrix} \tag{2.109}$$

where the terms $\{F_x\}$, $\{F_y\}$, and $\{m_z\}$ represent the $N \times 1$ vectors containing the generalized floor forces, $[K_x]$, $[K_y]$, and $[K_\vartheta]$ represent the $N \times N$ stiffness matrices in the direction of referred to, while $\{\xi\}$, $\{\eta\}$, and $\{\vartheta\}$ represent the $N \times 1$ vectors containing the generalized floor displacements.

To determine the individual terms of the submatrices stiffness $[K_x]$ and $[K_y]$, the Betti's Theorem is used, that is, the unitary concentrated forces acting in the two main directions are applied to the structure, and the transverse floor displacements

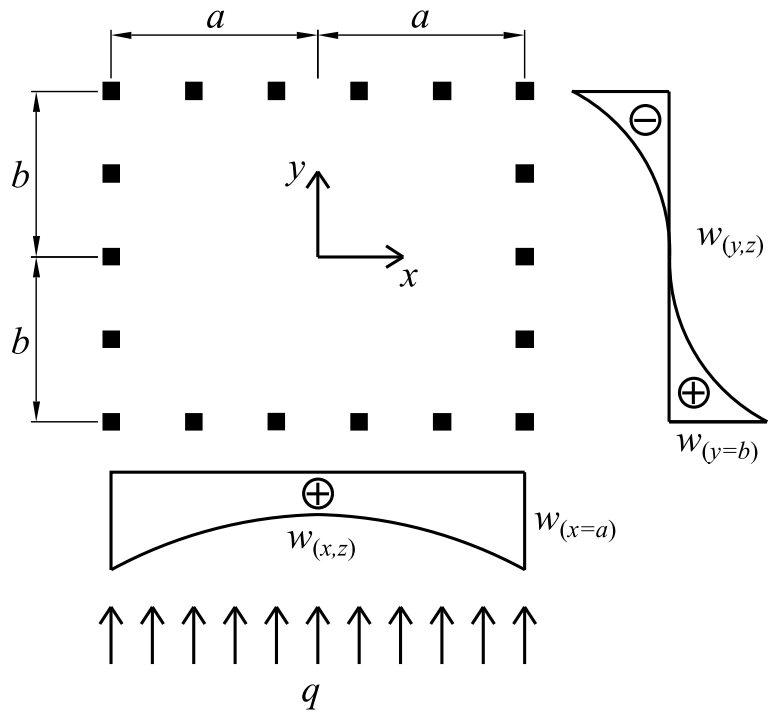

Figure 2.19: Floor plan of the building with distributions of axial displacements in the columns [187]

are evaluated. Rewriting everything in matrix form, the compliance matrices $[C_x]$ and $[C_y]$ with respect to x and y directions respectivey, will be obtained:

$$[C_x] = \begin{bmatrix} v_{x_{N,N}} & v_{x_{N-1,N}} & v_{x_{N-2,N}} & \cdots & v_{x_{1,N}} \\ v_{x_{N,N-1}} & v_{x_{N-1,N-1}} & v_{x_{N-2,N-1}} & \cdots & v_{x_{1,N-1}} \\ v_{x_{N,N-2}} & v_{x_{N-1,N-2}} & v_{x_{N-2,N-2}} & \cdots & v_{x_{1,N-2}} \\ \vdots & \vdots & \vdots & \ddots & \vdots \\ v_{x_{N,1}} & v_{x_{N-1,1}} & v_{x_{N-2,1}} & \cdots & v_{x_{1,1}} \end{bmatrix} \tag{2.110a}$$

$$[C_y] = \begin{bmatrix} v_{y_{N,N}} & v_{y_{N-1,N}} & v_{y_{N-2,N}} & \cdots & v_{y_{1,N}} \\ v_{y_{N,N-1}} & v_{y_{N-1,N-1}} & v_{y_{N-2,N-1}} & \cdots & v_{y_{1,N-1}} \\ v_{y_{N,N-2}} & v_{y_{N-1,N-2}} & v_{y_{N-2,N-2}} & \cdots & v_{y_{1,N-2}} \\ \vdots & \vdots & \vdots & \ddots & \vdots \\ v_{y_{N,1}} & v_{y_{N-1,1}} & v_{y_{N-2,1}} & \cdots & v_{y_{1,1}} \end{bmatrix} \tag{2.110b}$$

where the generic terms $v_{x_{i,j}}$ and $v_{y_{i,j}}$ indicate the transverse displacement (in x and y directions respectively) in correspondence of the j-th floor resulting from the application of a unitary concentrated force to i-th floor.

By definition, the stiffness sub-matrices $[K_x]$ and $[K_y]$ are evaluated:

$$[K_x] = [C_x]^{-1} \tag{2.111a}$$

$$[K_y] = [C_y]^{-1} \tag{2.111b}$$

Regarding the determination of the stiffness matrix $[K_\vartheta]$, by definition, can be written as:

$$[K_\vartheta] = 2\left([K_x^*]\, b^2 + \left[K_y^*\right] a^2\right) \tag{2.112}$$

where the terms $[K_x^*]$ and $\left[K_y^*\right]$ indicate the flexural stiffness of each frame developed in x and y directions, respectively. These last two terms are relative to the transverse displacements induced by the torsional moment and shall not be confused with terms relating to transverse displacements induced by horizontal loads (Equations 2.111). The transverse displacements in the direction of application of the load, separated in the quota-part due to the bending (v_M) and in the quota-part due to shear deformability (v_T), are evaluated with the following equations:

$$v_M = \frac{2}{H_M} \sum_{n=1}^{N} \left\{ C_{n,M} \cosh\left(\frac{\alpha_n a}{k}\right) \left[-\frac{\cos\left(\alpha_n z\right)}{\alpha_n} \right] + \frac{C_{n,M}}{\alpha_n} \cosh\left(\frac{\alpha_n a}{k}\right) \right\} \tag{2.113a}$$

$$v_T = \frac{2}{H_M} \sum_{n=1}^{N} \left\{ C_{n,T} \cosh\left(\frac{\alpha_n a}{k}\right) \left[-\frac{\cos\left(\alpha_n z\right)}{\alpha_n} \right] + \frac{C_{n,T}}{\alpha_n} \cosh\left(\frac{\alpha_n a}{k}\right) \right\} \tag{2.113b}$$

where H_M is the length of frame parallel to the load direction, and α_n is a parameter that holds $n\pi/2H$ (with $n = 1,2,3,...$).

The geometric parameter k is defined as follows:

$$k = \sqrt{\frac{12I}{hA_c s}} \tag{2.114}$$

where s is distance between the columns.

The coefficients $C_{n,M}$ and $C_{n,T}$ are defined as follows:

$$C_{n,M} = \frac{T_{n,M} H_{M,eq}}{2EI_{M,eq}} \left[\alpha_n^2 \cosh\left(\frac{\alpha_n a}{k}\right) + \frac{H_{M,eq}^2 12I}{2I_{M,eq} h s^2} \frac{\alpha_n}{k} \sinh\left(\frac{\alpha_n a}{k}\right) \right]^{-1} \tag{2.115a}$$

$$C_{n,T} = \frac{T_{n,T} H_{M,eq}}{2EI_{M,eq}} \left[\alpha_n^2 \cosh\left(\frac{\alpha_n a}{k}\right) + \frac{H_{M,eq}^2 12I}{2I_{M,eq} h s^2} \frac{\alpha_n}{k} \sinh\left(\frac{\alpha_n a}{k}\right) \right]^{-1} \tag{2.115b}$$

where $H_{M,eq}$ is the lenght of the frames parallel to the load direction, while $I_{M,eq}$ is the moment of inertia of the cross section of the cantilever beam equivalent to the frame parallel to the load, defined as:

$$I_{M,eq} = \frac{1}{12} H_{M,eq}^3 t_{eq} \tag{2.116}$$

The terms $T_{n,M}$ and $T_{n,T}$ derive from the Fourier series expansion of the shear stress, which evaluated for a concentrated load applied to the H_{max} level with respect to the base of the building. They can be rewritten in the following form:

$$T_{n,M} = P\left[\frac{4}{n\pi}\left(1 - \cos\left(\frac{n\pi}{2H} H_{max}\right)\right)\right] \tag{2.117a}$$

$$T_{n,T} = P^*\left[\frac{4}{n\pi}\left(1 - \cos\left(\frac{n\pi}{2H} H_{max}\right)\right)\right] \tag{2.117b}$$

where P indicates the intensity of the real concentrated horizontal load applied to each floor level of the structure, while P^* is the concentrated horizontal load that provides the contribution of flexural displacement equal to the contribution of shear deformability due to P, and is defined as:

$$P^*_{(z)} = P\frac{EI_{eq}}{G_{eq}A_{s,eq}}\left[\left(\frac{H}{2} - \frac{z}{6}\right)z\right]^{-1} \tag{2.118}$$

Given the N coefficients $C_{n,x} = C_{n,M} + C_{n,T}$, evaluated for the frame orthogonal to the load direction (Equations 2.115a and 2.115b), it is possible to evaluate the axial displacements at the generic height z, depending on the floor plan position of the column under consideration:

$$w_{(x,z)} = \sum_{n=1}^{N} C_{n,x} \cosh\left(\frac{\alpha_n x}{k}\right) \sin\left(\alpha_n z\right) \tag{2.119}$$

while the axial displacements of the frame parallel to the load direction are described by the following antisymmetric function:

$$w_{(y,z)} = \sum_{n=1}^{\infty} C_{n,y} \sinh\left(\frac{\alpha_n y}{k}\right) \sin\left(\alpha_n z\right) \tag{2.120}$$

Imposing the congruence of the axial displacements along the edge of the structure, that is:

$$w_{(x=a)} = w_{(y=b)} \tag{2.121}$$

the coefficients $C_{n,y}$ are equal to:

$$C_{n,y} = \frac{C_{n,x} \cosh\left(\frac{\alpha_n a}{k_x}\right)}{\sinh\left(\frac{\alpha_n b}{k_y}\right)} \tag{2.122}$$

where the terms k_x and k_y are the constants calculated by Equation (2.114) evaluated for the frame in x-direction and for the frame in y-direction, respectively.

Finally, it is possible to evaluate the normal stresses in the continuous equivalent membrane by means of the following relation:

$$n = s_1 E \sum_{n=1}^{N} C_{n,y} \sinh\left(\frac{\alpha_n y}{k}\right) \alpha_n \cos\left(\alpha_n z\right) \tag{2.123}$$

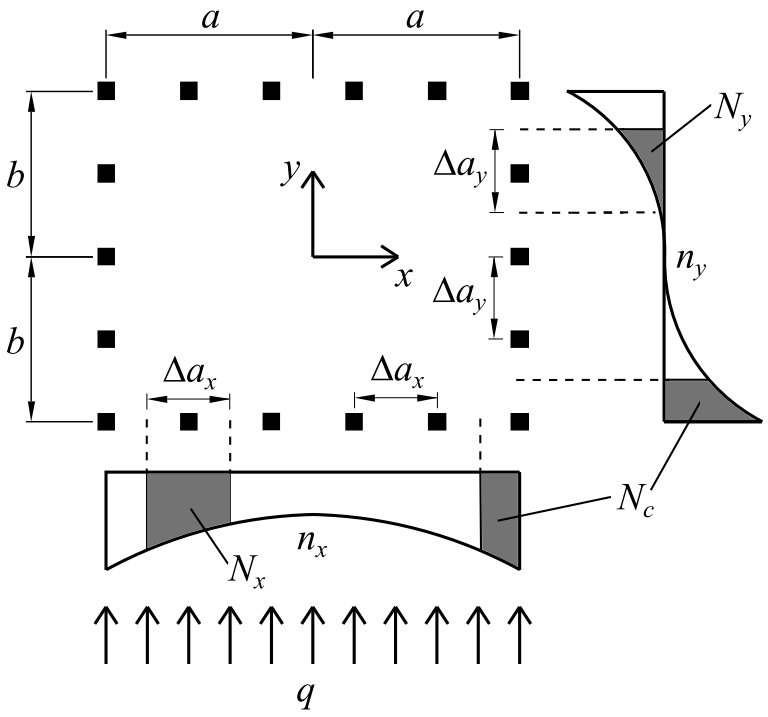

Figure 2.20: Distributions of axial forces in the columns [187]

Given the axial stress distributions, it is possible to determine the axial stresses acting on the internal columns of the frames, evaluates as:

$$N_{x(z)} = n_{(x=x_p,z)} \Delta a_x \tag{2.124a}$$

$$N_{y(z)} = n_{(y=y_p,z)} \Delta a_y \tag{2.124b}$$

while for the columns located in the corners of the structure, the axial stress is assessed as:

$$N_{c(z)} = n_{(x=a,z)} \frac{\Delta a_x}{2} + n_{(y=b,z)} \frac{\Delta a_y}{2} \tag{2.125}$$

Until now, a structure subject only to horizontal loads has been analyzed, but in the field of construction, a building can also be subject to torque moments (Figure 2.21a), for example, in the case where the center of the stiffness does not coincide with the center of the floor masses (where seismic forces are applied),

making it necessary to determine a further unknown factor of the problem, that is, the rigid plane rotations must be calculated. To do this it is necessary to introduce an additional calculation model in which the torsional moment m_z is subdivide into four equal equivalent forces, later indicated with $F_{m_z,x}$ and $F_{m_z,y}$, acting simultaneously on the construction, as shown in Figure (2.21b). In doing so, a geometrically symmetrical structure is obtained, but loaded in an antisymmetric manner.

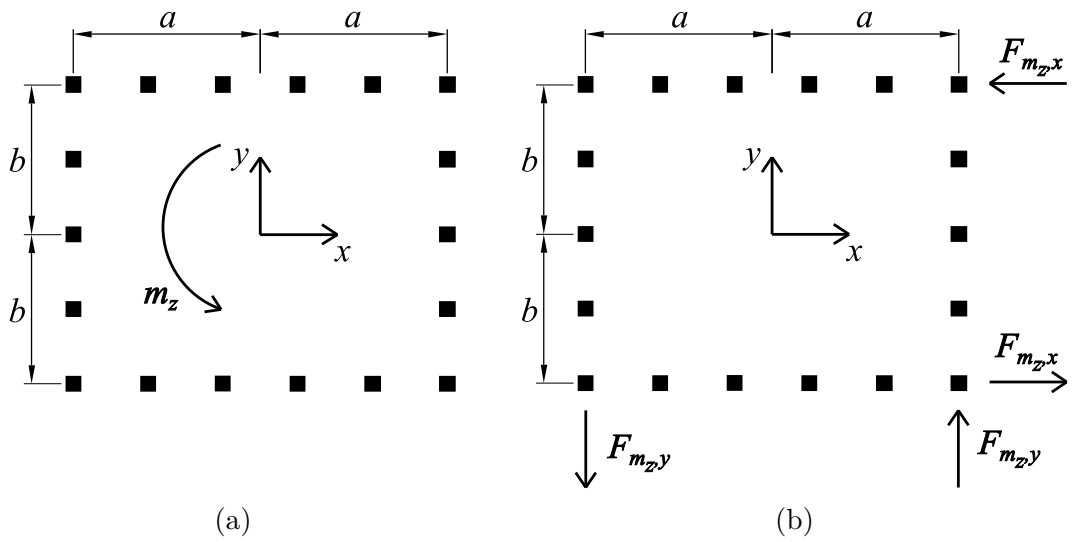

(a) (b)

Figure 2.21: (a) Actual torsional moment; (b) Four equal equivalent forces [187]

To evaluate the floor displacements, the same calculation philosophy already illustrated is used, but in this case all the frames with the same antisymmetric load condition, consequently the axial displacements are defined as:

$$w_{(x_L,z)} = \sum_{n=1}^{\infty} F_n\left(x_L\right) \sin\left(\alpha_n z\right) \tag{2.126}$$

where with x_L the axis of the local reference system direct along the development of each frame, is indicated, while the function F_n is formally defined as:

$$F_n(x_L) = C_{1n} e^{\frac{\alpha_n x_L}{k}} + C_{2n} e^{-\frac{\alpha_n x_L}{k}} \tag{2.127}$$

Since the frame is loaded in an antisymmetric way, the structural response in terms of displacement must also be antisymmetric, therefore it is evident that the function $F_n(x_L)$ must be antisymmetric:

$$F_n\left(x_L\right) = C_n \sinh\left(\frac{\alpha_n x_L}{k}\right) \tag{2.128}$$

Replacing Equation (2.128) in Equation (2.126), gives:

$$w_{(x_L,z)} = \sum_{n=1}^{\infty} C_n \sinh\left(\frac{\alpha_n x_L}{k}\right) \sin\left(\alpha_n z\right) \tag{2.129}$$

Eventually, after calculating the C_n coefficients relative to each frame (defined with $C_{n,x}$ and $C_{n,y}$), the transverse displacements of the floor are evaluated:

$$v_{x=a} = \frac{2}{2b} \sum_{n=1}^{\infty} \left\{ C_{n,x} \sinh\left(\frac{\alpha_n a}{k_x}\right) \left[-\frac{1}{\alpha_n} \cos\left(\alpha_n z\right)\right] + C_{n,x} \sinh\left(\frac{\alpha_n a}{k_x}\right) \frac{1}{\alpha_n} \right\} \tag{2.130}$$

In constructive reality, design buildings consisting only from four sides is an understatement as well as being highly influential from an architectural point of view, which is why over the years many buildings have been designed with a more or less regular polygonal floor plan. The calculation method presented in this section can also be extended to buildings with a non-rectangular floor plan, with the foresight to analyze the forces acting on each frame after appropriately breaking down the loads. Finally, by the Superposition Principle, the displacements and stresses are determined at each point of the structure.

2.5 Diagrid structures

Diagrid systems have been widely exploited in the last few decades because of their efficacy in resisting lateral forces, minimizing lateral displacements, and their suitability to realize complex-shaped structures allowing to achieve remarkable architectural effects [15]. The resisting mechanism is based on the axial forces in diagonal members, which are able to carry both lateral actions and vertical loads, thus leading to the uselessness of conventional vertical columns. Plenty of research has been conducted in the last ten years investigating diagrid behavior and characteristics. For example, Moon et al. [184], [185] proposed a simplified analytical methodology for the preliminary design of diagrid tube structures. Zhang et al. [281] generalized Moon's approach for the case of diagrid tubes composed of straight diagonals with gradually varying angles, whereas Mele et al. [174] proposed an hand-calculation methodology to investigate real case studies. More recently, Liu and Ma [164] made use of a modular procedure to evaluate the shear and bending stiffness for arbitrary polygonal diagrid tube structures, while Lacidogna et al. [153] developed a matrix-based method to perform the structural analysis of generic diagrid structures, providing information not only regarding the shear and bending behavior but also the torsional flexibility. In the literature it was also shown that diagrid structures are suitable for optimization procedures if changing geometrical parameters, such as the inclination of external diagonals [15], [185]. For example, Montuori et al. [183] performed Finite Element (FE) analyses in order to investigate the effect of different geometrical patterns (regular, variable angle

and variable density pattern) on the structural performance. FE calculations with similar aims were also carried out by Angelucci and Mollaioli [10], [11], [12], and Tomei et al. [253].

Finally, the structural analysis of an external diagrid system coupled with internal shear walls is carried by Lacidogna et al. [152]. In this work the structural behavior is investigated under both lateral forces and torque moments distributed along the height of the building. Different inclinations of the external diagonals are also considered, in order to explore the effect of this geometrical parameter on the lateral and torsional flexibility. Furthermore, the effect of the shear wall type, i.e. closed- or open-section, is investigated on the structural response, and a description of a multi-parameter approach, is presented, which allows to take into account variable inclinations of the external diagonals and considers a large set of possible geometrical patterns.

The method proposed by Lacidogna et al. [153] will be briefly explained in this work as it has allowed the direct calculation of the diagrid stiffness matrix.

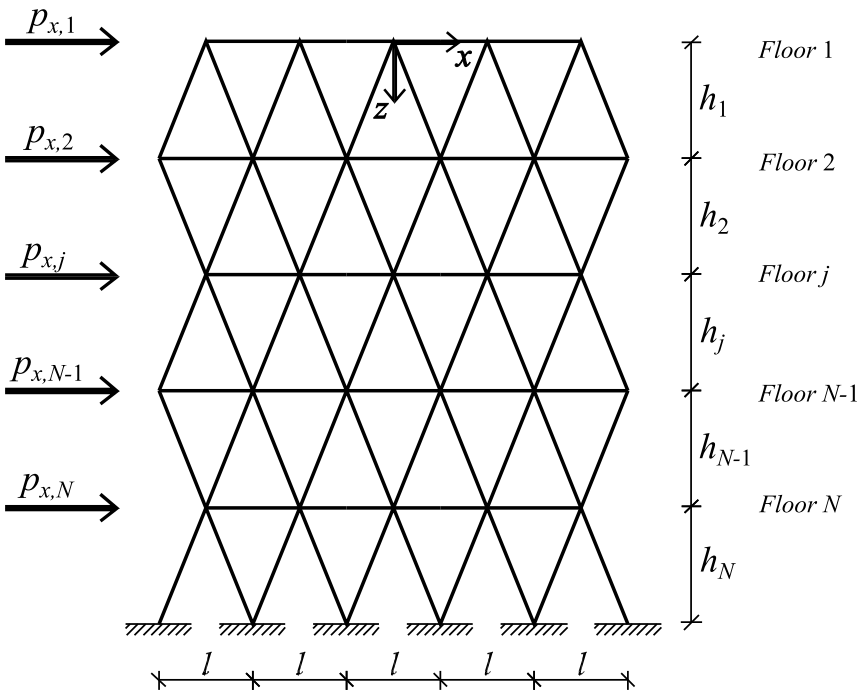

Figure 2.22: Plane diagrid structure

Consider a plane diagrid structure composed by N storeys, as shown in Figure (2.22). Since the system presents only 1 degree of freedom, that is the horizontal displacement of each floor in x-direction (ξ), the force-displacement relationship can be written as:

$$\begin{Bmatrix} p_{x,1} \\ p_{x,2} \\ p_{x,j} \\ \vdots \\ p_{x,N} \end{Bmatrix} = \begin{bmatrix} k_{x_{1,1}} & k_{x_{2,1}} & k_{x_{j,1}} & \cdots & k_{x_{N,1}} \\ k_{x_{1,2}} & k_{x_{2,2}} & k_{x_{j,2}} & \cdots & k_{x_{N,2}} \\ k_{x_{1,j}} & k_{x_{2,j}} & k_{x_{j,j}} & \cdots & k_{x_{N,j}} \\ \vdots & \vdots & \vdots & \ddots & \vdots \\ k_{x_{1,N}} & k_{x_{2,N}} & k_{x_{j,N}} & \cdots & k_{x_{N,N}} \end{bmatrix} \begin{Bmatrix} \xi_1 \\ \xi_2 \\ \xi_j \\ \vdots \\ \xi_N \end{Bmatrix} \tag{2.131}$$

or in compact form:

$$\{p_x\} = [K_x]\{\xi\} \tag{2.132}$$

The corresponding coefficient $k_{i,j}$ of the $N \times N$ stiffness matrix $[K_x]$ is obtained by imposing a horizontal unitary displacement to the j-th floor, keeping fixed all other floors, and calculating the total force that is generated in all the other i-th storeys of the structure. Obviously, as the diagrid can be assimilated to a truss structure, this force is affected by the axial deformation of the diagonal rods δ_d.

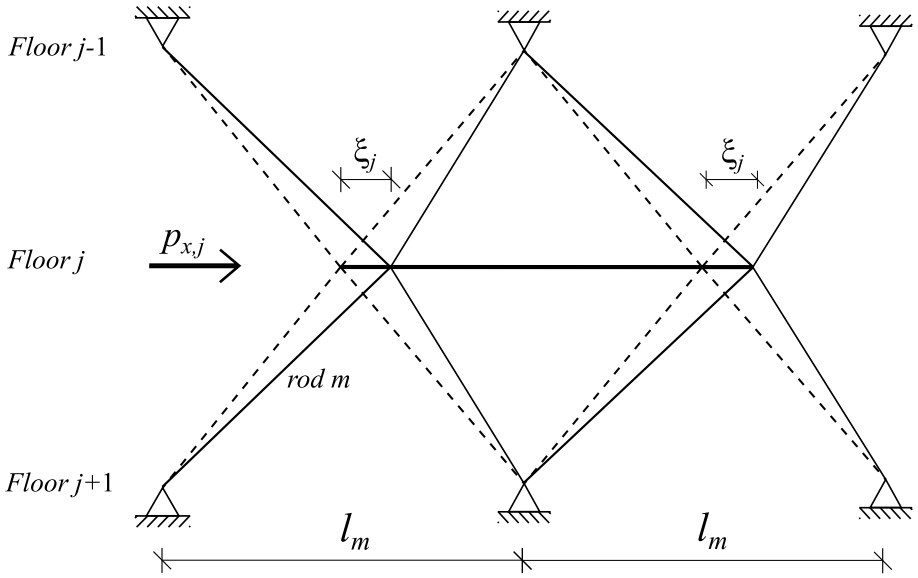

Figure 2.23: Imposed deformation δ_x of the j-th floor

Considering the generic m-th diagonal rod whose upper end is connected to the j-th floor to which the horizontal displacement ξ_j equal for all the rods because the floors are considered infinitely rigid, as shown in Figure (2.23), its axial elongation is equal to:

$$\delta_{d,m} = \xi_j \frac{L_m}{L_{d,m}} \tag{2.133}$$

where $L_m = l_m/2$ and $L_{d,m}$ is the actual length of the m-th diagonal rod. Since, by definition, a unitary horizontal displacement is imposed, the axial force in the

m-th rod is:

$$F_{d,m} = \frac{E_{d,m}A_{d,m}}{L_{d,m}}\delta_{d,m} = \frac{E_{d,m}A_{d,m}}{{L_{d,m}}^2}L_m\xi_j \tag{2.134}$$

where $E_{d,m}$ and $A_{d,m}$ indicate the normal elastic modulus and the area of the m-th diagonal rod, respectively. Projecting the axial stress $F_{d,m}$ along the horizontal direction, the stiffness of the m-th diagonal rod in the x-direction is obtained:

$$F_{x,m} = F_{d,m}\frac{L_m}{L_{d,m}} = \frac{E_{d,m}A_{d,m}}{{L_{d,m}}^3}{L_m}^2\xi_j = k_{x,m}\xi_j \tag{2.135}$$

Considering all M diagonal rods that converge in the j-th floor, the generic term $k_{i,j}$ of the stiffness matrix of the diagrid is obtained.

$$k_{i,j} = \sum_{m=1}^{M} k_{x,m} = \sum_{m=1}^{M} \frac{E_{d,m}A_{d,m}}{{L_{d,m}}^3}{L_m}^2 \tag{2.136}$$

Proceeding in this way assembles the stiffness matrix of the entire structure $[K_x]$.

Noted this stiffness matrix, and known the vector of horizontal loads applied to each floor $\{F_x\}$, the vector of transversal displacement $\{\xi\}$ of each floor is obtained:

$$\{\xi\} = [K_x]^{-1}\{p_x\} \tag{2.137}$$

Given the displacements of the j-th floor due to external load, the normal forces in each diagonal rod, which is a function of the drift $\xi_j - \xi_{j-1}$, are obtained:

$$N_{d,m} = \frac{E_{d,m}A_{d,m}}{{L_{d,m}}^3}L^2(\xi_j - \xi_{j-1}) \tag{2.138}$$

Following the same procedure, the contribution of rigid-rotation outside the floors can also be considered. In this case the structure has 2 degrees of freedom, and, to calculate the stiffness coefficients, it will be necessary to apply unitary rotations to the j-th floor and evaluate the reactive moments in i-th floors. This method provides more accurate results than the 1-DOF system, because it is also considered the component of vertical deformation of the diagonal rod, as shown in Figure (2.24).

The same procedure can also be applied to 3D diagrid systems, considering both a model a 3-DOF per floor (two translations in x and y directions, respectively, and rotation around the z axis), than at 6-DOF per floor. The latter model is the most complete (but also the most complex) and considers three displacements (ξ, η, and ζ) and three rotations with respect to x, y, and z axes (φ_x, φ_y, and ϑ).

Under these assumptions, the force-displacement relationship can be written as:

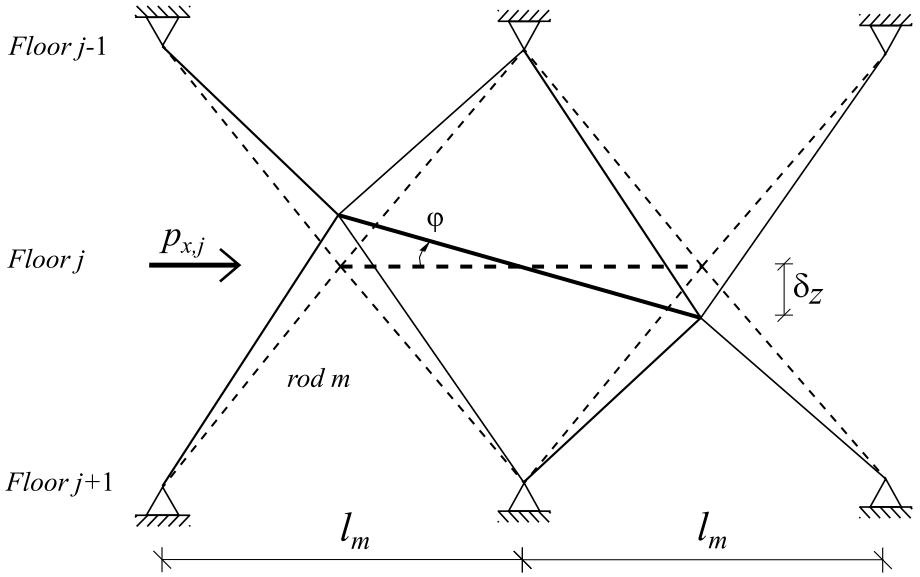

Figure 2.24: Imposed floor rotation φ of the j-th floor

$$\begin{Bmatrix} \{p_x\} \\ \{p_y\} \\ \{p_z\} \\ \{m_x\} \\ \{m_y\} \\ \{m_z\} \end{Bmatrix} = \begin{bmatrix} [K_{xx}] & [K_{yx}] & [K_{zx}] & [K_{\varphi_x x}] & [K_{\varphi_y x}] & [K_{\vartheta x}] \\ [K_{xy}] & [K_{yy}] & [K_{zy}] & [K_{\varphi_x y}] & [K_{\varphi_y y}] & [K_{\vartheta y}] \\ [K_{xz}] & [K_{yz}] & [K_{zz}] & [K_{\varphi_x z}] & [K_{\varphi_y z}] & [K_{\vartheta z}] \\ [K_{x\varphi_x}] & [K_{y\varphi_x}] & [K_{z\varphi_x}] & [K_{\varphi_x \varphi_x}] & [K_{\varphi_y \varphi_x}] & [K_{\vartheta \varphi_x}] \\ [K_{x\varphi_y}] & [K_{y\varphi_y}] & [K_{z\varphi_y}] & [K_{\varphi_x \varphi_y}] & [K_{\varphi_y \varphi_y}] & [K_{\vartheta \varphi_y}] \\ [K_{x\vartheta}] & [K_{y\vartheta}] & [K_{z\vartheta}] & [K_{\varphi_x \vartheta}] & [K_{\varphi_y \vartheta}] & [K_{\vartheta \vartheta}] \end{bmatrix} \begin{Bmatrix} \{\xi\} \\ \{\eta\} \\ \{\zeta\} \\ \{\varphi_x\} \\ \{\varphi_y\} \\ \{\vartheta\} \end{Bmatrix} \tag{2.139}$$

or in compact form:

$$\{F\} = [K]\{\delta\} \tag{2.140}$$

where $\{p_x\}$, $\{p_y\}$, and $\{p_z\}$ are the N-vectors containing respectively the floor forces in x, y, and z directions; $\{m_x\}$ and $\{m_y\}$ represents the N-vectors containing the bending moments with respect to the x and y axes; while $\{m_z\}$ is the N-vector containing the floor torsional moment with respect z axis. As for the floors displacements, $\{\xi\}$, $\{\eta\}$, and $\{\zeta\}$ are the N-vectors containing the displacements along x, y, and z axes respectively; $\{\varphi_x\}$ and $\{\varphi_y\}$ represent the N-vector containing the out-of-plane floor rotations with respect to x and y axes respectively, while $\{\vartheta\}$ is the floor rotations with respect to the vertical axis z.

2.6 Numerical examples

In order to confirm the validity of the analytical formulations previously illustrated, in this section some simple numerical examples are shown. In each example, only one type of vertical resistant element is taken into account, whose geometrical and mechanical characteristics are listed in figures and tables. Fixed the magnitude of the horizontal external load $\{F^*\}$ acting in the origin of the local reference system, and considering the stiffness matrix $[K^*]$ is assembled as shown in the previous sections, the vector $\{\delta^*\}$ containing the displacements of the local reference system origin of the bracing is evaluated using the following relationship:

$$\{\delta^*\} = [K^*]^{-1}\{F^*\} \tag{2.141}$$

Finally, the numerical results obtained using the analytical approach are compared with those obtained using commercial FEM software.

2.6.1 Shear wall

In this example the 60 meter-high shear wall shown in Figure (2.25) is considered, whose geometrical and mechanical characteristics are synthesized in Table 2.1. Since the element has a double symmetry floor plan and the load is applied in its centre of gravity, only x-direction transversal displacements are obtained, as shown in Figure (2.26).

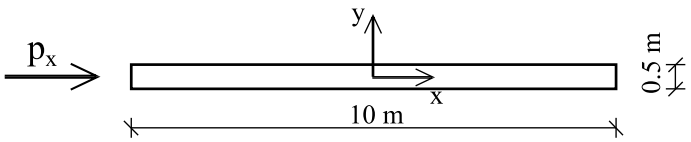

Figure 2.25: Rectangular shear wall floor plan

Table 2.1: Geometrical and mechanical characteristics of the shear wall

Number of storeys	15	-
Floor height	4	m
Normal elastic modulus	3×10^7	kN/m^2
Load p_x	100	kN/floor

As can be seen from Figure (2.26), the maximum difference between the analytical model and the FEM model is 2.6%.

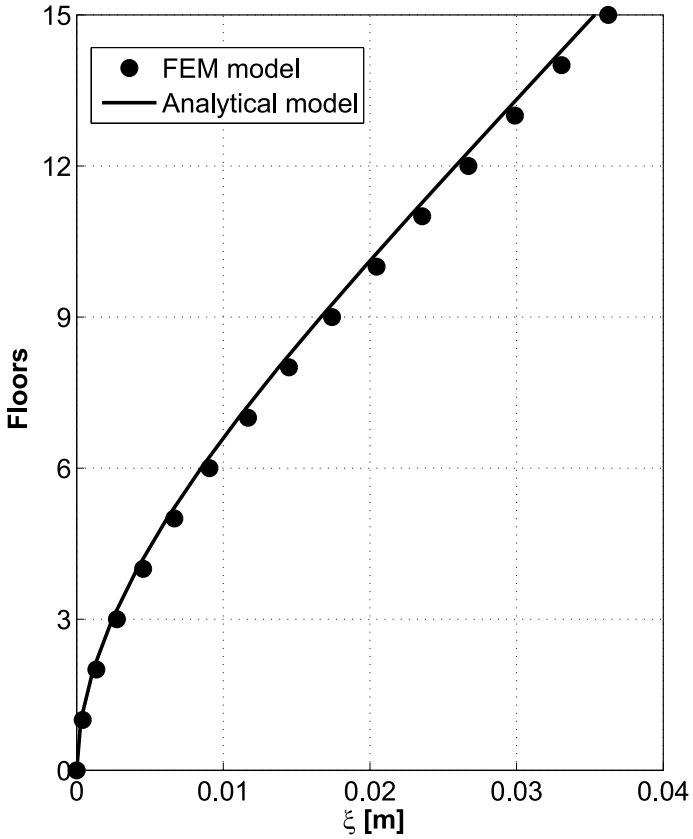

Figure 2.26: Rectangular shear wall transversal displacements

2.6.2 Thin-walled open-section shear wall

In this example the 60 meter-high thin-walled open-section shear wall shown in Figure (2.27) is considered, whose geometrical and mechanical characteristics are synthesized in Table 2.2.

Table 2.2: Geometrical and mechanical characteristics of the thin-walled open-section shear wall

Number of storeys	15	-
Floor height	4	m
Centre of gravity position	(0.00 , 0.00)	m
Shear centre position	(0.00 , 3.81)	m
Normal elastic modulus	3×10^7	kN/m^2
Load p_x	100	kN/floor

As it is well known, since the load $\{F^*\}$ is not applied in the shear centre of the

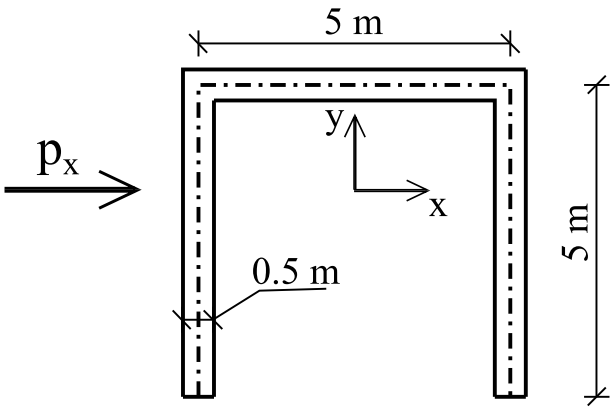

Figure 2.27: Thin-walled open-section shear wall floor plan

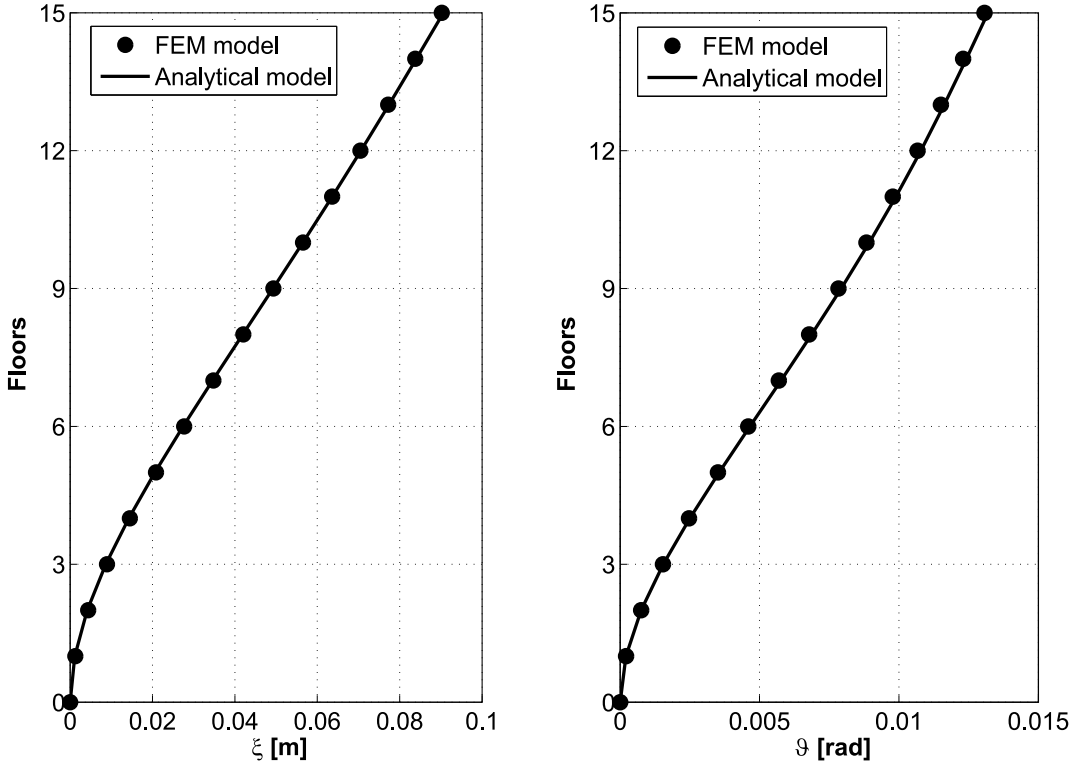

(a) (b)

Figure 2.28: Thin-walled open-section shear wall. (a) Transversal displacements; (b) Floor rotations

element, in addition to the x-direction transverse displacements, floor rotations ϑ are also generated as shown in Figures (2.28).

As it can be seen from Figure (2.28), the maximum differences between the

analytical model and the FEM model are -0.43% and -1.44% for transverse displacements and floor rotations respectively.

2.6.3 Plane frame

In this example the 60 meter-high plane frame shown in Figure (2.29) is considered, whose geometrical and mechanical characteristics are synthesized in Table 2.3.

Table 2.3: Geometrical and mechanical characteristics of the plane frame

Number of storeys	15	-
Floor height	4	m
Distance between the columns	4	m
Columns sizes	0.5×0.5	m
Beams sizes	0.5×0.8	m
Normal elastic modulus	3×10^7	kN/m^2
Load p_x	100	kN/floor

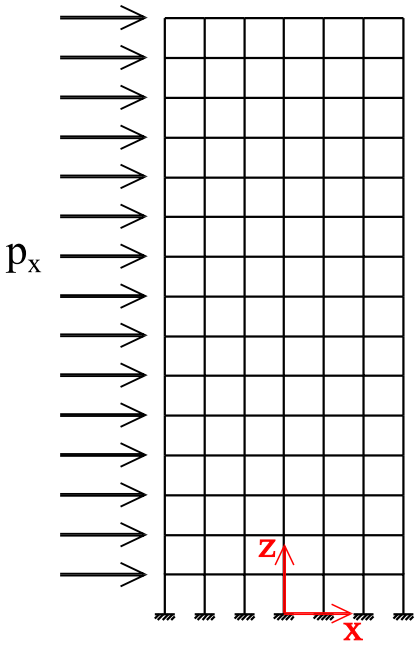

Figure 2.29: Plane frame front view

As shown in Figure (2.30) the maximum difference between the displacements obtained using the analytical formulation and those obtained using commercial FEM software is 4.7%.

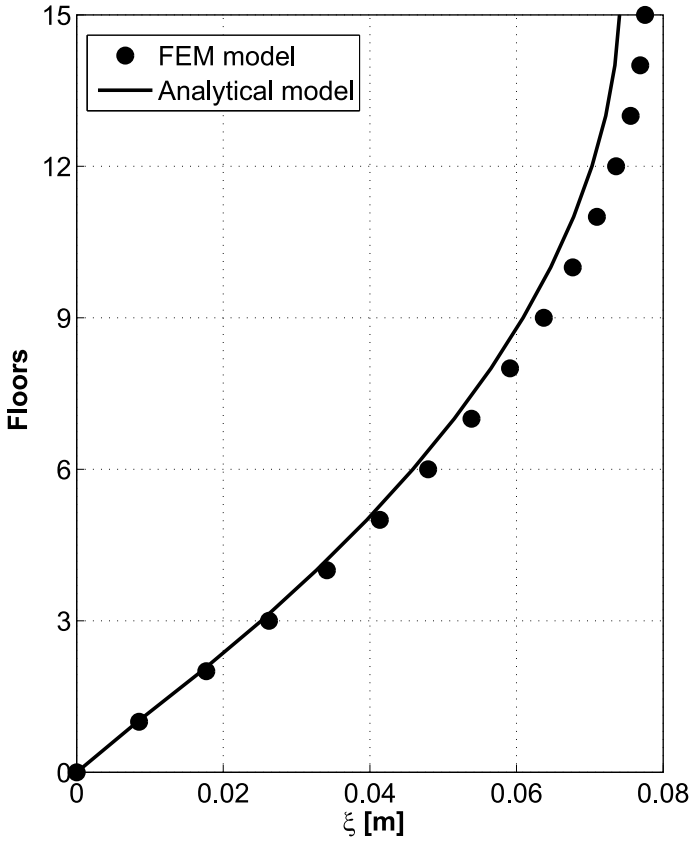

Figure 2.30: Plane frame transversal displacements

2.6.4 Braced frame

Let's consider now the same frame described in the previous section, with the addition of two diagonal rods for each storey as depicted in Figure (2.31). Each diagonal bar has the normal elastic modulus and cross section equal to 2.1×10^8 kN/m^2 and 7.85×10^{-2} m^2 respectively.

As shown in Figure (2.32), the maximum difference between the transversal displacements obtained using the analytical model and those obtained using the FEM software is 2.9%. These results do not change with respect to the position of the diagonal bars in the floor. In addition, comparing these values with those obtained by the model without the diagonal rods (Figure 2.30), it can be seen that by bracing the frame, the maximum transverse displacements are halved.

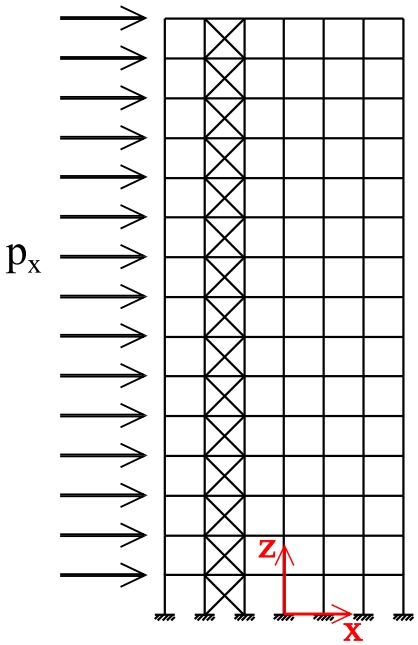

Figure 2.31: Braced frame front view

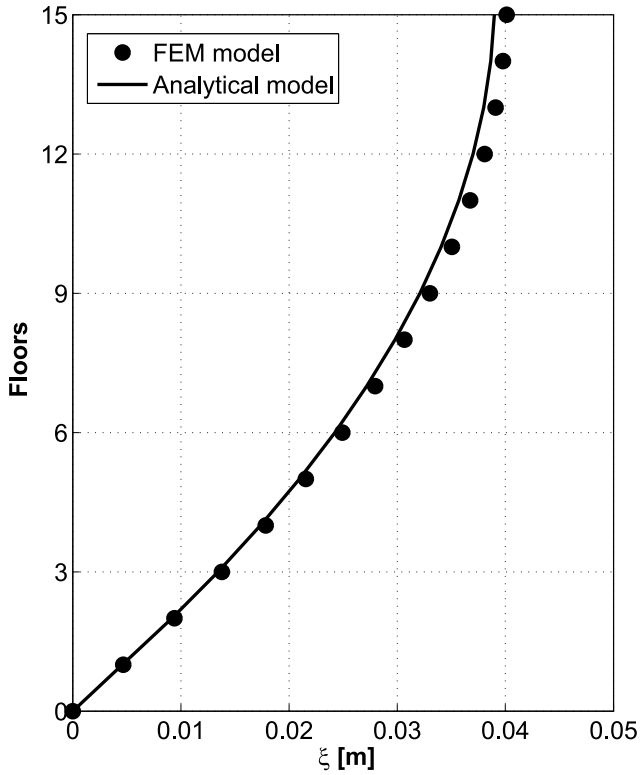

Figure 2.32: Braced frame transversal displacements

2.6.5 Framed tube

In this example a 120 meter-high framed tube structure shown in Figure (2.33) is considered, whose geometrical and mechanical characteristics are synthesized in Table 2.4. As depicted in Figure (2.34) the maximum difference between the displacements obtained using the analytical formulation and those obtained using commercial FEM software is 7.7%, but unlike previous cases, this value occurs about at the mid-height of the building and not at the top.

Table 2.4: Geometrical and mechanical characteristics of the framed tube structure

Number of storeys	40	-
Floor height	3	m
Distance between the columns	2	m
Columns sizes	0.5×0.5	m
Beams sizes	0.5×0.5	m
Normal elastic modulus	2×10^7	kN/m^2
Load p_x	100	kN/floor

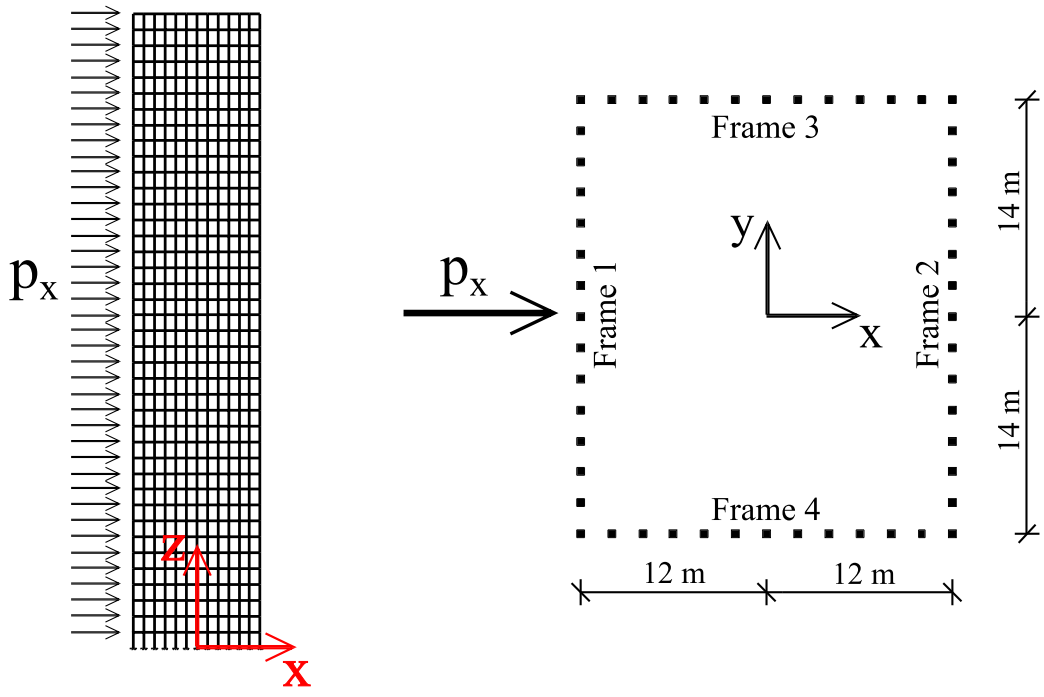

Figure 2.33: Framed tube structure. (a) Front view; (b) Floor plan

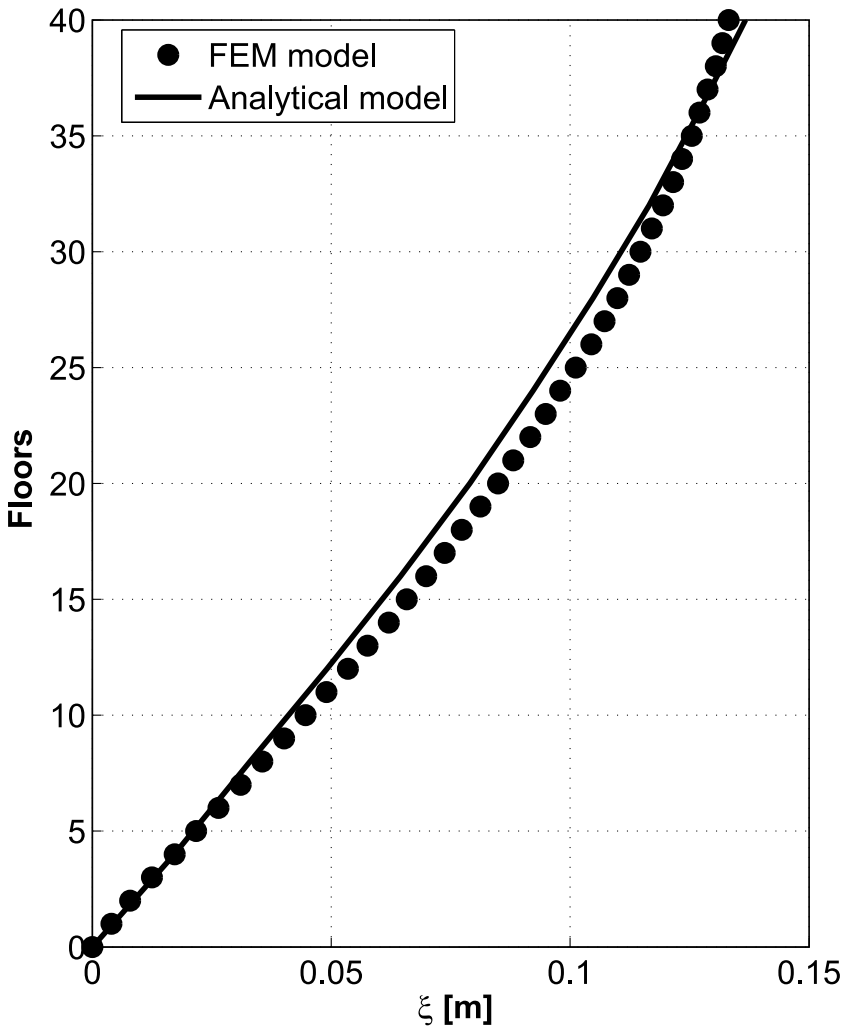

Figure 2.34: Framed tube transversal displacements

As illustrated in Section 2.4, since the main property of this type of structures is the shear lag effect, Figure (2.35) shows the intensity of the axial forces evaluated at the frame columns base section, where the non-linear trend of the normal stress can be appreciated. As can be seen, the columns belonging to frame 1 are all strained (Figure 2.35a) while, the columns belonging to frame 2 are all compressed (Figure 2.35b). In addition, it can be noted that the normal stress in the corner columns is more than three times higher with respect to the central frame columns. Figure (2.35c) is showing instead the trend of the normal stress in the columns belonging to frames 3 and 4. Also in this case the non-linear trend of the normal stress in the column is quite clear, and it can be seen that the central column is unloaded.

The maximum difference between the axial forces obtained using the analytical formulation and those obtained using commercial FEM software is 6.9%.

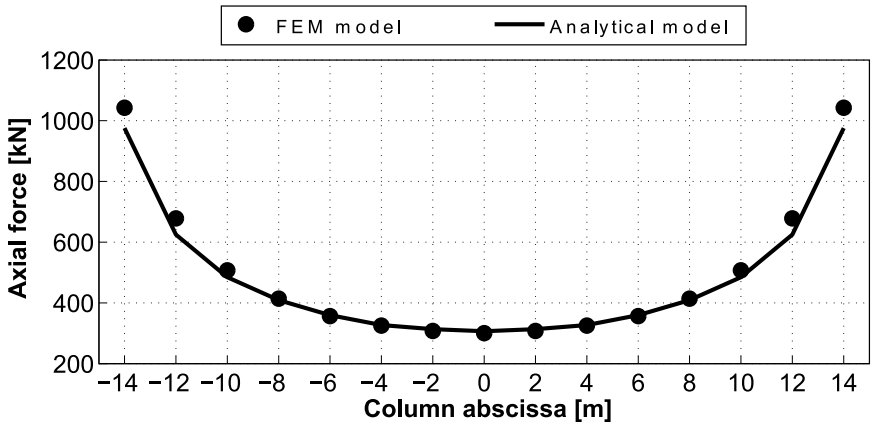

(a)

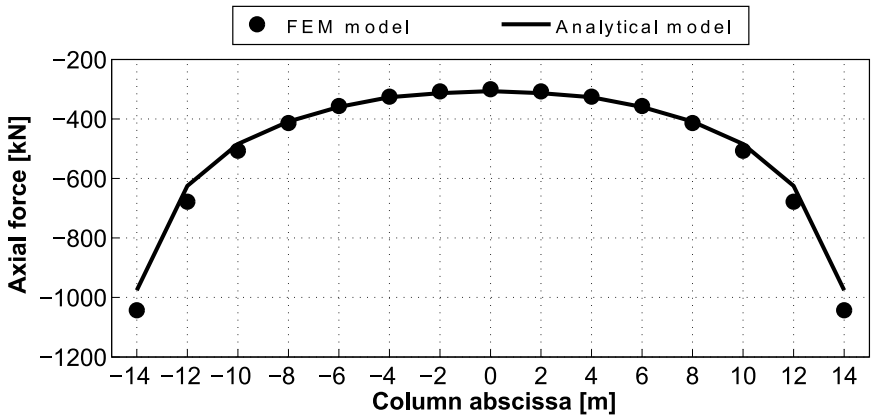

(b)

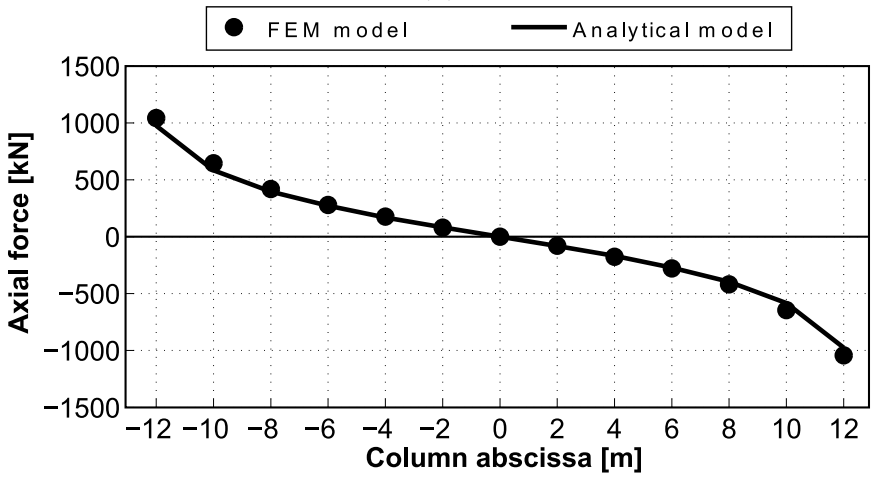

(c)

Figure 2.35: Normal stress at the base section of the columns. (a) Frame 1; (b) Frame 2; (c) Frames 3 and 4

The normal stress trend evaluated, as a function of the building height, in the corner column of frame 1 is shown in Figure (2.36). Also in this case the non-linear trend is clearly shown. Finally, it should be noted that from the bottom section and up to 2/3 of the entire height, the normal stress in the column is positive (tensile strength), while for the remaining part the column it is compressed.

This is attributable to the shear forces transmitted by the frames along the edge of the building. This effect contributes significantly to reducing the transversal displacements of the structure.

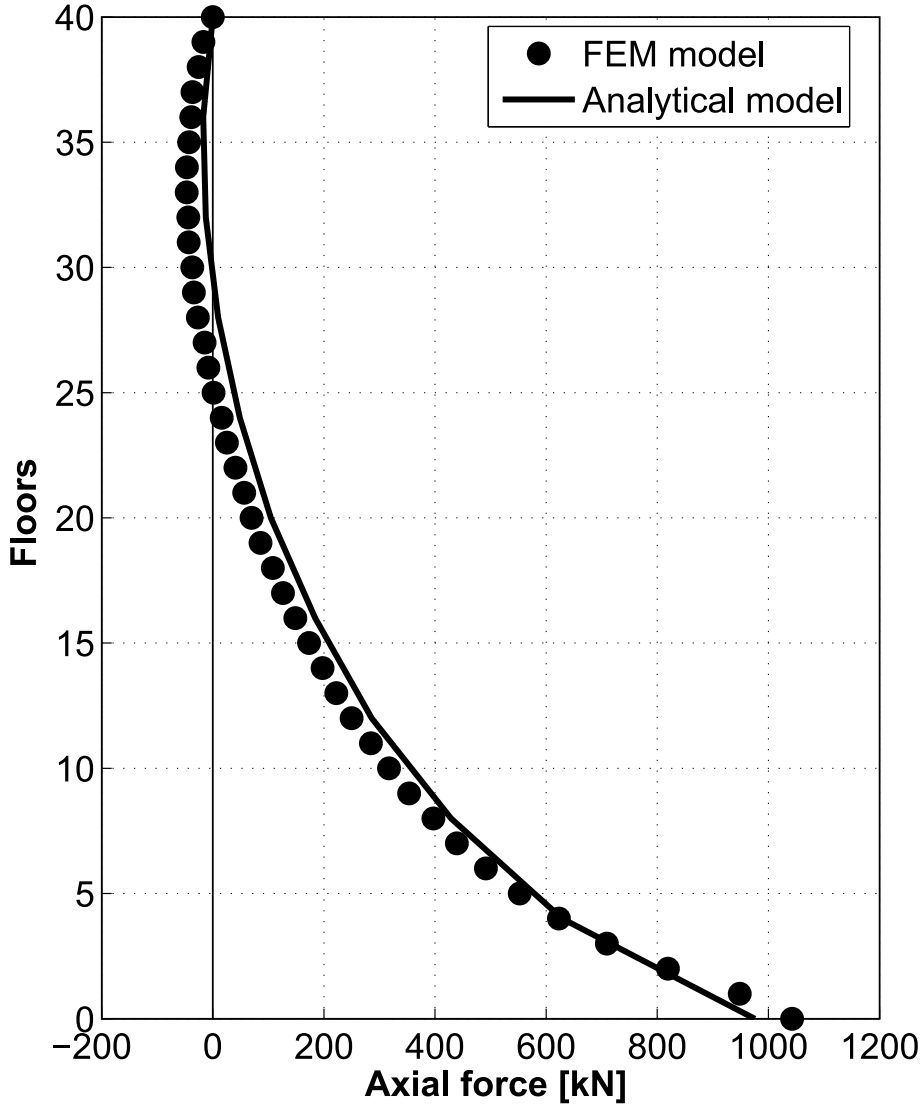

Figure 2.36: Normal stress in the corner column

2.6.6 Diagrid structure

In this example a 160 meter-high 3D diagrid structure shown in Figure (2.37) is considered, whose geometrical and mechanical characteristics are illustrated in Table 2.5.

Table 2.5: Geometrical and mechanical characteristics of the diagrid structure

Number of storeys	40	-
Floor height	4	m
diagonal rod cross section	0.1	m^2
Normal elastic modulus	2.1×10^8	kN/m^2
Load p_x	100	kN/floor

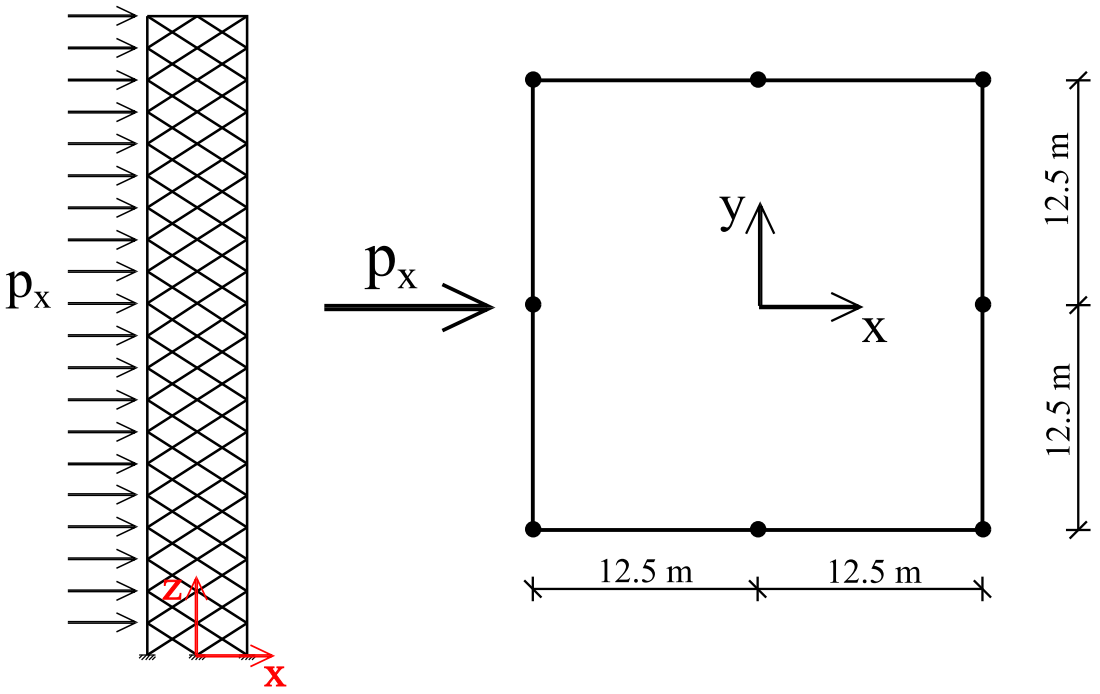

Figure 2.37: Diagrid structure. (a) Front view; (b) Floor plan

As shown in Figure (2.38), the transverse displacements obtained using the analytical model with 3-DOF per floor and those obtained using the FEM software are almost overlapping.

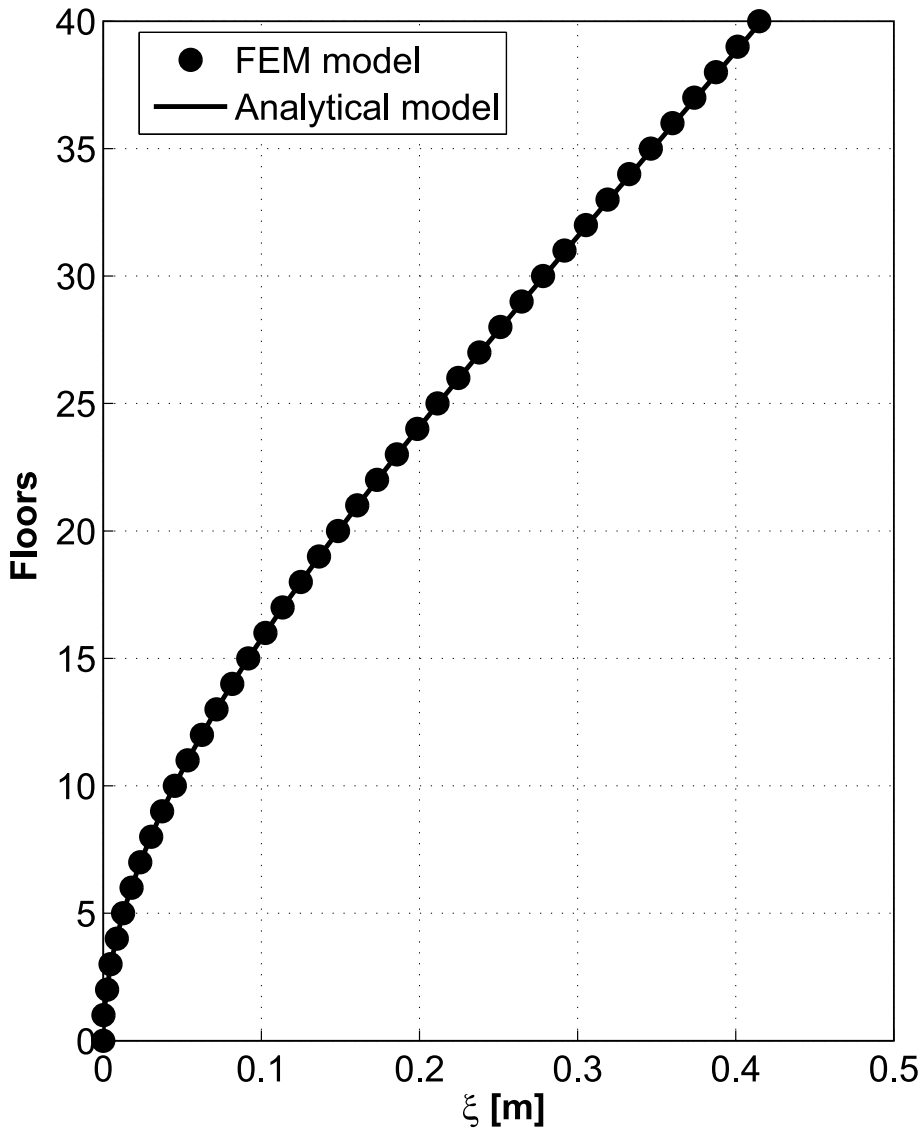

Figure 2.38: Diagrid structure transversal displacements

This result is obtained because, using both the analytical formulation and the finite element method, the structure is analyzed as a three-dimensional truss beam, namely in both models only the axial stiffness of the diagonal bars is considered.

Moreover, in both models the rods are hinged to each other.

Chapter 3

Static analysis

3.1 Analytical methods

The design of a high-rise building is a long and complex process that aims to define a structural system compatible with architectural restraints which is also, at the same time, capable of safely bearing gravitational and lateral loads [279].

Furthermore, the designer must respect strict regulations regarding lateral displacements and vibration control in order to ensure comfort to the occupants. To achieve these goals the design includes several stages: the conceptual stage, the preliminary design and finally the optimization and drafting of the executive project.

In the first phase the designer chooses the structural shape and the type of resistant elements to be used to ascertain horizontal actions. This phase is followed by the analysis of the actions that act on the building and the general dimensioning of the structures following the current technical regulations. Finally, in the optimization phase, we try to find the best compromise between the strength of the materials and the cost of building construction.

The development of easy-to-use commercial software codes with intuitive graphic interfaces made it possible to use the Finite Element Method (FEM) as a project tool. Currently, designers often use FEM software programs as a tool at all stages of the design process. However, along with this ease of use and to this power of calculation, there is also a certain danger in its use. Excessive confidence in the tool by the analyst can lead to errors. The reliability of a Finite Element (FE) calculation depends, more than on the tool, on how the simulation is set by the user and on the correct interpretation of inputs and outputs. This is due to the complexity and enormous amount of results provided, which lead to a certain difficulty in the identification of structural parameters that control the response of the structure and the interaction between its elements.

In addition, the FE software programs have a high computational cost due the high number of degrees of freedom of the structure. As pointed out by Howson [129], the use of FEM models is fundamental only for detailed and final stage design, and

not in the conceptual phase.

For this reason, several analytical methods have been developed over the years, often based on simplified calculation procedures and on approximations of structural behavior. In most cases models foresee the use of a linear elastic constitutive law, and no imperfections or deferred behaviors are expected over time (structural failure, shrinkage, creep, cracks, etc.); moreover the degrees of freedom are often reduced. These simplifications mean that the global model can offer a number of potential advantages as input data and analysis is certainly faster, and modeling is simpler and therefore less likely to be a potential source of errors. Finally, the clarification provided is satisfactory for the preliminary phase of the project. For this reason, analytical models have been developed to evaluate the stresses acting on the structural elements, estimate the displacements and evaluate the vibration shapes of the building. In addition, the use of this type of procedure provides a clear picture of the structural behavior, which allows the designers to obtain information on the key structural parameters that describe the behavior of the building.

As is known, high-rise buildings are particularly affected by horizontal actions such as wind and earthquake [3], [190]. These forces are absorbed by bracing of different shapes and sizes, which are consequently also subjected to shear forces, bending and torsional moments. The behavior of the bracing varies according to the shape it assumes: in the case of a rectangular, thin-walled closed-section or composed by shear walls converging in a single point, Saint Venant's Theory can be considered for analysis, while in the case of thin-walled open-sections, Vlasov's Theory is applied [261]. Over time these theories have been used to define the behavior of tall buildings subjected to horizontal forces and software programs have been developed to automate their study. In 1972 Wynhoven e Adams [273] studied the reduction of the ultimate bearing capacity of a structure subjected to loads that produce torsion. The torsional moment induces a rotation of the structure around its vertical axis, while horizontal forces cause a translation in their direction of application. This translation is increased by the effect of rotation.

Around the same time, Coull and Irwin [79], [83], [84], [85] presented a simple procedure for evaluating load distribution on a three-dimensional multi-storey structure. The method is based on the continuous connection technique and analyzes the load case consisting of bending and torsional moments. The studies also show how much of the load is absorbed by the bracings.

In 1973 Heidebrecht and Stafford Smith [122], [123] proposed an approximate method for analyzing the behavior of thin-walled open-section shear walls in tall buildings subjected to torsional moment. The procedure is the basis for the analysis of tall buildings. In the same year, Glück and Krauss [114] analyzed a group of thin-walled open-section cantilever beams, while Stamato and Mancini [231] created a method for the three-dimensional analysis of high buildings consisting of shear walls and frames of constant stiffness along the height. In this case, frames and shear walls are connect by slabs and a discreet number of storeys is assumed equivalent

to a continuous consisting of an infinite number of horizontal diaphragms without transverse stiffness, but infinitely rigid in its own plane. In the same years Biswas [30] also proposed a method for the three-dimensional analysis of a tall building subject to transverse loads.

In 1977 MacLeod e Hosny [166] proposed the analysis of the internal cores constituting the buildings, based on Vlasov's Theory [261]. The following year, Haris [121] presented an approximate method for determining the distribution of the lateral load and the displacement of tall buildings caused by the action of wind.

The frames making up the structure are transformed into equivalent cantilever beams in which the compliance matrix is obtained by applying a unit load to each floor and calculating the corresponding displacement. The stiffness matrix is obtained by inverting the compliance matrix.

The external load is redistributed on the basis of the rigidity of the various elements (shear walls or frames) to be reached by the calculation of displacements and rotations of the entire building. This procedure considers the problem to only one degree of freedom.

In the 1980's Mortelmans [186] and Taranath [242] re-proposed the analysis of tall buildings subjected to wind and earthquake based on the study of the stiffness matrix and the finite elements, a theme that was taken up in 1989 by Ha and Desbois [116].

In those years, the first attempts to create an automatic calculation code for the structural analysis of high-rise buildings also began [131]. Other methods, starting from aerospace engineering, subdivide the structure of building into a number of simple substructures and operate as the case of Finite Element (FE) approach, in which the substructures were considered as super-elements. The first to focus on this methodology were Leung [161], [162], Wong [272], followed, more recently, by Kim [140] and Steenbergen and Blaauwendraad [234].

3.2 The load distribution matrix between vertical bracings

In most buildings the horizontal resistant system consists of different elements which can vary from one to another according to their specific stiffness properties.

The use of in-parallel members is a structural solution which immediately appeared as a simple way of increasing the horizontal stiffening of high-rise structures [47].

From the design point of view, many studies were developed to identify the distribution of the external forces among the internal bracings.

The papers by Khan and Sbarounis [139], Rosman [221] and Beck [22] represent the first efforts to study this based on the continuum medium technique. This simplified technique was also taken up by other authors [81], [208], [225].

The general formulation of the problem of the external lateral loading distribution between the bracings of a threedimensional structure was presented in 1985 by A. Carpinteri [58], but in the last few years, this method of calculation has been further developed and improved [63], [64] for the purpose of analyzing a wider range of typologies of high-rise buildings [60], [65]. The effectiveness of this analytical code has been verified in some case studies carried out by the Authors in recent years [62], [188], [189]. The formulation, called the *General Algorithm*, has already been widely described in various works [61], [55], [63], and it is summarized in the following.

3.2.1 General Algorithm

The formulation is based on the following fundamental hypotheses:

- the structural material is homogeneous, isotropic, and obeys Hooke's law;
- the floor slabs are rigid in their own plane but their out-of-plane rigidity is negligible;
- in the transversal analysis, the axial deformation of the structural elements due to gravity loads is neglected.

The approach proves to be general, since it is possible to consider any type of vertical bracing, from simple frames to free-shaped tubular elements, provided that their own stiffness matrix is known.

Based on the previously mentioned hypotheses, an N-storey building is considered having M vertical bracings, each defined by an arbitrary position in the floor plan. The right-handed system XYZ defines the global coordinate system.

Since the slabs, which interconnect the bracings to each other, are considered to be infinitely rigid in their own planes, the degrees of freedom are represented by the transverse displacements of the single floors: two translations ξ and η in the X and Y directions, and the torsional rotation ϑ, for each storey. In the same way, the external load applied to the origin of the reference system is expressed by a $3N$-vector $\{F\}$, in which $2N$ shearing forces $\{p_x\}$, $\{p_y\}$, and N torsional moments $\{m_z\}$ are included (Figure 3.1):

$$\{F_i\} = \begin{Bmatrix} p_{x,i} \\ p_{y,i} \\ m_{z,i} \end{Bmatrix} \tag{3.1}$$

Being the right-handed system $X_i^* Y_i^* Z_i^*$ the local coordinate system of the i-th bracing, the $3N$-load vector $\{F_i^*\}$ and the $3N$-displacement vector $\{\delta_i^*\}$ describe the amount of external load carried by the i-th element and its transverse displacements, respectively. The loading vector $\{F_i^*\}$ can be reduced to $\{F_i\}$, which refers to the

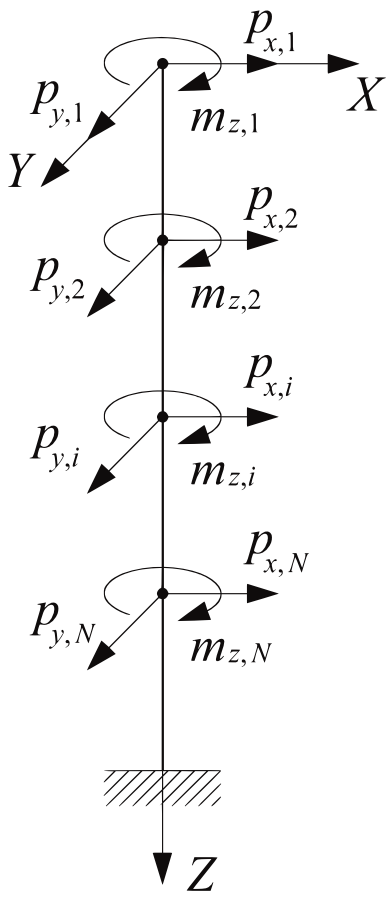

Figure 3.1: Scheme of a tall building in a right-handed coordinate system [63]

global coordinate system XYZ, by means of the following expressions, valid for each floor:

$$\left\{ \begin{array}{c} p^*_{x,i} \\ p^*_{y,i} \\ m^*_{z,i} \end{array} \right\} = \left[\begin{array}{cc} [N_i] & [0] \\ -\{u_z\} \wedge \{\psi_i\} & [1] \end{array} \right] \left\{ \begin{array}{c} p_{x,i} \\ p_{y,i} \\ m_{z,i} \end{array} \right\} \tag{3.2}$$

where $[1]$ is the $N \times N$ identity matrix and $[0]$ is the $2N \times N$ null matrix. The term $[N_i]$ represents the orthogonal rotation matrix from system XY to system $X^*_i Y^*_i$; $\{\psi_i\}$ is the coordinate vector of the origin of the local system in the global one; $\{u_z\}$ is the unit vector associated to the Z-direction.

The orthogonal $2N \times 2N$ matrix $[N_i]$, extended to consider all floors, can be represented by means of the angle φ_i between Y and Y^*_i axes (Figure 3.2):

$$\left[\begin{array}{c} N_i \end{array} \right] = \left[\begin{array}{cc} [\cos\varphi_i] & [\sin\varphi_i] \\ -[\sin\varphi_i] & [\cos\varphi_i] \end{array} \right] \tag{3.3}$$

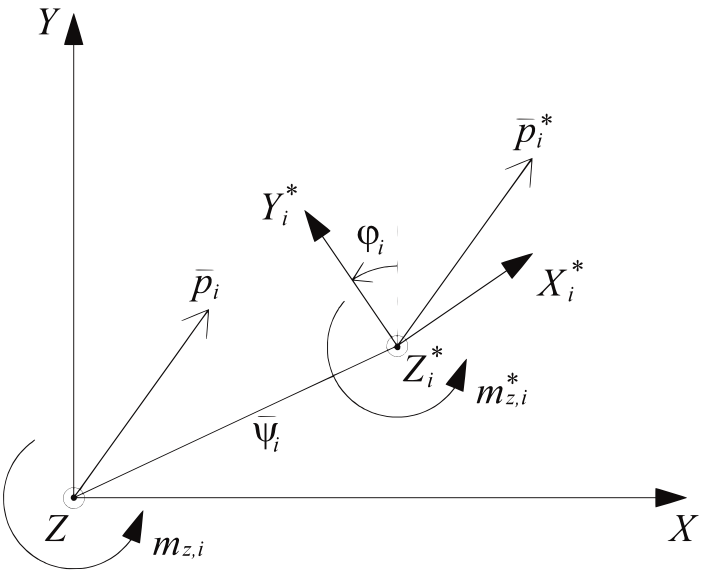

Figure 3.2: Global and local coordinate systems [63]

where each term is a diagonal $N \times N$ sub-matrix:

$$[\cos\varphi_i] = \begin{bmatrix} \cos\varphi_i & 0 & \cdots & 0 \\ 0 & \cos\varphi_i & \cdots & 0 \\ \vdots & \vdots & \ddots & \vdots \\ 0 & 0 & \cdots & \cos\varphi_i \end{bmatrix} \tag{3.4a}$$

$$[\sin\varphi_i] = \begin{bmatrix} \sin\varphi_i & 0 & \cdots & 0 \\ 0 & \sin\varphi_i & \cdots & 0 \\ \vdots & \vdots & \ddots & \vdots \\ 0 & 0 & \cdots & \sin\varphi_i \end{bmatrix} \tag{3.4b}$$

The vector product $\{u_z\} \wedge \{\psi_i\}$ can be written as:

$$\{u_z\} \wedge \{\psi_i\} = \begin{bmatrix} \vec{i} & \vec{j} & \vec{k} \\ 0 & 0 & 1 \\ x_i & y_i & 0 \end{bmatrix} = -y_i\vec{i} + x_i\vec{j} + 0\vec{k} = -y_i\vec{i} + x_i\vec{j} \tag{3.5}$$

where x_i and y_i are the coordinates of the origin of the local reference system of the i-th vertical bracing with respect to the global reference system.

For the sake of simplicity, in order to take into account the N floors of the structure, the $N \times 2N$ matrix $[C_i]^{\mathrm{T}}$ is introduced:

$$[C_i]^{\mathrm{T}} = \left[-\begin{bmatrix} y_{i,N} & 0 & \cdots & 0 \\ 0 & y_{i,N-1} & \cdots & 0 \\ \vdots & \vdots & \ddots & \vdots \\ 0 & 0 & \cdots & y_{i,1} \end{bmatrix} \begin{bmatrix} x_{i,N} & 0 & \cdots & 0 \\ 0 & x_{i,N-1} & \cdots & 0 \\ \vdots & \vdots & \ddots & \vdots \\ 0 & 0 & \cdots & x_{i,1} \end{bmatrix} \right]^{\mathrm{T}} \tag{3.6}$$

Taking into account all floors, Equation (3.2) can be re-written in the following form:

$$\{F_i^*\} = [A_i]\,\{F_i\} \tag{3.7}$$

Matrix $[A_i]$ gathers the information regarding the reciprocal rotation between the local and global coordinate systems and the location of the i-th bracing in the global reference system XY:

$$[A_i] = \begin{bmatrix} [N_i] & [0] \\ -[C_i]^{\mathrm{T}} & [1] \end{bmatrix} \tag{3.8}$$

The displacement vector $\{\delta_i\}$, constituted by $2N$ translations ξ_i, η_i, and N rotations ϑ_i, referred to the global reference system XY, are then connected to the displacement vector $\{\delta_i^*\}$ in the local coordinate system $X_i^*Y_i^*$ by the orthogonal matrix $[N_i]$:

$$\begin{Bmatrix} \xi_i^* \\ \eta_i^* \\ \vartheta_i^* \end{Bmatrix} = \begin{bmatrix} [N_i] & [0] \\ [0] & [1] \end{bmatrix} \begin{Bmatrix} \xi_i \\ \eta_i \\ \vartheta_i \end{Bmatrix} \tag{3.9}$$

Taking into account all floors, Equation (3.9) can be re-written in the following form:

$$\{\delta_i^*\} = [B_i]\,\{\delta_i\} \tag{3.10}$$

where matrix $[B_i]$ is similar to $[A_i]$, but the term $[C_i]^{\mathrm{T}}$ being reduced to a null matrix:

$$[B_i] = \begin{bmatrix} [N_i] & [0] \\ [0] & [1] \end{bmatrix} \tag{3.11}$$

A relation between $\{F_i^*\}$ and $\{\delta_i^*\}$ is considered known through the condensed stiffness matrix $[K_i^*]$, referred to the local coordinate system:

$$\{F_i^*\} = [K_i^*]\,\{\delta_i^*\} \tag{3.12}$$

Substituting Equations (3.7 and 3.10) into Equation (3.12), the load vector $\{F_i\}$ turns out to be connected to the displacement vector $\{\delta_i\}$ through a product

of matrices, which identifies the stiffness matrix $[K_i]$ of the i-th bracing in the global coordinate system XY:

$$\{F_i\} = \left([A_i]^{-1}\,[K_i^*]\,[B_i]\right)\{\delta_i\} = [K_i]\,\{\delta_i\} \tag{3.13}$$

Due to the presence of in-plane rigid slabs connecting the vertical cantilevers, the transverse displacements of each element can be computed considering only three generalised displacements ξ, η, and ϑ per floor. This step, extended to consider all floors, is performed through the matrix $[T_i]$, which takes into account the location of each bracing in the plan by means of the coordinates (x_i, y_i) and, therefore, the matrix $[C_i]$:

$$\{\delta_i\} = \begin{bmatrix} [1] & [C_i] \\ [0] & [1] \end{bmatrix}\{\delta\} = [T_i]\,\{\delta\} \tag{3.14}$$

being $\{\delta\}$ the floor displacement vector, *i.e.* the displacement vector associated to the origin of the global reference system. The substitution of Equation (3.14) into Equation (3.13) allows to identify the stiffness matrix of the i-th bracing, referred to the global coordinate system XYZ and to the generalised floor displacements ξ, η, and ϑ:

$$\{F_i\} = ([K_i]\,[T_i])\,\{\delta\} = \left[\overline{K}_i\right]\{\delta\} \tag{3.15}$$

For the global equilibrium, the external load $\{F\}$ applied to the structure is equal to the sum of the M vectors $\{F_i\}$. In this way a relationship between the external load and the floor displacements is obtained and the global stiffness matrix of the structure is computed. By means of this matrix, once the external load is defined, the displacements of the structure are acquired, from which the information regarding each single bracing can be deduced

$$\{F\} = \sum_{i=1}^{M}\{F_i\} = \left(\sum_{i=1}^{M}\left[\overline{K}_i\right]\right)\{\delta\} = \left[\overline{K}\right]\{\delta\} \tag{3.16}$$

and, therefore,

$$\{\delta\} = \left[\overline{K}\right]^{-1}\{F\} \tag{3.17}$$

Recalling Equation (3.15) and comparing it with Equation (3.17), an equation connecting the vectors $\{F\}$ and $\{F_i\}$ allows to define the amount of the external load carried by the i-th vertical stiffening element:

$$\{\delta\} = \left[\overline{K}\right]^{-1}\{F\} = \left[\overline{K}_i\right]^{-1}\{F_i\} \tag{3.18}$$

from which we obtain

$$\{F_i\} = \left[\overline{K}_i\right]\left[\overline{K}\right]^{-1}\{F\} = [R_i]\,\{F\} \tag{3.19}$$

The load distribution matrix $[R_i]$, shown in Equation (3.19), demonstrates that each bracing is subjected to a load $\{F_i\}$ which is connected with the external load $\{F\}$ through its own stiffness matrix and the inverse of the global stiffness matrix.

Once the generalised displacement vector $\{\delta\}$ is known, recalling Equations (3.12 and 3.14), the displacements and the forces related to the i-th bracing, in its local coordinate system, can be computed.

Consequently, since the loads applied to each element are clearly identified, a preliminary assessment can be easily performed.

Equation (3.19) solves the problem of the external load distribution between the resistant elements employed to stiffen a three-dimensional tall building. Such formulation proves to be general and can be adopted with any kind of structural elements, provided that their own condensed stiffness matrix $[K_i^*]$ is known.

Further benefits can be highlighted: firstly, an easy identification of the structural parameters, which govern the lateral behaviour of the building, can be performed; secondly, the formulation proves to be extremely clear and concise, limiting in this way the risk of unexpected errors and guaranteeing, in presence of very complex structures, relatively short times of modelling and analysis, if compared to Finite Element computations.

3.2.2 The numerical software program

The analytical formulation has been implemented in a numerical code by using Mathworks Matlab. With this model it is possible to compute the deformations and stresses acting on the horizontal stiffeners of high-rise buildings.

Such a formulation proves to be general and can be adopted with any kind of structural elements, provided that its own stiffness matrix is known. The main advantage of this approach is that it considers only three degrees of freedom for each storey, therefore it requires a shorter computation time if compared to the commercial Finite Element Method (FEM) software, which are mesh-dependent and are characterized by six degrees of freedom for each node.

Moreover, the proposed model produces results which are quite close to those achieved by the FEM, with differences generally less than 10%. This approximation is commonly accepted in the preliminary design stage of a high-rise building. The flow-chart of the numerical code is shown in Figure (3.3).

The entire calculation code, consisting of 37 functions for a total of more than 8,000 command lines, has a user-friendly graphics interface that allows a simple and intuitive input and output phase as shown in Figure (3.4).

The input phase consists of entering global data of the entire building, *i.e.* the total number of storeys, size and mass of the slabs (which may also have geometry different from one floor to another); geometrical and mechanical data on each individual vertical stiffening, which can be of the following typologies:

- rectangular shear walls;
- shear walls composed by thin plates converging in a single point;
- thin-walled closed- or open-section shear walls;
- plane frames and braced frames;
- 3D framed tube;
- 2D or 3D diagrid system.

For the insertion of the vertical bracings in the floor plan of the building, the user must first arbitrarily choose a global reference system to which the coordinates that describe all the braces will be expressed. After entering the data, the user can verify the correctness of the records by displaying the building plan on the screen with the position of all the elements indicated. Alternatively, the user can also view a three-dimensional model of the building, which can be observed from any point of view thanks to *orbit* tool that allows you to freely rotate the 3D model.

The last phase of the input consists in inserting the loads. The user must enter the values of the global horizontal concentrated loads p_x, p_y, and m_z referred to the center of the global reference system. These loads can be the same for all floors of the building, or different, as in the case of logarithmic distributions of the wind pressure proposed by the technical regulations [132], [232], [233].

Once the input phase is completed, the user can choose whether to perform a static analysis or a dynamic analysis (see Chapter 4) of the structure. By performing a static analysis, normally carried out in about 1 minute, the user can decide whether to view the results in terms of displacements or stresses. When using static analysis the graphs of the displacements of the global reference system origin, in the x and y directions, and the rotations around the vertical axis at each floor of the building, are generated. In addition to the displacement functions, it is also possible to view the first, second, third and fourth derivative functions.

It is also possible to view the three-dimensional displacements axonometric elevation of the building, as shown in the right window of the Figure (3.4).

In addition, for each vertical bracing it is possible to view the graphs of the bending moment, shear stress, bimoment, primary and secondary torsional moment (obviously where expected), according to the height of each floor of the structure.

If dynamic analysis is performed, it is instead possible to obtain a table containing the angular frequencies, the frequencies and the periods of all the modes of vibration of the structure ($3\times$*number of floors*). Furthermore, it is also possible to view the eigenvectors of the deformed modal shapes in the form of three-dimensional axonometric elevations of the entire building.

Finally, all the results can also be generated in tabular form in order to be easily manipulated, as well as with Matlab, even with the most common commercial software, such as Microsoft Excel.

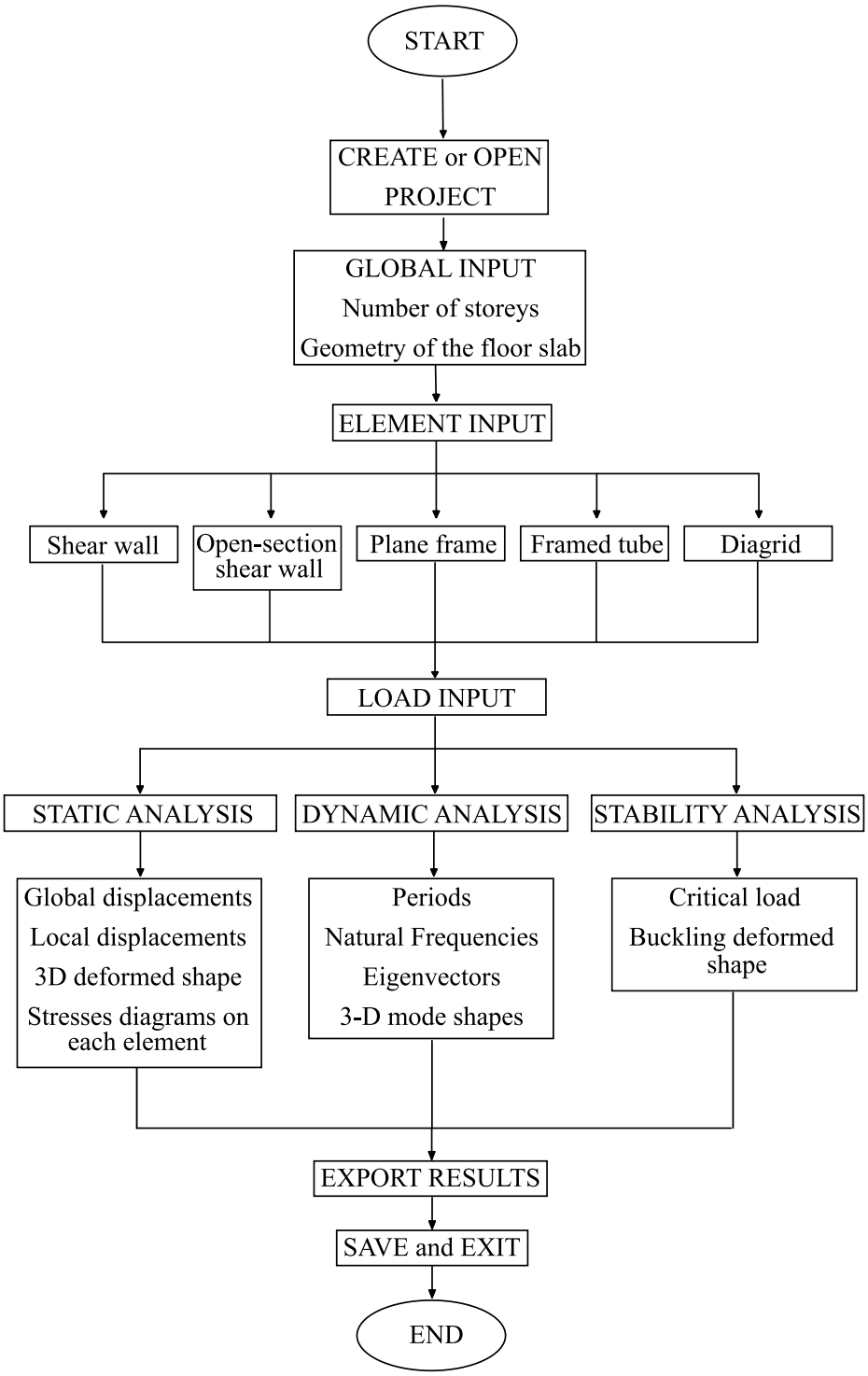

Figure 3.3: Flow-chart of the numerical code

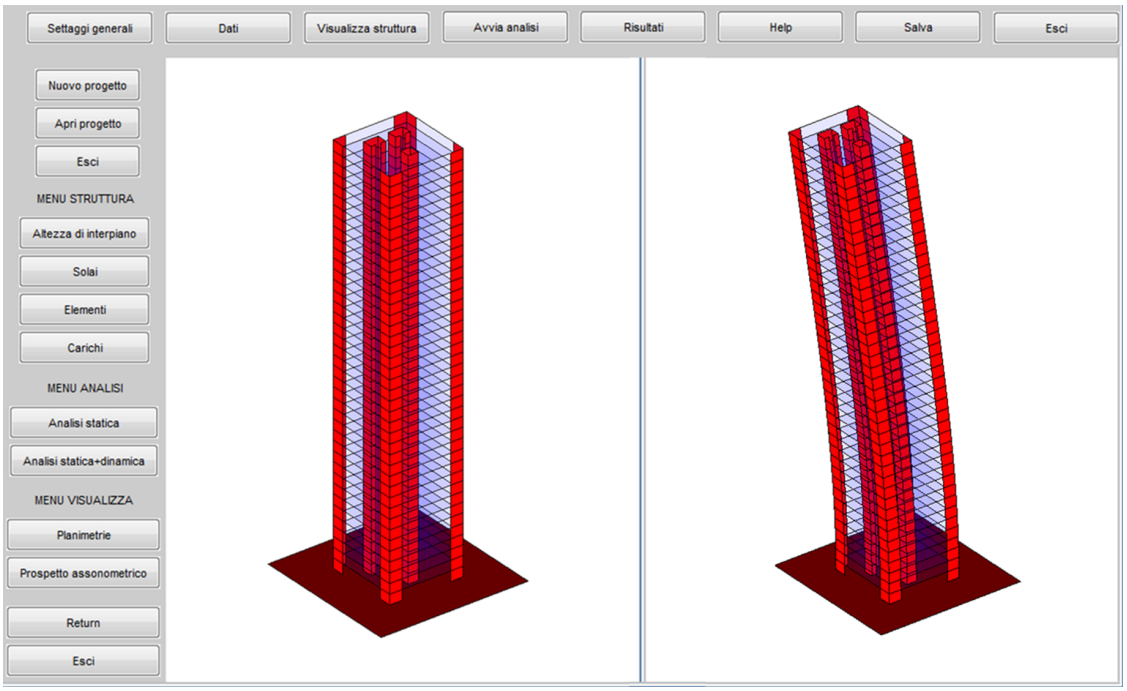

Figure 3.4: Main window of the numerical code

3.3 Numerical example

This section shows the calculation report of one of the highest buildings currently (2020) under construction in Italy, The Piedmont Region Headquarters Tower (Figure 3.5). The descriptions of the building, the calculation methods and the results have already been published in [188].

The building is situated in the south of the City of Turin in Italy (Figure 3.6).

Previously on this site, classified by the local authorities as an abandoned industrial area before the new constructions, there was the old manufacturing district of Fiat Avio. Near the new skyscraper, there is the "Oval" Olympic Winter Building, the Lingotto shopping center and auditorium. It is important to point out that the site will be well served by public transport by means of the new underground station on the Nizza street side, and the Lingotto railway station.

3.3.1 Description of the structure

The multi-storey building base is square, measuring 45 m on each side. The tower comprises 43 floors above the ground, each level is 4.27 m tall (except the entry-hall, which is 8.66 m tall), therefore its height is about 188 meters up to the last floor. Beyond this level there is a covered garden, 21-meters high, made of

Figure 3.5: Picture taken on August 30, 2018 [188]

steel and glass walls. Considering the roof of the garden, the building reaches 209 m in height. On the east side of the tower, there are the so-called *Satelliti*, i.e. non-structural slabs 11 m in length, linked to the façade. For this reason, these decorative elements do not influence the total structural stiffness of the building, and they are not taken into account in the analytical model. The east side façade is 180 m tall and it is composed of a self-supporting steel frame linked by means of a limited number of connections to the reinforced concrete structure. The building is characterized in its entire height by a regular structural scheme. In particular, the tower floor plan embeds 4 central cores with open thin sections and made of high performance concretes (Figure 3.7). Cores 1 and 3 are the same size on the plans and the same thickness (0.50 meters), like cores 2 and 4. These are arranged polar-symmetrically on the plan, in relation to the origin of the reference system, as shown in Figure 3.8).

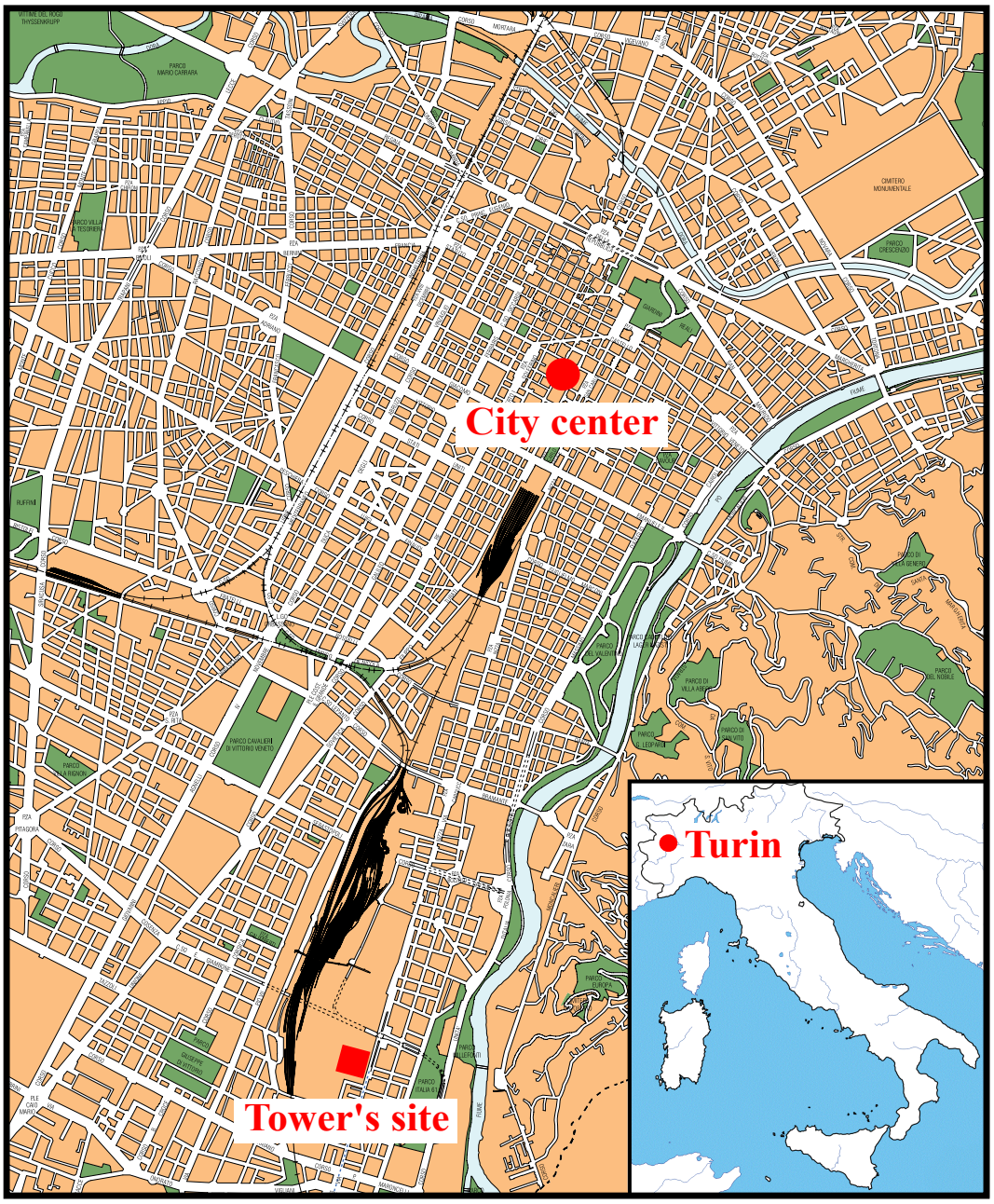

Figure 3.6: Location on the map [188]

From a structural point of view, the stiffness of these elements braces the tower by limiting transversal displacements in an optimal way.

Along the building perimeter, excepting the east side, there are columns spaced 6 meters from each other, which reach a height of 188 m. Due to architectural requirements, the reinforced concrete columns have constant rectangular cross section

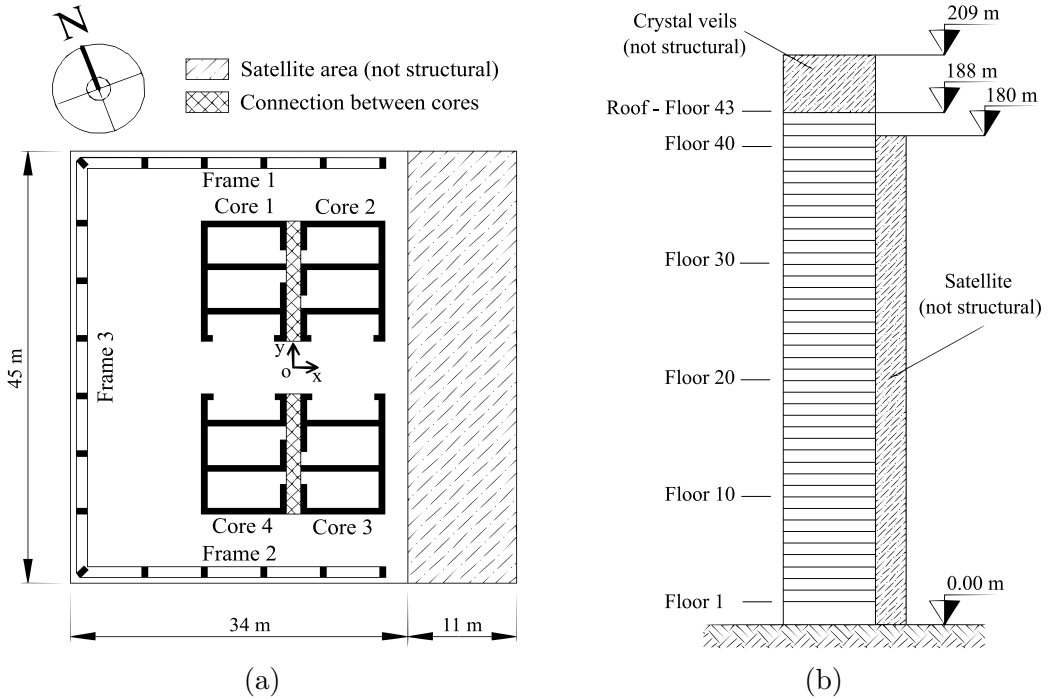

Figure 3.7: (a) Typical floor plan; (b) East-West elevation [188]

dimensions of about 1.10 m × 0.60 m, at all levels. The slabs, made of reinforced concrete, have a constant thickness of about 0.34 meters, while the slabs between the East and West cores (core pairs 1-2 and 3-4) are made of concrete with a thickness of about 0.50 meters. The increased thickness is due to the need to link the slabs to the vertical cores, increasing their resistance and, at the same time, reducing the transverse displacements of the entire building due to horizontal loads.

The slabs in lightweight concrete are made by means of the Bubble Deck technique [24], i.e. by using high density polyethylene (HDPE) bubbles with a diameter of 225 mm embedded in the concrete casting. Adopting this construction technique, it is possible to reduce the slab weight by about 20-25% compared to its unlightened weight. This lightening, moreover, allows a better seismic structural behaviour and a considerable reduction of the axial stresses in the vertical elements to be obtained.

Different strength classes of concretes, depending on the axial loads, were used to made the other types of vertical structural elements in the structure. In particular, on the first floors the columns are composed of C70/85 concrete class, while on the upper floors of C35/45 concrete class. The cores are made in C60/75 - C30/35 concrete class.

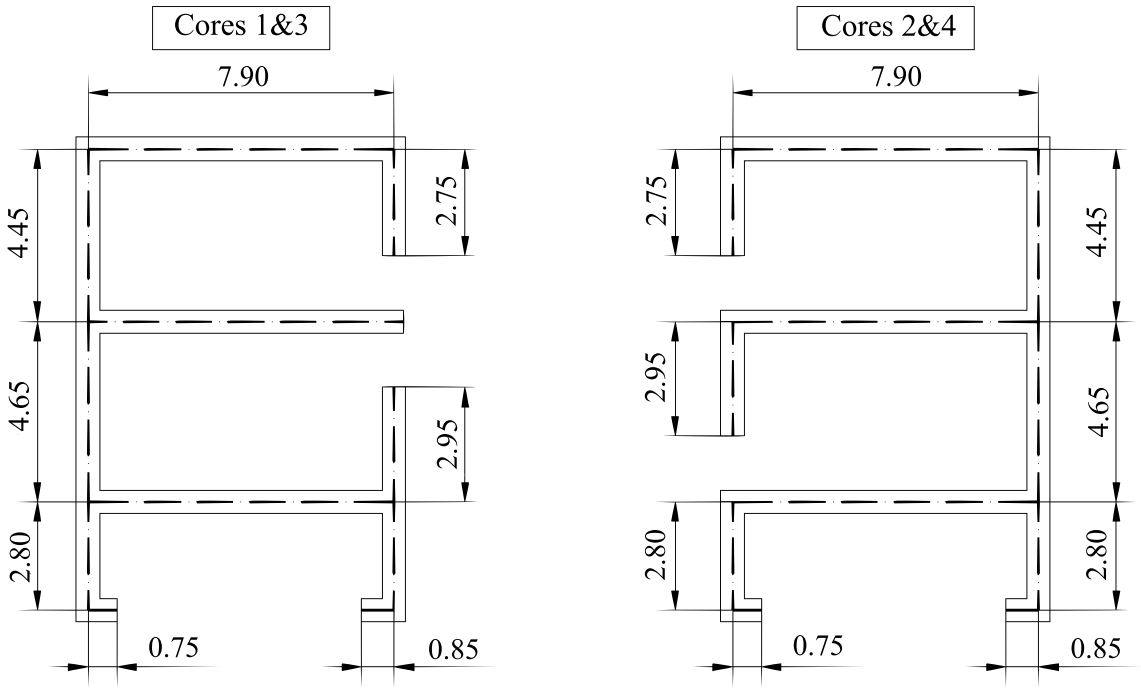

Figure 3.8: Geometry of the cores [188]

3.3.2 Wind load

Wind, which is usually considered to be horizontal in direction, exerts actions on constructions that vary in time and space, generally causing dynamic effects that have an extremely important effect on high-rise buildings. In this work, in particular, only the load combination that maximizes the torsional effects induced by the action of the wind was considered, not taking into account the vertical loads induced by the dead load of the structure. To analyze wind actions, sophisticated techniques that require experimental analysis of the structure in a wind tunnel can be used. In the preliminary phase, the lack of detailed knowledge of the structure does not allow the application of these methods, so we used simplified procedures.

In the following analysis, the procedure proposed by Italian Rules - D.M. 14th January 2008 [132], which reports the same formulation contained in the European Standard EN 1991 (Eurocode 1) [232], [233], was used. The calculation of wind forces depends on the geometric and dynamic characteristics of the structure, the geographical position and the characteristics of the site where the structure is located.

Therefore, it requires the determination of certain parameters, primarily the reference wind speed, which in this case corresponds to 25 m/s. Given the importance of the building, a return period of 200 years is considered. Using these data,

a kinetic reference pressure of 420.10 N/m^2 was obtained. The wind pressure acting on the building is given by the product between the kinetic reference pressure and other coefficients concerning the exposure, shape and dynamics of the structure, which can be calculated using a detailed procedure indicated in Eurocode 1. When the pressures acting on the vertical surfaces of the building are known, it is possible to calculate the forces to be applied to each floor in relation to the areas impacted by the wind. The graphs in (Figure 3.9) show the forces applied on each floor of the model, referring to the origin of the reference system as shown in (Figure 3.7a).

We can see that in correspondence to the last floor, at a height of 188 meters, there is a drastic increase in forces because the wind pressure acting on the surface of the veils was also considered. For the same reason, the forces applied on the first floor are greater, as the inter-floor space is 8.66 meters high. Finally, at a height of 183.73 meters, the F_y force is reduced as a result of the reduction of the area exposed to the wind.

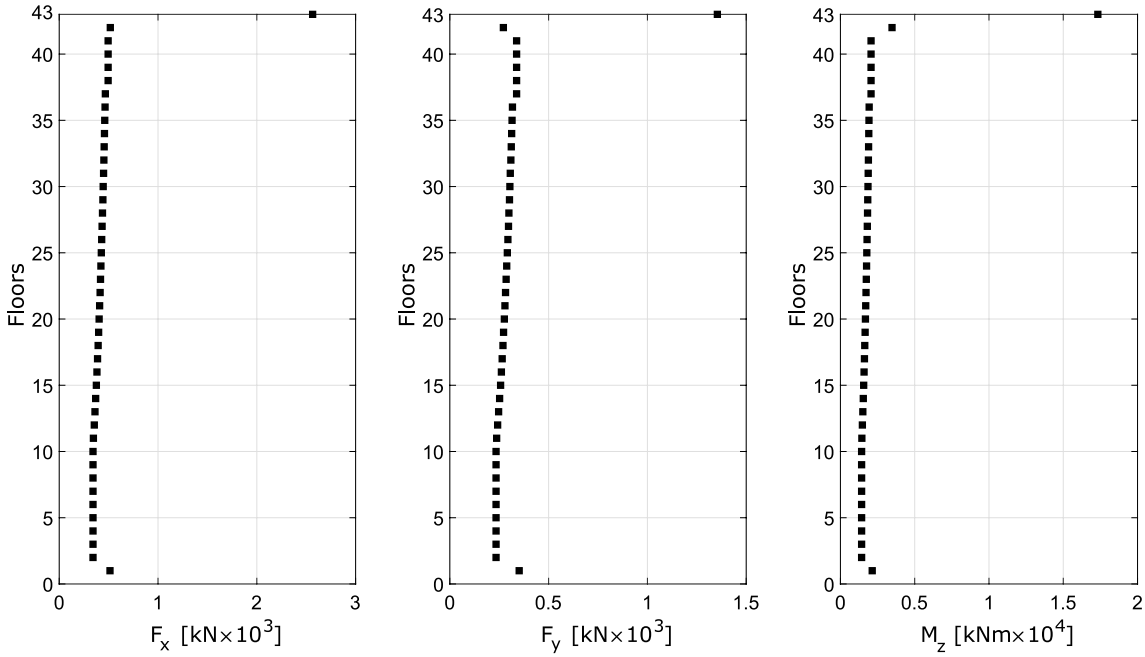

Figure 3.9: Wind loads on the structures referred to the centroid of floors [188]

3.3.3 Analytical model

The numerical model, implemented in the Matlab computation code, is based on Carpinteri's analytical formulation. The study of the structure was carried out on a simplified model of the building in which constant core thicknesses and constant mechanical properties along the height were considered. This choice is justified by

the fact that, in the preliminary design phase, we do not have complete knowledge of the behavior of the structure in order to optimize the sizing. Subsequently, once the main parameters that characterize structural behavior have been identified, the structure is optimized and, finally, a more accurate model can be analyzed with a commercial Finite Element software. For this reason, also the mechanical characteristics of the materials were homogenized with reference to the average resistance of the elements weighed on the number of floors. Following this procedure, an elastic modulus equal to 39 GPa was used for the frame elements, with 35 GPa for the cores, while a Poisson coefficient of 0.18 was assumed for all the elements. As far as the dynamic analysis is concerned, only the structural masses related to the slabs were considered. These were determined considering a specific weight of 18.75 kN/m^3. As already mentioned, core pairs 1-2 and 3-4 are connected by thickening the floor slabs. In this case, because the cores are less than two meters apart and the slabs are 0.50 meters thick, the connection can be considered infinitely rigid out of the plane.

To calculate this structure correctly, the original analytical formulation was changed, developing a computation method based on the equivalent flexural stiffness. Since the effect of the connection is to join the sections of the two cores, in addition to the local reference system of each core, it is also possible to define a further reference system for each pair of connected cores. The origin of this reference system lies in the centroid of the section made up of the two cores. Consequently, the geometric characteristics of each core (and therefore the local stiffness matrices) refer to this last reference system.

Finally, as previously illustrated, we calculate the global stiffness matrix and, in order to solve the structure from the distribution matrix, we obtain the forces acting on each core and, ultimately, the stresses and displacements of the structure.

The three-dimensional model of the building, created with the analytical calculation code, is shown in Figure (3.10).

Following the same assumptions adopted for the analytical model, in order to validate the results, a Finite Element Method Model (FEM model) was also created using a commercial software program. The three frames, four cores and infinitely rigid slabs in their plane were therefore modelled. Beam elements were used for the frame and shell elements were used for the cores, while the floors were modelled using rigid links that connect all the points of the floor plan to a master node coinciding with the geometric centroid of the slabs. At this point, the concentrated forces, corresponding to the externally applied loads for the static analysis and the mass of the floors for the dynamic analysis, were applied. All the structural elements are mutually interlocked and anchored to the ground. In this way, a FEM model similar to the analytical model was generated. The FEM model implemented is characterized by 69,212 nodes, 1,576 beam elements and 66,960 shell elements. The amount of data to be analyzed required a much longer computational time (about one hour) than the time required for the analytical

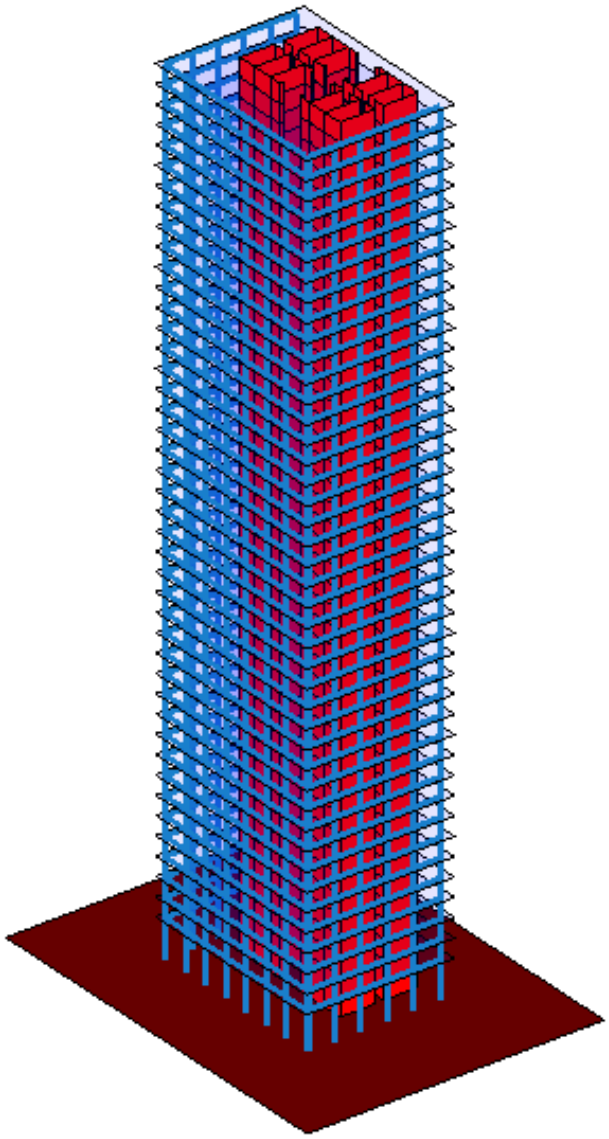

Figure 3.10: Three-dimensional model of the building

algorithm (a few minutes). The results of the structural analysis are summarized in graphs that show the comparisons between the Analytical Model and the Finite Element Model considering the horizontal displacements of the centroid of each floor, and the stresses and strains on the vertical resistant elements. As regards the stress computation, the effects due to bending and secondary torsion were considered, leaving out the component due to vertical forces. This choice was made because, as previously mentioned, the aim of this work is to study mainly the torsional effects in high-rise buildings, ignoring the effects due to vertical loads.

3.3.4 Displacements

Figure (3.11) shows the displacements of the structure in the x and y directions as well as the rotations of the floors. Three models have been created: two models are analytical and show the displacements obtained by applying the General Algorithm, considering cores 1-2 and 3-4, respectively, as not connected, or rigidly connected; the third model was obtained using a commercial FEM software program.

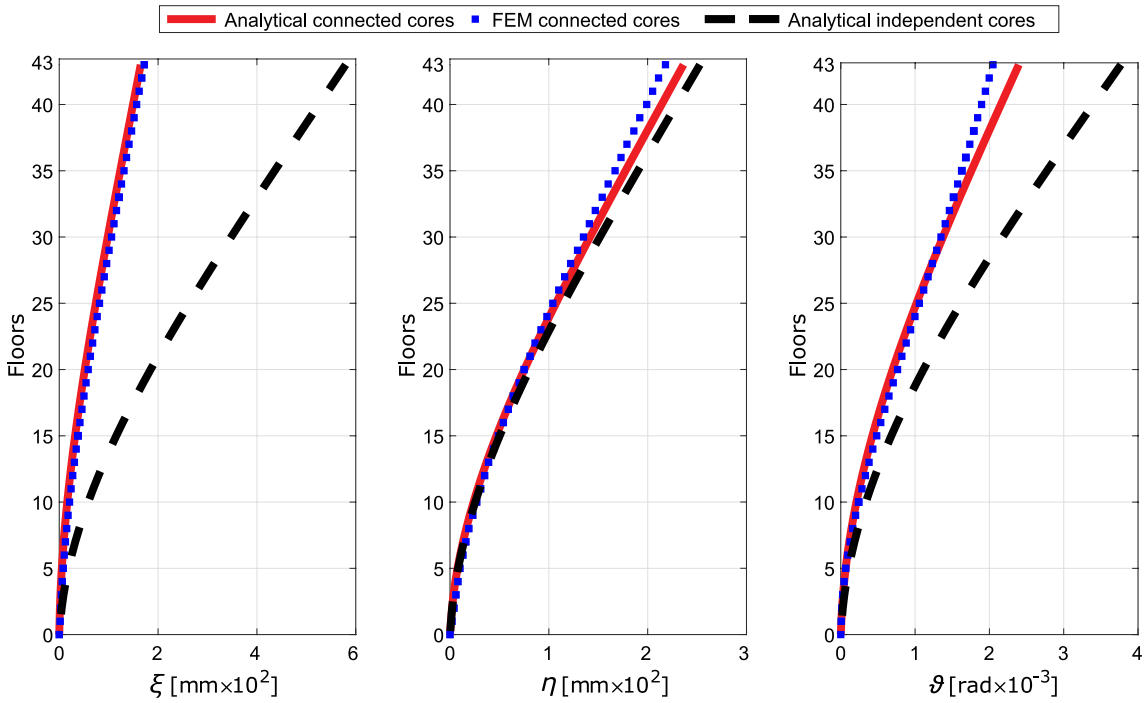

Figure 3.11: Displacements in x-direction (ξ), displacements in y-direction (η), and torsional rotations (ϑ) [188]

From the graphs, the rigid connection between the cores determines a reduction of about 70% of the transversal displacement in x-direction, and a reduction of 45% of the plane rotations. A slighter reduction of the displacement in y-direction is also evidenced. As a result, the analytical results of the model with the rigid connections show minimal differences compared to the FEM model.

With these graphs it has been demonstrated that the connection between two or more cores, achieved by thickening the floor, is a simple structural choice that permits a drastic reduction of the horizontal displacement at a negligible additional cost compared to other structural solutions (i.e. outrigger) that would allow the same deformation levels to be achieved.

3.3.5 Internal reactions

When the rigid rotations of floor ϑ are known, Vlasov's Theory can be used to determine bimoment B, the primary torsional moment M_z^{SV} and the secondary torsional moment M_z^{VL} acting on each bracing through the following equations:

$$B = -EJ_{\omega\omega}\vartheta'' \tag{3.20a}$$

$$M_z^{SV} = GI_t\vartheta' \tag{3.20b}$$

$$M_z^{VL} = -EJ_{\omega\omega}\vartheta''' \tag{3.20c}$$

where $J_{\omega\omega}$ and I_t indicate the sectorial moment of inertia and the torsional stiffness factor of the section of the considered core respectively, while E and G indicate the normal and shear elastic modulus of the core material, respectively.

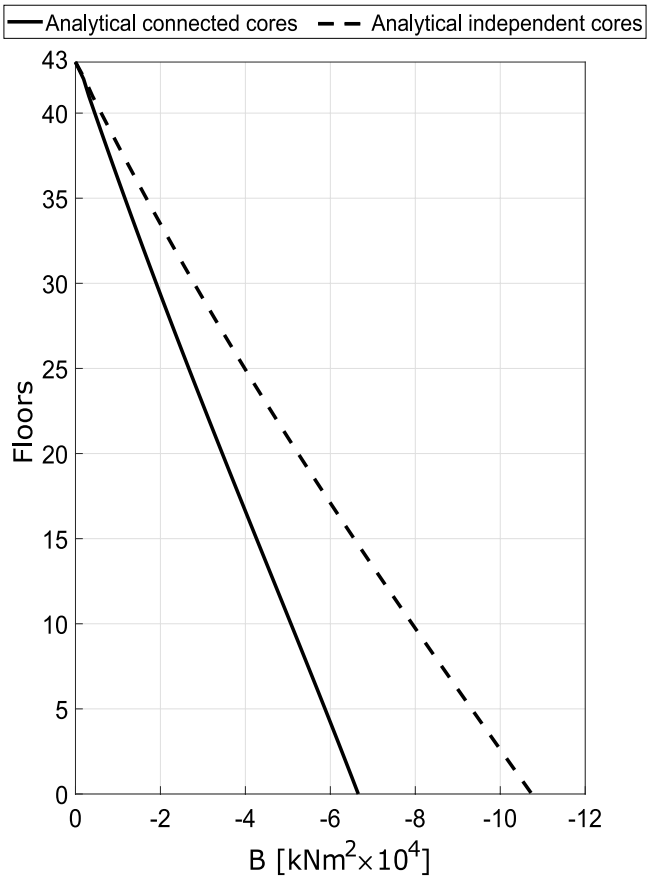

Figure 3.12: Bimoment on cores 1-3 [188]

Figure (3.12) shows bimoment on core 1, which is maximum at the base (warping prevented) and null at the top (free end). Also in this case the effect of the rigid connection with core 2 leads to a reduction in stress.

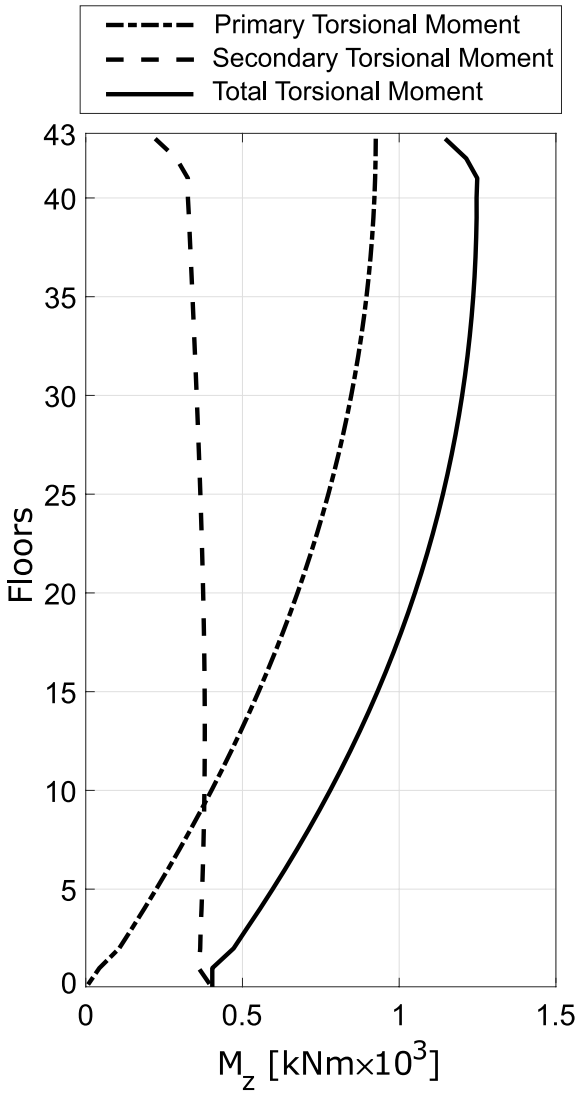

Figure 3.13: Primary, secondary and total torsional moments on cores 1-3 [188]

In the graphs shown in Figure (3.13) we can see that the total torsional moment can be subdivided into primary (derived from Saint Venant's Theory) and secondary (derived from Vlasov's Theory). It is important to note that, in the section at the base, the primary torsional moment is null. This result is a direct consequence of the formulated boundary conditions, i.e. the fixed constraint prevents the warping of the section (i.e. $\vartheta' = 0$). In the top section, however, the sum of the total torsional moment acting on the four cores is equal to the externally applied moment. In the intermediate sections, the trend is determined by the first and third derivative of the floor rotations as illustrated in Equations (3.20b and 3.20c).

Observing Figure (3.14), where the shear diagram is shown, we can see that

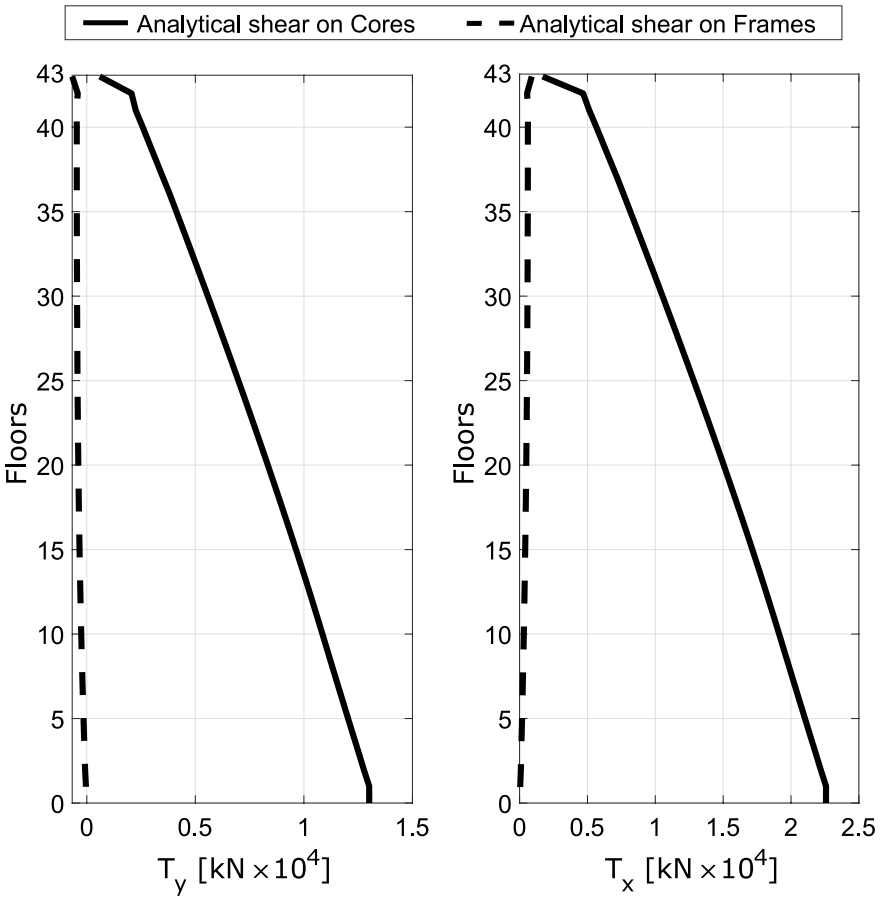

Figure 3.14: Shear forces on the cores and frames [188]

the frames, due to their weak stiffness, do not contribute to stiffening the structure with respect to the horizontal load. The horizontal load is almost entirely absorbed by the four central cores, while the frames, arranged around the perimeter of the building, take on considerable importance only in order to absorb the vertical loads.

3.3.6 Stresses

A schematic representation of core 1 is shown in Figure (3.15). Figure (3.16) shows the comparison between the stresses in the base section of core 1, evaluated by the analytical model with the independent and rigidly connected cores.

The standard stresses due to the wind load in the section of the base are obtained by the following equation:

$$\sigma_z = \frac{M_x}{J_{xx}} y - \frac{M_y}{J_{yy}} x + \frac{B}{J_{\omega\omega}} \omega \tag{3.21}$$

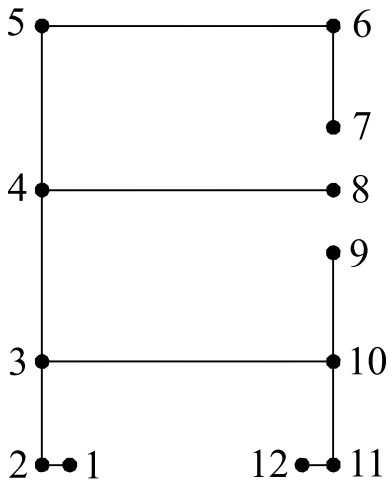

Figure 3.15: Numbering of the nodes of core 1 [188]

where M_x and M_y indicate the bending moment with reference to the x and y axes, B indicates bimoment, I_{xx} and J_{yy} indicate the moments of inertia with respect to x and y, and ω indicates the sectorial area.

Assuming that the bending moments of the two models are almost identical, we can make two important observations.

First of all, we can see that, by connecting the cores, the stresses due to M_y present the same sign in every point of the core because the neutral axis no longer referred to each core, but to the section made up of the two cores. In this case, the rigid connection causes tensile stress in all points of core 1 and compressive stress on all points of core 2.

The second observation concerns the modulus of stresses (3.17) in that, connecting the cores, the stress due to M_y is drastically reduced because the moment of inertia of the section made up of the two cores connected together is much greater than that of the single core. The same effect is seen on the stresses induced by bimoment, although in this case, the reduction of stress is due to the reduction of warping, because the sectorial moment of inertia is the same in both models.

However, in this case, the stresses induced by warping do not have much influence over bending stresses.

The result was predictable because the geometry of the building, in this case, is quite regular. Moreover, the designers, wishing to limit the torsional effects as much as possible, arranged the cores in such a way as to generate polar symmetry, limiting the effects due to the asymmetries present in each core.

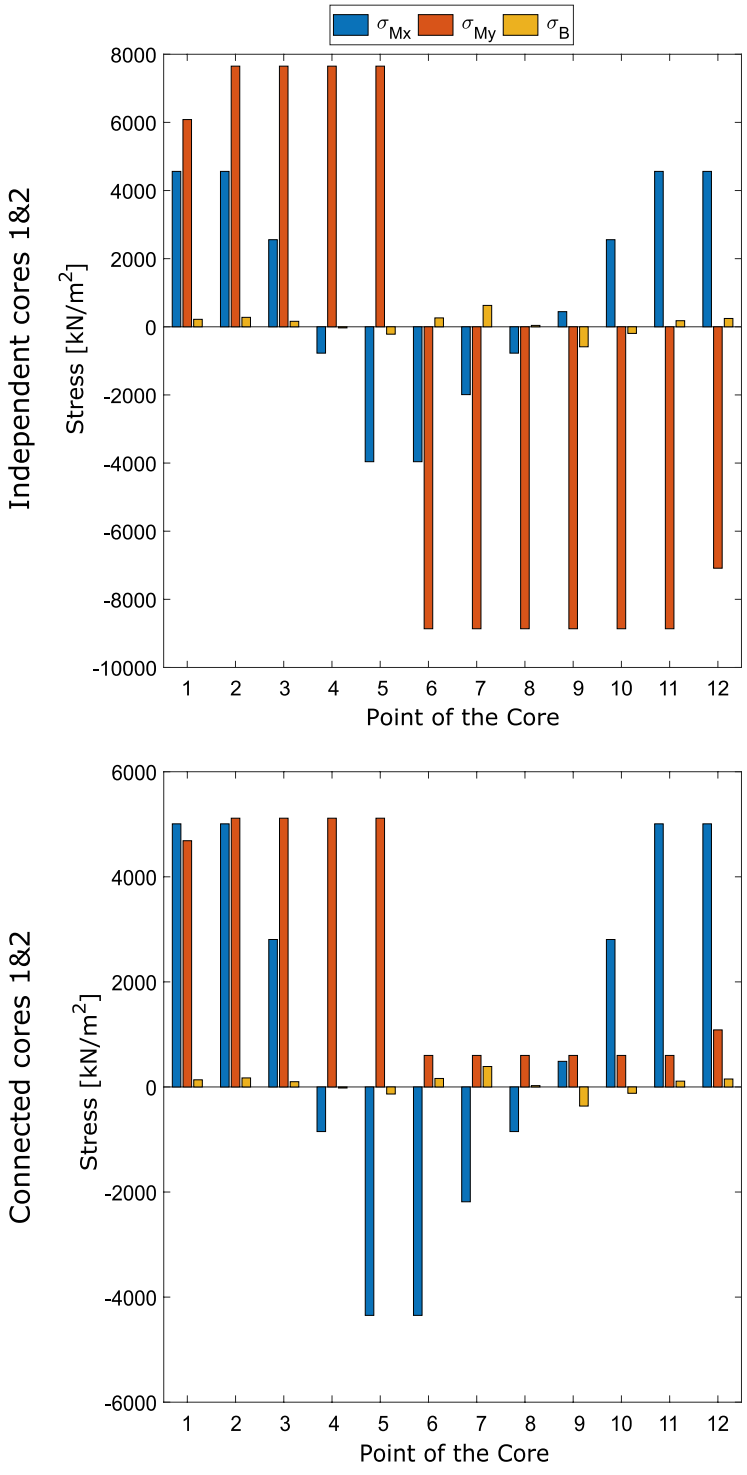

Figure 3.16: Vertical stresses on the core 1 [188]

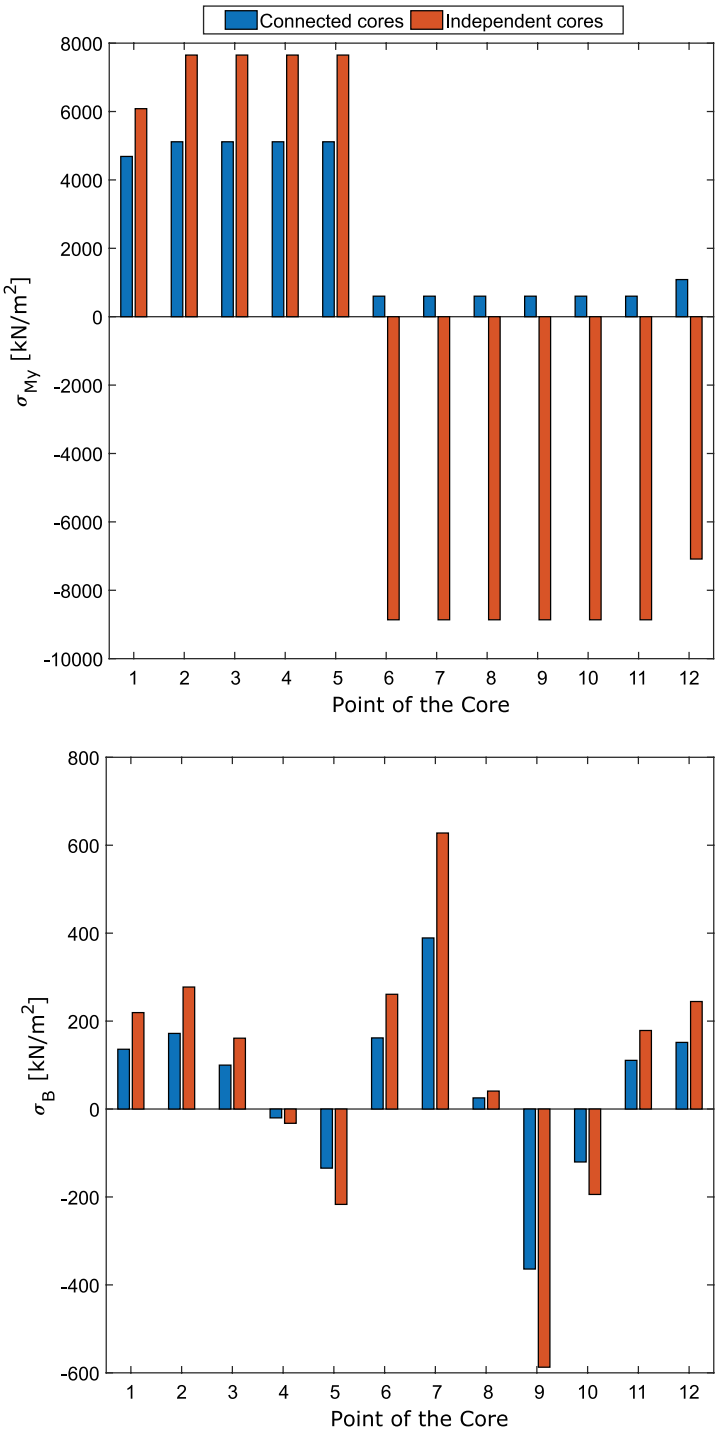

Figure 3.17: Comparison between vertical stresses due to the bending moment M_y (σ_{My}) and the bimoment (σ_B) in the core 1 [188]

In order to verify the reliability of the results of the analytical model for the core 1, a comparison with FEM model in terms of stresses are reported in Figure (3.18).

As can be observed, the differences in percentage between the results obtained using the analytical model and those obtained using the FEM model varies between +13.7% (point 6) and -4.5% (point 12), but the average difference in absolute terms is about +10%. This result emphasizes the reliability of the analytical formulation.

Moreover, by using the analytical calculation code it is possible to split the vertical stress into the contributions given by the two bending moments M_x, M_y, and bimoment B, as shown in Figure (3.16). Using commercial FEM software, this differentiation is generally not possible.

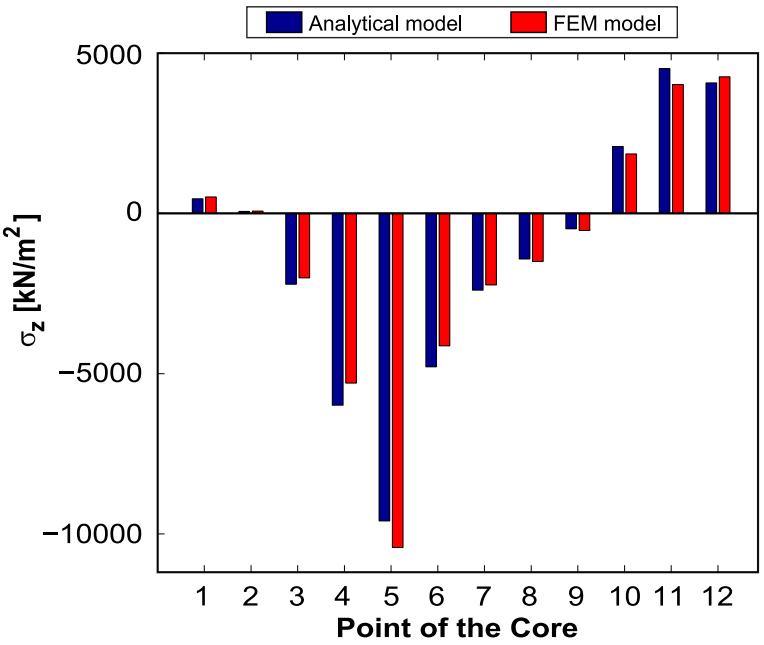

Figure 3.18: Comparison between vertical stresses for analytical and FEM model (rigidly connected cores)

3.3.7 Considerations on floor stiffness

As described in the previous sections, in the analytical formulation the floor slabs are rigid in their own plane, but their out-of-plane stiffness is neglected. Consequently, in order to validate the results obtained with the analytical calculation code, the FEM models shown in the previous sections were performed following the same hypothesis. In these FEM models, the floor slabs are not physical plate elements, but their effect was modeled using the rigid-links, namely a particular

type of constrains which allows only certain degrees-of-freedom of “slave nodes” to a “master node”. By setting the properties of the rigid-links, the displacements ξ, η, and ϑ of all the elements nodes included in each plane (slave nodes) are connected to a node located in the geometric center of the plane (master node), simulating the infinite in-plane stiffness of the slab. The displacements and rotations outside the plane, instead, are not transmitted between the nodes simulating in this way the null out-of-plane stiffness of the floors. This approach is commonly accepted in the preliminary design stages.

In this section, in order to confirm the validity of these simplified hypothesis, a more accurate FEM model in which the floors have their real stiffness is introduced.

As previously mentioned, the slabs in lightweight concrete are made by means of the Bubble Deck Technique, i.e. using high density polyethylene (HDPE) bubbles with a diameter of 225 mm embedded in a concrete casting. To perform a FEM model of this type of slab is very arduous, but some studies [26], [120], [135], [207] determined that it can be modeled using a "solid-plate" elements, with a thickness equal to that of the real slab, but using an homogeneous isotropic and linear material having the normal modulus of elasticity equal to 90% of the concrete of which it is really made. By considering these assumptions, this section shows the comparison in terms of displacements and stresses between the analytical model (the floor slabs are rigid in their own plane, but their out-of-plane rigidity is neglected), the FEM model in which the floors are modelled using rigid-links, and the FEM model in which the floors are modelled using 4-node plate elements with a thickness of 0.34 m, and normal elastic modulus of 27 GPa. Conversely, as already mentioned, core pairs 1-2 and 3-4 are connected by 0.50 meter thick concrete slabs.

To model this portion of the floor, 4-node plate elements with an elastic modulus of 35 GPa are employed. In Figure (3.19) the displacements obtained with the three models previously illustrated are shown. With regard to the x-direction displacements (ξ), the FEM model with rigid-link and the analytical model are more rigid with respect to the FEM model with real floor stiffness.This is due to the fact that in the first two models the connection between the cores pairs 1-2 was considered to be along the entire height of the building, while in the last FEM model the connection is only made at the level of each floor. With regard to displacements in the y-direction (η), the effect of the stiffness outside the plane means that the displacements are fewer than those analytical calculated and those obtained with the rigid links FEM model. With regard to the floor rotations (ϑ) the effect of the real stiffness outside the plane involves that the spins smaller on the lower floors of the building, but larger on the upper floors if compared with those obtained with the other two models. However, as can be seen from Table 3.1, despite considering the real stiffness of the floors in-plane and out-of-plane, the differences between the three models are very slight.

In addition to the comparison in terms of displacement, as depicted in Figure (3.20), a comparison of the normal stresses evaluated at the base of core 1 is also

made. Also in this case, as shown in Table 3.2, the differences between the three models are very slight.

In conclusion, in this section it has been shown that making complex calculation models, in which the real stiffness of the floors is considered, produces minimal differences compared to simplified models. On the other hand, making complex models involves a longer creation time and a considerable increase in calculation time because the number of DOFs, and therefore the unknowns of the numerical problem, increase dramatically. Consequently, in the preliminary design stages, it is advisable to use simplified models that are easy to implement and lead to acceptable and realistic results in a short calculation time.

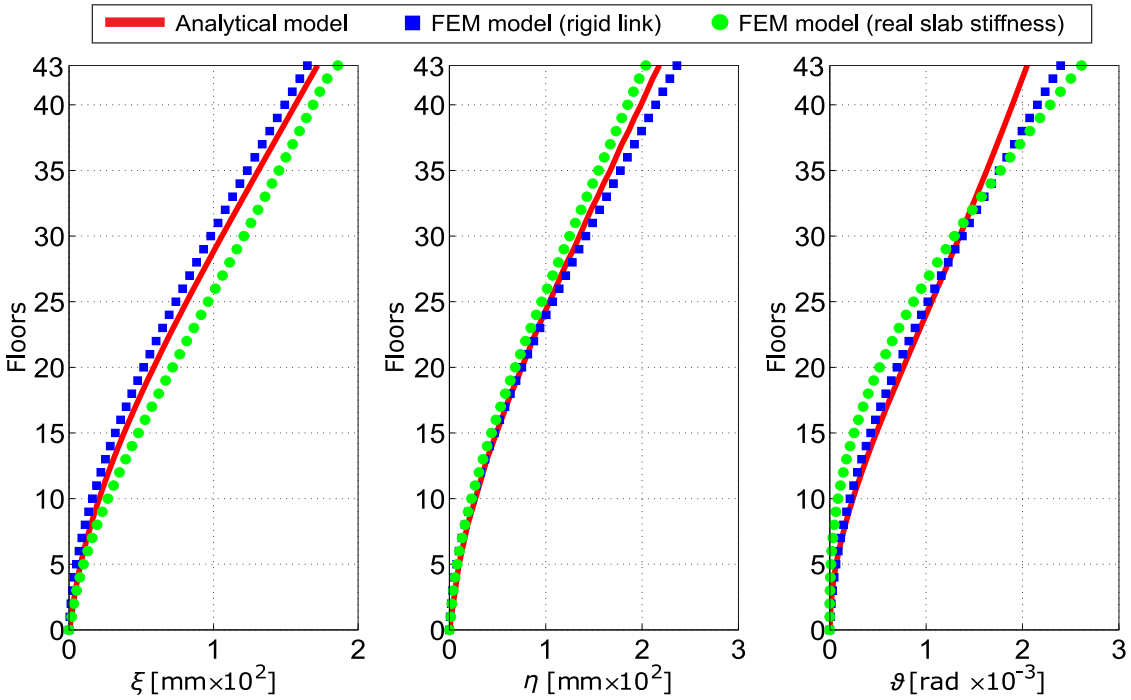

Figure 3.19: Comparison of building displacements

Table 3.1: Percentage differences of displacements

Models	ξ		η		ϑ	
	Max	Aver.	Max	Aver.	Max	Aver.
FEM(rigid) - FEM(real stiff.)	12.89	8.39	11.88	6.63	8.76	6.27
Analytical - FEM(rigid)	6.81	4.48	7.69	3.42	14.55	7.17
Analytical - FEM(real stiff.)	8.25	5.13	6.91	3.55	18.82	13.24

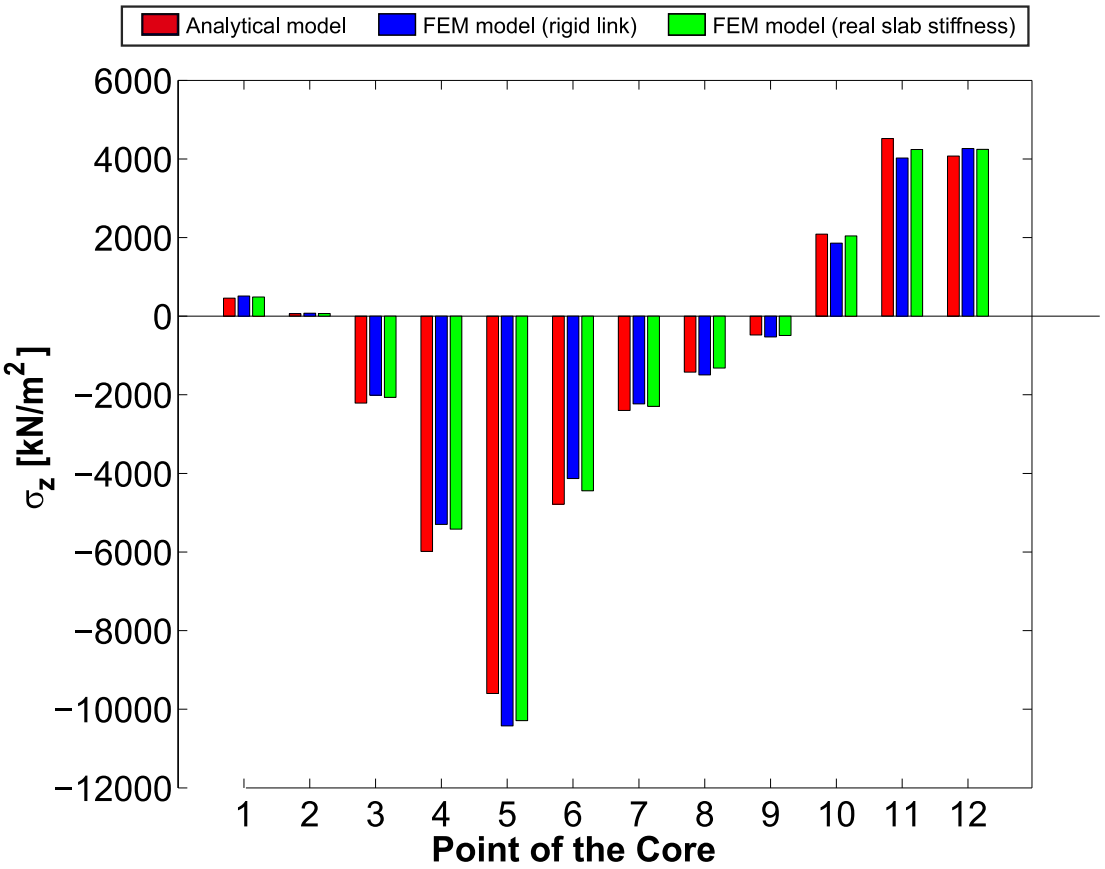

Figure 3.20: Comparison between vertical stresses in the base section of core 1

Table 3.2: Percentage differences of vertical stresses in the base section of core 1

Models	**Points of the core**					
	1	2	3	4	5	6
FEM(rigid) - FEM(real stiff.)	-4.85	-9.54	2.81	2.28	-1.28	7.58
Analytical - FEM(rigid)	12.23	14.13	-8.99	-11.49	8.63	-13.67
Analytical - FEM(real stiff.)	6.79	3.24	-6.43	-9.47	7.24	-7.13

Models	**Points of the core**					
	7	8	9	10	11	12
FEM(rigid) - FEM(real stiff.)	2.79	-11.87	-7.33	9.85	5.46	-0.46
Analytical - FEM(rigid)	-6.82	5.09	11.13	-10.87	-10.97	4.68
Analytical - FEM(real stiff.)	-4.23	-7.38	2.98	-2.10	-6.11	4.20

Chapter 4

Dynamic analysis

In this chapter, a semi-analytical formulation for the evaluation of the free vibrations of a three-dimensional tall building is proposed.

The methodology is intended to be used by engineers in the preliminary design phases as it allows the evaluation of the dynamic response of high-rise buildings consisting of thin-walled closed- or open-section shear walls, frames, framed tubes, and diagrid systems. If thin-walled open-section shear walls are present, the stiffness matrix of the element is evaluated considering Vlasov's Theory using the methodology shown in Section 2.2.1.

Using the procedure called *General Algorithm*, which allows to assembly the stiffness matrices of the individual vertical bracing elements, it is possible to model the structure as a single equivalent cantilever beam. Furthermore, assuming that the floors are infinitely rigid in their own plane, the degrees of freedom (DOF) of the structural system are reduced to only three per floor: two translations in the x and y directions and a rigid rotation of the floor around the vertical axis of the building.

This results in a drastic reduction of calculation times compared with those necessary to carry out the same analysis using commercial software that implements Finite Element models. The potential of the proposed method is confirmed by a numerical example, which demonstrates the benefits of this procedure.

4.1 Introduction

In recent decades there has been a rapid increase in the number of high-rise buildings [4] and many of these are built in highly seismic areas. As a result, the study of their dynamic behavior has aroused the interest of engineers around the world. The main objective of designers is to increase structural safety and reduce the amplitude of the oscillations in order to guarantee the integrity and comfort of the occupants [44], [133].

Considering that seismic forces are proportional to the mass of the structure itself, and that the response of the structure depends on the rigidity of the structure, it is deduced, in a somewhat counterintuitive way, the more rigid structures are subject to greater inertial forces than more flexible ones. For this reason, high-rise buildings, as well as long-span bridges, are generally not very susceptible to the effects of an earthquake [243]. However this does not mean that the dynamic study should be omitted or underestimated.

In the design process, particular attention must be paid to the determination of the center of stiffness of the entire building. In fact, considering that the forces of inertia are applied in the center of mass of each floor, the further this point is away from the center of stiffnesses the greater the torsional effects due to the action of horizontal loads [244].

Since many tall buildings have an irregular floor plan, which often changes geometry from one floor to another, it is very complex to match the stiffness center and the geometric center of gravity of each floor [155]. For this reason, it is essential to study the dynamic response of the building by carrying out three-dimensional flexural and torsional coupled analysis [90].

Today, most engineers use commercial Finite Element software to perform structural analysis even in the preliminary design stages. This software, although simple to use, involve long calculation times and results that are difficult to interpret, especially if dynamic nonlinear pushover analysis is performed. Alternatively, the analytical methods present in literature can be used, but these often involve complex and difficult calculations to carry out in a hand.

In this context, the analytical procedure proposed in this section is inserted, which implemented in a calculation code, allows to evaluate with a good approximation the frequencies of vibration and the modal shapes of a high-rise building in short times and with little outlay of resources [189]. For this reason, the proposed method can be an excellent aid for designers who can use it in the preliminary design phases.

In literature there are two types of study: the former define mathematical models for analyzing the behavior of a single beam, while the latter are intended to define analytical models, generally more complex than the former, for the dynamic behavior of a whole building. In the latter case, it becomes essential to consider the mass of the floors connecting the various vertical structural elements.

4.1.1 Literature review for the analysis of a thin-walled open-section beam

From an analytical point of view, the evaluation of the dynamic response of a thin-walled open-section beam has attracted the attention of many researchers. In 1940 Garland [108] described the behavior of a cantilever beam using the Rayleigh-Ritz method [70]. Among the results obtained, a graph is shown that summarizes

the variation of the natural vibration frequencies as a function of the geometric characteristics of the beam. However, he himself admits that the analytical solutions are approximate and do not necessarily obtain the vibration frequencies for high order modes.

In the early 1950s, Timoshenko [252] studied the dynamic behavior of beams in which the geometric center of gravity did not coincide with the shear center and consequently coupled bending and torsional vibrations occurred. By using energy methods, he was able to obtain the exact solution just for beams that were simply supported, while for beams which were, he obtained approximate values. A few years later, Gere [109], [110] extended this formulation to be able to analyze thin-walled open-section beams, with various constraint conditions. Further simplified approaches based on Vlasov's Theory [261] and on Wagner-Kappus Theory [13] were proposed by Bishop et al. [28], [29].

The first attempts to determine the exact solution in the case of coupled bending and torsional vibrations in thin-walled open-section beams were conducted by Dokumaci [92] in a work published in 1987. Numerical results are given to explain the effect of the shear centre offset on the natural frequencies.

A few years later, this method was extended by Bishop [27] also taking into account the deformation of the section. At the end of the 1990s, Yaman [275] extended this formulation by also introducing an external force while Tanaka e Bercin [241] implemented the exact formulation proposed by Dokumaci and Bishop using Mathematica, a software capable of solving differential equations. This work can be considered a first step towards the automation of the calculation of modal shapes and the periods of vibration, as it allows the analysis of a beam however it is restrained.

The effects on dynamic behavior due to shear deformability, which is neglected in the classical Vlasov's Theory, as well as the variability of the geometry of the section along the axis of the beam were examined by Ambrosini [5], [6], [7], [8] using the state variables.

Nonsymmetrical thin-walled open-section beams have been studied by Arpaci [14] and Kim [141].

In 2003 Di Egidio et al. [95], [96], using Vlasov's kinematical hypotheses, formulated a non-linear one-dimensional model for the dynamics of the thin-walled open-section beam. With this method, three non-linear differential equations of motion are derived using the Hamilton principle [90]. Numerical and experimental results confirm the validity of the analytical model [97], and the role of the internal resonances related to the nonlinear warping coupling terms is considered [94].

Alongside the analytical approaches, numerical procedures based on shape functions have also been developed, such as the methods proposed by Zhang [283], Chen [69], and Hu [130].

Finally, an interesting experimental study is proposed by Klausbruckner and Pryputniewicz [145].

4.1.2 Literature review for the analysis of an high-rise building

In the preliminary stages of the design of a high-rise building, it is essential to estimate with good approximation the possible vibrating mode shapes of the structure in order to guarantee to future occupants the necessary conditions of comfort.

Among the first studies on the dynamic behavior of a building, is the work of Mallick [171] who analyzed a shear walls structure. A similar model was taken up in 1981 by Paulay [192]. The case in which the core is composed by thin-walled open-section shear walls connected by rigid floors was treated by Mendelson [176], [177] who examined the structural response of a non-symmetrical multi-storey structure with or without damping effect. Approximate analytical methods for estimating the vibration periods of high-rise buildings composed by many structural elements were presented by Stafford Smith and Crowe [229], and some years later by Wang [266] and Zalka [277].

In the mid-1990s, Pekau published two works [193], [194] in which the Finite Story Method is used, that is the global behaviour of the building depends on the nodal displacements of two-storey substructures into which the whole construction is split.

For the dynamic analysis of coupled shear walls, Swaddiwudhipong [235], [236] used the continuum medium technique that can model the tip connection generated by the floors, as a continuum having equivalent geometric properties and also considers the axial deformation by the Galerkin Method. In 2007, Meftah [173] formulated a simple analytical method that uses the Galerkin technique, for the evaluation of the free vibrations of buildings braced by shear walls and open-section elements.

In 2009 Bozdogan presents a formulation that, using the transfer matrix method [42], allows approximated dynamic analysis of a symmetric wall-frame building [37] and thin-walled open-section structures [41]. In the following years this procedure was optimized as the multi-storey structure was modeled as an equivalent cantilever beam [39] and the shear walls and frames were assumed to be flexural and shear cantilever beam structures [38]. Finally, applying the Differential Transform Method to convert the differential equation into an algebraic equation, the same author considered the free vibration analysis of the tube-in-tube tall buildings [40].

In 2015 Piccardo et al. [197] formulated an equivalent nonlinear one-dimensional shear-shear torsional beam model which reproduces, the dynamic behavior of tower buildings through a heuristic identification method. Subsequently, taking inspiration from fluid-elastic models, this method was extended to take account of non-linearities generated by the stretching of the columns [198], and the mechanical non-linearities [200], which are often believed to be unimportant but do affect the amplitude of motion. Recently these same authors have proposed a model for static

and dynamic analysis of tall buildings based on the Timoshenko equivalent column [199]. There are also techniques in the literature that can evaluate the dynamic behavior of tall buildings with not only shear walls, but also braced frame systems [35], [172], outrigger [191], [227], and tube-in-tube structures [156], [160], [265].

Eventually, it is interesting to note how the seismic performance of the building can vary according to the actual rigidity of the floors [157], [168], or in buildings with a large bottom podium [284].

In the present work, a formulation is proposed for the three-dimensional analysis of a high building based on the General Algorithm illustrated in Chapter 3. The basic formulation has already been published in some works [47], [57], [63], while in the present elaboration it has been extended in order to analyze the greatest possible type of high-rise buildings, for example framed tube or diagrid, as well as for structures in which there are simultaneously cores of different heights, and irregular buildings in floor plan or in height. Furthermore, the algorithms of the calculation code in which it is implemented have been improved and enhanced.

4.2 Dynamic analysis of high-rise buildings

An N-storey high-rise building with M vertical bracings is considered. An arbitrary global reference system and a local reference system with origin in the shear center of each resistant element are introduced; the vectors $\{\xi\}$, $\{\eta\}$, and $\{\vartheta\}$ containing the displacements of the origin of the global reference system are designed. It is possible to define the vectors containing the displacements of the shear center $\{\xi_{C,i}\}$ and $\{\eta_{C,i}\}$ of the i-th resistant element as:

$$\{\xi_{C,i}\} = \{\xi\} - y_i\{\vartheta\} \tag{4.1a}$$

$$\{\eta_{C,i}\} = \{\eta\} + x_i\{\vartheta\} \tag{4.1b}$$

where x_i and y_i are the coordinates of the shear center of the i-th bracing, referring to the global reference system. In a similar way and as is illustrated in the previous chapters, the entire building (Figure 4.1a) is modeled as an equivalent cantilever beam in which the masses of the floors are concentrated in the gravity center of their own, as shown in Figure (4.1b).

Considering that the dynamic equation of the system in absence of viscous dissipations can be written as:

$$[m]\{\ddot{\delta}\} + [k]\{\delta\} = \{0\} \tag{4.2}$$

for the j-th floor it is possible to write the equation of dynamic equilibrium in x-direction:

$$m_j\ddot{\xi}_{G,j} + \sum_{i=0}^{M}\left(\{k_{x_{i,j}}\}\{\xi_{C,i}\}\right) = 0 \tag{4.3}$$

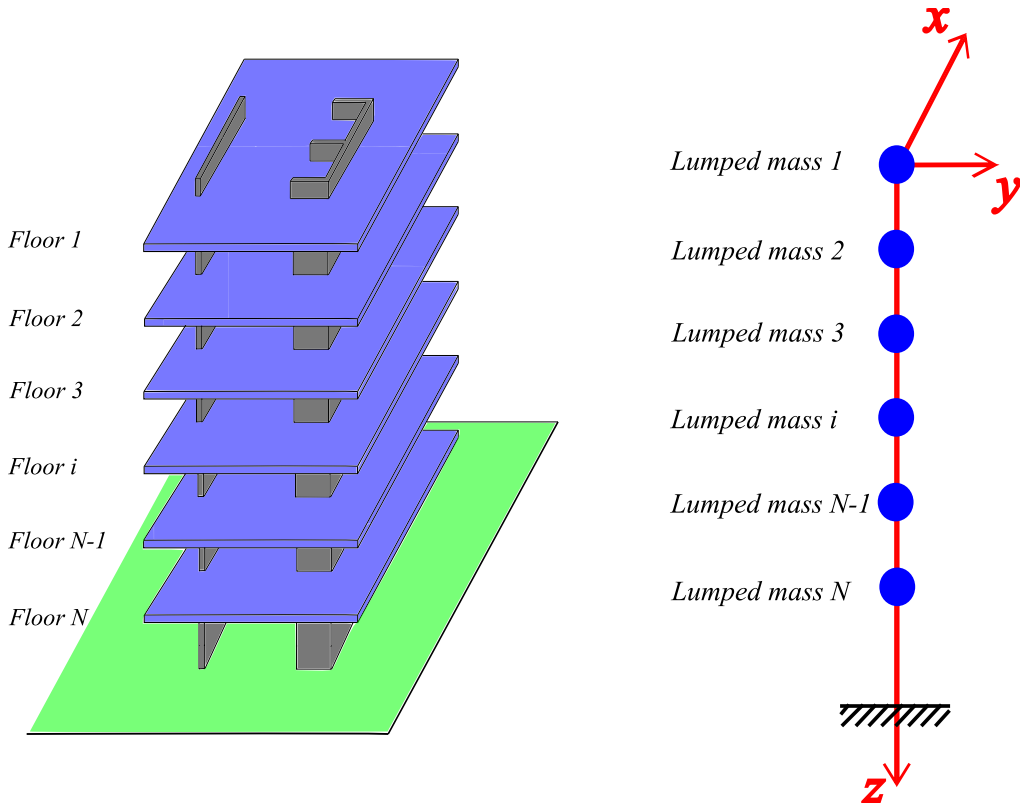

(a) (b)

Figure 4.1: (a) 3D-model of the building; (b) Equivalent cantilever beam with lumped masses

where m_j and $\ddot{\xi}_{G,j}$ are mass and acceleration in x-direction of the j-th storey, respectively, $\{k_{x_{i,j}}\}$ is the vector corresponding to the j-th row of the local stiffness matrix (estimated for the x-direction only) of the i-th resistant element, and $\{\xi_{C,i}\}$ is the vector containing the i-th vertical bracing displacements in x-direction of the shear center of all floors. Considering Equation (4.1a), the term $\ddot{\xi}_{G,j}$ can be written as:

$$\ddot{\xi}_{G,j} = \ddot{\xi}_j - y_{m,j}\ddot{\vartheta}_j \tag{4.4}$$

where ξ_j and ϑ_j are respectively the x-direction displacements and the rotation angle of the global reference system origin of the j-th floor, while, $y_{m,j}$ is the coordinate of the center of mass of the j-th floor with respect to the origin of the global reference system. Replacing Equations (4.1a and 4.4) into Equation (4.3), we obtain:

$$m_j\left(\ddot{\xi}_j - y_{m,j}\ddot{\vartheta}_j\right) + \sum_{i=0}^{M}\Big[\{k_{x_{i,j}}\}\left(\{\xi\} - y_i\{\vartheta\}\right)\Big] = 0 \tag{4.5}$$

If we consider all the N storeys of the building, we obtain the following system of equations:

$$\begin{gathered} m_1\left(\ddot{\xi}_1 - y_{m,1}\ddot{\vartheta}_1\right) + \sum_{i=0}^{M}\Big[\{k_{x_{i,1}}\}\Big(\{\xi\} - y_i\{\vartheta\}\Big)\Big] = 0 \\ m_2\left(\ddot{\xi}_2 - y_{m,2}\ddot{\vartheta}_2\right) + \sum_{i=0}^{M}\Big[\{k_{x_{i,2}}\}\Big(\{\xi\} - y_i\{\vartheta\}\Big)\Big] = 0 \\ \vdots \\ m_N\left(\ddot{\xi}_N - y_{m,N}\ddot{\vartheta}_N\right) + \sum_{i=0}^{M}\Big[\{k_{x_{i,N}}\}\Big(\{\xi\} - y_i\{\vartheta\}\Big)\Big] = 0 \end{gathered} \tag{4.6}$$

Introducing the matrices:

$$[M_{xx}] = \begin{bmatrix} m_1 & 0 & \cdots & 0 \\ 0 & m_2 & \cdots & 0 \\ \vdots & \vdots & \ddots & \vdots \\ 0 & 0 & \cdots & m_N \end{bmatrix} \tag{4.7a}$$

$$[M_{x\vartheta}] = \begin{bmatrix} -m_1 y_{m,1} & 0 & \cdots & 0 \\ 0 & -m_2 y_{m,2} & \cdots & 0 \\ \vdots & \vdots & \ddots & \vdots \\ 0 & 0 & \cdots & -m_N y_{m,N} \end{bmatrix} \tag{4.7b}$$

$$[K_{x_i}] = \begin{bmatrix} \{k_{x_{i,1}}\} \\ \vdots \\ \{k_{x_{i,N}}\} \end{bmatrix} \tag{4.7c}$$

the system of Equations (4.6) can be written in compact form:

$$[M_{xx}]\{\ddot{\xi}\} + [M_{x\vartheta}]\{\ddot{\vartheta}\} + \sum_{i=0}^{M}[K_{x_i}]\{\xi\} - \sum_{i=0}^{M}\Big(y_i[K_{x_i}]\Big)\{\vartheta\} = \{0\} \tag{4.8}$$

Defining the following matrices:

$$[K_{xx}] = \sum_{i=0}^{M}[K_{x_i}] \tag{4.9a}$$

$$[K_{x\vartheta}] = -\sum_{i=0}^{M}\Big(y_i[K_{x_i}]\Big) \tag{4.9b}$$

where $[K_{xx}]$ indicates the stiffness matrix of the entire building evaluated for x-direction only, the equation of the dynamic equilibrium can be written as:

$$[M_{xx}]\{\ddot{\xi}\} + [M_{x\vartheta}]\{\ddot{\vartheta}\} + [K_{xx}]\{\xi\} + [K_{x\vartheta}]\{\vartheta\} = \{0\} \tag{4.10}$$

In a completely analogical way, the equation of dynamic equilibrium in the y-direction can be written as:

$$[M_{yy}]\{\ddot{\eta}\} + [M_{y\vartheta}]\{\ddot{\vartheta}\} + [K_{yy}]\{\eta\} + [K_{y\vartheta}]\{\vartheta\} = \{0\} \tag{4.11}$$

where η indicates the y-direction displacement vector of the global reference system origin, while the matrices are defined as follows:

$$[M_{yy}] = \begin{bmatrix} m_1 & 0 & \cdots & 0 \\ 0 & m_2 & \cdots & 0 \\ \vdots & \vdots & \ddots & \vdots \\ 0 & 0 & \cdots & m_N \end{bmatrix} \tag{4.12a}$$

$$[M_{y\vartheta}] = \begin{bmatrix} m_1 x_{m,1} & 0 & \cdots & 0 \\ 0 & m_2 x_{m,2} & \cdots & 0 \\ \vdots & \vdots & \ddots & \vdots \\ 0 & 0 & \cdots & m_N x_{m,N} \end{bmatrix} \tag{4.12b}$$

$$[K_{yy}] = \sum_{i=0}^{M} \begin{bmatrix} \{k_{y_{i,1}}\} \\ \vdots \\ \{k_{y_{i,N}}\} \end{bmatrix} = \sum_{i=0}^{M} [K_{y_i}] \tag{4.12c}$$

$$[K_{y\vartheta}] = \sum_{i=0}^{M} x_i \begin{bmatrix} \{k_{y_{i,1}}\} \\ \vdots \\ \{k_{y_{i,N}}\} \end{bmatrix} = \sum_{i=0}^{M} x_i [K_{y_i}] \tag{4.12d}$$

The equation of the dynamic equilibrium rotation for the j-th floor and for the i-th vertical bracing can be written as:

$$\begin{aligned} &- \left(\{k_{x_{i,j}}\}\{\xi_{C,i}\}\right) y_{i,j} + \left(\{k_{y_{i,j}}\}\{\eta_{C,i}\}\right) x_{i,j} - \left(m_j \ddot{\xi}_{G,j}\right) y_{m,j} + \\ &+ \left(m_j \ddot{\eta}_{G,j}\right) x_{m,j} + I_{\mathrm{G},j} \ddot{\vartheta}_j = 0 \end{aligned} \tag{4.13}$$

in which the terms $\left(\{k_{x_{i,j}}\}\{\xi_{C,i}\}\right)$ and $\left(\{k_{y_{i,j}}\}\{\eta_{C,i}\}\right)$ are the elastic forces in x and y directions, the terms $\left(m_j \ddot{\xi}_{G,j}\right)$ and $\left(m_j \ddot{\eta}_{G,j}\right)$ are the inertia forces, while the term $I_{\mathrm{G},j}\ddot{\vartheta}_j$ represents the relative angular moment of the j-th floor in which the polar moment of inertia appears to refer to the center of gravity of the floor. By inserting Equations (4.1 and 4.4), and the analogous equation written for the y-direction in Equation (4.13), we obtain:

$$\begin{aligned} &- \left[\{k_{x_{i,j}}\}\left(\{\xi\} - y_i\{\vartheta\}\right)\right] y_{i,j} + \left[\{k_{y_{i,j}}\}\left(\{\eta\} + x_i\{\vartheta\}\right)\right] x_{i,j} + \\ &- \left[m_j\left(\ddot{\xi}_j - y_{m,j}\ddot{\vartheta}_j\right)\right] y_{m,j} + \left[m_j\left(\ddot{\eta}_j + x_{m,j}\ddot{\vartheta}_j\right)\right] x_{m,j} + I_{\mathrm{G},j}\ddot{\vartheta}_j = 0 \end{aligned} \tag{4.14}$$

and carrying out the calculations,

$$\begin{aligned} &- y_{i,j}\left\{k_{x_{i,j}}\right\}\{\xi\} + y_{i,j}^2\left\{k_{x_{i,j}}\right\}\{\vartheta\} + x_{i,j}\left\{k_{y_{i,j}}\right\}\{\eta\} + x_{i,j}^2\left\{k_{y_{i,j}}\right\}\{\vartheta\} + \\ &- m_j y_{m,j}\ddot{\xi}_j + m_j y_{m,j}^2\ddot{\vartheta}_j + m_j x_{m,j}\ddot{\eta}_j + m_j x_{m,j}^2\ddot{\vartheta}_j + I_{\mathrm{G},j}\ddot{\vartheta}_j = 0 \end{aligned} \tag{4.15}$$

For the Huygens-Steiner theorem, the angular moment which refers to the origin of the global reference system can be written as:

$$I_{\mathrm{O},j} = I_{\mathrm{G},j} + m_j\left(x_m^2 + y_m^2\right) = I_{\mathrm{G},j} + m_j r_m^2 \tag{4.16}$$

from which it follows that:

$$\begin{aligned} &- y_{i,j}\left\{k_{x_{i,j}}\right\}\{\xi\} + y_{i,j}^2\left\{k_{x_{i,j}}\right\}\{\vartheta\} + x_{i,j}\left\{k_{y_{i,j}}\right\}\{\eta\} + x_{i,j}^2\left\{k_{y_{i,j}}\right\}\{\vartheta\} + \\ &- m_j y_{m,j}\ddot{\xi}_j + m_j x_{m,j}\ddot{\eta}_j + I_{\mathrm{O},j}\ddot{\vartheta}_j = 0 \end{aligned} \tag{4.17}$$

Considering all the N storeys of the building, and all the M resistant vertical elements, we get a system of equations that, after introducing the matrices:

$$[M_{\vartheta\vartheta}] = \begin{bmatrix} I_{\mathrm{O},1} & 0 & \cdots & 0 \\ 0 & I_{\mathrm{O},2} & \cdots & 0 \\ \vdots & \vdots & \ddots & \vdots \\ 0 & 0 & \cdots & I_{\mathrm{O},N} \end{bmatrix} \tag{4.18a}$$

$$[K_{\vartheta\vartheta}] = \sum_{i=0}^{M}[K_{x_i}]\,y_i^2 + \sum_{i=0}^{M}[K_{y_i}]\,x_i^2 \tag{4.18b}$$

takes the following formulation:

$$[M_{x\vartheta}]\left\{\ddot{\xi}\right\} + [M_{y\vartheta}]\{\ddot{\eta}\} + [M_{\vartheta\vartheta}]\left\{\ddot{\vartheta}\right\} + [K_{x\vartheta}]\{\xi\} + [K_{y\vartheta}]\{\eta\} + [K_{\vartheta\vartheta}]\{\vartheta\} = \{0\} \tag{4.19}$$

The three-dimensional problem can be described by a system of three differential equations, each of which relates to the dynamic equilibrium in x-direction (4.10), y-direction (4.11), and to the rotation around the vertical axis of the structure (4.19).

Defining the mass matrix:

$$[M] = \begin{bmatrix} [M_{xx}] & [0] & [M_{x\vartheta}] \\ [0] & [M_{yy}] & [M_{y\vartheta}] \\ [M_{\vartheta x}] & [M_{\vartheta y}] & [M_{\vartheta\vartheta}] \end{bmatrix} \tag{4.20}$$

and the stiffness matrix:

$$[K] = \begin{bmatrix} [K_{xx}] & [0] & [K_{x\vartheta}] \\ [0] & [K_{yy}] & [K_{y\vartheta}] \\ [K_{\vartheta x}] & [K_{\vartheta y}] & [K_{\vartheta\vartheta}] \end{bmatrix} \tag{4.21}$$

the previously introduced system can be written in compact form as:

$$[M]\left\{\ddot{\delta}\right\} + [K]\{\delta\} = \{0\} \tag{4.22}$$

Assuming that the displacement vector $\{\delta\}$ is given by the product of a vector depending only on the spatial coordinate $\{\zeta(z)\}$ for a scalar depending only on time $\psi(t)$:

$$\{\delta\} = \{\zeta(z)\}\,\psi(t) \tag{4.23}$$

and replacing Equation (4.23) into Equation (4.22), we obtain:

$$[M]\{\zeta(z)\}\,\ddot{\psi}(t) + [K]\{\zeta(z)\}\,\psi(t) = \{0\} \tag{4.24}$$

Pre-multiplying both terms for $\{\zeta(z)\}^{\mathrm{T}}$,

$$\{\zeta(z)\}^{\mathrm{T}}[M]\{\zeta(z)\}\,\ddot{\psi}(t) + \{\zeta(z)\}^{\mathrm{T}}[K]\{\zeta(z)\}\,\psi(t) = \{0\} \tag{4.25}$$

and splitting the terms, it is possible to write:

$$\frac{\{\zeta(z)\}^{\mathrm{T}}[K]\{\zeta(z)\}}{\{\zeta(z)\}^{\mathrm{T}}[M]\{\zeta(z)\}} = \frac{\ddot{\psi}(t)}{\psi(t)} = \omega_n^2 \tag{4.26}$$

where the terms ω_n are the angular frequencies of the system.

Equation (4.26) can be written as two decoupled equations:

$$\ddot{\psi}(t) + \omega_n^2\psi(t) = 0 \tag{4.27a}$$

$$\{\zeta(z)\}^{\mathrm{T}}\left([K] - \omega_n^2[M]\right)\{\zeta(z)\} = \{0\} \tag{4.27b}$$

The solution of Equation (4.27a) can be expressed in the form:

$$\psi(t) = A\cos(\omega_n t) + B\sin(\omega_n t) = 0 \tag{4.28}$$

in which A and B are constants whose values are deducted from the initial conditions of the problem.

Equation (4.27b) is instead an eigenvalue problem and is solved by imposing that:

$$\det\left([K] - \omega_n^2[M]\right) = 0 \tag{4.29}$$

In this way it is possible to determine the $3N$ values of ω_n from which the natural frequencies ($f_n = \omega_n/2\pi$) and periods of vibration of the building ($T_n = 1/f_n$) are derived. Noting the n values of the angular frequencies, it is possible to determine the $3N$ eigenvectors $\{\zeta(z)\}$ that represent the building's deformed shapes relative to every mode of vibration.

In doing so, for each period of vibration, a deformed configuration is determined relative to the origin of the global reference system. By subsequently applying the General Algorithm, it is possible to define the displacements of all storeys of the i-th stiffening element and, therefore, the stresses acting on it.

4.3 Numerical example

In this section there will be illustrated the results that have been obtained investigating the Piedmont Region Headquarters Tower in Turin, already been published in [188]. The description of the building and the static analysis has already been addressed in Section 3.3; while the dynamic analysis carried out by applying the analytical formulation has determined the primary natural frequencies of the structure and the relative modes shape of vibration.

As far as the dynamic analysis is concerned, we considered the volume weight of the slabs to be 18.75 kN/m^3 and consequently the mass of each floor was calculated.

The numerical code was used to calculate the vibration frequencies (Table 4.1) and the mode shapes of the structure.

Table 4.1: Natural frequencies estimate for the first ten modes

Mode [-]	**Analytical model** [**Hz**]	**FEM model** [**Hz**]	**Percentage difference** [%]
1	0.178	0.201	12.92
2	0.195	0.222	13.85
3	0.577	0.671	16.29
4	1.276	1.214	-4.86
5	1.899	1.857	-2.21
6	2.133	1.898	-11.02
7	3.528	3.314	-6.07
8	5.252	4.837	-7.90
9	5.957	5.726	-3.88
10	6.894	6.501	-5.70

The natural frequencies of the first ten vibration modes are shown in Figure (4.2). In this case too, the rigid connection between cores 1-2 and 3-4 makes

it possible to obtain the vibration frequencies of the analytical model that lean towards those of the FEM model. In addition, the graph shows greater accuracy for the first vibration modes, and while there are larger differences for the others, this can be accepted as a first approximation.

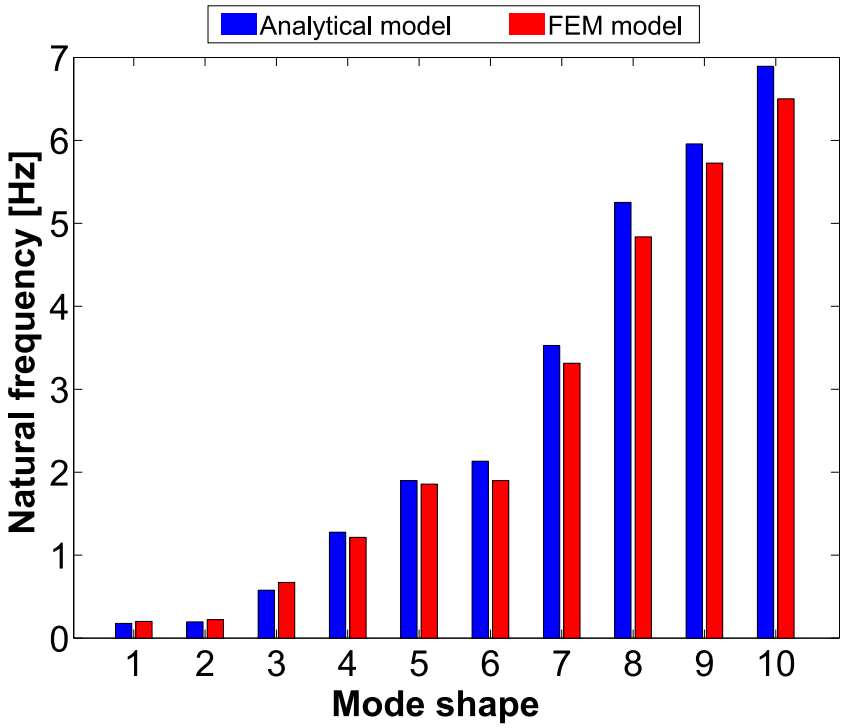

Figure 4.2: Comparison between FEM and analytical natural frequencies

The first six eigenvectors representing the dimensionless displacements of the origin of the global reference system (rigid connection between cores 1-2 and 3-4), are shown in the Figures (4.3, 4.4, 4.5, 4.6, 4.7, and 4.8).

Eventually, the Figure (4.9) shows the first six modes of vibration on the 3D model of the structure. In the first three vibration modes, nodal sections in deformed shapes do not appear, whereas, in the following three, they manifest themselves.

In particular, as can be observed in Figure (4.9), the first modal shape is predominantly bending, while second and third are predominantly torsional. The fourth mode shape is predominantly bending, but present one nodal section. The fifth and sixth are predominantly torsional modes, with one nodal section.

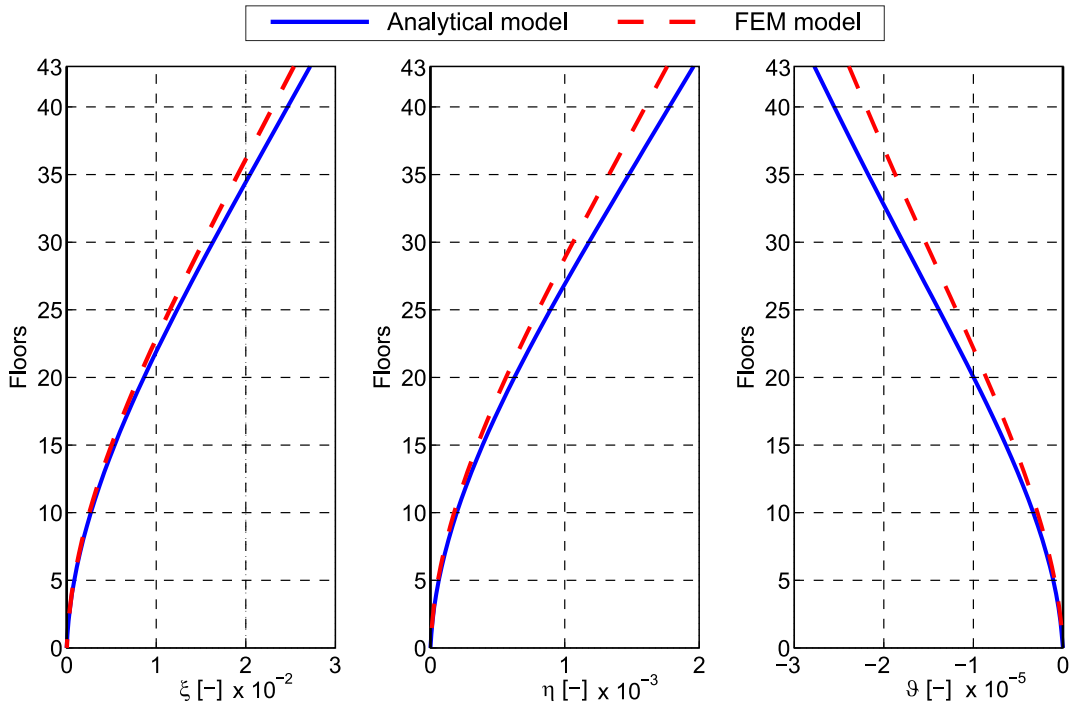

Figure 4.3: Dimensionless eigenvectors of the 1st mode

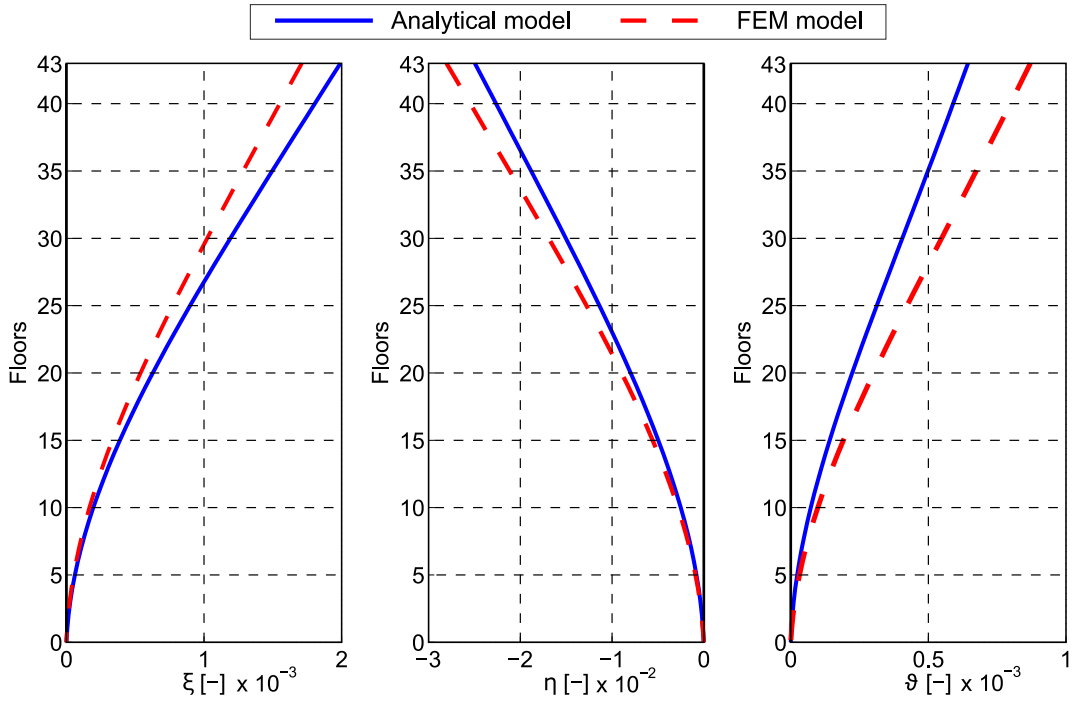

Figure 4.4: Dimensionless eigenvectors of the 2nd mode

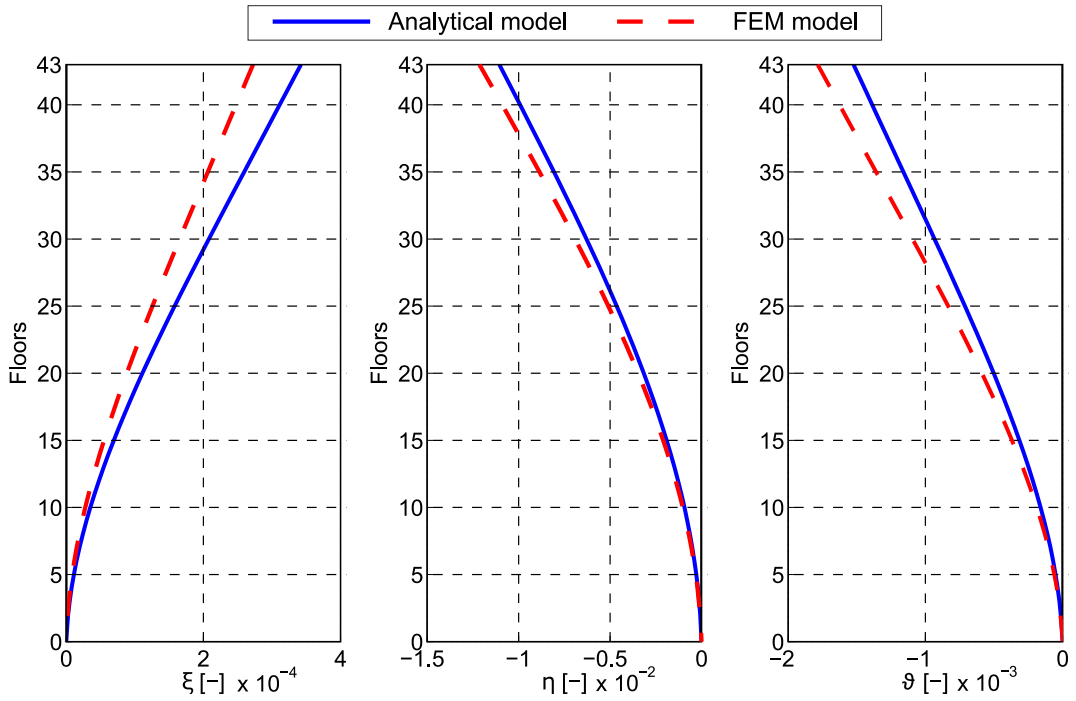

Figure 4.5: Dimensionless eigenvectors of the 3rd mode

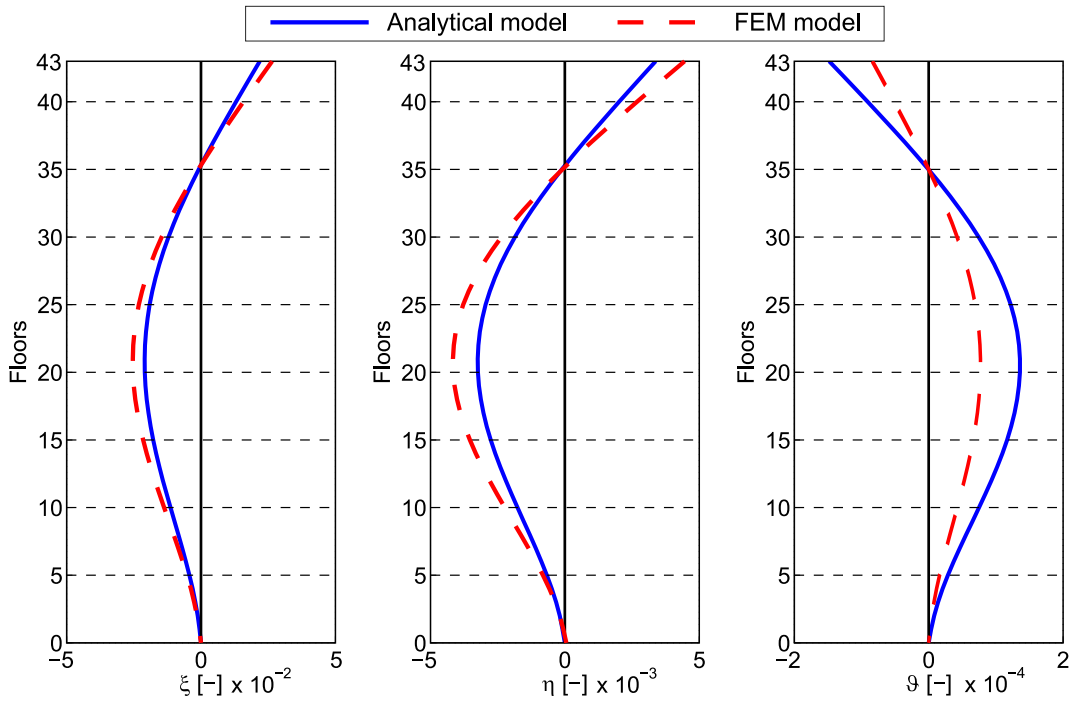

Figure 4.6: Dimensionless eigenvectors of the 4th mode

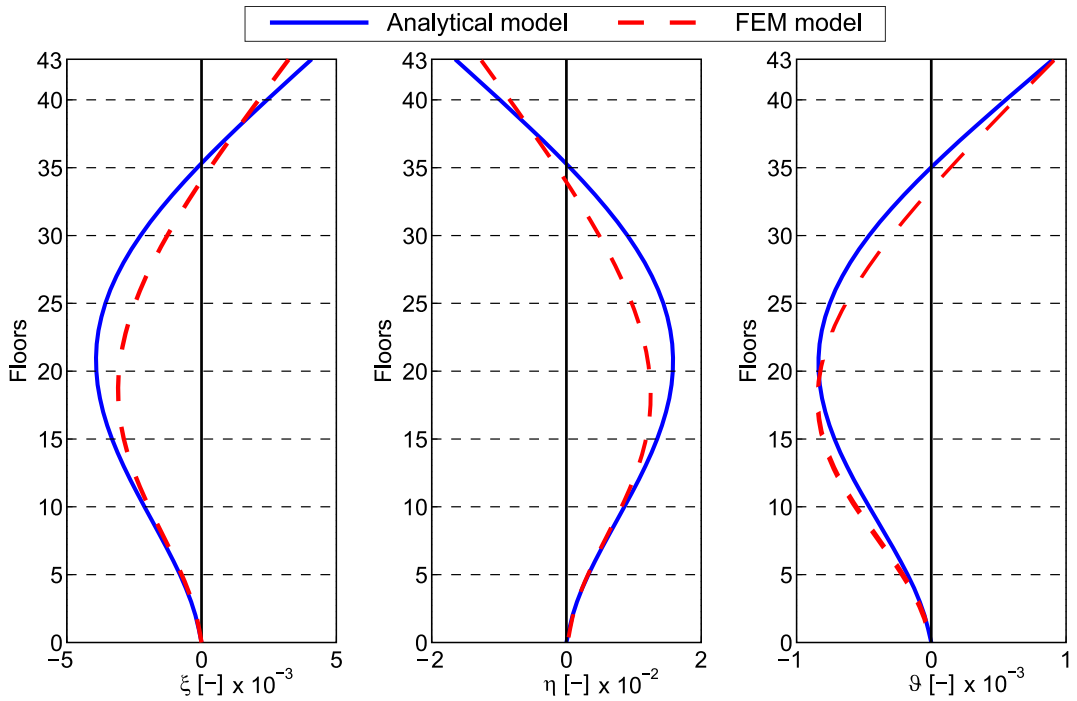

Figure 4.7: Dimensionless eigenvectors of the 5th mode

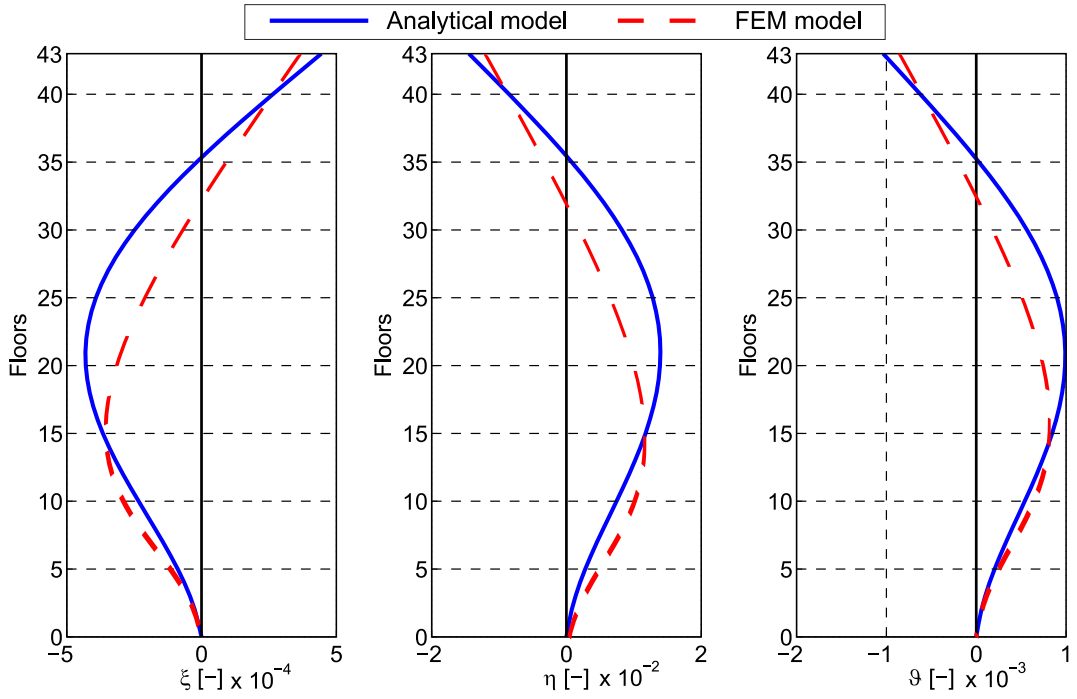

Figure 4.8: Dimensionless eigenvectors of the 6th mode

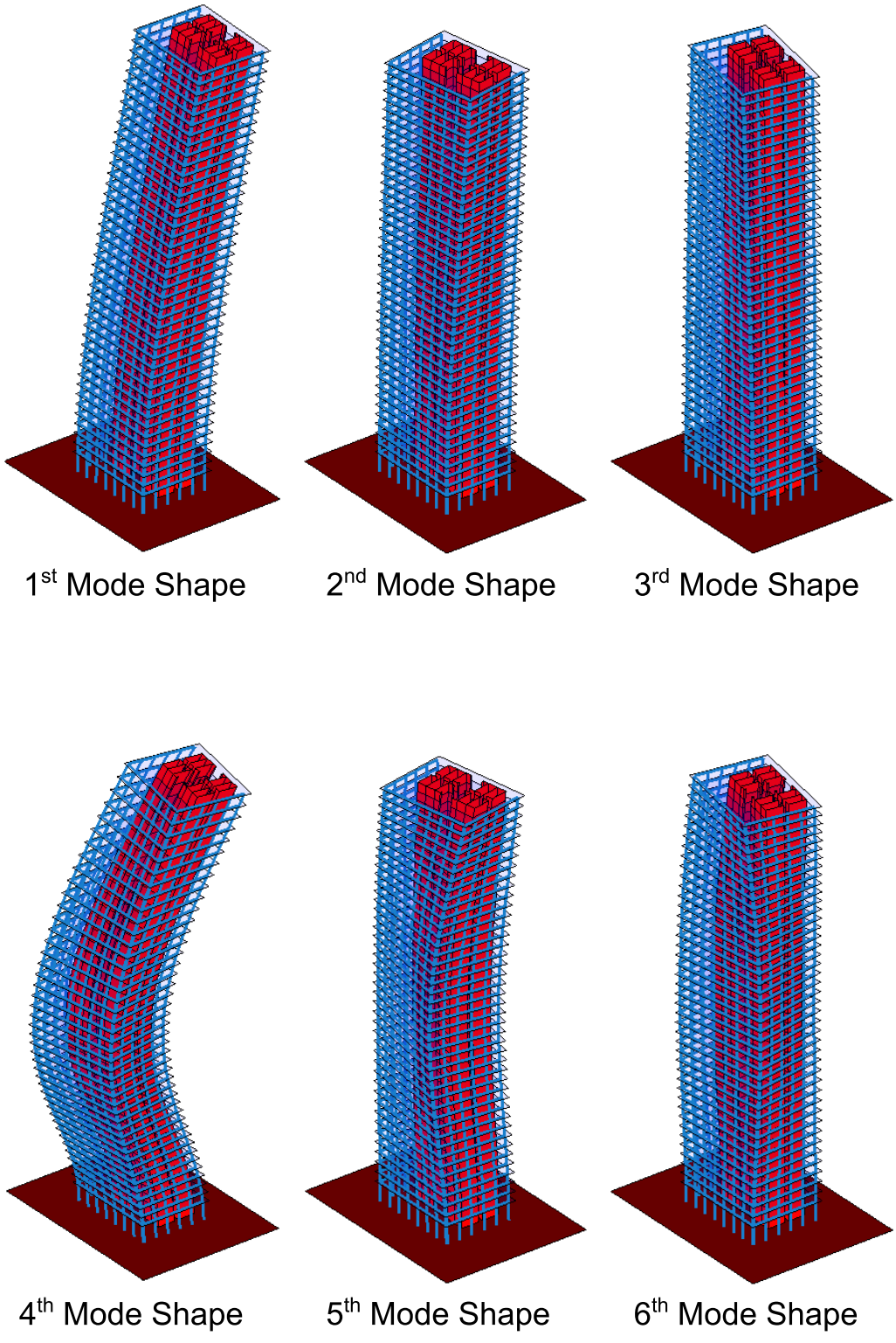

Figure 4.9: First six 3-D mode shapes of the building

Chapter 5

Stability analysis

In the field of structural mechanics, the study of stability is a very important process because if underestimated in the design stages, it can lead to the collapse of the individual structural element and in some cases of the entire building or a substantial portion of it. The collapse of an element due to instability occurs before it reaches the ultimate stress of the material, values that are generally assumed for the dimensioning of it. This collapse phenomenon occurs following the loss of equilibrium of the element, and affects the beams which are highly slender. This is achieved when the load applied to the structure reaches a critical value, or the maximum value that the element can withstand without undergoing large deformations that lead to collapse. This value of the load depends on the geometry cross section, length and restraints of the beam, as well as its mechanical characteristics.

For complex structures, it is often useful to define the multiplier of external loads, or the coefficient that, if multiplied by the value of the external load actually applied to the structure, leads to collapse due to instability. Given this, the load multiplier can be interpreted as a safety factor, as, the more this value is greater than the unit (which would lead to the loss of equilibrium), the farther the structure is from the condition of collapsing. There are two types of loss of equilibrium, called respectively *axial buckling*, mainly due to a critical axial load, and *lateral-torsional buckling*, due to the critical flexural-torsional bending moment that makes the structural element bend and twist at the same time. In general, these two types of collapse are related to each other and cannot be studied independently.

This work will illustrate a three-dimensional formulation, based on Vlasov's Theory, which makes it possible to determine the values of critical loads that lead to collapse by instability of a generic thin-walled open-section beam. This formulation is quite general, and it will be demonstrated that, using appropriate hypotheses, it is possible obtain the Euler and Prandtl equations that describe the axial buckling and lateral-torsional buckling respectively. Finally, by inserting these equations into the General Algorithm, it is possible to determine the multiplier of the external loads that leads to collapse due to global instability of a high-rise building.

5.1 Literature review

The phenomenon of instability is a topic that has received a great deal of attention from academics, but although the first works date back to the middle of the 18th Century, instability remains a complex theme and over the years there have not been many particularly innovative studies. This is confirmed by the fact that even today there is often reference made to models introduced by Euler (axial buckling) and Prandtl (lateral-torsional buckling) more than a century ago.

The first study on elastic stability is reported in Euler's Treatise of 1759 [99] in which axial buckling and axial critical load leading to loss of equilibrium of a straight beam are defined. But is was only in 1899 that Michell [180] realized the possibility that there might be a phenomenon of instability in very long beams subject to transverse loads. Around the same time Prandtl [205] affirmed a theory that describes the loss of equilibrium by flexion-torsion of a beam subject to bending moment.

In the mid-30s the German engineer Wagner published a work (first in German [264], and later in English [263]) in which he provided the equations for the determination of the critical forces that determine the torsional instability of the thin-walled open-section beams present in the structures of aircraft. In this formulation, in order to determine the normal stresses due to twisting, Wagner used a law similar to that of the sectorial areas introduced by Vlasov in 1936 [260].

In the same years Znamenskii published an article [285] in which he used the Ritz-Timoshenko method to obtain approximate expressions for critical torsional force. It should also be noted that, in examining torsional deformations, both Wagner and Znamenskii hypothesized that the center of torsion coincides with the shear center. In fact, as was demonstrated a few years later by the studies of Vlasov [262], this statement is true only in the event that the shear center coincides with the geometrical centroid of the section. The center of torsion generally does not coincide with the shear center: the equations obtained by Wagner are only applicable when the section of the beam has two axes of symmetry. The experiments conducted by Boloban in 1936 [34] on aircraft spars showed that in beams subject to torsion, axial instability occurs for critical forces considerably lower than the theoretical values described by Euler.

In the same year F. and H. Bleich published a work [32] dedicated to the problem of torsion and stability of thin-walled section beams. Using an energetic method to describe the problem, the authors obtained a system of three differential equations.

However, these authors hypothesized that after deformation the sections remain plane, and considered that the resulting stresses be applied in the geometric centroid of the section. This led to the loss of one of the three roots of the corresponding solving equation and, considering that the equations are coupled together, gave incorrect results for the other two.

The stability of a beam with a polygonal section was studied in 1937 by Kappus

[136], while Lundquist e Fligg [165] determined the position of the center of rotation corresponding to the minimum critical load. The stability in pure bending of a rectangular beam made of strain-hardened material was studied in 1952 by Hill and Clark [126] and by Wittrick [271]. The stability of an I-beam in pure bending assuming a purely plastic character of the process of buckling was examined by Flint [101] in 1953, while the stability of eccentrically compressed thin-walled section beams was studied by Chuvikin [71] in 1954.

In these same years the academics who contributed most to generating a general theory on the instability of the thin-walled open-section beam, although with different methodologies, were Bleich, Timoshenko, and Vlasov. In particular, Bleich [31] used a procedure describing the total potential energy of the beam as the difference between its deformation energy and the work of external loads. Timoshenko [248], [250] instead used the static method, that is, he wrote the equilibrium equations of the forces in the deformed shape configuration, while Vlasov [261], [262] used an energetic method in which the stresses that are generated in a beam subject to deformation are transformed into fictitious external loads.

Many years later, Anderson [9] and Attard [16] carried out experimental studies on mono-symmetric thin-walled open-section cantilever beams that confirmed results obtained using the analytical formulations proposed by Timoshenko and Vlasov.

Over the years, several analytical efforts have followed to rewrite the stability theory of thin-walled open-section beams. To describe the problem, following the theories of Bleich and Valsov, many researchers use an energy approach. The use of this method is the ideal solution to analyze the local stability of a structural element but involves excessive calculations when applied to more complex structures.

Among others, we can mention the works of Ghobarah [111] and Roberts [216]: they took up Vlasov's Theory by removing the hypothesis of annulment of shear forces on the middle line of the section. Yang and McGuire [276], and Kitipornchai and Chan [144] improved the deformation energy considering all linear terms and all non-linear terms. In the first of these studies, the beam with doubly symmetrical sections are analyzed, while in the second, L- and T-section beams (with null warping) are analyzed. While greatly complicating the calculations, their results are confirmed as special cases of the classical theory.

In 1985, on the basis of the general theory of elastic stability due to Koiter [125], [146], [147], Pignataro et al. [202] performed a post-buckling analysis of simply supported channel beams under uniform compression focused on eulerian and flexural torsional simultaneous buckling modes interaction.

The total potential energy was written up to third order terms in order to investigate buckling phenomena. This technique was subsequently improved and the initial imperfection effects were taken into account [201]. In 1990s, Pi [195] wrote a new formulation considering the rotation components of the second order, while Trahair [255] rewrote the deformation energy in a simplified form considering

only linear terms.

Ronagh [217], [218], instead, studied the instability of the beams with variable section while Mohri [182] studied the post-buckling behavior of thin-walled open-sections bars. In 2016 Taig et al. [237] presented an analytical approach for stability analysis of thin-walled beams implemented within the framework of the Generalised Beam Theory [196], [212]. In this manner, it is possible to account for the deformability of the cross section in both pre-buckling and buckling analyses.

In addition to these analytical works, numerical procedures using the Finite Element Method [20], [68] began to spread since the 1970s thanks to the development of the first calculators. More recently, Tong and Zhang [254], [282] performed comparative simulations of beams under different load conditions by using FEM models. Their studies show using a comparative numerical analysis that, all other conditions being equal, some theories commonly accepted today lead to critical load values that are also different from each other.

5.2 Stability analysis of thin-walled open-section beams

Consider a slender prismatic thin-walled open-section element without symmetry (Figure 5.1), where ξ and η are the displacements according to x and y axes, respectively, and ϑ is the angle of rotation with respect to the z axis.

A load system is applied to the beam, restrained to both the ends by cylindrical hinges, consisting of two distributed forces $p_x(z)$ and $p_y(z)$ directed in x and y directions, respectively, and by a distributed torsional moment $m_z(z)$, along the axis of the beam. Furthermore, one axial force N and two bending moments $\bar{M}_x$ and $\bar{M}_y$, are applied to the ends of the beam, as shown in Figure (5.2).

The assumptions behind the formulation are the following:

- the shape of the cross section remains unchanged after deformation;
- the element is deformable only by bending and twisting;
- Vlasov's Theory is valid.

In the present formulation, an energy method is used by which it is possible to determine the equilibrium conditions of the system (that is, the critical concentrated loads that determine instability) by requiring the annulment of the variation of the total potential energy of the beam, calculated as the difference between the elastic deformation energy and the work of external loads.

Using Clapeyron Theorem and considering that the bending moments and the bimoment are energetically orthogonal to each other, the elastic deformation energy Φ can be written as:

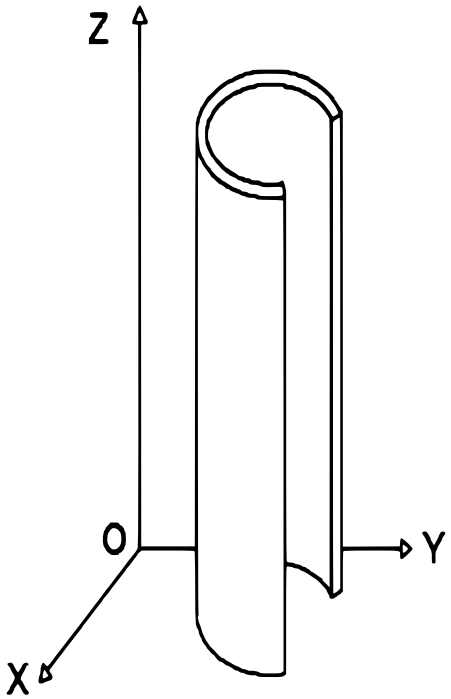

Figure 5.1: Thin-walled open-section beam

$$\Phi = \frac{1}{2}\int_0^L \left[-M_y\xi'' - M_x\eta'' - B\vartheta'' + M_z\vartheta'\right]\mathrm{d}l \tag{5.1}$$

Recalling Vlasov's Equations,

$$N = E\left(A\zeta' - S_y\xi'' - S_x\eta'' - S_\omega\vartheta''\right) \tag{5.2a}$$

$$M_y = E\left(S_y\zeta' - I_{yy}\xi'' - I_{yx}\eta'' - I_{y\omega}\vartheta''\right) \tag{5.2b}$$

$$M_x = E\left(-S_x\zeta' - I_{xy}\xi'' - I_{xx}\eta'' - I_{x\omega}\vartheta''\right) \tag{5.2c}$$

$$B = E\left(S_\omega\zeta' - I_{\omega y}\xi'' - I_{\omega x}\eta'' - I_{\omega\omega}\vartheta''\right) \tag{5.2d}$$

if the sectorial area is evaluated with respect to the sectorial centroid, the sectorial static moment S_ω is null for definition. Therefore, from Equation (5.2a), evaluated with respect to the geometric center of gravity of the section ($S_y = S_x = 0$), it is possible to calculate the value of function ζ'

$$\zeta' = \frac{N}{EA} \tag{5.3}$$

Physically ζ' represents the axial deformation of the beam. By inserting Equation (5.3) into Equations (5.2b, 5.2c, and 5.2d), and making the following assumptions:

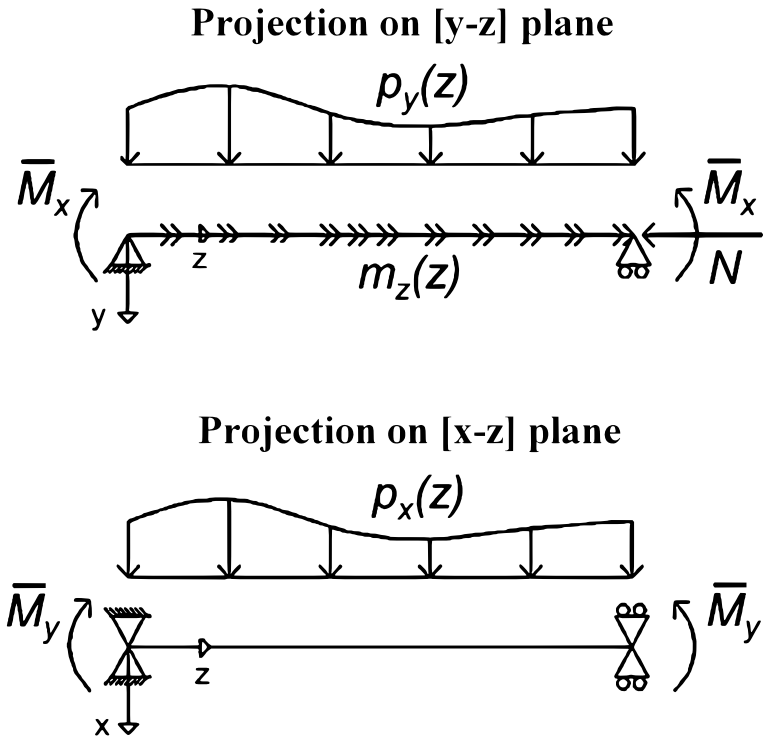

Figure 5.2: Load system applied to the beam

- the origin of the reference system coincides with the shear center of the section

$$I_{y\omega} = I_{x\omega} = 0;$$

- the axes of the reference system are principal

$$I_{xy} = I_{yx} = 0;$$

- the sectorial area is evaluated with respect to the sectorial centroid

$$S_\omega = 0;$$

the following relationships can be deduced:

$$M_y = E\left(S_y \frac{N}{EA} - I_{yy}\xi''\right) \tag{5.4a}$$

$$M_x = E\left(-S_x \frac{N}{EA} - I_{xx}\eta''\right) \tag{5.4b}$$

$$B = -EI_{\omega\omega}\vartheta'' \tag{5.4c}$$

Noting that:

$$S_y = Ax_G \Longrightarrow S_y \frac{N}{EA} = \frac{Nx_G}{E} \tag{5.5a}$$

$$S_x = Ay_G \Longrightarrow S_x \frac{N}{EA} = \frac{Ny_G}{E} \tag{5.5b}$$

Equations (5.4) can be rewritten as follows:

$$M_y = Nx_G - EI_{yy}\xi'' \tag{5.6a}$$

$$M_x = -Ny_G - EI_{xx}\eta'' \tag{5.6b}$$

$$B = -EI_{\omega\omega}\vartheta'' \tag{5.6c}$$

As can be observed, the presence of the axial force N does not allow a perfect diagonalization of Vlasov's Equations. Eventually, it is important to remember that the moments of inertia are evaluated with respect to the shear center of the section, while the terms x_G and y_G indicate the coordinates of the geometric center of gravity of the section evaluated with respect to its shear center.

The primary torsional moment, according to Saint Venant's Theory, can be written as:

$$M_z = GI_t\vartheta' \tag{5.7}$$

Inserting Equations (5.6 and 5.7) into Equation (5.1), the elastic deformation energy Φ takes the following form:

$$\Phi = \frac{1}{2}\int_0^L \left[-Nx_G\xi'' + EI_{yy}\xi''^2 + Ny_G\eta'' + EI_{xx}\eta''^2 + EI_{\omega\omega}\vartheta''^2 + GI_t\vartheta'^2\right]\mathrm{d}l \tag{5.8}$$

The variation is equal to:

$$\begin{aligned}\delta\Phi = \int_0^L \Big[&-\frac{1}{2}Nx_G\xi''\delta\xi'' + EI_{yy}\xi''\delta\xi'' + \frac{1}{2}Ny_G\eta''\delta\eta'' + EI_{xx}\eta''\delta\eta'' + \\ &+ EI_{\omega\omega}\vartheta''\delta\vartheta'' + GI_t\vartheta'\delta\vartheta'\Big]\mathrm{d}l\end{aligned} \tag{5.9}$$

which integrated by parts provides:

$$\begin{aligned}\delta\Phi = &\left[\frac{1}{2}\left(-Nx_G\xi''\delta\xi' + Nx_G\xi'''\delta\xi\right) + EI_{yy}\xi''\delta\xi' - EI_{yy}\xi'''\delta\xi + \right.\\ &+\frac{1}{2}\left(Ny_G\eta''\delta\eta' - Ny_G\eta'''\delta\eta\right) + EI_{xx}\eta''\delta\eta' - EI_{xx}\eta'''\delta\eta + \\ &\left.+ EI_{\omega\omega}\vartheta''\delta\vartheta' - EI_{\omega\omega}\vartheta'''\delta\vartheta + GI_t\vartheta'\delta\vartheta\right]_0^L + \\ &+\int_0^L\left(-\frac{1}{2}Nx_G\xi^{IV}\delta\xi + EI_{yy}\xi^{IV}\delta\xi + \frac{1}{2}Ny_G\eta^{IV}\delta\eta + EI_{xx}\eta^{IV}\delta\eta + \right.\\ &\left.+ EI_{\omega\omega}\vartheta^{IV}\delta\vartheta - GI_t\vartheta''\delta\vartheta\right)\mathrm{d}l\end{aligned} \tag{5.10}$$

To evaluate the work of concentrated loads N, $\bar{M}_x$, and $\bar{M}_y$, a longitudinal strip of the beam having infinitesimal area $\mathrm{d}A$ is considered, as shown in Figure (5.3).

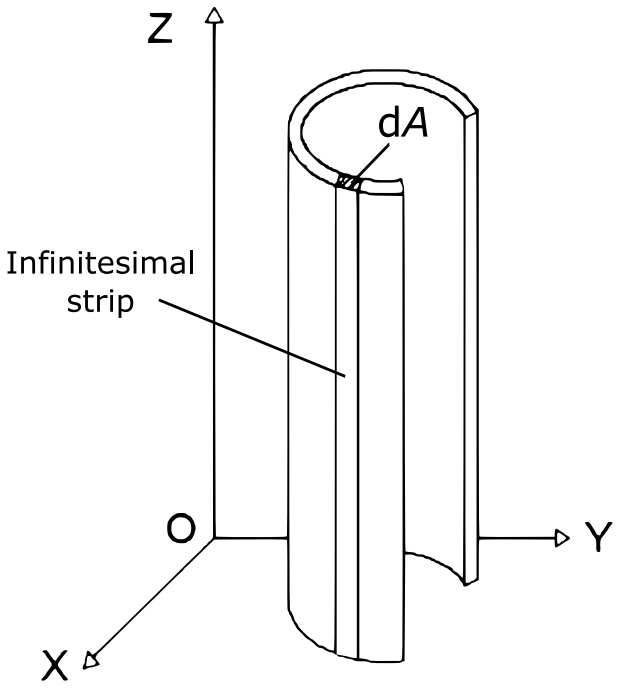

Figure 5.3: Thin-walled open-section beam with infinitesimal strip

By replacing the loads with a statically equivalent stress field, evaluated by Navier's formula, it is possible to write the equation of the work done by external forces relative to an infinitesimal strip of beam. Integrating on the entire area obtains the total work of concentrated loads.

With reference to the generic beam strip, whose position is identified by the coordinates (x, y), the normal stress σ_z, equivalent to the concentrated external loads applied at the end of the beam, is equal to:

$$\sigma_z = \frac{N}{A} + \frac{\bar{M}_x}{I_{xx}}(y - y_G) - \frac{\bar{M}_y}{I_{yy}}(x - x_G) \tag{5.11}$$

The total work of the concentrated external loads is written as:

$$L_{conc} = \int_0^L \int_A [\sigma_z \Delta \mathrm{d}A]\,\mathrm{d}l \tag{5.12}$$

where the term $\Delta = \mathrm{d}l - \mathrm{d}z$ expresses the approach of the constraints due to the inflection with respect to the x and y axes, as shown in Figure (5.4).

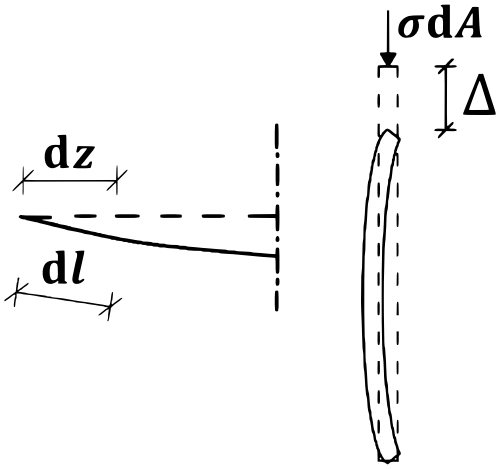

Figure 5.4: Graphics representation of the term Δ

The displacement Δ, due to the axial displacement of the point of application of the force N, can be evaluated in function of the first derivatives of transverse displacements ξ and η, and must be calculated as the vectorial sum of the two displacement components Δ_{xz} and Δ_{yz} on the $[xz]$ and $[yz]$ planes:

$$\Delta = \Delta_{xz} + \Delta_{yz} \tag{5.13}$$

The displacement component Δ_{yz} can be written as:

$$\Delta_{yz} = \mathrm{d}l - \mathrm{d}z_y = \mathrm{d}l - \mathrm{d}l\cos\varphi_x = (1 - \cos\varphi_x)\,\mathrm{d}l \tag{5.14}$$

and expanding the $\cos\varphi_x$ function in the Taylor series, we get:

$$\cos\phi_x \cong 1 - \frac{\varphi_x^2}{2} \tag{5.15}$$

Carrying out similar considerations also for the displacement component Δ_{xz} and performing the appropriate substitutions, the displacement components can be rewritten in the following form:

$$\Delta_{yz} \cong \left(1 - 1 + \frac{\varphi_x^2}{2}\right) \mathrm{d}l \cong \frac{\varphi_x^2}{2} \mathrm{d}l \cong \frac{1}{2}\xi'^2 \tag{5.16a}$$

$$\Delta_{xz} \cong \left(1 - 1 + \frac{\varphi_y^2}{2}\right) \mathrm{d}l \cong \frac{\varphi_y^2}{2} \mathrm{d}l \cong \frac{1}{2}\eta'^2 \tag{5.16b}$$

Finally, the total displacement can be written as:

$$\Delta \cong \frac{1}{2}\left[\xi'^2 + \eta'^2\right] \tag{5.17}$$

Since we are considering a generic beam strip, which does not commonly coincide with the shear center of the section, Equation (5.17) generalizes as:

$$\Delta \cong \frac{1}{2}\left[\left(\frac{\mathrm{d}\Delta x}{\mathrm{d}z}\right)^2 + \left(\frac{\mathrm{d}\Delta y}{\mathrm{d}z}\right)^2\right] \tag{5.18}$$

in which the displacements Δ_x and Δ_y are respectively:

$$\Delta_x = \xi - \vartheta y \tag{5.19a}$$

$$\Delta_y = \eta + \vartheta x \tag{5.19b}$$

Ultimately, the axial displacement of the point of application of the force N can be written as:

$$\begin{aligned} \Delta &\cong \frac{1}{2}\left[\left(\xi' - \vartheta' y\right)^2 + \left(\eta' + \vartheta' x\right)^2\right] \cong \\ &\cong \left[\frac{1}{2}\left(\xi'^2 + \eta'^2\right) + \frac{1}{2}\left(y^2 + x^2\right)\vartheta'^2 - \xi'\vartheta' y + \eta'\vartheta' x\right] \end{aligned} \tag{5.20}$$

By inserting Equation (5.20) in Equation (5.11), the deformation work due to concentrated external loads N, $\bar{M}_x$, and $\bar{M}_y$, can be written as:

$$\begin{aligned} L_{conc} = \int_0^L \int_A \Bigg[&\left(\frac{N}{A} + \frac{\bar{M}_x}{I_{xx}}\left(y - y_G\right) - \frac{\bar{M}_y}{I_{yy}}\left(x - x_G\right)\right) \\ &\left(\frac{1}{2}\left(\xi'^2 + \eta'^2\right) + \frac{1}{2}\left(y^2 + x^2\right)\vartheta'^2 - \xi'\vartheta' y + \eta'\vartheta' x\right)\Bigg] \mathrm{d}A\mathrm{d}l \end{aligned} \tag{5.21}$$

For simplicity of exposure, the contributions of N, $\bar{M}_x$, and $\bar{M}_y$, are calculated separately, obtaining the following formulations.

The work of the axial force N is:

$$\begin{aligned} L_N = &\int_0^L \Bigg[\int_A \frac{1}{2}\frac{N}{A}\left(\xi'^2 + \eta'^2\right) \mathrm{d}A + \int_A \frac{1}{2}\frac{N}{A}\vartheta'^2\left(y^2 + x^2\right)\mathrm{d}A + \\ &- \int_A \frac{N}{A}\xi'\vartheta' y \mathrm{d}A + \int_A \frac{N}{A}\eta'\vartheta' x \mathrm{d}A \Bigg] \mathrm{d}l \\ &\int_0^L \left[\frac{N}{2}\left(\xi'^2 + \eta'^2\right) + \frac{N}{2A} I_P \vartheta'^2 - \frac{N}{A} S_x \xi'\vartheta' + \frac{N}{A} S_y \eta'\vartheta' \right] \mathrm{d}l \end{aligned} \tag{5.22}$$

The variation is equal to:

$$\begin{aligned} \delta L_N = &\int_0^L N\left(\xi'\delta\xi' + \eta'\delta\eta'\right)\mathrm{d}l + \int_0^L \frac{N}{A} I_P \vartheta'\delta\vartheta' \mathrm{d}l + \\ &- \int_0^L \frac{N}{A} S_x \left(\delta\xi'\vartheta' + \xi'\delta\vartheta'\right)\mathrm{d}l + \int_0^L \frac{N}{A} S_y \left(\delta\eta'\vartheta' + \eta'\delta\vartheta'\right)\mathrm{d}l \end{aligned} \tag{5.23}$$

which integrated by parts provides:

$$\begin{aligned} \delta L_N = &\Bigg[N\xi'\delta\xi + N\eta'\delta\eta + \frac{N}{A}\Big(I_P\vartheta'\delta\vartheta - S_x\vartheta'\delta\xi - S_x\xi'\delta\vartheta + \\ &+ S_y\vartheta'\delta\eta + S_y\eta'\delta\vartheta \Big) \Bigg]_0^L + \\ &- \int_0^L \Bigg[N\xi''\delta\xi + N\eta''\delta\eta + \frac{N}{A}\Big(I_P\vartheta''\delta\vartheta - S_x\vartheta''\delta\xi - S_x\xi''\delta\vartheta + \\ &+ S_y\vartheta''\delta\eta + S_y\eta''\delta\vartheta \Big) \Bigg] \mathrm{d}l \end{aligned} \tag{5.24}$$

The work of the bending moment $\bar{M}_x$ is:

$$\begin{aligned} L_{\bar{M}_x} = &\int_0^L \Bigg[\int_A \frac{1}{2}\frac{\bar{M}_x}{I_{xx}}\left(y - y_G\right)\left(\xi'^2 + \eta'^2\right)\mathrm{d}A + \\ &+ \int_A \frac{1}{2}\frac{\bar{M}_x}{I_{xx}}\left(y - y_G\right)\left(y^2 + x^2\right)\vartheta'^2 \mathrm{d}A + \\ &- \int_A \frac{\bar{M}_x}{I_{xx}}\left(y - y_G\right)\xi'\vartheta' y \mathrm{d}A + \\ &+ \int_A \frac{\bar{M}_x}{I_{xx}}\left(y - y_G\right)\eta'\vartheta' x \mathrm{d}A \Bigg] \mathrm{d}l \end{aligned} \tag{5.25}$$

where defining the terms:

$$\int_A \frac{y-y_G}{I_{xx}}\mathrm{d}A = a_x \tag{5.26a}$$

$$\int_A \frac{y-y_G}{I_{xx}}x\mathrm{d}A = b_x \tag{5.26b}$$

$$\int_A \frac{y-y_G}{I_{xx}}y\mathrm{d}A = c_x \tag{5.26c}$$

$$\int_A \frac{y-y_G}{I_{xx}}\left(y^2+x^2\right)\mathrm{d}A = d_x \tag{5.26d}$$

it is possible to write:

$$L_{\bar{M}_x} = \bar{M}_x \int_0^L \left[\frac{1}{2}a_x\left(\xi'^2+\eta'^2\right)+\frac{1}{2}d_x\vartheta'^2 - c_x\xi'\vartheta' + b_x\eta'\vartheta'\right]\mathrm{d}l \tag{5.27}$$

The variation is equal to:

$$\begin{aligned}\delta L_{\bar{M}_x} = \bar{M}_x \int_0^L \Big[& a_x\left(\xi'\delta\xi'+\eta'\delta\eta'\right)+d_x\vartheta'\delta\vartheta'+ \\ & -c_x\left(\xi'\delta\vartheta'+\vartheta'\delta\xi'\right)+b_x\left(\eta'\delta\vartheta'+\vartheta'\delta\eta'\right)\Big]\mathrm{d}l\end{aligned} \tag{5.28}$$

which integrated by parts provides:

$$\begin{aligned}\delta L_{\bar{M}_x} = \bar{M}_x \Big\{ & \Big[a_x\left(\xi'\delta\xi+\eta'\delta\eta\right)+d_x\vartheta'\delta\vartheta - c_x\left(\vartheta'\delta\xi+\xi'\delta\vartheta\right)+ \\ & +b_x\left(\vartheta'\delta\eta+\eta'\delta\vartheta\right)\Big]_0^L - \int_0^L \Big[a_x\left(\xi''\delta\xi+\eta''\delta\eta\right)+ \\ & +d_x\vartheta''\delta\vartheta - c_x\left(\vartheta''\delta\xi+\xi''\delta\vartheta\right)+b_x\left(\vartheta''\delta\eta+\eta''\delta\vartheta\right)\Big]\mathrm{d}l\Big\}\end{aligned} \tag{5.29}$$

The work of the bending moment $\bar{M}_y$ is:

$$\begin{aligned}L_{\bar{M}_y} = \int_0^L \Big[& -\int_A \frac{1}{2}\frac{\bar{M}_y}{I_{yy}}\left(x-x_G\right)\left(\xi'^2+\eta'^2\right)\mathrm{d}A+ \\ & -\int_A \frac{1}{2}\frac{\bar{M}_y}{I_{yy}}\left(x-x_G\right)\left(y^2+x^2\right)\vartheta'^2\mathrm{d}A+ \\ & +\int_A \frac{\bar{M}_y}{I_{yy}}\left(x-x_G\right)\xi'\vartheta' y\mathrm{d}A+ \\ & -\int_A \frac{\bar{M}_y}{I_{yy}}\left(x-x_G\right)\eta'\vartheta' x\mathrm{d}A\Big]\mathrm{d}l\end{aligned} \tag{5.30}$$

where defining the terms:

$$\int_A \frac{x - x_G}{I_{yy}} \mathrm{d}A = a_y \tag{5.31a}$$

$$\int_A \frac{x - x_G}{I_{yy}} x \mathrm{d}A = b_y \tag{5.31b}$$

$$\int_A \frac{x - x_G}{I_{yy}} y \mathrm{d}A = c_y \tag{5.31c}$$

$$\int_A \frac{x - x_G}{I_{yy}} \left(y^2 + x^2\right) \mathrm{d}A = d_y \tag{5.31d}$$

it is possible to write:

$$L_{\bar{M}_y} = \bar{M}_y \int_0^L \left[-\frac{1}{2} a_y \left(\xi'^2 + \eta'^2\right) - \frac{1}{2} d_y \vartheta'^2 + c_y \xi' \vartheta' - b_y \eta' \vartheta' \right] \mathrm{d}l \tag{5.32}$$

The variation is equal to:

$$\begin{aligned} \delta L_{\bar{M}_y} = - \bar{M}_y \int_0^L \Big[& a_y \left(\xi' \delta\xi' + \eta' \delta\eta'\right) + d_y \vartheta' \delta\vartheta' + \\ & + c_y \left(\xi' \delta\vartheta' + \vartheta' \delta\xi'\right) + b_y \left(\eta' \delta\vartheta' + \vartheta' \delta\eta'\right) \Big] \mathrm{d}l \end{aligned} \tag{5.33}$$

which integrated by parts provides:

$$\begin{aligned} \delta L_{\bar{M}_y} = - \bar{M}_y \Big\{ & \Big[a_y \left(\xi' \delta\xi + \eta' \delta\eta\right) + d_y \vartheta' \delta\vartheta + c_y \left(\vartheta' \delta\xi + \xi' \delta\vartheta\right) + \\ & - b_y \left(\vartheta' \delta\eta + \eta' \delta\vartheta\right) \Big]_0^L + \int_0^L \Big[a_y \left(\xi'' \delta\xi + \eta'' \delta\eta\right) + \\ & + d_y \vartheta'' \delta\vartheta + c_y \left(\vartheta'' \delta\xi + \xi'' \delta\vartheta\right) - b_y \left(\vartheta'' \delta\eta + \eta'' \delta\vartheta\right) \Big] \mathrm{d}l \Big\} \end{aligned} \tag{5.34}$$

Adding the contributions of the variations of the concentrated loads works, results in:

$$
\begin{aligned}
&\delta L_{conc} = \delta L_N + \delta L_{\bar{M}_x} + \delta L_{\bar{M}_y} = \\
&= \left[N\xi'\delta\xi + N\eta'\delta\eta + \frac{N}{A}\Big(I_P\vartheta'\delta\vartheta - S_x\vartheta'\delta\xi - S_x\xi'\delta\vartheta + S_y\vartheta'\delta\eta + S_y\eta'\delta\vartheta \Big) \right]_0^L + \\
&\bar{M}_x \left\{ \left[a_x\Big(\xi'\delta\xi + \eta'\delta\eta \Big) + d_x\vartheta'\delta\vartheta - c_x\Big(\vartheta'\delta\xi + \xi'\delta\vartheta \Big) + b_x\Big(\vartheta'\delta\eta + \eta'\delta\vartheta \Big) \right]_0^L \right\} + \\
&- \bar{M}_y \left\{ \left[a_y\Big(\xi'\delta\xi + \eta'\delta\eta \Big) + d_y\vartheta'\delta\vartheta + c_y\Big(\vartheta'\delta\xi + \xi'\delta\vartheta \Big) - b_y\Big(\vartheta'\delta\eta + \eta'\delta\vartheta \Big) \right]_0^L \right\} + \\
&- \int_0^L \left[N\xi''\delta\xi + N\eta''\delta\eta + \frac{N}{A}\Big(I_P\vartheta''\delta\vartheta - S_x\vartheta''\delta\xi - S_x\xi''\delta\vartheta + S_y\vartheta''\delta\eta + S_y\eta''\delta\vartheta \Big) \right] \mathrm{d}l + \\
&- \bar{M}_x \left\{ \int_0^L \left[a_x\Big(\xi''\delta\xi + \eta''\delta\eta \Big) + d_x\vartheta''\delta\vartheta - c_x\Big(\vartheta''\delta\xi + \xi''\delta\vartheta \Big) + b_x\Big(\vartheta''\delta\eta + \eta''\delta\vartheta \Big) \right] \mathrm{d}l \right\} + \\
&- \bar{M}_y \left\{ \int_0^L \left[a_y\Big(\xi''\delta\xi + \eta''\delta\eta \Big) + d_y\vartheta''\delta\vartheta + c_y\Big(\vartheta''\delta\xi + \xi''\delta\vartheta \Big) - b_y\Big(\vartheta''\delta\eta + \eta''\delta\vartheta \Big) \right] \mathrm{d}l \right\}
\end{aligned}
\tag{5.35}
$$

The work of the distributed external loads p_x, p_y, and m_z, is written as:

$$
L_{distr} = \int_0^L \int_A \Big(p_x\xi + p_y\eta + m_z\vartheta \Big) \mathrm{d}l \tag{5.36}
$$

and the variation is equal to:

$$
\delta L_{distr} = \int_0^L \int_A \Big(p_x\delta\xi + p_y\delta\eta + m_z\delta\vartheta \Big) \mathrm{d}l \tag{5.37}
$$

Since the objective of the problem is to determine equilibrium configurations (or critical loads), the variation of the total potential energy δW of the beam is determined and it is set equal to zero, that is:

$$
\delta W = \delta\Phi - \delta L_{conc} - \delta L_{distr} = 0 \tag{5.38}
$$

By inserting Equations (5.10, 5.35, and 5.37), in Equation (5.38), two equations are obtained which must be satisfied.

The first equation contains the finite terms, and is verified at the end points of the beam, that is for $z = 0, L$:

$$
\begin{aligned}
&\left[\frac{1}{2}\left(-Nx_G\xi''\delta\xi' + Nx_G\xi'''\delta\xi\right) + EI_{yy}\xi''\delta\xi' - EI_{yy}\xi'''\delta\xi + \right.\\
&+ \frac{1}{2}\left(Ny_G\eta''\delta\eta' - Ny_G\eta'''\delta\eta\right) + EI_{xx}\eta''\delta\eta' - EI_{xx}\eta'''\delta\eta + \\
&\left. + EI_{\omega\omega}\vartheta''\delta\vartheta' - EI_{\omega\omega}\vartheta'''\delta\vartheta + GI_t\vartheta'\delta\vartheta\right]_0^L + \\
&+ \left[N\xi'\delta\xi + N\eta'\delta\eta + \frac{N}{A}\left(I_P\vartheta'\delta\vartheta - S_x\vartheta'\delta\xi - S_x\xi'\delta\vartheta + S_y\vartheta'\delta\eta + S_y\eta'\delta\vartheta\right)\right]_0^L + \\
&\bar{M}_x\left\{\left[a_x\left(\xi'\delta\xi + \eta'\delta\eta\right) + d_x\vartheta'\delta\vartheta - c_x\left(\vartheta'\delta\xi + \xi'\delta\vartheta\right) + b_x\left(\vartheta'\delta\eta + \eta'\delta\vartheta\right)\right]_0^L\right\} + \\
&- \bar{M}_y\left\{\left[a_y\left(\xi'\delta\xi + \eta'\delta\eta\right) + d_y\vartheta'\delta\vartheta + c_y\left(\vartheta'\delta\xi + \xi'\delta\vartheta\right) - b_y\left(\vartheta'\delta\eta + \eta'\delta\vartheta\right)\right]_0^L\right\} = 0
\end{aligned}
\tag{5.39}
$$

The second equation is instead integral:

$$
\begin{aligned}
&\int_0^L\left(-\frac{1}{2}Nx_G\xi^{IV}\delta\xi + EI_{yy}\xi^{IV}\delta\xi + \frac{1}{2}Ny_G\eta^{IV}\delta\eta + EI_{xx}\eta^{IV}\delta\eta + \right.\\
&\left. + EI_{\omega\omega}\vartheta^{IV}\delta\vartheta - GI_t\vartheta''\delta\vartheta\right)\mathrm{d}l + \\
&+ \int_0^L\left[N\xi''\delta\xi + N\eta''\delta\eta + \frac{N}{A}\left(I_P\vartheta''\delta\vartheta - S_x\vartheta''\delta\xi - S_x\xi''\delta\vartheta + S_y\vartheta''\delta\eta + S_y\eta''\delta\vartheta\right)\right]\mathrm{d}l + \\
&- \bar{M}_x\left\{\int_0^L\left[a_x\left(\xi''\delta\xi + \eta''\delta\eta\right) + d_x\vartheta''\delta\vartheta - c_x\left(\vartheta''\delta\xi + \xi''\delta\vartheta\right) + b_x\left(\vartheta''\delta\eta + \eta''\delta\vartheta\right)\right]\mathrm{d}l\right\} + \\
&- \bar{M}_y\left\{\int_0^L\left[a_y\left(\xi''\delta\xi + \eta''\delta\eta\right) + d_y\vartheta''\delta\vartheta + c_y\left(\vartheta''\delta\xi + \xi''\delta\vartheta\right) - b_y\left(\vartheta''\delta\eta + \eta''\delta\vartheta\right)\right]\mathrm{d}l\right\} + \\
&- \int_0^L\int_A\left(p_x\delta\xi + p_y\delta\eta + m_z\delta\vartheta\right)\mathrm{d}l = 0
\end{aligned}
\tag{5.40}
$$

By separating the terms of Equation (5.40) as a function of their variation $\delta\xi$, $\delta\eta$, and $\delta\vartheta$, it is possible to write a system of three equations in three unknowns:

$$
\begin{aligned}
&EI_{yy}\xi^{IV} - \frac{1}{2}Nx_G\xi^{IV} + N\xi'' - \frac{N}{A}S_x\vartheta'' + \bar{M}_x a_x\xi'' + \\
&- \bar{M}_x c_x\vartheta'' - \bar{M}_y a_y\xi'' + \bar{M}_y c_y\vartheta'' = p_x
\end{aligned}
\tag{5.41a}
$$

$$EI_{xx}\eta^{IV} + \frac{1}{2}Ny_G\eta^{IV} + N\eta'' + \frac{N}{A}S_y\vartheta'' + \bar{M}_x a_x\eta'' + \\ + \bar{M}_x b_x\vartheta'' - \bar{M}_y a_y\eta'' - \bar{M}_y b_y\vartheta'' = p_y \tag{5.41b}$$

$$EI_{\omega\omega}\vartheta^{IV} - GI_t\vartheta'' + \frac{N}{A}I_P\vartheta'' - \frac{N}{A}S_x\xi'' + \frac{N}{A}S_e\eta'' + \bar{M}_x d_x\vartheta'' + \\ - \bar{M}_x c_x\xi'' + \bar{M}_x b_x\eta'' - \bar{M}_y d_y\vartheta'' + \bar{M}_y c_y\xi'' - \bar{M}_y b_y\eta'' = m_z \tag{5.41c}$$

The previous system of three equations can be rewritten in a compact form:

$$E\left[J\right]\left\{\delta^{IV}\right\} + G\left[J_t\right]\left\{\delta''\right\} + \left[\left\{N\right\}^{\mathrm{T}}\left\{C_g\right\}\right]\left\{\delta''\right\} = \left\{F\right\} \tag{5.42}$$

where the matrices are defined as follows:

$$\left[J\right] = \begin{bmatrix} I_{yy} & 0 & 0 \\ 0 & I_{xx} & 0 \\ 0 & 0 & I_{\omega\omega} \end{bmatrix} + \frac{N}{E}\begin{bmatrix} -\frac{1}{2}x_G & 0 & 0 \\ 0 & +\frac{1}{2}y_G & 0 \\ 0 & 0 & 0 \end{bmatrix} \tag{5.43a}$$

$$\left[J_t\right] = \begin{bmatrix} 0 & 0 & 0 \\ 0 & 0 & 0 \\ 0 & 0 & -I_t \end{bmatrix} \tag{5.43b}$$

$$\left\{N\right\} = \begin{Bmatrix} N \\ \bar{M}_x \\ \bar{M}_y \end{Bmatrix} \tag{5.43c}$$

$$\left\{C_g\right\} = \left\{ \begin{bmatrix} 1 & 0 & -S_x/A \\ 0 & 1 & S_y/A \\ -S_x/A & S_y/A & I_P/A \end{bmatrix} \quad \begin{bmatrix} a_x & 0 & -c_x \\ 0 & a_x & b_x \\ -c_x & b_x & d_x \end{bmatrix} \quad \begin{bmatrix} -a_y & 0 & c_y \\ 0 & -a_y & -b_y \\ c_y & -b_y & -d_y \end{bmatrix} \right\} \tag{5.43d}$$

$$\left\{F\right\} = \begin{Bmatrix} p_x \\ p_y \\ m_z \end{Bmatrix} \tag{5.43e}$$

$$\left\{\delta\right\} = \begin{Bmatrix} \xi \\ \eta \\ \vartheta \end{Bmatrix} \tag{5.43f}$$

The matrix $[J]$ consists of two terms: the first is the tensor of moments of inertia already defined in the previous chapters, while the second, which can be interpreted

as a matrix of geometric stiffness, depends on the axial force and from the cross section geometry. In case the shear center coincides with the geometric center of gravity of the section, this term is annulled because $x_G = y_G = 0$.

The matrix $[J_t]$ contains only the term related to the torsional stiffness factor and describes the primary torsion due to Saint Venant's Theory.

The vector $\{N\}$ contains the values of concentrated loads at the ends of the beam. This term can be interpreted as the eigenvalue of the problem.

The vector $\{C_g\}$ is associated to this term: it composed by three matrices, each of size 3×3, which contain some geometric coefficients that describe the cross section of the beam.

The $\{F\}$ and $\{\delta\}$ vectors respectively contain the values of the transverse distributed external loads and the generalized displacements of the beam.

In conclusion, by imposing the boundary conditions, it is possible to define the values of the critical loads that determine the instability of the beam. For each of the two ends of the beam it is possible to identify six boundary conditions which may be statics or kinematics. In particular, depending on the type of constraint present, it can be written:

$$Clamped\ end \Longrightarrow \left\{ \begin{array}{c} \xi = 0 \\ \eta = 0 \\ \vartheta = 0 \end{array} \right\} \ ; \ \left\{ \begin{array}{c} \xi' = 0 \\ \eta' = 0 \\ \vartheta' = 0 \end{array} \right\} \tag{5.44a}$$

$$Hinged\ end \Longrightarrow \left\{ \begin{array}{c} \xi = 0 \\ \eta = 0 \\ \vartheta = 0 \end{array} \right\} \ ; \ \left\{ \begin{array}{c} \xi'' = 0 \\ \eta'' = 0 \\ \vartheta'' = 0 \end{array} \right\} \tag{5.44b}$$

$$Free\ end \Longrightarrow \left\{ \begin{array}{c} \xi'' = 0 \\ \eta'' = 0 \\ \vartheta'' = 0 \end{array} \right\} \ ; \ \left\{ \begin{array}{c} \xi''' = 0 \\ \eta''' = 0 \\ GI_t\vartheta' - EI_{\omega\omega}\vartheta''' = 0 \end{array} \right\} \tag{5.44c}$$

5.2.1 Particular cases

The equations written so far are absolutely general. We will now address some particular cases for geometry or for load conditions.

As a first particular case, consider a thin-walled open-section beams unstressed by loads concentrated at its ends, that is $\{N\} = \{0\}$. The Equation (5.42) takes the following form:

$$\left[\begin{array}{ccc} EI_{yy} & 0 & 0 \\ 0 & EI_{xx} & 0 \\ 0 & 0 & EI_{\omega\omega} \end{array} \right] \left\{ \begin{array}{c} \xi^{IV} \\ \eta^{IV} \\ \vartheta^{IV} \end{array} \right\} + \left[\begin{array}{ccc} 0 & 0 & 0 \\ 0 & 0 & 0 \\ 0 & 0 & -GI_t \end{array} \right] \left\{ \begin{array}{c} \xi'' \\ \eta'' \\ \vartheta'' \end{array} \right\} = \left\{ \begin{array}{c} p_x \\ p_y \\ m_z \end{array} \right\} \tag{5.45}$$

As seen from this system of equations, the first two are the classic equations of the elastic line, while the third,

$$EI_{\omega\omega}\vartheta^{IV} - GI_t\vartheta'' = m_z \tag{5.46}$$

is the equation of the non-uniform torsion obtained by energy and not using the static method proposed by Vlasov (Equation 2.55).

As a second particular case, consider a beam on which the bending moments applied to the ends are null ($\bar{M}_x = \bar{M}_y = 0$); the distributed moment m_z is also null.

Since the beam, of length L and constrained at its ends by cylindrical hinges, does not have an open-section, it can be analyzed considering Saint Venant's Theory, ($I_{\omega\omega} = 0$, and $\vartheta' = cost \Longrightarrow \vartheta'' = 0$), and if the shear center coincides with the center of gravity of the section ($S_x = S_y = 0$), then under these hypotheses Equation (5.42) assumes the following form:

$$\begin{bmatrix} EI_{yy} & 0 \\ 0 & EI_{xx} \end{bmatrix} \begin{Bmatrix} \xi^{IV} \\ \eta^{IV} \end{Bmatrix} + \begin{bmatrix} N & 0 \\ 0 & N \end{bmatrix} \begin{Bmatrix} \xi'' \\ \eta'' \end{Bmatrix} = \begin{Bmatrix} p_x \\ p_y \end{Bmatrix} \tag{5.47}$$

This system contains two decoupled equations each of which represents the elastic line equation with second-order effects valid respectively in the $[yz]$ plane and $[xz]$ plane. If $p_x = p_y = 0$, the value of the Euler critical axial force is obtained:

$$N_{cr} = \min\left(\frac{\pi^2 EI_{yy}}{L^2}; \frac{\pi^2 EI_{xx}}{L^2}\right) \tag{5.48}$$

The exact critical load for a cantilever beam subject to a uniformly distributed axial load has been evaluated by Timoshenko [250], and, further, taking into account the influence of discrete number s of actual concentrated loads applied over the height of the beam (i.e., the dead load due to the horizontal slab of the high-rise buildings), it is possible to apply a reduction factor α [127], [278], [280]. The axial buckling load at the clamped base of the cantilever beam is equal to:

$$N_{cr} = \min\left(3.176\alpha\frac{\pi^2 EI_{yy}}{(2L)^2}; 3.176\alpha\frac{\pi^2 EI_{xx}}{(2L)^2}\right) \tag{5.49}$$

where

$$\alpha = \frac{s}{s + 1.588} \tag{5.50}$$

As a third particular case, consider that the only load acting on the beam is the bending moment $\bar{M}_x$ ($N = \bar{M}_y = p_x = p_y = m_z = 0$). Since the beam cross section has double symmetry (the shear center coincides with the center of gravity) and $I_{\omega\omega} = 0$, it is easy to determine, through Equations (5.26 and 5.31), that $a_x = a_y = b_x = c_y = d_x = d_y = 0$, while $c_x = b_y = 1$. Under these assumptions, Equation (5.42) takes the following form:

$$\begin{bmatrix} EI_{yy} & 0 & 0 \\ 0 & EI_{xx} & 0 \\ 0 & 0 & 0 \end{bmatrix} \begin{Bmatrix} \xi^{IV} \\ \eta^{IV} \\ \vartheta^{IV} \end{Bmatrix} + \begin{bmatrix} 0 & 0 & 0 \\ 0 & 0 & 0 \\ 0 & 0 & -GI_t \end{bmatrix} \begin{Bmatrix} \xi'' \\ \eta'' \\ \vartheta'' \end{Bmatrix} + \\ + \begin{bmatrix} 0 & 0 & -\bar{M}_x \\ 0 & 0 & 0 \\ -\bar{M}_x & 0 & 0 \end{bmatrix} \begin{Bmatrix} \xi'' \\ \eta'' \\ \vartheta'' \end{Bmatrix} = \begin{Bmatrix} 0 \\ 0 \\ 0 \end{Bmatrix} \tag{5.51}$$

which can be rewritten as:

$$\begin{cases} EI_{yy}\xi^{IV} - \bar{M}_x\vartheta'' = 0 \\ \bar{M}_x\xi'' + GI_t\vartheta'' = 0 \end{cases} \tag{5.52}$$

Finding ϑ'' of the second equation and replacing it in the first one, we obtain:

$$\xi^{IV} + \frac{\bar{M}_x^2}{EGI_{yy}I_t}\xi'' = 0 \tag{5.53}$$

On the other hand, if we derive the second equation of the system (5.52) twice and replace it in the first one, we obtain:

$$\vartheta^{IV} + \frac{\bar{M}_x^2}{EGI_{yy}I_t}\vartheta'' = 0 \tag{5.54}$$

Equations (5.53 and 5.54) are the relations obtained by Prandtl to describe the lateral-torsional buckling.

If the beam, of length L is constrained at its ends by cylindrical hinges, the solution of Equations (5.53 and 5.54) is the same and provides the value of the critical bending moment equal to:

$$M_{x,cr} = \frac{\pi}{L}\sqrt{EGI_{yy}I_t} \tag{5.55}$$

In case a beam is analyzed, where the previous hypotheses remain valid, but with $I_{\omega\omega} \neq 0$, Equation (5.42) takes the following form:

$$\begin{bmatrix} EI_{yy} & 0 & 0 \\ 0 & EI_{xx} & 0 \\ 0 & 0 & EI_{\omega\omega} \end{bmatrix} \begin{Bmatrix} \xi^{IV} \\ \eta^{IV} \\ \vartheta^{IV} \end{Bmatrix} + \begin{bmatrix} 0 & 0 & 0 \\ 0 & 0 & 0 \\ 0 & 0 & -GI_t \end{bmatrix} \begin{Bmatrix} \xi'' \\ \eta'' \\ \vartheta'' \end{Bmatrix} + \\ + \begin{bmatrix} 0 & 0 & -\bar{M}_x \\ 0 & 0 & 0 \\ -\bar{M}_x & 0 & 0 \end{bmatrix} \begin{Bmatrix} \xi'' \\ \eta'' \\ \vartheta'' \end{Bmatrix} = \begin{Bmatrix} 0 \\ 0 \\ 0 \end{Bmatrix} \tag{5.56}$$

Considering that:

$$\xi'' = \frac{\bar{M}_x}{EI_{yy}}\vartheta \tag{5.57}$$

the third equation of system (5.56) can be written as:

$$EI_{\omega\omega}\vartheta^{IV} - GI_t\vartheta'' - \frac{\bar{M}_x^2}{EI_{yy}}\vartheta = 0 \tag{5.58}$$

This is the equation of non-uniform torsion with flexural-torsional buckling effects.

This equation can also be obtained conceptually, considering the overlapping of the effects of the non-uniform torsion Equation (5.46) and the equation of the flexural-torsional instability of Prandtl (5.54). If the beam, of length L, is constrained at its ends by cylindrical hinges, by imposing the appropriate boundary conditions (Equations 5.44), the solution of Equation (5.58) provides the value of the critical bending moment [203]:

$$M_{x,cr} = \frac{\pi}{L}\sqrt{EI_{yy}GI_t + \left(\frac{\pi}{L}\right)^2 E^2 I_{yy} I_{\omega\omega}} \tag{5.59}$$

Comparing Equation (5.59) with Equation (5.55), it can be deduced that the presence of the term $I_{\omega\omega} \neq 0$ leads to an increase in the value of the critical bending moment $M_{x,cr}$. As already pointed out in Chapter 2, the analysis of a thin-walled open-section using Vlasov's Theory involves an increase in its stiffness compared to the value that would be obtained by using Saint Venant's Theory.

The analogous treatment can be done if the only load present on the beam is the bending moment $\bar{M}_y$, obtaining:

$$M_{y,cr} = \frac{\pi}{L}\sqrt{EI_{xx}GI_t + \left(\frac{\pi}{L}\right)^2 E^2 I_{xx} I_{\omega\omega}} \tag{5.60}$$

For the cantilever beam under uniformly distributed load case, the bending moment is a second-order parabolic function. Consequently, no-closed form solutions of Equation (5.58) to be sought by analytical procedures are available, and an alternative approximate numerical method should be use [107]. In this case, the eigenvalue of Equation (5.58), that is the lateral-torsional buckling moment with respect to y axis, is equal to:

$$M_{x,cr} = 2.046\frac{\pi}{L}\sqrt{EI_{yy}GI_t + \left(\frac{\pi}{L}\right)^2 E^2 I_{yy} I_{\omega\omega}} \tag{5.61}$$

Drawing the diagram of Equation (5.61) as a function of the height of the beam, we obtain a curve very similar to Euler's hyperbola as shown in Figure (5.5).

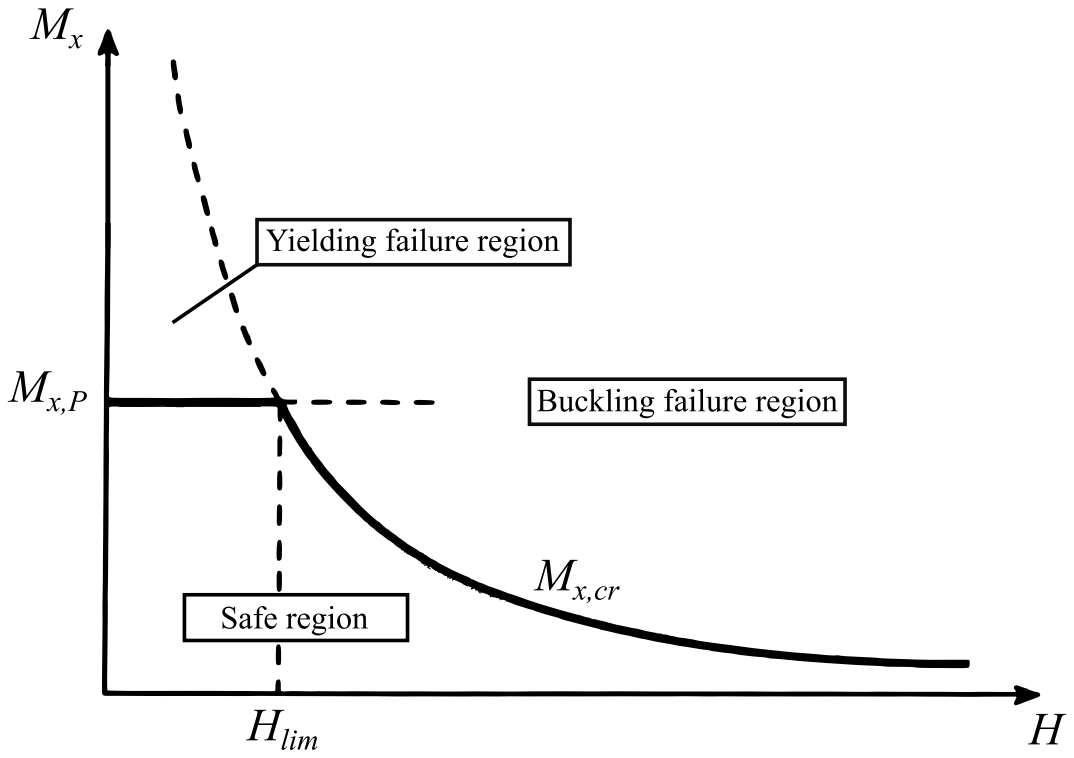

Figure 5.5: Lateral-torsional buckling moment as a function of the height of the beam

This curve envisages lateral-torsional buckling moment tending to zero as the height of the beam tends to infinity and, conversely, lateral-torsional buckling moment tending to infinity as the height of the beam tends to zero. The latter tendency is unlikely, because the failure due to yielding:

$$M_{x,P} = W_x \sigma_P \tag{5.62}$$

where W_x and σ_P are the elastic section modulus with respect to the x-axis and the yield stress of the beam, respectively.

If there were no interaction between the two critical phenomena, there would be a point of discontinuity in the passage from one to the other, corresponding to the limit height of the cantilever beam (H_{lim}).

In this section it has been shown that the remarkable cases present in literature (Euler's Problem, Prandtl's Problem, Non-uniform Torsion Theory) can be described by Equation (5.42), which proves to be quite general.

5.3 Contribution of shear deformability

In the previous formulation, the hypothesis was made that the beam is deformable only by bending and twisting. In a first approximation the hypothesis is widely satisfied, but in order to generalize the treatment as much as possible, in this section it is considered that the beam is also deformable by shearing stresses.

In consideration of this, the total deformation energy of the beam Φ^T can be written as the sum of the derformative contribution due to bending and twisting, Φ^B, and the deformative contribution Φ^S due to shear stresses and the secondary torsional moment:

$$\Phi^T = \Phi^B + \Phi^S \tag{5.63}$$

The term Φ^B has been widely discussed and can be assessed using Equation (5.8), while by using Clapeyron Theorem, the elastic deformation energy due to shearing stresses is written as:

$$\Phi^S = -\frac{1}{2}\int_V \tau_{zs}\gamma_{zs}\mathrm{d}V = \frac{1}{2G}\int_0^L \left[\int_A \tau_{zs}^2 \mathrm{d}A\right]\mathrm{d}l \tag{5.64}$$

By choosing the global reference system with origin in the shear center of the section, the shearing stresses can be assessed using Equation (2.82).

By making substitutions, Equation (5.64) can be written as:

$$\Phi^S = -\frac{1}{2G}\int_0^L \left[\int_A \left(\frac{T_x S_y(s)}{I_{yy} b} + \frac{T_y S_x(s)}{I_{xx} b} + \frac{M_z^{VL} S_\omega(s)}{I_{\omega\omega} b}\right)^2 \mathrm{d}A\right]\mathrm{d}l \tag{5.65}$$

and then,

$$\begin{aligned}\Phi^S = &-\frac{1}{2G}\int_0^L \left[\frac{T_x^2}{I_{yy}^2}\int_A \left(\frac{S_y(s)^2}{b^2}\right)\mathrm{d}A + \frac{T_y^2}{I_{xx}^2}\int_A \left(\frac{S_x(s)^2}{b^2}\right)\mathrm{d}A + \right.\\ &+ \frac{{M_z^{VL}}^2}{I_{\omega\omega}^2}\int_A \left(\frac{S_\omega(s)^2}{b^2}\right)\mathrm{d}A + 2\frac{T_x T_y}{I_{yy} I_{xx}}\int_A \left(\frac{S_y(s) S_x(s)}{b^2}\right)\mathrm{d}A + \\ &\left.+ 2\frac{T_x M_z^{VL}}{I_{yy} I_{\omega\omega}}\int_A \left(\frac{S_y(s) S_\omega(s)}{b^2}\right)\mathrm{d}A + 2\frac{T_y M_z^{VL}}{I_{xx} I_{\omega\omega}}\int_A \left(\frac{S_x(s) S_\omega(s)}{b^2}\right)\mathrm{d}A\right]\mathrm{d}l\end{aligned} \tag{5.66}$$

As can be seen, the shear stresses T_x, T_y and the secondary torsional moment M_z^{VL} are not energetically orthogonal to each other. The constant terms, that depend only on the geometry of the section, are introduced:

$$t_x = \frac{A}{I_{yy}^2}\int_A \left(\frac{S_y(s)^2}{b^2}\right)\mathrm{d}A \tag{5.67a}$$

$$t_y = \frac{A}{I_{xx}^2}\int_A\left(\frac{S_x(s)^2}{b^2}\right)\mathrm{d}A \tag{5.67b}$$

$$t_\omega = \frac{A}{I_{\omega\omega}^2}\int_A\left(\frac{S_\omega(s)^2}{b^2}\right)\mathrm{d}A \tag{5.67c}$$

$$t_{xy} = \frac{A}{I_{xx}I_{yy}}\int_A\left(\frac{S_x(s)S_y(s)}{b^2}\right)\mathrm{d}A \tag{5.67d}$$

$$t_{x\omega} = \frac{A}{I_{xx}I_{\omega\omega}}\int_A\left(\frac{S_x(s)S_\omega(s)}{b^2}\right)\mathrm{d}A \tag{5.67e}$$

$$t_{y\omega} = \frac{A}{I_{yy}I_{\omega\omega}}\int_A\left(\frac{S_y(s)S_\omega(s)}{b^2}\right)\mathrm{d}A \tag{5.67f}$$

In Equations (5.67a, 5.67b, and 5.67d), the well-known shear factors introduced by Jourawski [56] are recognizable, while Equations (5.67c, 5.67e, and 5.67f) are constant coefficients, formally similar to the previous ones, but related to the sectorial characteristic. For this reason, they can be called *sectorial shear factors*.

By substituting Equations (2.53 and 5.67) in Equation (5.66), the shear deformation energy equation of the thin-walled open-section beam section is obtained.

$$\begin{aligned}\Phi^S = &-\frac{E^2}{2GA}\int_0^L\Big[t_x I_{yy}^2\xi'''^2 + t_y I_{xx}^2\eta'''^2 + t_\omega I_{\omega\omega}^2\vartheta'''^2 + \\ &+ 2\Big(t_{xy}I_{yy}I_{xx}\xi'''\eta''' + t_{x\omega}I_{yy}I_{\omega\omega}\xi'''\vartheta''' + t_{y\omega}I_{xx}I_{\omega\omega}\eta'''\vartheta'''\Big)\Big]\mathrm{d}l\end{aligned} \tag{5.68}$$

the variation is equal to:

$$\begin{aligned}\delta\Phi^S = &-\frac{E^2}{GA}\int_0^L\Big\{t_x I_{yy}^2\xi'''\delta\xi''' + t_y I_{xx}^2\eta'''\delta\eta''' + t_\omega I_{\omega\omega}^2\vartheta'''\delta\vartheta''' + \\ &+ 2\Big[t_{xy}I_{yy}I_{xx}\Big(\xi'''\eta'''\delta\xi''' + \xi'''\eta'''\delta\eta'''\Big) + t_{x\omega}I_{yy}I_{\omega\omega}\Big(\xi'''\vartheta'''\delta\xi''' + \\ &+ \xi'''\vartheta'''\delta\vartheta'''\Big) + t_{y\omega}I_{xx}I_{\omega\omega}\Big(\eta'''\vartheta'''\delta\eta''' + \eta'''\vartheta'''\delta\vartheta'''\Big)\Big]\Big\}\mathrm{d}l\end{aligned} \tag{5.69}$$

which integrated three times by parts, and consider only the integral equation, provides:

$$
\begin{aligned}
\delta\Phi^S =& \frac{E^2}{GA}\int_0^L \left[t_x I_{yy}^2 \xi^{VI}\delta\xi + t_y I_{xx}^2 \eta^{VI}\delta\eta + t_\omega I_{\omega\omega}^2 \vartheta^{VI}\delta\vartheta\right]\mathrm{d}l + \\
&+ \frac{E^2 t_{xy} I_{yy} I_{xx}}{GA}\int_0^L \left[\xi^{VI}\eta''' + 3\xi^{V}\eta^{IV} + 3\xi^{IV}\eta^{V} + \xi'''\eta^{VI}\right]\delta\xi\mathrm{d}l + \\
&+ \frac{E^2 t_{xy} I_{yy} I_{xx}}{GA}\int_0^L \left[\xi^{VI}\eta''' + 3\xi^{V}\eta^{IV} + 3\xi^{IV}\eta^{V} + \xi'''\eta^{VI}\right]\delta\eta\mathrm{d}l + \\
&+ \frac{E^2 t_{y\omega} I_{yy} I_{\omega\omega}}{GA}\int_0^L \left[\xi^{VI}\vartheta''' + 3\xi^{V}\vartheta^{IV} + 3\xi^{IV}\vartheta^{V} + \xi'''\vartheta^{VI}\right]\delta\xi\mathrm{d}l + \\
&+ \frac{E^2 t_{y\omega} I_{yy} I_{\omega\omega}}{GA}\int_0^L \left[\xi^{VI}\vartheta''' + 3\xi^{V}\vartheta^{IV} + 3\xi^{IV}\vartheta^{V} + \xi'''\vartheta^{VI}\right]\delta\vartheta\mathrm{d}l + \\
&+ \frac{E^2 t_{x\omega} I_{xx} I_{\omega\omega}}{GA}\int_0^L \left[\eta^{VI}\vartheta''' + 3\eta^{V}\vartheta^{IV} + 3\eta^{IV}\vartheta^{V} + \eta'''\vartheta^{VI}\right]\delta\eta\mathrm{d}l + \\
&+ \frac{E^2 t_{x\omega} I_{xx} I_{\omega\omega}}{GA}\int_0^L \left[\eta^{VI}\vartheta''' + 3\eta^{V}\vartheta^{IV} + 3\eta^{IV}\vartheta^{V} + \eta'''\vartheta^{VI}\right]\delta\vartheta\mathrm{d}l
\end{aligned}
\tag{5.70}
$$

Adding this term to Equation (5.38), the variation of the total potential energy δW of the beam also considering its shear deformability is determined.

Following the procedure illustrated above, setting $\delta W = 0$, and separating the terms that derive from them according to their variation, $\delta\xi$, $\delta\eta$, and $\delta\vartheta$, it is possible to write a system of three equations in three unknowns.

For beams with a symmetrical cross section, the problem is simplified considerably since the shear factors t_{xy}, $t_{x\omega}$, and $t_{y\omega}$, are null. In this case the solved equation takes the form:

$$
\frac{E^2}{GA}\left[J_v\right]\left\{\delta^{VI}\right\} + E\left[J\right]\left\{\delta^{IV}\right\} + G\left[J_t\right]\left\{\delta''\right\} + \left[\left\{N\right\}^{\mathrm{T}}\left\{C_g\right\}\right]\left\{\delta''\right\} = \left\{F\right\} \tag{5.71}
$$

where:

$$
\left[J_v\right] = \begin{bmatrix} t_x I_{yy}^2 & 0 & 0 \\ 0 & t_y I_{xx}^2 & 0 \\ 0 & 0 & t_\omega I_{\omega\omega}^2 \end{bmatrix} \tag{5.72}
$$

Interestingly, the contribution of shear deformability translates from the addition to Equation (5.42) of a shear stiffness term that multiplies the vector containing the sixth derivatives of the displacements.

In order to solve this sixth order differential equation and determine the vector $\{N\}$ of the critical loads, as is known, it is necessary to have 18 boundary conditions, 9 for each end of the beam. At the time of writing the present work, not all boundary conditions, which are necessary to solve the problem, have been defined yet.

5.4 Stability analysis of thin-walled open-section shear walls

In Section 5.2, the stability of a generic beam was studied. Now, a method that allows the analysis of a thin-walled open-section shear wall that is part of the vertical stiffening system of a high-rise building, will be illustrated, and, with this procedure, it is possible to calculate the critical loads that determine its instability.

In Chapter 2 it was illustrated that a generic bracing, be it a thin-walled closed- or open-section, can be modeled as an equivalent cantilever beam using appropriate techniques.

Consider an n-storey thin-walled open-section shear wall on which the external distributed loads p_x, p_y, and m_z, are applied. The entire bracing can be modeled as a series of n beams, of a length equal to the inter-story h, rigidly connected to each other. Numbering the beams from top to bottom, assuming that the material is the same for the entire height, and neglecting the shear deformability, it is possible to write Equation (5.42) for each individual beam, obtaining in this way a system of n fourth order differential equations:

$$\begin{aligned}
&E\,[J_1]\left\{{\delta_1}^{IV}\right\} + G\,[J_{t1}]\,\{\delta_1{}''\} + \left[\{N_1\}^{\mathrm{T}}\left\{C_{g1}\right\}\right]\{\delta_1{}''\} = \{F_1\}\\
&E\,[J_2]\left\{{\delta_2}^{IV}\right\} + G\,[J_{t2}]\,\{\delta_2{}''\} + \left[\{N_2\}^{\mathrm{T}}\left\{C_{g2}\right\}\right]\{\delta_2{}''\} = \{F_2\}\\
&\qquad\qquad\cdots\\
&E\,[J_n]\left\{{\delta_n}^{IV}\right\} + G\,[J_{tn}]\,\{\delta_n{}''\} + \left[\{N_n\}^{\mathrm{T}}\left\{C_{gn}\right\}\right]\{\delta_n{}''\} = \{F_n\}
\end{aligned} \tag{5.73}$$

where each of the matrices has dimension 3×3, while the vectors have dimension 3×1.

By introducing the matrices, each having dimensions $3n \times 3n$,

$$[J^*] = \begin{bmatrix} [J_1] & 0 & \cdots & 0 \\ 0 & [J_2] & \cdots & 0 \\ \vdots & \vdots & \ddots & \vdots \\ 0 & 0 & \cdots & [J_n] \end{bmatrix} \tag{5.74a}$$

$$[J_t^*] = \begin{bmatrix} [J_{t1}] & 0 & \cdots & 0 \\ 0 & [J_{t2}] & \cdots & 0 \\ \vdots & \vdots & \ddots & \vdots \\ 0 & 0 & \cdots & [J_{tn}] \end{bmatrix} \tag{5.74b}$$

$$[C_g{}^*] = \begin{bmatrix} \left[C_{g1}\right] & 0 & \cdots & 0 \\ 0 & \left[C_{g2}\right] & \cdots & 0 \\ \vdots & \vdots & \ddots & \vdots \\ 0 & 0 & \cdots & \left[C_{gn}\right] \end{bmatrix} \tag{5.74c}$$

and the vectors, each having dimensions $3n \times 1$,

$$\{\delta^*\} = \begin{Bmatrix} \{\delta_1{}^*\} \\ \{\delta_2{}^*\} \\ \vdots \\ \{\delta_n{}^*\} \end{Bmatrix} \tag{5.75a}$$

$$\{N^*\} = \begin{Bmatrix} \{N_1{}^*\} \\ \{N_2{}^*\} \\ \vdots \\ \{N_n{}^*\} \end{Bmatrix} \tag{5.75b}$$

$$\{F^*\} = \begin{Bmatrix} \{F_1{}^*\} \\ \{F_2{}^*\} \\ \vdots \\ \{F_n{}^*\} \end{Bmatrix} \tag{5.75c}$$

the following equation, valid for the entire shear wall, can be written:

$$E\,[J^*]\left\{\delta^{*IV}\right\} + G\,[J_t{}^*]\left\{\delta^{*\prime\prime}\right\} + \left[\{N^*\}^{\mathrm{T}}\,\{C_g{}^*\}\right]\left\{\delta^{*\prime\prime}\right\} = \{F^*\} \tag{5.76}$$

To solve this system of $3n$ fourth order differential equations, it is necessary to define the boundary conditions.

Assuming that the shear wall is subject to the external horizontal distributed load in the x and y directions, respectively, the boundary conditions can be schematically summarized as follows.

At the base of the shear wall (node $n+1$) there is a full restraint, therefore kinematic conditions require that $\{\delta_{n+1}\} = \{0\}$ and $\{\delta'_{n+1}\} = \{0\}$.

At the top (node 1), there is no constraint; as a result the static conditions impose that the two bending moments and the bimoment are null ($\{\delta''_1\} = \{0\}$), just as the two shear forces in the x and y directions, respectively, ($\xi'''_1 = \eta'''_1 = 0$), and the total torsional moment ($GI_t\vartheta'_1 - EI_{\omega\omega}\vartheta'''_1 = 0$), must be null.

For all j-th intermediate nodes the conditions of continuity of the displacement function $\{\delta_j\}$ and of its first derivative $\{\delta'_j\}$ must be valid.

By solving Equation (5.76), the vector containing the critical loads $\{N^*\}$ is obtained. This vector contains the values of the critical axial force N_{cr} and the two critical bending moments $M_{x,cr}$ and $M_{y,cr}$, evaluated for each floor of the shear wall.

In general, for the verification against axial stability ($N \leq N_{cr}$), the most unfavorable conditions occur in the lower floors, where the maximum axial force due to dead load is concentrated. Moreover, since tall buildings have on the ground floor the entrance hall which usually has height of $10-15$ meters (the storeys above generally are $3-4$ meters in height), and considering Equation (5.48), it is easy to verify that in the lower floors the critical axial load is low.

Regarding the verification against lateral-torsional buckling ($M_x \leq M_{x,cr} \cup M_y \leq M_{y,cr}$), the problem is generally more complex as it is necessary to first evaluate the values of M_x and M_y due to the actual external distributed loads that are applied to the shear wall.

On the other hand, by performing static analysis, it is possible to evaluate the floor displacements $\{\delta\}$ due to the external load, and the bending moments, as shown in the Equation (2.46a). By inverting these relationships and replacing the values of $M_{x,cr}$ and $M_{y,cr}$, it is possible to obtain the deformed shape of the structure (buckling shape). By applying Equation (2.46c) we obtain the values of the external critical loads $p_{x,cr}$ and $p_{y,cr}$. These values can also be defined as a function of the actual horizontal loads p_x and p_y acting on the bracing, through constants:

$$p_{x,cr} = \lambda_x p_x \tag{5.77a}$$

$$p_{y,cr} = \lambda_y p_y \tag{5.77b}$$

The constants λ_x and λ_y are defined as multipliers of the external loads for the x and y directions, respectively.

As illustrated in Chapter 3, if in the high-rise building more than one vertical bracing is present, by knowing their stiffness matrices and applying the General Algorithm, it is possible to determine the load distribution matrix $[R_i]$, and consequently the portion of external load that is absorbed by i-th bracing, as illustrated in Equation (3.19).

By evaluating Equations (5.76 and 5.77) for each i-th vertical bracing, it is possible to determine the values of the multipliers of the global external loads acting on the building:

$$\Lambda_x = \min\left(\lambda_{x,i}\right) \tag{5.78a}$$

$$\Lambda_y = \min\left(\lambda_{y,i}\right) \tag{5.78b}$$

Physically, the multipliers of the external load can be interpreted as safety factors. If the coefficient Λ_x or Λ_y is equal to 1, it means that the load applied to the building generates instability. The more the coefficients Λ_x and Λ_y are greater than 1, the further the building is from collapse due to instability.

Chapter 6

Conclusions

This thesis illustrates the main results of the research that I have conducted, under the supervision of Prof. Alberto Carpinteri and Prof. Giuseppe Lacidogna, in the three years of my doctoral studies.

As shown in Chapter 1, the number of high-rise buildings being built in the world, as well as their height, is constantly increasing. This upward trend has been made possible by the introduction of new building materials and the creation of calculation models which allow the control of a building's transversal displacements, construction speed, and structural lightness while providing greater freedom in architectural choices. On the other hand, the complexity of designing this type of building has significantly increased.

In order to deal with these engineering problems, in recent decades the development of computer tools, both hardware and software, has had considerable impetus and improvement, especially in the context of Finite Element Method (FEM) software programs. New generations of engineers often completely rely on commercial software, frequently without evaluating whether the results they obtain are compatible with the real behavior of the building. Especially in the initial stages of design, where it is very important to understand how a structure behaves following the application of loads, the use of this complex and expensive FEM software is not necessary, indeed it can also be harmful. In this context, simplified analytical formulations have been developed which describe the behavior of tall buildings in an uncomplicated, intuitive way and with the use of simple resources and techniques.

As shown in Chapter 2, the first analytical methods were developed in the 1960s and 1970s, when computer tools were rare and complex to use and almost unknown to designers. Today, many consider these formulations obsolete and outclassed, but as shown in this present work, if properly used, they provide results that match those obtained using FEM software. With the creation of the General Algorithm by Prof. Alberto Carpinteri, described in Chapter 3, the basis was laid for the realization of structural software based on these methods.

Over the years the General Algorithm has been improved and optimized, implementing formulations not only to carry out static analysis, but, as shown in Chapter 4, also to perform dynamic analyses and estimate the mode shapes, natural frequencies, and periods of vibration of a high-rise building.

Finally, as described in Chapter 5 of this thesis, the foundations have been laid for the stability analysis of a high-rise building. This type of analysis, often underestimated by designers, is very important in the design process because nowadays taller and leaner buildings are being built.

6.1 Objectives achieved

Numerous objectives have been achieved through this doctoral thesis which, in a number of cases, represent the completion of the analytical formulation devised a few years ago by Prof. Alberto Carpinteri. In particular, the functions that allow the definition of the stiffness matrices of framed tube and diagrid structures have been implemented in the General Algorithm. This has greatly expanded the possibilities of using the software, because nowadays many high-rise buildings are made using these construction techniques. Furthermore, while in the scientific literature there are numerous analytical formulations that allow the analysis of only one type of vertical bracing (thin-walled closed- or open-section shear walls, frames, braced frames, framed tube or diagrid), the intrinsic potential of the General Algorithm allow the displacements and stresses to be determined in buildings where there are simultaneously multiple types of vertical bracings. In this way it is possible to understand how the external horizontal load is distributed among the various vertical bracings and which is the most stressed element.

As far as dynamic analysis is concerned, the analytical formulations have been extended in order to evaluate the mode shapes, natural frequencies, and periods of vibration of high-rise buildings which have an irregular floor plan or are composed of vertical bracings of different heights. Furthermore, in this doctoral thesis the possibility of analyzing buildings in which there is a mass damper has been introduced.

Eventually, a new and original analytical formulation has been developed for the stability study of thin-walled open-section beams. This complex three-dimensional formulation, based on Vlasov's Theory, has proved to be generally applicable and can be used to evaluate the stability of a beam with any constraint and load conditions. To demonstrate the effectiveness of the method, some particular cases known in literature have been evaluated. By imposing some simplifying hypotheses, the formulation has been particularized by obtaining the equations that allow the critical axial load (Euler's problem) and the critical flexural moment (Prandtl's problem) to be established, and the non-uniform torsion equation with flexotorsional destabilizing effects has been determined.

A further development, which also included the effects of deformation energy relating to the shearing stresses due to shear forces and to the secondary torsional moment, has been evaluated, obtaining a sixth order differential equation.

In this formulation some coefficients have been introduced which, analogously to Jourawski's Theory, have been defined shear factors related to the sectorial area.

Finally, using the General Algorithm, it is possible to evaluate the stability of a generic thin-walled shear wall, and consequently of a high-rise building. In this case the unknowns of the problem are the multipliers of the external loads, which can be interpreted as safety factors against the collapse instability of the building.

6.2 Future developments

The results obtained in this work are not to be considered conclusive. Instead, they can represent an original starting point for further study, in order to evaluate the behavior of a structure in the most realistic possible way. In this regards, a fundamental hypothesis of the General Algorithm consists in the fact that out of their plane floors have null rigidity. This simplifying assumption gives conservative results since it provides greater displacements and stresses than the solution with floors having a real out-of-plane rigidity. Removing the assumption of null rigidity should involve the not simple addition to the analytical formulation of further elastic constraints at the level of each floor. In this way it will be possible to further reduce the gap, already very small (usually less than 10%) between the results obtained using the analytical code and those obtained using commercial FEM software.

As regards dynamic analysis, it is planned to introduce algorithms into the analytical formulation that allow the determination of the modal participation factors and the evaluation of the stresses on the structural elements, defined by carrying out the modal analysis. Furthermore, it is also planned to introduce the automatic evaluation of the structure elastic response spectrum, and consequently the seismic forces acting on the building, into the code. The reason why this procedure has not yet been implemented in the software is that it presents some differences according to the legislation to be used.

As for the stability analysis, the formulation presented in this thesis will soon be implemented in the analytical calculation code. The clarity of the final expressions, made even more evident by the matrix form, bodes well for quick and convenient use in the field of automatic calculation. Finally, by replacing static loads with dynamic forces, the problem can be further extended in order to assess stability under dynamic conditions. After introducing these algorithms into our analytic calculation code, we will be able to affirm that we have developed a powerful software that can be distributed to designers all over the world to test its effectiveness on real structures.

Bibliography

[1] G. Abdel-Sayed. "Effective width of steel deck-plates in bridges". In: *Journal of the Structural Division* 95 (1969), pp. 1459–1474.

[2] H.R. Aggarwal and E.T. Cranch. "A theory of torsional and coupled bending torsional waves in thin-walled open section beams". In: *Journal of Applied Mechanics* 34 (1967), pp. 337–343.

[3] S.A.K. Ahuja and P.K. Gupta. "Wind loads on tall buildings with steps". In: *Journal of Academia and Industrial Research* 1 (2013), pp. 766–768.

[4] M.M. Ali and K.S. Moon. "Structural developments in tall buildings: current trends and future prospects". In: *Architectural Science Review* 50 (2007), pp. 205–223.

[5] R.D. Ambrosini. "Experimental validation of free vibrations from nonsymmetrical thin walled beams". In: *Engineering Structures* 32 (2010), pp. 1324–1332.

[6] R.D. Ambrosini. "On free vibration of nonsymmetrical thin-walled beams". In: *Thin-walled Structures* 47 (2009), pp. 629–636.

[7] R.D. Ambrosini, J.D. Riera, and R.F. Danesi. "A modified Vlasov theory for dynamic analysis of thin-walled and variable open section beams". In: *Engineering Structures* 22 (2000), pp. 890–900.

[8] R.D. Ambrosini, J.D. Riera, and R.F. Danesi. "Dynamic analysis of thin-walled and variable open section beams with shear flexibility". In: *International Journal for Numerical Methods in Engineering* 38 (1995), pp. 2867–2885.

[9] J.M. Anderson and N.S. Trahair. "Stability of monosymmetric beams and cantilevers". In: *Journal of the Structural Division* 98 (1972), pp. 269–286.

[10] G. Angelucci and F. Mollaioli. "Diagrid structural systems for tall buildings: Changing pattern configuration through topological assessments". In: *The Structural Design of Tall and Special Buildings* 26 (2017), Article number e1396.

[11] G. Angelucci and F. Mollaioli. "Voronoi-Like grid systems for tall buildings". In: *Frontiers in Built Environment* 4 (2018), Article number 78.

[12] G. Angelucci, F. Mollaioli, and O. Al Shawa. "Evaluation of optimal lateral resisting systems for tall buildings subject to horizontal loads". In: *Procedia Manufacturing* 44 (2020), pp. 457–464.

[13] J.H. Argyris. "The open tube: A study of thin-walled structures such as interspar wing cut-outs and open-section stringers". In: *Aircraft Engineering and Aerospace Technology* 26 (1954), pp. 102–112.

[14] A. Arpaci and E. Bozdag. "On free vibration analysis of thin-walled beams with nonsymmetrical open cross-sections". In: *Computers and Structures* 80 (2002), pp. 691–695.

[15] E. Asadi and H. Adeli. "Diagrid: An innovative, sustainable, and efficient structural system". In: *The Structural Design of Tall and Special Buildings* 26 (2017), Article number e1358.

[16] M.M. Attard and M.A. Bradford. "Bifurcation experiments on monosymmetric cantilevers". In: *Proceedings of 12th Australasian Conference on the Mechanics of Structures and Materials, Brisbane* (1990), pp. 207–213.

[17] R. Avini, P. Kumar, and S.J. Hughes. "Wind loading on high-rise buildings and the comfort effects on the occupants". In: *Sustainable Cities and Society* 45 (2019), pp. 378–394.

[18] C. Bach and R. Baumann. *Elastizität und festigkeit*. (In German). Springer, 1924.

[19] R. Baldacci. *Fondamenti di meccanica delle strutture*. (In Italian). U.T.E.T., 1976.

[20] R.S. Barsoum and R.H. Gallagher. "Finite element analysis of torsional and torsional-flexural stability problems". In: *International Journal for Numerical Methods in Engineering* 2 (1970), pp. 335–352.

[21] Z.P. Bažant and M. Christensen. "Continuous approximation of large regular frames and the problem of a substitute frame". In: *American Concrete Institute* Special Publication No.36 (1973), pp. 257–278.

[22] H. Beck. "Contribution to the analysis of coupled shear walls". In: *American Concrete Institute Journal Proceedings* 59 (1962), pp. 1055–1070.

[23] O. Belluzzi. *Scienza delle costruzioni*. (In Italian). Zanichelli, 1950.

[24] R. Bhowmik, S. Mukherjee, A. Das, and S. Banerjee. "Review on bubble deck with spherical hollow balls". In: *International Journal of Civil Engineering and Technology* 8 (2017), pp. 979–987.

[25] D.P. Billington. *The tower and the bridge: The new art of structural engineering*. Princeton University Press, 1985.

[26] M. Bindea, C.M. Chezan, and A. Puskas. "Numerical analysis of flat slabs with spherical voids subjected to shear force". In: *Journal of Applied Engineering Sciences* 5 (2015), pp. 7–13.

[27] R.E.D. Bishop, S.M. Cannon, and S. Miao. "On coupled bending and torsional vibration of uniform beams". In: *Journal of Sound and Vibration* 131 (1989), pp. 457–464.

[28] R.E.D. Bishop, W.G. Price, and Z.X. Cheng. "A note on the dynamical behaviour of uniform beams having open channel section". In: *Journal of Sound and Vibration* 99 (1985), pp. 155–167.

[29] R.E.D. Bishop, W.G. Price, and Z.X. Cheng. "On the structural dynamics of a Vlasov beam". In: *Proceedings of the Royal Society of London. Series A, Mathematical and Physical Sciences* 388 (1983), pp. 49–73.

[30] J.K. Biswas and W.K. Tso. "Three-dimensional analysis of shear wall buildings to lateral load". In: *Journal of the Structural Division* 100 (1974), pp. 1019–1036.

[31] F. Bleich. *Buckling strength of metal structures*. McGraw-Hill, 1952.

[32] F. Bleich and H. Bleich. "Biegung, drellung und knickung von stäben aus dünnen wänden". (In German). In: *Vorbericht Zweiter Kongress Internationale Vereinigung für Brückenbau und Hochbau, Berlin* (1936).

[33] D. Bluestone. "Preservation and renewal in post-world war II Chicago". In: *Journal of Architectural Education* 47 (1994), pp. 210–223.

[34] N.A. Boloban. "Issledovanie dyuralyuminievykh profilei". (In Russian, Trans: A study of duraluminium profiles). In: *Sawodskaja Laboratorija* 5 (1936), pp. 482–483.

[35] M. Bosco, A. Ghersi, E.M. Marino, and P.P. Rossi. "Prediction of the seismic response of steel frames with concentric diagonal bracings". In: *The Open Construction and Building Technology Journal* 7 (2013), pp. 118–128.

[36] L.F. Boswell and Q. Li. "Consideration of the relationship between torsion, distortion and warping of thin-walled beams". In: *Thin-walled Structures* 21 (1995), pp. 147–161.

[37] K.B. Bozdogan. "An approximate method for static and dynamic analyses of symmetric wall-frame buildings". In: *The Structural Design of Tall and Special Buildings* 18 (2009), pp. 279–290.

[38] K.B. Bozdogan. "Free vibration analysis of asymmetric shear wall-frame buildings using modified finite element-transfer matrix method". In: *Structural Engineering and Mechanics* 46 (2013), pp. 1–17.

[39] K.B. Bozdogan. "Free vibration analysis of asymmetric-plan shear wall and core buildings using one-dimensional finite element". In: *Arabian Journal for Science and Engineering* 38 (2013), pp. 1041–1045.

[40] K.B. Bozdogan and D. Ozturk. "Free vibration analysis of the tube-in-tube tall buildings with the differential transform method". In: *Advances in Structural Engineering* 17 (2014), pp. 1271–1279.

[41] K.B. Bozdogan and D. Ozturk. "Vibration analysis of asymmetric shear wall and thin walled open section structures using transfer matrix method". In: *Structural Engineering and Mechanics* 33 (2009), pp. 95–107.

[42] K.B. Bozdogan and D. Ozturk. "Vibration analysis of asymmetric shear wall structures using the transfer matrix method". In: *Iranian Journal of Science and Technology* 34 (2010), pp. 1–14.

[43] H.A. Brooks. "Chicago School: Metamorphosis of a term". In: *Journal of the Society of Architectural Historians* 25 (1966), pp. 115–118.

[44] M.D. Burton, K.C.S. Kwok, and A. Abdelrazaq. "Wind-induced motion of tall buildings: Designing for occupant comfort". In: *International Journal of High-rise Buildings* 4 (2015), pp. 1–8.

[45] K.A. Čališev. "Izračunavanje višestruko statički neodredenik sistema pomoću postepenih aproksimacija". (In Croatian). In: *Tehnički List Udruženja Jugoslavenskih Inženjera i Arhitekata* 5 (1923), pp. 125–158.

[46] K.A. Čališev. "O dopunitbenim naprezanjima rešetkastih nosača". (In Croatian). In: *Tehnički List Udruženja Jugoslavenskih Inženjera i Arhitekata* 4 (1922), pp. 1–6.

[47] S. Cammarano. "Static and dynamic analysis of high-rise building". PhD thesis. Politecnico di Torino, 2014.

[48] S. Cammarano, G. Lacidogna, B. Montrucchio, and A. Carpinteri. "Experimental evaluation of the warping deformation in thin-walled open section profiles". In: *Advancement of Optical Methods in Experimental Mechanics. Conference Proceedings of the Society for Experimental Mechanics Series* 3 (2015), pp. 231–242.

[49] D. Capuani, M. Merli, and M Savoia. "An equivalent continuum approach for coupled shear walls". In: *Engineering Structures* 16 (1994), pp. 63–73.

[50] D. Capuani, M. Merli, and M Savoia. "Dynamic analysis of coupled shear wall-frame systems". In: *Journal of Sound and Vibration* 192 (1996), pp. 867–883.

[51] D. Capuani, M. Savoia, and F. Laudiero. "Continuum model for analysis of multiply connected perforated cores". In: *Journal of Engineering Mechanics* 120 (1994), pp. 1641–1660.

[52] M. Capurso. “Sul calcolo dei sistemi spaziali di controventamento”. (In Italian). In: *Giornale del Genio Civile* Fasc. 1°-2°-3° (1981), pp. 27–42.

[53] M. Capurso. “Sul calcolo delle travi di parete sottile in presenza di forze e distorsioni”. (In Italian). In: *La Ricerca Scientifica* 6. NOTE I-II (1964), pp. 213–286.

[54] M. Capurso. “Sul calcolo delle travi di parete sottile in presenza di forze e distorsioni”. (In Italian). In: *La Ricerca Scientifica* 7. NOTE III-V (1964), pp. 5–106.

[55] A. Carpinteri. *Advanced structural mechanics*. CRC Press, 2017.

[56] A. Carpinteri. *Structural mechanics fundamentals*. CRC Press, 2014.

[57] A. Carpinteri and S. Cammarano. “A simplified approach for the dynamic analysis of high-rise structures”. In: *Dynamics of Civil Structures. Conference Proceedings of the Society for Experimental Mechanics Series* 4 (2014), pp. 509–520.

[58] A. Carpinteri and An. Carpinteri. “Lateral loading distribution between the elements of a three-dimensional civil structure”. In: *Computers and Structures* 21 (1985), pp. 563–580.

[59] A. Carpinteri, G. Lacidogna, B. Montrucchio, and S. Cammarano. “The effect of the warping deformation on the structural behaviour of thin-walled open section shear walls”. In: *Thin-walled Structures* 84 (2014), pp. 335–343.

[60] A. Carpinteri, G. Lacidogna, and S. Cammarano. “Conceptual design of tall and unconventionally shaped structures: A handy analytical method”. In: *Advances in Structural Engineering* 17 (2014), pp. 767–783.

[61] A. Carpinteri, G. Lacidogna, and S. Cammarano. “Formulazione analitica per la progettazione dei controventi verticali in edifici di grande altezza”. (In Italian). In: *XXIV Giornate Italiane della Costruzione in Acciaio (CTA), Torino, 30 Settembre-2 Ottobre* (2013), pp. 982–989.

[62] A. Carpinteri, G. Lacidogna, and S. Cammarano. “Structural analysis of high-rise buildings under horizontal loads: A study on the Intesa Sanpaolo Tower in Turin”. In: *Engineering Structures* 56 (2013), pp. 1362–1371.

[63] A. Carpinteri, G. Lacidogna, and G. Nitti. “Open and closed shear-walls in high-rise structural systems: Static and dynamic analysis”. In: *Curved and Layered Structures* 3 (2016), pp. 154–171.

[64] A. Carpinteri, G. Lacidogna, and S. Puzzi. “A global approach for three-dimensional analysis of tall buildings”. In: *The Structural Design of Tall and Special Buildings* 19 (2010), pp. 518–536.

[65] A. Carpinteri, M. Corrado, G. Lacidogna, and S. Cammarano. "Lateral load effects on tall shear wall structures of different height". In: *Structural Engineering and Mechanics* 41 (2012), pp. 313–337.

[66] P.C.K. Chan, W.K. Tso, and A.C. Heidebrecht. "Effect of normal frames on shear walls". In: *Building Science* 9 (1974), pp. 197–209.

[67] S.T. Chang and F.A. Zheng. "Negative shear lag in cantilever box girder with constant depth". In: *Journal of Structural Engineering* 113 (1987), pp. 20–35.

[68] W.F. Chen and T. Atsuta. *Theory of beam columns. Space behaviour and design*. McGraw-Hill, 1977.

[69] X. Chen and K.K. Tamma. "Dynamic response of elastic thin-walled structures influenced by coupling effects". In: *Computers and Structures* 51 (1994), pp. 91–105.

[70] A.K. Chopra. *Dynamics of structures, theory and application to earthquake engineering*. Prentice Hall, 2001.

[71] G.M. Chuvikin. "Ustoichivost' ploskoi deformatsii vnetsentrenno szhatykh sterzhnei pri sravnimykh glavnykh momentakh inerrtsii secheniya". (In Russian, Trans: Stability in plane deformation of eccentrically compressed beams with comparable principal moments of section). In: *Issledovaniya po Teorii Sooruzhenii, VI Gosstroiizdat* 1 (1954).

[72] G. Cocchi. "Estensione del metodo di Cross ai telai con nodi spostabili". (In Italian). In: *Giornale del Genio Civile* luglio-agosto (1946).

[73] C.W. Condit. *The Chicago School of Architecture: A history of commercial and public building in the Chicago area, 1875-1925*. University of Chicago Press, 1964.

[74] J.J. Connor and C.C. Poungare. "Simple model for design of framed-tube structures". In: *Journal of the Structural Division* 117 (1991), pp. 3623–3644.

[75] A. Coull and A. Ahmed. "Deflections of framed-tube structures". In: *Journal of the Structural Division* 104 (1978), pp. 857–862.

[76] A. Coull and B. Bose. "Simplified analysis of framed-tube structures". In: *Journal of the Structural Division* 101 (1975), pp. 2223–2240.

[77] A. Coull and B. Bose. "Torsion of frame-tube structures". In: *Journal of the Structural Division* 102 (1976), pp. 2366–2370.

[78] A. Coull and W.Y. Chee. "Coupling action of slabs in hull-core structures". In: *Journal of Structural Engineering* 110 (1984), pp. 213–227.

[79] A. Coull and W.Y. Chee. "Design of floor slabs coupling shear walls". In: *Journal of Structural Engineering* 109 (1983), pp. 109–125.

[80] A. Coull and W.Y. Chee. "Stresses in slabs coupling flanged shear walls". In: *Journal of Structural Engineering* 110 (1984), pp. 105–119.

[81] A. Coull and J.R. Choudhury. "Stresses and deflections in coupled shear walls". In: *ACI Journal Proceedings* 64 (1967), pp. 65–72.

[82] A. Coull and A.A. El Hag. "Effective coupling of shear-walls by floor slabs". In: *ACI Journal Proceedings* 72 (1975), pp. 429–431.

[83] A. Coull and A.W. Irwin. "Analysis of load distribution in multi-storey shear wall structures". In: *Structural Engineer* 48 (1970), pp. 301–306.

[84] A. Coull and A.W. Irwin. "Model investigations of shear wall structures". In: *Journal of the Structural Division* 98 (1972), pp. 1223–1237.

[85] A. Coull and A.W. Irwin. "Torsional analysis of multi-story shear-wall structures". In: *ACI Special Publication* 35 (1973), pp. 211–238.

[86] A. Coull and R.D. Puri. "Analysis of pierced shear walls". In: *Journal of the Structural Division* 94 (1968), pp. 71–82.

[87] A. Coull and N.K. Subedi. "Framed-tube structures for high-rise buildings". In: *Journal of the Structural Division* 97 (1971), pp. 2097–2105.

[88] H. Cross. "Analysis of continuous frames by distributing fixed-end moments". In: *Proeedings of American Society of Civil Engineers* 56 (1930), pp. 919–928.

[89] H. Cross and N.D. Morgan. *Continuous frames of reinforced concrete*. Wiley, 1932.

[90] T.K. Datta. *Seismic analysis of structures*. John Wiley & Sons, 2010.

[91] P. Deamer. *Architecture and capitalism: 1845 to the present*. Routledge, 2014.

[92] E. Dokumaci. "An exact solution for coupled bending and torsion vibrations of uniform beams having single cross-sectional symmetry". In: *Journal of Sound and Vibration* 119 (1987), pp. 443–449.

[93] L. Dufort, M. Grédiac, and Y. Surrel. "Experimental evidence of the cross-section warping in short composite beams under three point-bending". In: *Composite Structures* 51 (2001), pp. 37–47.

[94] A. Di Egidio, A. Contento, and F. Vestroni. "The role of nonlinear torsional contributions on the stability of flexural-torsional oscillations of open-cross section beams". In: *Journal of Sound and Vibration* 358 (2015), pp. 236–250.

[95] A. Di Egidio, A. Luongo, and F. Vestroni. "A non-linear model for the dynamics of open cross-section thin-walled beams - Part I: formulation". In: *International Journal of Non-Linear Mechanics* 38 (2003), pp. 1067–1081.

[96] A. Di Egidio, A. Luongo, and F. Vestroni. "A non-linear model for the dynamics of open cross-section thin-walled beams - Part II: forced motion". In: *International Journal of Non-Linear Mechanics* 38 (2003), pp. 1083–1094.

[97] A. Di Egidio and F. Vestroni. "Static behavior and bifurcation of a monosymmetric open cross-section thin-walled beam: Numerical and experimental analysis". In: *International Journal of Solids and Structures* 48 (2011), pp. 1894–1905.

[98] M. Eisenberger. "Nonuniform torsional analysis of variable and open cross-section bars". In: *Thin-walled Structures* 21 (1995), pp. 93–105.

[99] L. Euler. "Sur la force des colonnes". (In French). In: *Mémoires de l'Académie des Sciences de Berlin* 13 (1759), pp. 252–282.

[100] C. Fischer and B. Kasal. "Analysis of light-frame, low-rise buildings under simulated lateral wind loads". In: *Wind and Structures* 12 (2009), pp. 89–101.

[101] A.R. Flint. "The stability and strength of stocky beams". In: *Journal of Mechanics and Physics of Solid* 1 (1953), pp. 90–102.

[102] D.A. Foutch and P.C. Chang. "A shear lag anomaly". In: *Journal of the Structural Division* 108 (1982), pp. 1653–1658.

[103] V. Franciosi. *Scienza delle costruzioni*. (In Italian). Liguori, 1971.

[104] V. Franciosi. "Un metodo di rapida convergenza per il calcolo dei telai a nodi spostabili". (In Italian). In: *L'Industria Italiana del Cemento* o (1949), pp. 221–261.

[105] N. Frazier. *Louis Sullivan and the Chicago School*. Knickerbocker Press, 1998.

[106] R.H. Gallangher. *A correlation study of methods of matrix structural analysis*. Pergamon Press, 1964.

[107] M.L. Gambhir. *Stability Analysis and Design of Structures*. Springer, 2004.

[108] C.F. Garland. "The normal modes of vibrations of beams having noncollinear elastic and mass axes". In: *Journal of Applied Mechanics ASME* 7 (1940), pp. 97–105.

[109] J.M. Gere. "Torsional vibrations of beams of thin-walled open section". In: *Journal of Applied Mechanics ASME* 21 (1954), pp. 381–387.

[110] J.M. Gere and Y.K. Lin. "Coupled vibrations of thin-walled beams of open cross section". In: *Journal of Applied Mechanics ASME* 25 (1958), pp. 373–378.

[111] A.A. Ghobarah and W.K. Tso. "Parametric stability of thin-walled beams of open section". In: *Journal of Applied Mechanics ASME* 39 (1972), pp. 201–206.

[112] E. Giangreco. *Teoria e tecnica delle costruzioni*. (In Italian). Liguori, 1966.

[113] J. Glück. "Lateral-load analysis of asymmetric multistory structures". In: *Journal of the Structural Division* 96 (1970), pp. 317–333.

[114] J. Glück and M. Krauss. "Stress analysis of group of interconnected thin-walled cantilevers". In: *Journal of the Structural Division* 99 (1973), pp. 2143–2165.

[115] L.E. Grinter. "Analysis of continuous frames by balancing angle changes". In: *Transactions of the American Society of Civil Engineers* 102 (1937), pp. 995–1011.

[116] K.H. Ha and M. Desbois. "Finite elements for tall buildings analysis". In: *Computers and Structures* 33 (1989), pp. 249–255.

[117] K.H. Ha, P. Fazio, and O. Moselhi. "Orthotropic membrane for tall building analysis". In: *Journal of the Structural Division* 104 (1978), pp. 1495–1505.

[118] H. Haji-Kazemi and M. Company. "Exact method of analysis of shear lag in framed Tube structures". In: *The Structural Design of Tall Building* 11 (2002), pp. 375–388.

[119] A.G. Hansora, P.N. Nimodiya, and K.P. Gehlot. "Numerical analysis of wind loads on tapered shape tall buildings". In: *International Journal of Science Technology and Engineering* 1 (2015), pp. 92–97.

[120] I.S.I. Harba and M.A. Hammed. "Numerical analysis of shear strength behavior of self-compact reinforced concrete two-way bubble deck slab with shear reinforcement". In: *IOP Conference Series: Materials Science and Engineering* 518 (2019).

[121] A.K. Haris. "Approximate stiffness analysis of high-rise buildings". In: *Journal of the Structural Division* 104 (1978), pp. 681–696.

[122] A.C. Heidebrecht and B. Stafford Smith. "Approximate analysis of open-section shear walls subjected to torsional loading". In: *Journal of the Structural Division* 99 (1973), pp. 2355–2373.

[123] A.C. Heidebrecht and B. Stafford Smith. "Approximate analysis of tall wall-frame structures". In: *Journal of the Structural Division* 99 (1973), pp. 199–221.

[124] A.C. Heidebrecht and R.D. Swift. "Analysis of asymmetrical coupled shear walls". In: *Journal of the Structural Division* 97 (1971), pp. 1407–1422.

[125] A.M.A. Van der Heijden. *W.T. Koiter's elastic stability of solids and structures*. Cambridge University Press, 2009.

[126] H. Hill and J. Clark. "Lateral buckling of eccentrically loaded I- and H-section columns". In: *Proceedings of the First National Congress of Applied Mechanics* (1952).

[127] J.C.D. Hoenderkamp. "Critical loads of lateral load resisting structures for tall buildings". In: *The Structural Design of Tall Buildings* 11 (2002), pp. 221–232.

[128] J.C.D. Hoenderkamp and H. Snijder. "Approximate analysis of high-rise frames with flexible connections". In: *The Structural Design of Tall Buildings* 9 (2000), pp. 233–248.

[129] W.P. Howson. "Global analysis: Back to the future". In: *The Structural Engineer* 84 (2006), pp. 18–21.

[130] Y. Hu, X. Jin, and B. Chen. "A finite element model for static and dynamic analysis of thin-walled beams with asymmetric cross-sections". In: *Computers and Structures* 61 (1996), pp. 897–908.

[131] J. Humar and J. Khandoker. "A computer program for three-dimensional analysis of buildings". In: *Computers and Structures* 11 (1980), pp. 369–387.

[132] Ministero delle Infrastrutture e dei Trasporti. "DM 14/01/2008: Norme tecniche per le costruzioni". (In Italian). In: *Gazzetta Ufficiale* Serie Generale n.29 del 04-02-2008 - Suppl. Ordinario n. 30 (2008).

[133] P. Jayachandran. "Design of tall buildings preliminary design and optimization". In: *International Conference on Tall Buildings and Industrial Structures, Coimbatore, India, January 8-10* (2003).

[134] F.A. Johann. "Impact of structural design criteria on the comfort assessment of tall buildings". In: *Journal of Wind Engineering and Industrial Aerodynamics* 180 (2018), pp. 231–248.

[135] R. John and J. Varghese. "A study on behavior of bubble deck slab using Ansys". In: *International Journal of Innovative Science, Engineering and Technology* 2 (2015), pp. 560–563.

[136] R. Kappus. "Drillknicken zentrisch gedrückter stäbe mit offenem profil im elastischen bereich". (In German). In: *Luftfahrtforschung* 14 (1937).

[137] A.H. Khan and B. Stafford Smith. "A simple method of analysis for deflection and stresses in wall-frame structures". In: *Building and Enviromental* 11 (1976), pp. 69–78.

[138] F.R. Khan. *Tubular structures for tall buildings. Handbook of concrete engineering.* Van Nostrand Reinhold Co., 1974.

[139] F.R. Khan and J.A. Sbarounis. "Interaction of shear walls and frames". In: *Journal of the Structural Division* 90 (1964), pp. 285–335.

[140] H.S. Kim and D.G. Lee. "Analysis of shear wall with openings using super elements". In: *Engineering Structures* 25 (2003), pp. 981–891.

[141] N. Kim and M. Kim. "Exact dynamic-static stiffness matrices of non-symmetric thin-walled beams considering coupled shear deformation effects". In: *Thin-walled Structures* 43 (2005), pp. 701–734.

[142] YC. Kim and J. Kanda. "Wind pressures on tapered and set-back tall buildings". In: *Journal of Fluids and Structures* 39 (2013), pp. 306–321.

[143] YM. Kim, K. Youa, and N. Kob. "Across-wind responses of an aeroelastic tapered tall building". In: *Journal of Wind Engineering and Industrial Aerodynamics* 96 (2008), pp. 1307–1319.

[144] S. Kitipornchai and S.L. Chan. "Nonlinear finite element analysis of angle and T beam-columns". In: *Journal of Structural Engineering* 113 (1987), pp. 721–739.

[145] M.J. Klausbruckner and R.J. Pryputniewicz. "Theoretical and experimental study of coupled vibrations of channel beams". In: *Journal of Sound and Vibration* 183 (1995), pp. 239–252.

[146] W.T. Koiter. "Over de stabiliteit van hetelastisch evenwicht". (In Dutch). PhD thesis. H. J. Paris, Amsterdam, English translation as NASA TT F-10, 833 (1967) and AFFDL Report TR 70-25 (1970), 1945.

[147] W.T. Koiter. *Theory of elastic stability*. McGraw-Hill, 1979.

[148] P. Kuhn and P.T. Chiarito. "Shear lag in beams. Methods of analysis and experimental analysis". In: *National Advisory Committee for Aeronautics* 739 (1941).

[149] P. Kuhn and J.P. Peterson. "Shear lag in axially loaded panels". In: *National Advisory Committee for Aeronautics* 1728 (1946).

[150] A.K.H. Kwan. "Simple method for approximate analysis of framed tube structures". In: *Journal of Structural Engineering* 120 (1994), pp. 1221–1239.

[151] G. Lacidogna. "Tall buildings: Secondary effects on the structural behaviour". In: *Structures and Buildings* 6 (2017), pp. 391–405.

[152] G. Lacidogna, G. Nitti, D. Scaramozzino, and A. Carpinteri. "Diagrid systems coupled with closed- and open-section shear walls: Optimization of geometrical characteristics in tall buildings". In: *Procedia Manufacturing* 44 (2020), pp. 402–409.

[153] G. Lacidogna, D. Scaramozzino, and A. Carpinteri. "A matrix-based method for the structural analysis of diagrid systems". In: *Engineering Structures* 193 (2019), pp. 340–352.

[154] A.L. Lang and R.L. Bisplinghoff. "Some results of sweptback wing structural studies". In: *Journal of the Aeronautical Sciences* 18 (1951), pp. 705–717.

[155] O. Lavan and M. De Stefano. *Seismic behaviour and design of irregular and complex civil structures*. Springer, 2013.

[156] T. Lavanya and R.S. Sridhar. "Dynamic analysis of tube-in-tube tall buildings". In: *International Research Journal of Engineering and Technology* 4 (2017), pp. 2357–2362.

[157] D. Lee, H. Kim, and M. Chun. "Efficient seismic analysis of high-rise building structures with the effect of the floor slabs". In: *Engineering Structures* 24 (2002), pp. 613–623.

[158] J. Lee, M. Bang, and J.Y. Kim. "An analytical model for high-rise wall-frame structures with outriggers". In: *The Structural Design of Tall and Special Buildings* 17 (2008), pp. 839–851.

[159] K. Lee, Y. Loo, and H. Guan. "Simple analysis of framed-tube structures with multiple internal tubes". In: *Journal of Structural Engineering* 150 (2001), pp. 450–460.

[160] W.H. Lee. "Free vibration analysis for tube-in-tube tall buildings". In: *Journal of Sound and Vibration* 303 (2007), pp. 287–304.

[161] A. Leung. "Microcomputer analysis of three-dimensional tall buildings". In: *Computers and Structures* 21 (1985), pp. 639–661.

[162] A. Leung and S.C. Wong. "Local-global distribution factors method for tall building frame". In: *Computers and Structures* 29 (1988), pp. 497–502.

[163] T.C. Liauw and K.W. Leung. "Torsion analysis of core wall structures by transfer matrix method". In: *The Structural Engineer* 53 (1975), pp. 187–194.

[164] C. Liu and K. Ma. "Calculation model of lateral stiffness of high-rise diagrid tube structures based on the modular method". In: *The Structural Design of Tall and Special Buildings* 26 (2017), pp. 124–145.

[165] E.E. Lundquist and C.M. Fligg. "A theory for primary failure of straight centrally loaded columns". In: *National Advisory Committee for Aeronautics, Technical Memorandum* 582 (1937), pp. 141–167.

[166] A. MacLeod and H.M. Hosny. "Frame analysis of shear-wall cores". In: *Journal of the Structural Division* 103 (1977), pp. 2037–2047.

[167] R. Mahjoub, R. Rahgozar, and H. Saffari. "Simple analysis of tube frame system of tall building by using of deformation functions". In: *Australian Journal of Basic and Applied Sciences* 5 (2011), pp. 1475–1482.

[168] S. Mahmoud. "Horizontally connected high-rise buildings under earthquake loadings". In: *Ain Shams Engineering Journal* 10 (2019), pp. 227–241.

[169] R. Maillart. "Zur frage der biegung". (In German). In: *Schweizerische Bauzeitung* 18 (1921), pp. 195–197.

[170] D.J. Malcolm and R.G. Redwood. "Shear lag in stiffened box girders". In: *Journal of the Structural Division* 7 (1970), pp. 1403–1419.

[171] D.V. Mallick and R. Dungar. "Dynamic characteristics of core wall structures subjected to torsion and bending". In: *The Structural Engineer* 55 (1977), pp. 251–261.

[172] V. Mazzotta, E. Brunesi, and R. Nascimbene. "Numerical modeling and seismic analysis of tall steel buildings with braced frame systems". In: *Periodica Polytechnica Civil Engineering* 61 (2017), pp. 196–208.

[173] S.A. Meftah, A. Tounsi, and A.B. Abbas. "A simplified approach for seismic calculation of a tall buildings braced by shear walls and thin walled open section structures". In: *Engineering Structures* 29 (2007), pp. 2576–2585.

[174] E. Mele, M. Toreno, G. Brandonisio, and A. De Luca. "Diagrid structures for tall buildings: Case studies and design considerations". In: *The Structural Design of Tall and Special Buildings* 23 (2014), pp. 124–145.

[175] M. Memon and T.D. Narwani. "Experimental investigations regarding behavior of tall buildings subjected to lateral loading". In: *Journal of Quality and Technology Management* 4 (2008), pp. 39–50.

[176] E. Mendelson and M. Baruch. "Damped earthquake response of non-symmetric multistorey structures". In: *The Structural Engineer* 53 (1975), pp. 165–171.

[177] E. Mendelson and M. Baruch. "Earthquake response of non-symmetric multistorey structures". In: *The Structural Engineer* 51 (1973), pp. 61–70.

[178] P. Mendis. "Warping analysis of concrete cores". In: *The Structural Design of Tall Buildings* 10 (2001), pp. 43–52.

[179] D. Michael. "Torsional coupling of core walls in tall buildings". In: *The Structural Engineer* 47 (1969), pp. 67–72.

[180] A.G.M. Michell. "Elastic stability of long beams under transverse forces". In: *Philosophical Magazine* 48 (1899), pp. 298–309.

[181] H.C. Miller. *The Chicago School of Architecture*. United States Department of the Interior, 1973.

[182] F. Mohri, L. Azrar, and M. Potier-Ferry. "Flexural-torsional post-buckling analysis of thin-walled elements with open sections". In: *Thin-walled Structures* 39 (2001), pp. 907–938.

[183] G.M. Montuori, E. Mele, G. Brandonisio, and A. De Luca. "Geometrical patterns for diagrid buildings: Exploring alternative design strategies from the structural point of view". In: *Engineering Structures* 71 (2014), pp. 112–127.

[184] K.S. Moon. "Stiffness-based design methodology for steel braced tube structures: A sustainable approach". In: *Engineering Structures* 32 (2010), pp. 3163–3170.

[185] K.S. Moon, J.J. Connor, and J.E. Fernandez. "Diagrid structural systems for tall buildings: Characteristics and methodology for preliminary design". In: *The Structural Design of Tall and Special Buildings* 16 (2007), pp. 205–230.

[186] F. Mortelmans, G. Roeck, and D. Gemert. "Approximate method for lateral load analysis of high-rise buildings". In: *Journal of the Structural Division* 107 (1981), pp. 1589–1610.

[187] G. Nitti. "Formulazione analitica per il calcolo degli edifici di grande altezza realizzati mediante involucri tubolari intelaiati". (In Italian). MA thesis. Politecnico di Torino, 2015.

[188] G. Nitti, G. Lacidogna, and A. Carpinteri. "Structural analysis of high-rise buildings under horizontal loads: A study on the Piedmont Region Headquarters Tower in Turin". In: *The Open Construction and Building Technology Journal* 13 (2019), pp. 81–96.

[189] G. Nitti, G. Lacidogna, and A. Carpinteri. "Tall buildings subjected to horizontal loading: Analysis of two case studies by an in-house numerical code". In: *Proceedings of the 23rd Conference of the Italian Association of Theoretical and Applied Mechanics* 1 (2017), pp. 292–300.

[190] S. Park, E. Simiu, and D. Yeo. "Equivalent static wind loads vs. database-assisted design of tall buildings: An assessment". In: *Engineering Structures* 186 (2019), pp. 553–563.

[191] D.M. Patil and K.K. Sangle. "Seismic behaviour of outrigger braced systems in high rise 2-D steel buildings". In: *Structures* 8 (2016), pp. 1–16.

[192] T. Paulay and R.G. Taylor. "Slab coupling of earthquake-resisting shear walls". In: *ACI Journal Proceedings* 78 (1981), pp. 130–140.

[193] O.A. Pekau, L. Lin, and Z.A. Zielinski. "Static and dynamic analysis of tall tube-intube structures by finite story method". In: *Engineering Structures* 18 (1996), pp. 515–527.

[194] O.A. Pekau, Z.A. Zielinski, and L. Lin. "Displacement and natural frequencies of tall building structures by finite story method". In: *Computers and Structures* 54 (1995), pp. 1–13.

[195] Y.L. Pi, N.S. Trahair, and S. Rajasekaran. "Energy equation for beam lateral buckling". In: *Journal of Structural Engineering* 118 (1992), pp. 1462–1479.

[196] G. Piccardo, A. Ferrarotti, and A. Luongo. "Nonlinear generalized beam theory for open thin-walled members". In: *Mathematics and Mechanics of Solids* 22 (2017), pp. 1907–1921.

[197] G. Piccardo, F. Tubino, and A. Luongo. "A shear-shear torsional beam model for nonlinear aeroelastic analysis of tower buildings". In: *Zeitschrift fur Angewandte Mathematik und Physik* 66 (2015), pp. 1895–1913.

[198] G. Piccardo, F. Tubino, and A. Luongo. "Equivalent nonlinear beam model for the 3-D analysis of shear-type buildings: Application to aeroelastic instability". In: *International Journal of Non-Linear Mechanics* 80 (2016), pp. 52–65.

[199] G. Piccardo, F. Tubino, and A. Luongo. "Equivalent Timoshenko linear beam model for the static and dynamic analysis of tower buildings". In: *Applied Mathematical Modelling* 71 (2019), pp. 77–95.

[200] G. Piccardo, F. Tubino, and A. Luongo. "On the effect of mechanical nonlinearities on vortex-induced lock-in vibrations". In: *Mathematics and Mechanics of Solids* 22 (2017), pp. 1922–1935.

[201] M. Pignataro and A. Luongo. "Asymmetric interactive buckling of thin-walled columns with initial imperfections". In: *Thin-walled Structures* 5 (1987), pp. 365–382.

[202] M. Pignataro, A. Luongo, and N. Rizzi. "On the effect of the local overall interaction on the postbuckling of uniformly compressed channels". In: *Thin-walled Structures* 3 (1985), pp. 293–321.

[203] M. Pignataro, N. Rizzi, and A. Luongo. *Stabilità, biforcazione e comportamento postcritico delle strutture elastiche*. (In Italian). E.S.A., 1988.

[204] P. Pozzati. *Teoria e tecnica delle strutture*. (In Italian). UTET, 1977.

[205] L. Prandtl. *Kipperscheinungen*. (In German). Thesis, 1899.

[206] A. Prokic. "Thin-walled beams with open and closed cross-sections". In: *Computers and Structures* 47 (1993), pp. 1065–1070.

[207] T. Pundir and R. Joshi. "To study the behaviour of conventional slab and buble deck slab". In: *International Journal of Advance Research and Innovative Ideas in Education* 6 (2020), pp. 1082–1088.

[208] A. Qadeer and B. Stafford Smith. "The bending stiffness of slabs connecting shear walls". In: *ACI Journal Proceedings* 66 (1969), pp. 464–473.

[209] R. Rahgozar, A.R. Ahmadi, M. Ghelichi, Y. Goudarzi, M. Malekinejad, and P. Rahgozar. "Parametric stress distribution and displacement functions for tall buildings under lateral loads". In: *Structural Design of Tall and Special Buildings* 23 (2014), pp. 22–41.

[210] R. Rahgozar, A.R. Ahmadi, and Y. Sharifi. "A simple mathematical model for approximate analysis of tall buildings". In: *Applied Mathematical Modelling* 34 (2010), pp. 2437–2451.

[211] S. Rajasekaran. "Equations for tapered thin-walled beams of generic open section". In: *Journal of Engineering Mechanics* 120 (1994), pp. 1607–1629.

[212] G. Ranzi and A. Luongo. "A new approach for thin-walled member analysis in the framework of GBT". In: *Thin-walled Structures* 49 (2011), pp. 1404–1414.

[213] E. Reissner. "Analysis of shear lag in box beams by the principle of minimum potential energy". In: *Quarterly Applied Mathematics* 4 (1946), pp. 268–278.

[214] E. Reissner. "Least work solutions of shear lag problems". In: *Journal of the Aeronautical Sciences* 8 (1941), pp. 284–291.

[215] S. Rendek and I. Balaz. "Distortion of thin-walled beams". In: *Thin-walled Structures* 42 (2004), pp. 255–277.

[216] T.M. Roberts. "Second order strains and instability of thin-walled bars of open cross-section". In: *International Journal of Mechanical Sciences* 13 (1981), pp. 297–306.

[217] H.R. Ronagh, M.A. Bradford, and M.M. Attard. "Nonlinear analysis of thin-walled members of variable cross-section, part I: theory". In: *Computers and Structures* 77 (2000), pp. 285–299.

[218] H.R. Ronagh, M.A. Bradford, and M.M. Attard. "Nonlinear analysis of thin-walled members of variable cross-section, part II: Application". In: *Computers and Structures* 77 (2000), pp. 301–313.

[219] R. Rosman. "An approximate method of analysis of walls of multistorey buildings". In: *Civil Engineering and Public Works Review* 59 (1964), pp. 67–69.

[220] R. Rosman. *Analysis of pierced shear walls*. Wilhelm Ernst and Sohn, 1965.

[221] R. Rosman. "Approximate analysis of shear walls subjected to loads". In: *ACI Journal Proceedings* 6 (1964), pp. 717–733.

[222] R. Rosman. "Torsion of perforated concrete shafts". In: *Journal of the Structural Division* 95 (1969), pp. 991–1010.

[223] A. Rutenberg and A.C. Heidebrecht. "Approximate analysis of asymmetric wall-frame structures". In: *Building Science* 10 (1975), pp. 27–35.

[224] M. Sarkisian. *Designing tall buildings: Structure as architecture*. Routledge, 2016.

[225] J. Schwaighofer. "Door opening in shear walls". In: *ACI Journal Proceedings* 11 (1967), pp. 730–734.

[226] J. Schwaighofer and M.P. Collins. "Experimental study of the behaviour of reinforced concrete coupling slabs". In: *ACI Journal Proceedings* 74 (1977), pp. 123–127.

[227] P. Sharma and G. Singh. "Dynamic analysis of outrigger systems in high rise building against lateral loading". In: *International Journal of Civil Engineering and Technology* 9 (2018), pp. 61–70.

[228] B. Stafford Smith and A. Coull. *Tall building structures: Analysis and design*. John Wiley & Sons, 1991.

[229] B. Stafford Smith and E. Crowe. "Estimating periods of vibration of tall building". In: *Journal of Structural Engineering* 112 (1986), pp. 1005–1019.

[230] R. Smith. "Deflection limits in tall buildings: Are they useful?" In: *ASCE Structures Congress, April 14-16, Las Vegas, Nevada, USA* (2011).

[231] M.C. Stamato and E. Mancini. "Three-dimensional interaction of walls and frames". In: *Journal of the Structural Division* 99 (1973), pp. 2375–2390.

[232] European Committee for Standardization. "Eurocode 1: Actions on structures - Part 1-1: General actions - Densities, self-weight, imposed loads for buildings". In: EN 1991-1-1:2002 (2002).

[233] European Committee for Standardization. "Eurocode 1: Actions on structures - Part 1-4: General actions - Wind actions". In: EN 1991-1-4:2005 (2005).

[234] R.D.J.M. Steenbergen and J. Blaauwendraad. "Closed-form super element method for tall buildings of irregular geometry". In: *International Journal of Solids and Structures* 44 (2007), pp. 5576–5597.

[235] S. Swaddiwudhipong, S. Lee, and Q. Zhou. "Effect of axial deformation on vibration of tall buildings". In: *The Structural Design of Tall and Special Buildings* 10 (2001), pp. 79–91.

[236] S. Swaddiwudhipong, S. Piriyakoontorn, Y. Lim, and S. Lee. "Analysis of tall buildings considering the effect of axial deformation by the Galerkin method". In: *Computers and Structures* 32 (1989), pp. 1363–1369.

[237] G. Taig, G. Ranzi, and A. Luongo. "GBT pre-buckling and buckling analyses of thin-walled members under axial and transverse loads". In: *Continuum Mechanics and Thermodynamics* 28 (2016), pp. 41–66.

[238] H. Takabatake and O. Matsuoka. "The elastic theory of thin-walled open cross sections with local deformations". In: *International Journal of Solids and Structures* 19 (1983), pp. 1065–1088.

[239] H. Takabatake, R. Takesako, and M. Kobayashi. "A simplified analysis of doubly symmetric tube structures". In: *The Structural Design of Tall and Special Buildings* 4 (1995), pp. 137–153.

[240] Y. Tamura et al. "Aerodynamic and response characteristics of supertall buildings with various configurations". In: *Proceedings of the 8th Asia-Pacific Conference on Wind Engineering (APCWE-VII), Chennai, India* (2013), k219–k243.

[241] M. Tanaka and A.N. Bercin. "Free vibration solution for uniform beams of nonsymmetrical cross section using Mathematica". In: *Computers and Structures* 71 (1999), pp. 1–8.

[242] B.S. Taranath. *Structural analysis and design of tall buildings*. McGraw-Hill, 1988.

[243] B.S. Taranath. *Structural analysis and design of tall buildings. Steel and composite construction*. CRC Press, 2012.

[244] B.S. Taranath. *Wind and earthquake resistant buildings*. Marcel Dekker, 2005.

[245] B.S. Taranath and B. Stafford Smith. "Torsion analysis of shear core structures". In: *American Concrete Institute* 35 (1973), pp. 239–264.

[246] M.B. Tate. "Shear lag in tension panels and box beams". In: *Iowa State College Bulletin Engineering Report No. 3* (1950).

[247] S.P. Timoshenko. "Ob ustoichivosti ploskoi formy izgiba dvutavrovoi balki". (In Russian, Trans: On the stability in plane bending of an I-beam). In: *Izvestiya St. Petersburg Politekhnicheskogo Instituta* IV-V (1905-1906).

[248] S.P. Timoshenko. *The Collected Papers of Stephen P. Timoshenko*. McGraw-Hill, 1953.

[249] S.P. Timoshenko. "Theory of bending, torsion and buckling of thin-walled members of open cross section". In: *Journal of the Franklin Institute* 239 (1945), pp. 201–361.

[250] S.P. Timoshenko and J.M. Gere. *Theory of elastic stability*. McGraw-Hill, 1961.

[251] S.P. Timoshenko and D.H. Young. *Theory of structures*. McGraw-Hill, 1945.

[252] S.P. Timoshenko and D.H. Young. *Vibration problems in engineering*. Van Nostrand, 1955.

[253] V. Tomei, M. Imbimbo, and E. Mele. "Optimization of structural patterns for tall buildings: The case of diagrid". In: *Engineering Structures* 171 (2018), pp. 280–297.

[254] G. Tong and L. Zhang. "A new derivation of the buckling theory of thin-walled beams". In: *Proceedings of the Third International Conference on Advances in Steel Structures 9-11 December, Hong Kong, China* (2002), pp. 129–137.

[255] N.S. Trahair. *Flexural-torsional buckling of structures*. CRC Press, 1993.

[256] W.K. Tso and J.K. Biswas. "General analysis of nonplanar coupled shear walls". In: *Journal of the Structural Division* 99 (1973), pp. 365–380.

[257] W.K. Tso and H.B. Chan. "Dynamic analysis of plane coupled shear walls". In: *Journal of the Engineering Mechanics Division* 97 (1971), pp. 33–48.

[258] V. Vlasov. "Kruchenie i ustoichivost' tonkostennykh otkrytykh profilei". (In Russian, Trans: Torsion and stability of thin-walled open sections). In: *Stroitel'naya Promyshlennost'* 6-7 (1938).

[259] V. Vlasov. "Kruchenie, ustoichivost' i kolebaniya tonkostennykh sterzhnei". (In Russian, Trans: Torsion, stability and vibration of thin-walled beams). In: *Prikladnaya Matematika i Mekhanika* 3 (1939).

[260] V. Vlasov. "Raschet rebristykh svodov-obolochek i balok iz tonkostennykh profilei na sovmestnoe deistvie izgiba i krucheniya". (In Russian, Trans: Design of ribben arch-shells, thin-walled beams for combined bending, and torsion). In: *Proekt i Standart* 8,9,10 (1936).

[261] V. Vlasov. *Thin-walled elastic beams*. Israeli program for scientific translation, US Science Foundation, 1961.

[262] V. Vlasov. *Tonkostennyye uprugie sterzhni*. (In Russian, Trans: Thin-walled elastic beams). Stroiizdat, 1940.

[263] H. Wagner and W. Pretschner. "Torsion and buckling of open sections". In: *National Advisory Committee for Aeronautics, Technical Memorandum* 784 (1936).

[264] H. Wagner and W. Pretschner. "Verdrehung und knickung von offenen profilen". (In German). In: *Luftfahrtforschung* 11 (1934), pp. 174–180.

[265] Q. Wang. "Sturm-Liouville equation for free vibration of a tube-in-tube tall building". In: *Journal of Sound and Vibration* 191 (1996), pp. 349–355.

[266] Y. Wang, C. Arnaouti, and S. Guo. "A simple approximate formulation for the first two frequencies of asymmetric wall-frame multi-storey building structures". In: *Journal of Sound and Vibration* 236 (2000), pp. 141–160.

[267] J. Wdowicki and E. Wdowicka. "System of programs for analysis of three-dimensional shear wall structures". In: *The Structural Design of Tall and Special Buildings* 2 (1993), pp. 295–305.

[268] J. Wdowicki and E. Wdowicka. "Three-dimensional analysis of asymmetric shear wall structures with connecting and stiffening beams". In: *Engineering Structures* 42 (2012), pp. 362–370.

[269] C. Weber. "Übertragung des drehmomentes in balken mit doppelflanschigem querschnitt". (In German). In: *Zeitschrift für Angewandte Mathematik und Mechanik* 6 (1926).

[270] C. Willis. *Empire State Building. 21 mesi per costruire il grattacielo più alto del mondo*. (In Italian). Mondadori Electa, 2004.

[271] W.H. Wittrick. "Lateral instability of rectangular beams of strain-hardening material under uniform bending". In: *Journal of the Aeronautical Sciences* 19 (1952), pp. 835–843.

[272] C.W. Wong and S.L. Lau. "Simplified finite element analysis of three-dimensional tall building structures". In: *Computers and Structures* 33 (1989), pp. 821–830.

[273] J.H. Wynhoven and P.F. Adams. "Behavior of structures under loads causing torsion". In: *Journal of the Structural Division* 98 (1972), pp. 1361–1376.

[274] J. Xie. "Aerodynamic optimization in super-tall building designs". In: *The Seventh International Colloquium on Bluff Body Aerodynamics and its Applications (BBAA7), Shanghai, China, September 2-6* (2012), pp. 104–111.

[275] Y. Yaman. "Vibration of open-section channels: a coupled flexural and torsional wave analysis". In: *Journal of Sound and Vibration* 204 (1997), pp. 131–158.

[276] Y.B. Yang and W. McGuire. "Stiffness matrix for geometric nonlinear analysis". In: *Journal of Structural Engineering* 112 (1986), pp. 853–877.

[277] K.A. Zalka. "A simplified method for calculation of the natural frequencies of wall-frame buildings". In: *Engineering Structures* 23 (2001), pp. 1544–1555.

[278] K.A. Zalka. "Full-height buckling of frameworks with cross-bracing". In: *Proceedings of the Institute of Civil Engineers* 134 (1999), pp. 181–191.

[279] K.A. Zalka. *Global structural analysis of buildings*. CRC Press, 2000.

[280] K.A. Zalka. *Structural analysis of multi-storey buildings*. CRC Press, 2020.

[281] C. Zhang, F. Zhao, and Y. Liu. "Diagrid tube structures composed of straight diagonals with gradually varying angles". In: *The Structural Design of Tall and Special Buildings* 21 (2012), pp. 283–295.

[282] L. Zhang and G.S. Tong. "Elastic flexural-torsional buckling of thin-walled cantilivers". In: *Thin-walled Structures* 46 (2008), pp. 27–37.

[283] Z. Zhang and S. Chen. "A new method for the vibration of thin-walled beams". In: *Computers and Structures* 39 (1991), pp. 597–601.

[284] Y. Zhou, P. Chen, C. Wang, L. Zhang, and L. Lu. "Seismic performance evaluation of tall, multitower reinforced concrete buildings with large bottom podiums". In: *Structural Concrete* 19 (2018), pp. 1591–1607.

[285] P.M. Znamenskii. "Obshchaya ustoishivost' dlinnukh otkrytykh profilei pri prodol'nom szhatii". (In Russian, Trans: The general stability of long open sections under longitudinal compression). In: *Tekhnika Vozdushnogo Flota* 12 (1934), pp. 174–180.

[286] D. Zupan and M. Saje. "The linearized three-dimensional beam theory of naturally curved and twisted beams: The strain vectors formulation". In: *Computer Methods in Applied Mechanics and Engineering* 195 (2006), pp. 4557–4578.

This Ph.D. thesis has been typeset by means of the TEX-system facilities. The typesetting engine was pdfLATEX. The document class was `toptesi`, by Claudio Beccari, with option `tipotesi=scudo`. This class is available in every up-to-date and complete TEX-system installation.